AER/AGS Report 91

Alberta Energy Regulator

Regional Geological and Hydrogeological Characterization of the Calgary-Lethbridge Corridor in the South Saskatchewan Regional Planning Area

AGS
ALBERTA GEOLOGICAL SURVEY

AER/AGS Report 91

Regional Geological and Hydrogeological Characterization of the Calgary-Lethbridge Corridor in the South Saskatchewan Regional Planning Area

L.A. Atkinson, J.E. Liggett, G. Hartman, N. Nakevska,
S. Mei, K.E. MacCormack and D. Palombi

Alberta Energy Regulator
Alberta Geological Survey

February 2017

©Her Majesty the Queen in Right of Alberta, 2017
ISBN 978-1-4601-0158-2

The Alberta Energy Regulator/Alberta Geological Survey (AER/AGS), its employees and contractors make no warranty, guarantee or representation, express or implied, or assume any legal liability regarding the correctness, accuracy, completeness or reliability of this publication. Any references to proprietary software and/or any use of proprietary data formats do not constitute endorsement by AER/AGS of any manufacturer's product.

If you use information from this publication in other publications or presentations, please acknowledge the AER/AGS. We recommend the following reference format:

Atkinson, L.A., Liggett, J.E., Hartman, G., Nakevska, N., Mei, S., MacCormack, K.E. and Palombi, D. (2017): Regional geological and hydrogeological characterization of the Calgary-Lethbridge Corridor in the South Saskatchewan regional planning area; Alberta Energy Regulator, AER/AGS Report 91, 175 p.

Published February 2017 by:
Alberta Energy Regulator
Alberta Geological Survey
4th Floor, Twin Atria Building
4999 – 98th Avenue
Edmonton, AB T6B 2X3
Canada

Tel: 780.638.4491
Fax: 780.422.1459
E-mail: AGS-Info@aer.ca
Website: ags.aer.ca

Contents

Acknowledgements x
Abstract xi
1 Introduction 1
1.1 Objectives 1
1.2 Structure 1
2 Study Area 3
3 Geological Setting 9
3.1 Regional Neogene–Quaternary Sediment Geology 9
3.2 Regional Upper Cretaceous–Paleogene Bedrock Geology 13
4 CLC Hydrostratigraphic Model 13
4.1 Development of a Regional Hydrostratigraphic Framework 13
4.2 Hydrostratigraphic Modelling 19
4.2.1 Input Data and Hydrostratigraphic Model Construction 19
4.2.2 Hydrostratigraphic Model Compilation 26
4.2.3 Limitations of the Hydrostratigraphic Model 26
4.3 Analysis of the Distribution of Permeable Bedrock 30
5 Hydrogeology 33
5.1 CLC Wells and Water Supply 35
5.2 Methodology for Mapping Potentiometric Surfaces 35
5.3 Methodology for Mapping Total Dissolved Solids 42
5.4 Analysis of Hydrostratigraphic Units 43
5.5 Recharge, Discharge, and Vertical Gradients 50
5.5.1 Recharge 50
5.5.2 Discharge 54
5.5.3 Vertical Hydraulic Head Gradients 56
5.6 Hydrogeological Implications of the Distribution of Permeable Bedrock 59
6 Provincial Observation Wells 66
7 Summary 66
8 References 70
Appendix 1 – Methodology Workflows 75
Appendix 2 – Hydrostratigraphic Model Data Distribution and Gridded Surface Statistics 81
Appendix 3 – Hydrostratigraphic and Hydrogeological Maps 88
Appendix 4 – Recharge Modelling 131
Appendix 5 – Slice Mapping Results 138
Appendix 6 – Field Photos 166

Tables

Table 1. Geological description of thirteen unconsolidated and bedrock HSUs modelled within the CLC as well as the two erosional surfaces used to constrain the hydrostratigraphic model. 20
Table 2. Data input/quality for unconsolidated HSUs and the bedrock topography grid. 22
Table 3. Data input and quality for bedrock HSUs. 25
Table 4. Hydrogeological summary of mapped HSUs in the CLC. 46
Table 5. Summary of average annual results of the VSMB modelling for those simulations that resulted in groundwater recharge. 53
Table 6. Active GOWN wells in the CLC 67
Table A1-1. AWWID wells that are included or excluded as water supply wells. 78

Table A1-2. Selection criteria for water supply wells and well counts after each step. 79
Table A1-3. Selection criteria for AWWID wells with hydraulic information and well counts after each step. 79
Table A1-4. Selection criteria for DSTs from oil and gas wells and number of DSTs remaining after each step. 79
Table A1-5. Selection criteria for AWWID chemical analyses and number of analyses after each step. 80
Table A1-6. Selection criteria for formation water from oil and gas wells and number of analyses after each step. 80
Table A2-1. Number of subsurface hydrostratigraphic assignments used in the CLC model. 81
Table A2-2. Hydrostratigraphic model: grid elevation, thickness, and error statistics. 82
Table A2-3. Grid errors between measured data points and interpolated potentiometric surface and maps of TDS concentration. 87
Table A4-1. Four climate stations were used in the VSMB modelling and their individual characteristics for model input. 131
Table A4-2. Soil properties used for the VSMB simulations. 131
Table A4-3. Three crop coefficient inputs used for wheat. 133
Table A4-4. Three crop coefficient inputs used for grass. 134
Table A4-5. Three drying curve coefficients for VSMB. 134
Table A4-6. Parameters common to all VSMB simulations. 134
Table A4-7. Average annual recharge (AET) and surface runoff from the VSMB simulation of eight hydrological years. 136

Figures

Figure 1. Location map of the CLC showing elevations (m asl) and major surface features. 2
Figure 2. Physiographic regions and districts as defined by Pettapiece (1986) and underlain by the land surface topography. 4
Figure 3. Hydrology of the CLC shown with the land surface topography. 5
Figure 4. Average annual precipitation (30 year normal from 1981 through 2010). 6
Figure 5. Average annual PET (30 year normal from 1981 through 2010) determined by ACIS with a modified Priestly-Taylor equation. 7
Figure 6. Average annual AET (30 year normal from 1981 through 2010) determined by ACIS for wheat crops. 8
Figure 7. Southwest to northeast schematic cross-section showing the four tectono-fluvial cycles recognized in southern Alberta. 10
Figure 8. Bedrock topography overlain by domains partitioned based on the interpretation of the topographic expression of the bedrock surface and the expected suite of sediments that lie within each domain. 11
Figure 9. Updated surficial geology compilation in the CLC. 12
Figure 10. Stratigraphic column of bedrock units of the southwestern plains. 14
Figure 11. Bedrock units and their stratigraphic equivalents that subcrop in the CLC. 15
Figure 12. Schematic cross-section through the Upper Cretaceous−Paleogene bedrock strata showing the typical depth and lateral extent of bedrock units in the southern portion of the CLC. 16
Figure 13. Schematic cross-section through Neogene–Quaternary HSUs S1, C, and S2. 17
Figure 14. Summary of stratigraphy and related hydrostratigraphy for the CLC study area. 18
Figure 15. Updated bedrock topography and the location and names of paleovalley thalwegs. 23
Figure 16. Sediment thickness created by subtracting the bedrock topography from the DEM. 24

Figure 17. 3D hydrostratigraphic model of the CLC study area showing the thirteen unconsolidated and bedrock HSUs. 27
Figure 18. Bedrock geology map taken directly from the hydrostratigraphic model shown in Figure 17, where modelled bedrock units are truncated by the modelled bedrock topography grid. 28
Figure 19. Cross-section through the southern part of the modelled area (see inset) showing the gridded surfaces from the hydrostratigraphic model. 29
Figure 20. (a) West-east cross-section showing the 81 slices that were evaluated within three different intervals. (b) Example NGR sandstone map of slice 1 of the top of bedrock. 31
Figure 21. Merged slice 11 and the ≥0.60 NGR polygon. 32
Figure 22. Data density map for merged slice 11. 34
Figure 23. Allocation of water supply wells. 36
Figure 24. Water supply wells per ATS section in unconsolidated HSUs. 37
Figure 25. Water supply wells per ATS section in bedrock HSUs. 38
Figure 26. Average recommended pumping rate per section for water supply wells in unconsolidated HSUs. 39
Figure 27. Average recommended pumping rate per section for water supply wells in bedrock HSUs. 40
Figure 28. Three cross-sections showing the gridded surfaces from the hydrostratigraphic model 44
Figure 29. Estimate of potential recharge based on average available precipitation. 51
Figure 30. Schematic of the VSMB model with multiple soil layers. 52
Figure 31. An example of the variation in annual recharge from the Brocket AGDM climate station. 53
Figure 32. Average monthly recharge by climate station from those simulations with recharge. 54
Figure 33. Springs and flowing artesian wells in the CLC. 55
Figure 34. Hydraulic head difference between potentiometric surfaces from wells with mid-screen depths of 0–20 m and 40–60 m, respectively, showing upwards and downwards flow potential. Also shown is the well data used to create the surface at each depth interval. 57
Figure 35. Hydraulic head difference between potentiometric surfaces from wells with mid-screen depths of 0–20 m and 40–60 m, respectively, showing upwards and downwards flow potential. Also shown are the locations of springs and flowing artesian wells. 58
Figure 36. Hydraulic head versus elevation for two townships and wells in the Scollard / Willow Creek HSU. 59
Figure 37. Vertical gradients for all GPS- or LSD-located wells per township and per section. 60
Figure 38. Comparison of flow potential directions for the tomographic-like approach and the section-based approach. 61
Figure 39. Pseudo-3D rendering of the 13 merged net-gross ratio (NGR) slices as well as the top 50 m depth slice below the bedrock surface in the CLC model. 63
Figure 40. NGR subcrop map using averaged NGR data available within 50 m below the bedrock topography surface. 64
Figure 41. Data density map for the 50 m NGR subcrop map. 65
Figure A1-1. Workflow diagram for the updated surficial map compilation. 75
Figure A1-2. Workflow diagram for the construction of the hydrostratigraphic model. 76
Figure A1-3. Workflow diagram for the net-to-gross sandstone slice map analysis. 77
Figure A2-1. Data quality and distribution for the bedrock topography grid (blue). 83
Figure A2-2. Data quality and distribution for the HSU S2 grid (blue). 84
Figure A2-3. Data quality and distribution for the HSU C grid (blue). 85
Figure A2-4. Data quality and distribution for the HSU S1 grid (blue). 86

Figure A3-1. Thickness and extent of HSU S2 as well as average screen depth per ATS section for water supply wells. 89
Figure A3-2. Hydraulic heads and chemical analyses from available HSU S2 wells. 90
Figure A3-3. Depth to recorded water level from available HSU S2 wells. 91
Figure A3-4. Thickness and extent of HSU C as well as average screen depth per ATS section for water supply wells. 92
Figure A3-5. Potentiometric surface for HSU C. Note that the connection of the coarse-grained lenses was not mapped within HSU C. 93
Figure A3-6. Depth to potentiometric surface for HSU C. 94
Figure A3-7. Concentration of TDS in HSU C. 95
Figure A3-8. Thickness and extent of HSU S1 as well as average screen depth per ATS section for water supply wells. 96
Figure A3-9. Potentiometric surface for HSU S1. 97
Figure A3-10. Depth to potentiometric surface for HSU S1. 98
Figure A3-11. Concentration of TDS in HSU S1. 99
Figure A3-12. Thickness, extent, and subcrop of the Paskapoo / Porcupine Hills HSU. 100
Figure A3-13. Average screen depth per ATS section for water supply wells in the Paskapoo / Porcupine Hills HSU. 101
Figure A3-14. Potentiometric surface for the Paskapoo / Porcupine Hills HSU. 102
Figure A3-15. Depth to potentiometric surface for the Paskapoo / Porcupine Hills HSU. 103
Figure A3-16. Concentration of TDS in the Paskapoo / Porcupine Hills HSU. 104
Figure A3-17. Thickness, extent, and subcrop area of the Scollard / Willow Creek HSU. 105
Figure A3-18. Average screen depth per ATS section for water supply wells in the Scollard / Willow Creek HSU. 106
Figure A3-19. Potentiometric surface for the Scollard / Willow Creek HSU. 107
Figure A3-20. Depth to potentiometric surface for the Scollard / Willow Creek HSU. 108
Figure A3-21. Concentration of TDS in the Scollard / Willow Creek HSU. 109
Figure A3-22. Thickness and extent of the Battle HSU. This HSU does not subcrop in the CLC. 110
Figure A3-23. Hydraulic heads and TDS concentration from available Battle HSU wells. 111
Figure A3-24. Depth to potentiometric surface in available wells for the Battle HSU. 112
Figure A3-25. Thickness, extent, and subcrop area of the Horseshoe Canyon / St. Mary River HSU. 113
Figure A3-26. Average screen depth per ATS section for water supply wells in the Horseshoe Canyon / St. Mary River HSU. 114
Figure A3-27. Potentiometric surface for the Horseshoe Canyon / St. Mary River HSU. 115
Figure A3-28. Depth to potentiometric surface for the Horseshoe Canyon / St. Mary River HSU. 116
Figure A3-29. Concentration of TDS in the St. Mary River / Horseshoe Canyon HSU. 117
Figure A3-30. Thickness and extent of the upper tongue of the Bearpaw HSU. 118
Figure A3-31. Thickness and extent of the Horseshoe Canyon / St. Mary River HSU (Strathmore Mb), which separates the upper and lower tongues of the Bearpaw HSU. 119
Figure A3-32. Thickness, extent, and subcrop of the Bearpaw HSU (lower tongue and undifferentiated portion). 120
Figure A3-33. Potentiometric surface, hydraulic heads, and TDS for the Bearpaw HSU. 121
Figure A3-34. Depth to potentiometric surface for the Bearpaw HSU. 122
Figure A3-35. Thickness, extent, and subcrop of the undifferentiated Belly River HSU. 123
Figure A3-36. Potentiometric surfaces of the undifferentiated Belly River HSU. 124
Figure A3-37. Depth to potentiometric surface for the undifferentiated Belly River HSU. 125
Figure A3-38. Concentration of TDS in the undifferentiated Belly River HSU. 126
Figure A3-39. Thickness and extent of the Foremost HSU. 127
Figure A3-40. Hydraulic heads in available wells in the Foremost HSU. 128

Figure A3-41. Depth to potentiometric surface in available wells in the Foremost HSU. 129
Figure A3-42. Concentration of TDS in the Foremost HSU. 130
Figure A4-1. Texture of the parent material of the dominant soil type in each soils polygon in the CLC. 132
Figure A4-2. Plot of C horizon texture of the dominant soil type in each soils polygon. 133
Figure A5-1. West–east cross-section showing the 81 slices that were evaluated within three different intervals 139
Figure A5-2. Merged slice 13 and the ≥0.60 NGR polygon. 140
Figure A5-3. Data density map for merged slice 13. 141
Figure A5-4. Merged slice 12 and the ≥0.60 NGR polygon. 142
Figure A5-5. Data density map for merged slice 12. 143
Figure A5-6. Merged slice 11 and the ≥0.60 NGR polygon. 144
Figure A5-7. Data density map for merged slice 11. 145
Figure A5-8. Merged slice 10 and the ≥0.60 NGR polygon. 146
Figure A5-9. Data density map for merged slice 10. 147
Figure A5-10. Merged slice 9 and the ≥0.60 NGR polygon. 148
Figure A5-11. Data density map for merged slice 9. 149
Figure A5-12. Merged slice 8 and the ≥0.60 NGR polygon. 150
Figure A5-13. Data density map for merged slice 8. 151
Figure A5-14. Merged slice 7 and the ≥0.60 NGR polygon. 152
Figure A5-15. Data density map for merged slice 7. 153
Figure A5-16. Merged slice 6 and the ≥0.60 NGR polygon. 154
Figure A5-17. Data density map for merged slice 6. 155
Figure A5-18. Merged slice 5 and the ≥0.60 NGR polygon. 156
Figure A5-19. Data density map for merged slice 5. 157
Figure A5-20. Merged slice 4 and the ≥0.60 NGR polygon. 158
Figure A5-21. Data density map for merged slice 4. 159
Figure A5-22. Merged slice 3 and the ≥0.60 NGR polygon. 160
Figure A5-23. Data density map for merged slice 3. 161
Figure A5-24. Merged slice 2 and the ≥0.60 NGR polygon. 162
Figure A5-25. Data density map for merged slice 2. 163
Figure A5-26. Merged slice 1 and the ≥0.60 NGR polygon. 164
Figure A5-27. Data density map for merged slice 1. 165
Figure A6-1. Map of field site locations within the CLC. 166
Figure A6-2. Field site 1: Clast- to matrix-supported pebble–cobble gravel and sand (3 m thick) exposed in excavation. 167
Figure A6-3. Field site 2: Clast-supported pebble–cobble gravel and sand (3 m thick) and overlying diamicton (1 m thick) exposed in excavation. 168
Figure A6-4. Field site 3: Clast- to matrix-supported pebble–cobble gravel and sand (4 m thick) exposed in excavation. 169
Figure A6-5. Field site 4: Crudely stratified clast-supported pebble–cobble gravel with sand lenses (6 m thick) and overlying silt diamicton (2.5 m thick) exposed in excavation. 170
Figure A6-6. Field site 5: Crudely bedded clast- to matrix-supported pebble–cobble gravel and sand (6 m thick) and overlying diamicton (1 m thick) exposed in excavation. 171
Figure A6-7. Field site 7: Interbedded sandstone/mudstone bedrock (>24 m thick) overlain by diamicton and silt/clay (approximately 8 m and 3 m thick respectively) exposed in valley wall. 172

Figure A6-8. Field site 8: Units exposed in Oldman River section from bottom to top: shale (>3.5 m thick), gravel (7 m thick), diamicton (8.5 m thick), laterally extensive siltstone bedrock (1.5 m thick; displaced), bedded silt (3.5 m thick), diamicton (6.5 m thick), bedded silt (>4 m thick). 173
Figure A6-9. Field site 9: Interbedded sandstone/shale bedrock and overlying colluviated Quaternary material exposed in St. Mary River section. 174
Figure A6-10. Field site 10: Units exposed in Oldman River section from bottom to top: sandstone (>8 m thick), sand and gravel (6 m thick), massive to crudely stratified diamicton (20 m thick), laminated to bedded sand and silt (12 m thick).....175

Acknowledgements

The authors wish to thank P. Glombick and D. Bechtel (formerly of the AGS) for technical work performed as well as for helpful discussions facilitating completion of this work. The AGS Bedrock Framework Team provided the bedrock grid data from the Geological Framework of Alberta. Climate data in the Calgary-Lethbridge Corridor was provided by Alberta Agriculture and Forestry's AgroClimatic Information Service (http://agriculture.alberta.ca/acis/ [accessed April 2015]). We thank Dr. Masaki Hayashi at the University of Calgary for use of and support for the VSMB recharge model. The authors also acknowledge K. Parks and M. Grobe for the science review, and A. Dalton for technical editing. Finally, we would like to thank S. Wallace, C. Leidl, and S. Gordon at Alberta Environment and Parks for comments on an earlier draft version of this report and for their continued support through the Provincial Groundwater Inventory Program.

Abstract

In partnership with Alberta Environment and Parks (EP), the Alberta Geological Survey (AGS) undertook a study in the Calgary-Lethbridge Corridor (CLC) area of southern Alberta to support the development of a management approach for groundwater in the region. The study's objective was to compile existing geological and hydrogeological information for the CLC and interpret it within a regional-scale hydrostratigraphic framework. This characterization is the foundation for future work in the CLC such as refining the bedrock hydrostratigraphy, defining subregional aquifer units and their properties (hydraulic and chemical), defining groundwater management units, and informing the development of a groundwater monitoring framework.

The interval of geological interest relating to the shallow subsurface hydrostratigraphic framework of the CLC includes Upper Cretaceous–Paleogene bedrock strata overlain by Neogene–Quaternary sediments. This report details the methods and results of dividing this interval into three Neogene–Quaternary hydrostratigraphic units (HSU) and ten Upper Cretaceous−Paleogene HSUs, as well as mapping hydrogeological properties within these units. The study included the following activities:

- establishment of a regional hydrostratigraphic framework of the CLC with which to guide modelling of 3D surfaces for the hydrostratigraphic model and mapping of hydrogeological properties;
- creation of a hydrostratigraphic model of (a) the Neogene–Quaternary sediments, focusing on the spatial distribution of coarse- and fine-grained sediments, and (b) the Upper Cretaceous−Paleogene bedrock units, focusing on a stratigraphic, formation-based approach;
- analysis of the spatial distribution of potentially permeable sandstone within modelled bedrock units using measured rock properties from geophysical log information collected to ground surface;
- production of potentiometric surface and total dissolved solids maps from water level and water chemistry data for each unit represented in the hydrostratigraphic model; and
- estimation of the regional recharge and discharge areas, including an analysis of vertical gradients and numerical modelling of potential recharge.

The development of the regional hydrostratigraphic framework, modelling of 3D gridded surfaces of the unconsolidated and bedrock HSUs, and analysis of the distribution of permeable rocks within bedrock units all form the basis for the analysis of the regional hydrogeology in the CLC. The delineation of HSUs within the regional hydrostratigraphic framework differed between the unconsolidated Neogene–Quaternary succession and the bedrock strata. In the Neogene–Quaternary succession, three unconsolidated HSUs were delineated based on units that were laterally extensive, mappable at a regional scale (1–100 km), and had similar bulk physical material properties (e.g., texture) that are typically related to permeability. These HSUs include two coarse-grained units consisting of sand and/or gravel (HSU S2 and S1), confined to paleovalleys and upland areas, as well as an intervening fine-grained unit (HSU C). HSU S1 forms an important aquifer, overlying the bedrock units and confined by the dominantly fine-grained sediments of HSU C. Within HSU C, thin lenses of coarse-grained materials provide an important water source, although these lenses are not laterally-extensive. Thin, discontinuous, coarse-grained materials of HSU S2 occur at the modern land surface and are not readily used for water supply, although they could be important groundwater recharge areas.

The Upper Cretaceous−Paleogene bedrock HSUs, which underlie Neogene–Quaternary HSUs, collectively comprise an eastward-thinning wedge of bedrock strata. Bedrock HSUs were delineated based on previous stratigraphic divisions and geological mapping and include, in ascending order including lateral equivalents, Upper Cretaceous Pakowki / upper Lea Park HSU, Foremost HSU, undifferentiated Belly River HSU, Bearpaw HSU, Horseshoe Canyon / St. Mary River HSU, uppermost Cretaceous and lowermost Paleogene Scollard / Willow Creek HSU, and Paleogene Paskapoo / Porcupine

Hills HSU. Of these bedrock units, the Battle HSU, Pakowki / upper Lea Park HSU, and Bearpaw HSU are important aquitards, although some permeable layers do exist in the Bearpaw HSU, which provide water supply in the CLC. The remaining bedrock HSUs (Paskapoo / Porcupine Hills HSU, Scollard / Willow Creek HSU, Horseshoe Canyon / St. Mary River HSU, undifferentiated Belly River HSU, and Foremost HSU) generally act as aquifers. Further subdivision of these thick and extensive bedrock HSUs was undertaken to analyze the distribution of rock properties within modelled bedrock units to illustrate zones that likely contain more permeable sandstone bodies. This analysis is extremely helpful for understanding the distribution of potentially permeable bodies, particularly when no hydraulic data is available in the subsurface. This analysis represents an important step towards refining the hydrostratigraphic framework in the bedrock and delineating aquifers for the purposes of groundwater management, especially for deeper HSUs, which are currently not being exploited and hence for which little hydrogeological information is available.

Analysis of the hydrogeological information in the Alberta Water Well Information Database shows a very high density of water supply wells in the area south of Calgary, with upwards of 96 wells per section (~1.6 × 1.6 km). These water supply wells also show that groundwater is mainly sourced from bedrock HSUs in the CLC, although there are areas (generally along paleovalleys) where groundwater is sourced from a mixture of bedrock and unconsolidated HSUs. Potentiometric surface maps of each HSU show a strong link between hydraulic head and local-scale variations of the land surface and bedrock topography, with topographically high areas expressing high hydraulic head, and topographically low areas expressing lower hydraulic head. The associated depth to potentiometric surface maps identify areas which, regionally, are likely under unconfined, confined (‘artesian’), or flowing artesian conditions. Combining the maps of potentiometric surface, depth to potentiometric surface, total dissolved solids, thickness of sediment and bedrock HSUs, water supply wells, and the distribution of potential permeability from rock properties within modelled bedrock units can aid in identifying potential recharge areas or groundwater management units in the CLC.

Numerical modelling of recharge shows that annual recharge is highly variable, varying from 0 to +120 mm/yr. Average annual recharge varied between 10 and 58 mm/yr from simulations of climate conditions at four different weather stations throughout the CLC. These values are consistent with previously published estimates of groundwater recharge in the southern prairies. Mapping of vertical gradients using two different methods can be used to aid in interpretation of potential recharge and discharge areas, although the different mapping methods in some cases produced contradictory results.

Results of this work contribute to a better understanding of the regional hydrogeology of the CLC, which is required in order to guide future studies relating to land-use planning and groundwater monitoring. This regional study also provides the first step in focusing future subregional studies to further define and characterize aquifer units for groundwater management and to better understand surface water-groundwater interactions around specific water bodies.

1 Introduction

In the area covered under the *South Saskatchewan Regional Plan* (SSRP; Government of Alberta, 2014), Alberta Environment and Parks (EP) committed to the development and implementation of a management approach for groundwater in the region by the end of 2017. This included

- confirming priority issues and areas of concern and accelerating monitoring at existing wells in the areas of concern by the end of 2014,
- developing and implementing a regional monitoring program to focus on priority issues by the end of 2016,
- continuing to map groundwater in southern Alberta under the Provincial Groundwater Inventory Program, and
- developing policy direction related to the connectivity of groundwater to nearby surface water sources.

To assist with these activities, EP requested the support of the Alberta Geological Survey (AGS).

The AGS evaluated priority issues and areas of concern in early 2013. This evaluation was subsequently presented to internal and external stakeholders during a workshop held in Calgary in June 2013. As an outcome of this workshop, EP prioritized the Calgary-Lethbridge Corridor (CLC) within the SSRP area, and it was agreed that the AGS would focus on a regional geological and hydrogeological characterization in the CLC before EP developed a regional monitoring strategy. This report presents this characterization and supports groundwater mapping under the Provincial Groundwater Inventory Program.

1.1 Objectives

The objective of this study is to characterize the regional hydrogeology in the CLC (Figure 1) by interpreting existing geological and hydrogeological information using a regional hydrostratigraphic framework. The study achieved the following:

- created a regional hydrostratigraphic framework for the CLC, focusing on
  - delineating the spatial distribution of coarse-grained sediments and identify intervening units that may behave hydraulically as confining units in the Neogene–Quaternary sediments (Sections 3.1, 4.1, and 4.2) and
  - a formation-based approach to mapping and understanding the lateral continuity of lithologically similar materials in the bedrock strata (Sections 3.2, 4.1, and 4.2);
- analyzed the distribution of rock properties within modelled bedrock units to illustrate zones that likely contain more permeable sandstone bodies (Sections 4.3 and 5.6);
- used water level and water chemistry data to produce potentiometric surface and total dissolved solids (TDS) maps for each unit represented in the hydrostratigraphic model (Sections 5.2 and 5.4); and
- estimated the regional recharge and discharge areas, including analysis of vertical gradients and numerical modelling of potential recharge (Section 5.5).

1.2 Structure

This report is organized into seven main sections followed by six supplementary appendices. The main sections focus on the CLC study area, geological setting, hydrostratigraphic modelling, and hydrogeological mapping with key examples presented as figures. The appendices include supplementary diagrams, tables, maps, and photos that are not discussed in the main sections of the report but are an important component of the integrated geological and hydrogeological characterization. In order to minimize boundary effects at the edge of the CLC study area, all maps produced in this report and

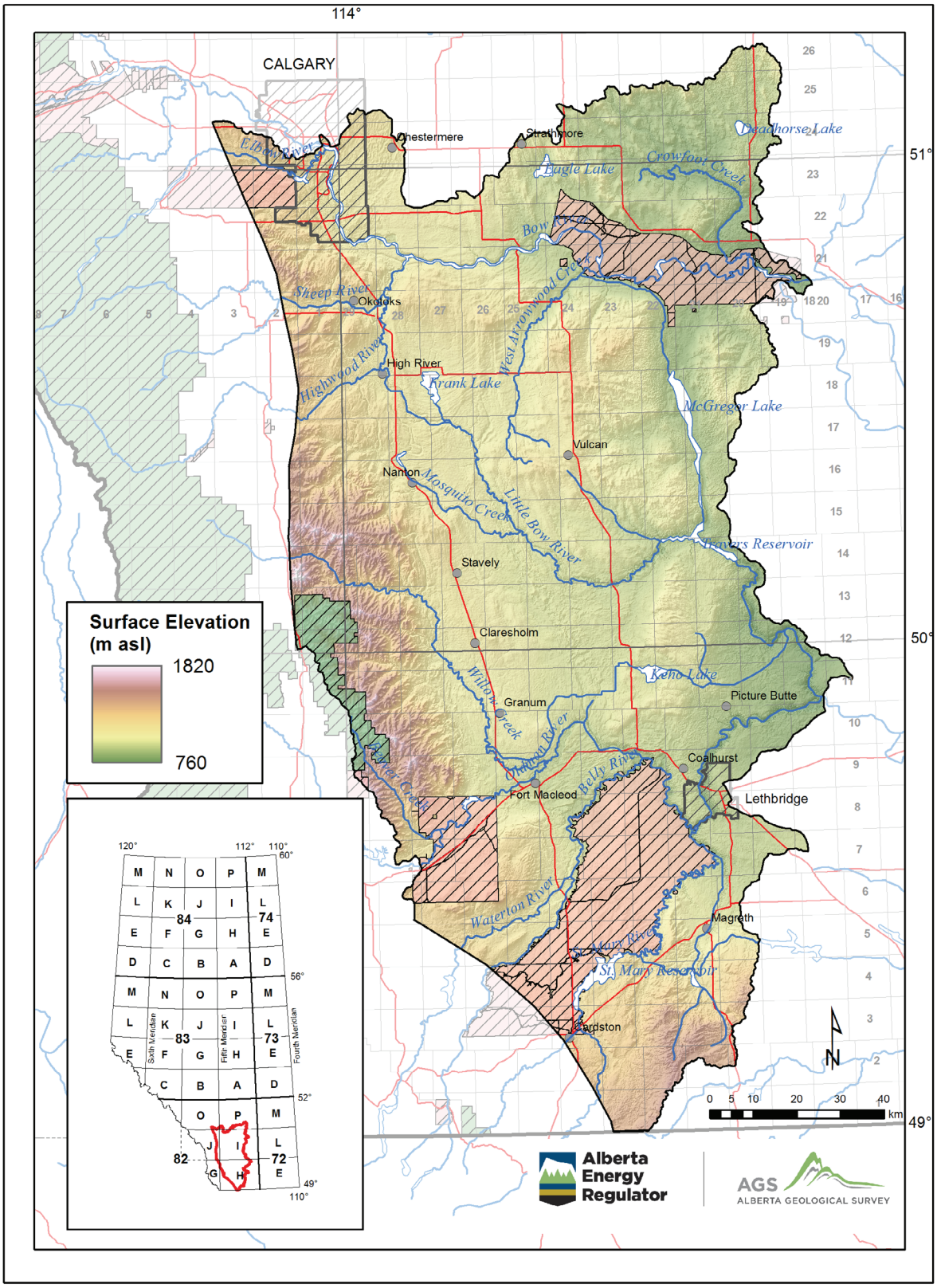

Figure 1. Location map of the CLC showing elevations (m asl) and major surface features. Pink hatched areas outline First Nations reserves. Green hatched shading shows location of the forested portion (Green Area) of public land.

appendices include data within a 10 km buffer zone extended outside the CLC boundary during the interpolation process; although, map extents and statistics presented in this report include only the area within the CLC boundary unless otherwise indicated.

The six supplementary appendices are labelled Appendix 1 through 6. Appendix 1 (A1) provides detailed workflow information used to create the hydrostratigraphic model as well as selection criteria for data used to create hydrogeological maps. A comprehensive suite of maps and tables have been created and are compiled in Appendix 2 (A2), which provide further information for each of the thirteen units interpreted as part of the hydrostratigraphic framework. Accompanying hydrogeological maps are overlain on plan view maps of modelled hydrostratigraphic units in Appendix 3 (A3) to illustrate the spatial distribution of hydraulic properties mapped in the CLC. Appendix 4 (A4) includes information about the input parameters used and simulation results generated for the recharge modelling. Appendix 5 (A5) provides individual maps for each slice used to analyze the distribution of rock properties within the bedrock strata. Lastly, Appendix 6 (A6) presents a number of photos taken in 2013 and 2014, from field excursions conducted to collect data for input into the hydrostratigraphic model. The information presented in the six appendices together with the main sections of the report provides a more detailed understanding of the geology and hydrogeology of the CLC and can be used as the foundation for future studies relating to land-use planning and groundwater monitoring.

2 Study Area

The CLC, located in southern Alberta, occupies an area of 21 159 km^2 (Figure 1) and covers portions of six National Topography System (NTS) map areas, including 82 G, H, I, J, O, and P. The study area lies in the southwestern corner of the Canadian Interior Plains (Bostock, 1967) and is bounded to the west by the Rocky Mountain Foothills (Pettapiece, 1986) and to the south by the USA international border. Three physiographic regions have been recognized in the CLC: the Southern Alberta Uplands along the west and south boundaries, the Western Alberta Plains, and the Eastern Alberta Plains (Pettapiece, 1986; Figure 2). Within these regions, various physiographic districts have been identified. Mean elevation and relief decrease northeastward across the study area.

The CLC is situated within the South Saskatchewan River Basin and contains parts of the Bow and Oldman River sub-basins (Figure 3). The major rivers are the Bow, Little Bow, Oldman, Belly, and St. Mary. Most of the rivers in the CLC are controlled by dams and weirs, and significant volumes of water are withdrawn for irrigation and other uses. Information on the sub-basins and water allocation from these rivers can be found in reports such as *Water for Life* (Golder Associates Ltd., 2008), *From the Mountains to the Sea* (PFSRB, 2009), *Oldman State of the Watershed Report* (Oldman Watershed Council, 2010), and *Bow River Basin State of the Watershed Summary* (Bow River Basin Council, 2010).

The climate in the CLC is semi-arid with significant east-west gradients in climate and hydrological conditions such as precipitation, potential evapotranspiration (PET; the rate at which evapotranspiration would occur over a uniformly vegetated area given an unlimited supply of water), and actual evapotranspiration (AET; the actual amount of evapotranspiration accounting for limitations of water and energy). Average annual precipitation (Figure 4), PET (Figure 5), and AET (Figure 6) data were obtained from Alberta Agriculture and Rural Development's (AARD's) Alberta AgroClimatic Information Service (ACIS; http://agriculture.alberta.ca/acis/ [June 2015]). While PET increases eastward, AET increases westward. This is because although PET is high in the eastern portion of the CLC, precipitation is lower; therefore, less water is available to actually be evapotranspired.

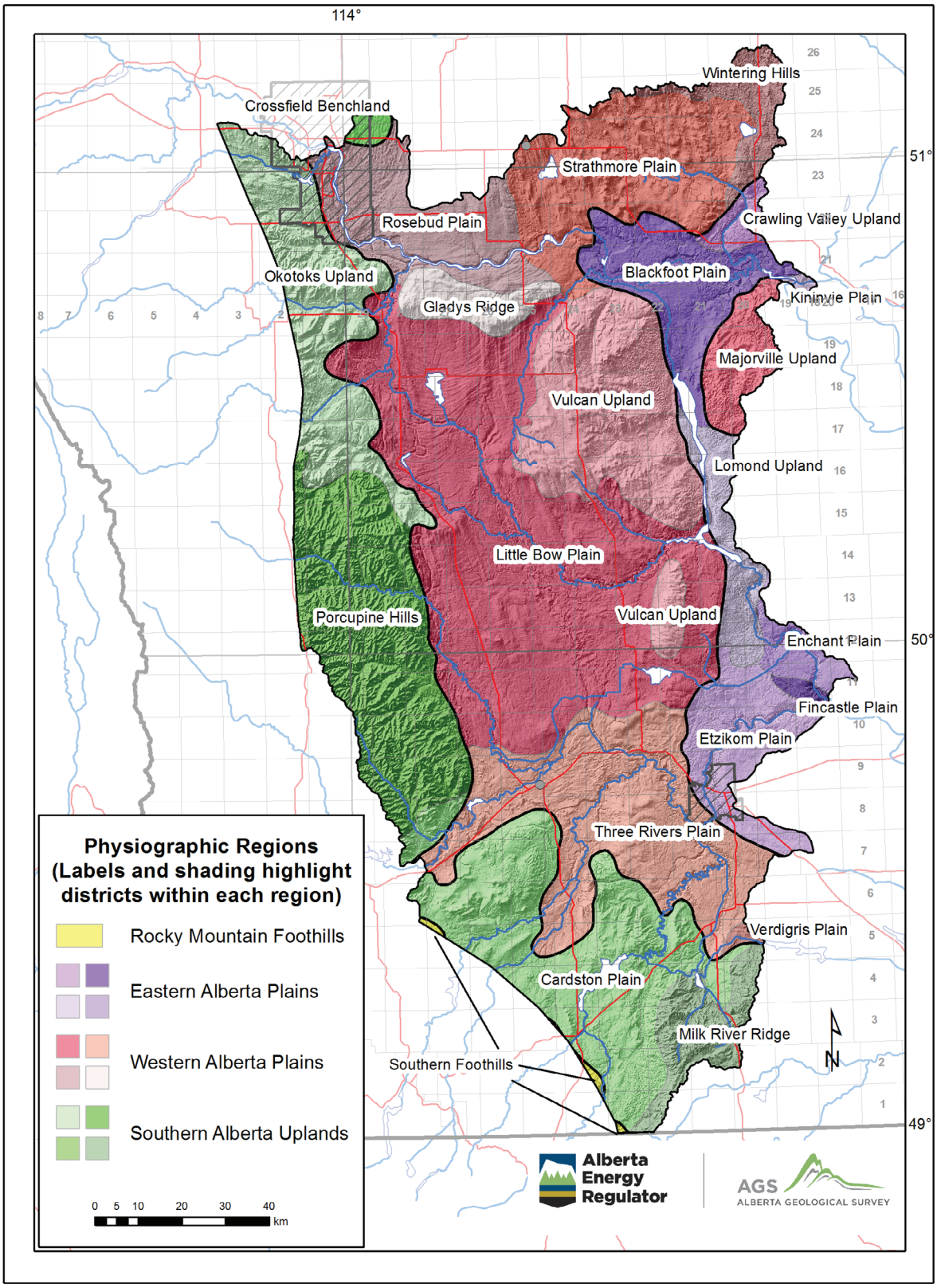

Figure 2. Physiographic regions and districts as defined by Pettapiece (1986) and underlain by the land surface topography.

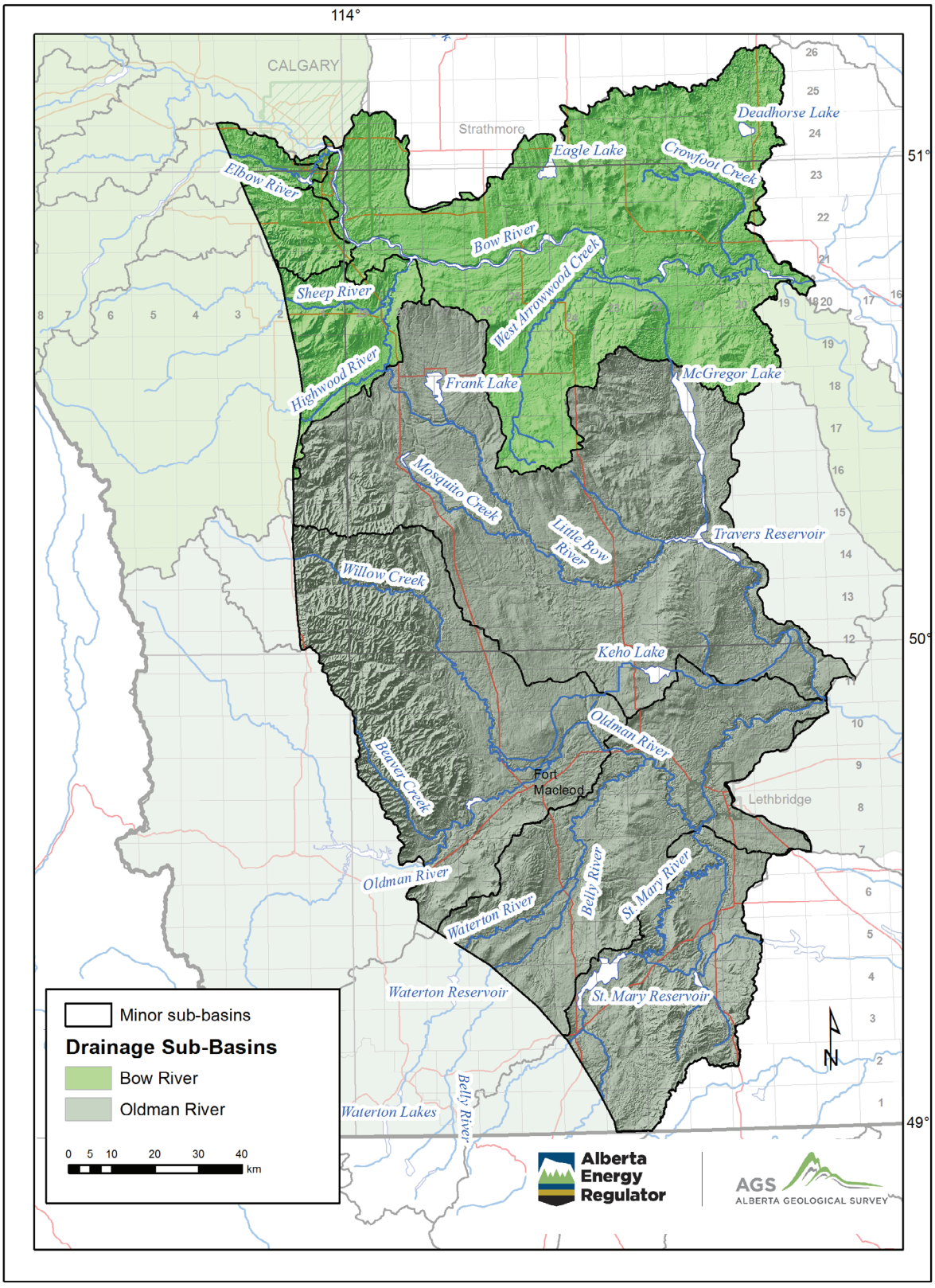

Figure 3. Hydrology of the CLC shown with the land surface topography.

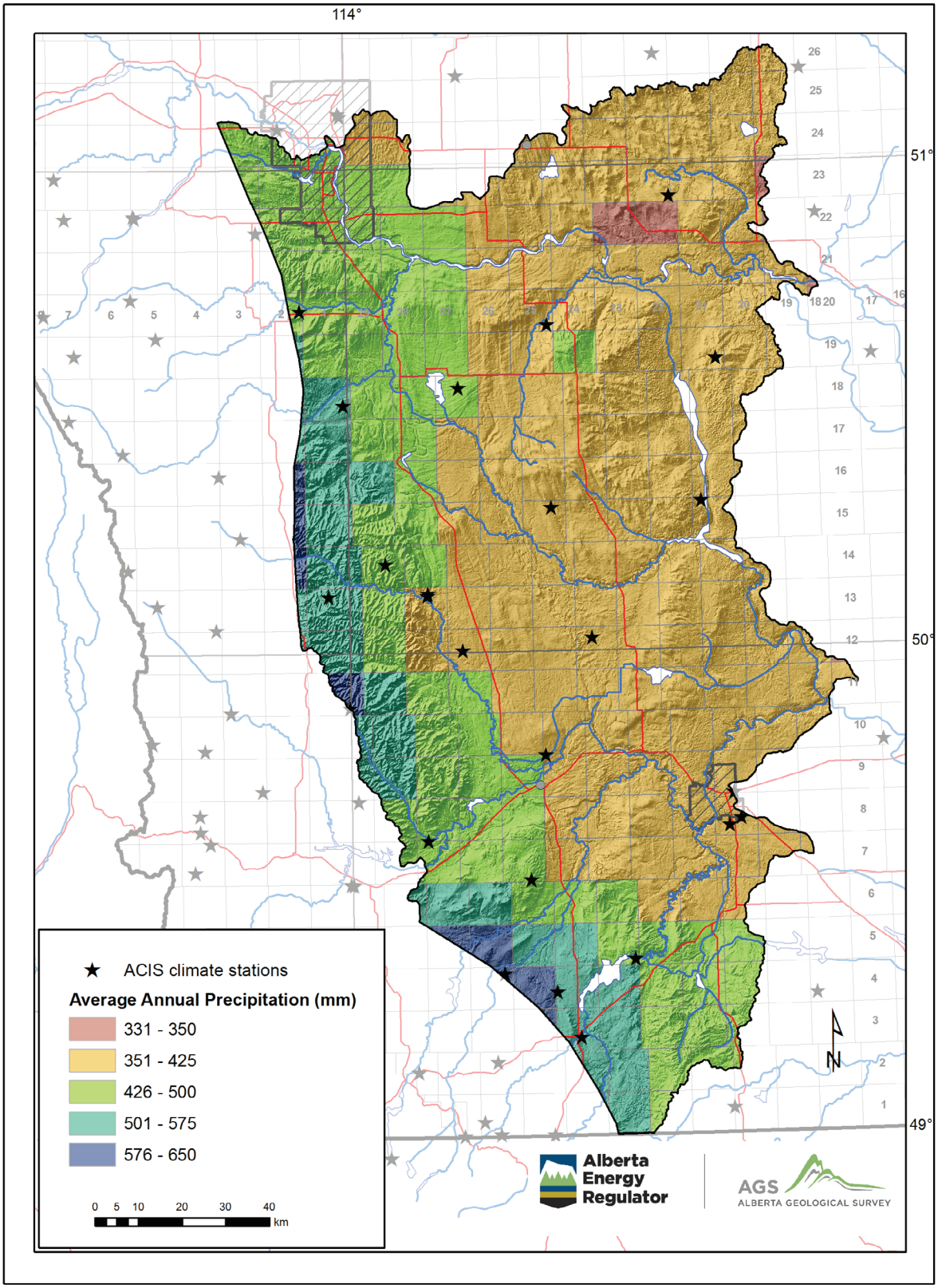

Figure 4. Average annual precipitation (30 year normal from 1981 through 2010). ACIS climate stations include those run by Environment Canada, Alberta Environment and Parks, and Nav Canada, in addition to their own. Interpolated data is provided on a per-township basis. Land surface topography and major rivers are also shown.

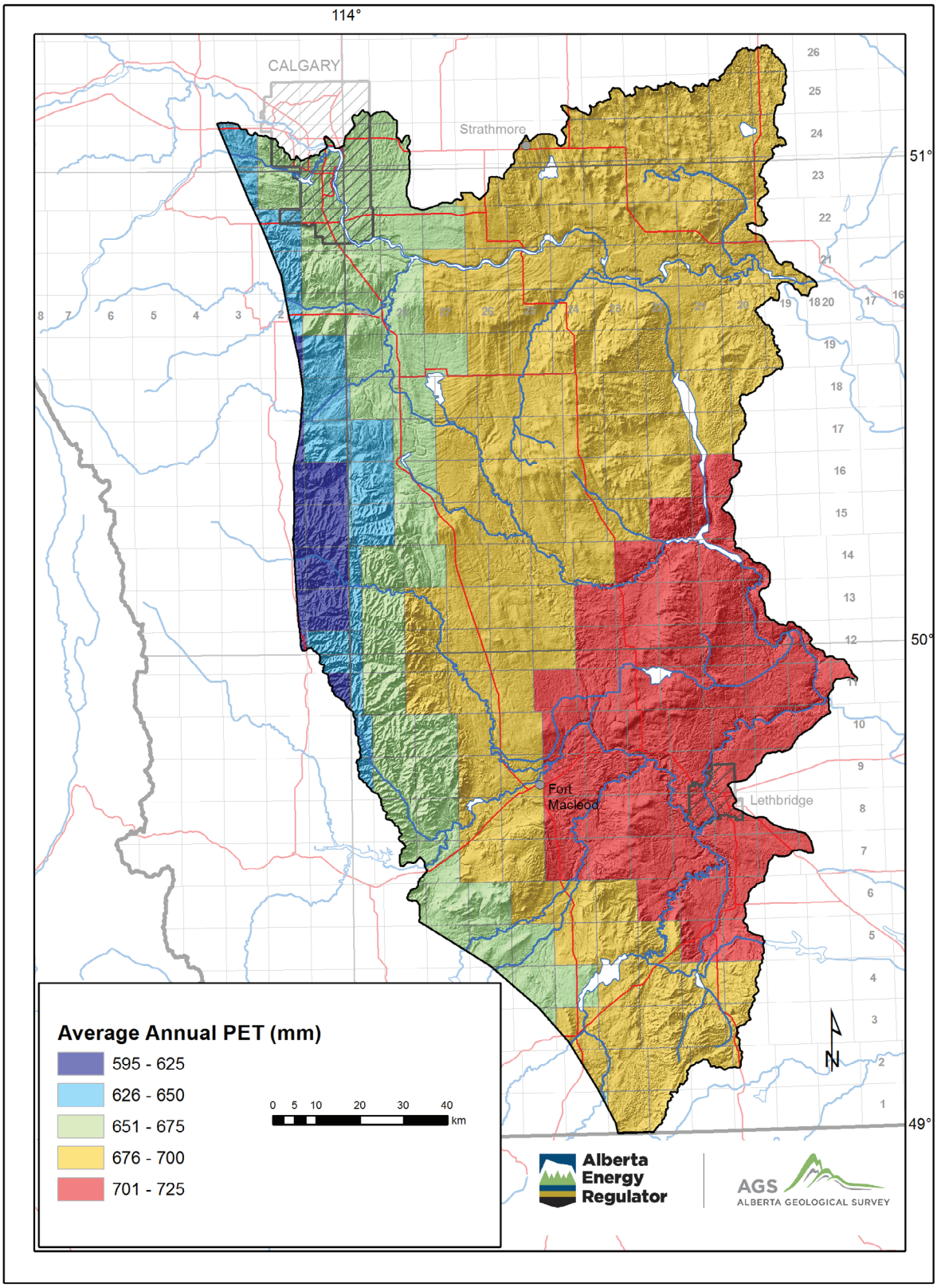

Figure 5. Average annual PET (30 year normal from 1981 through 2010) determined by ACIS with a modified Priestly-Taylor equation.

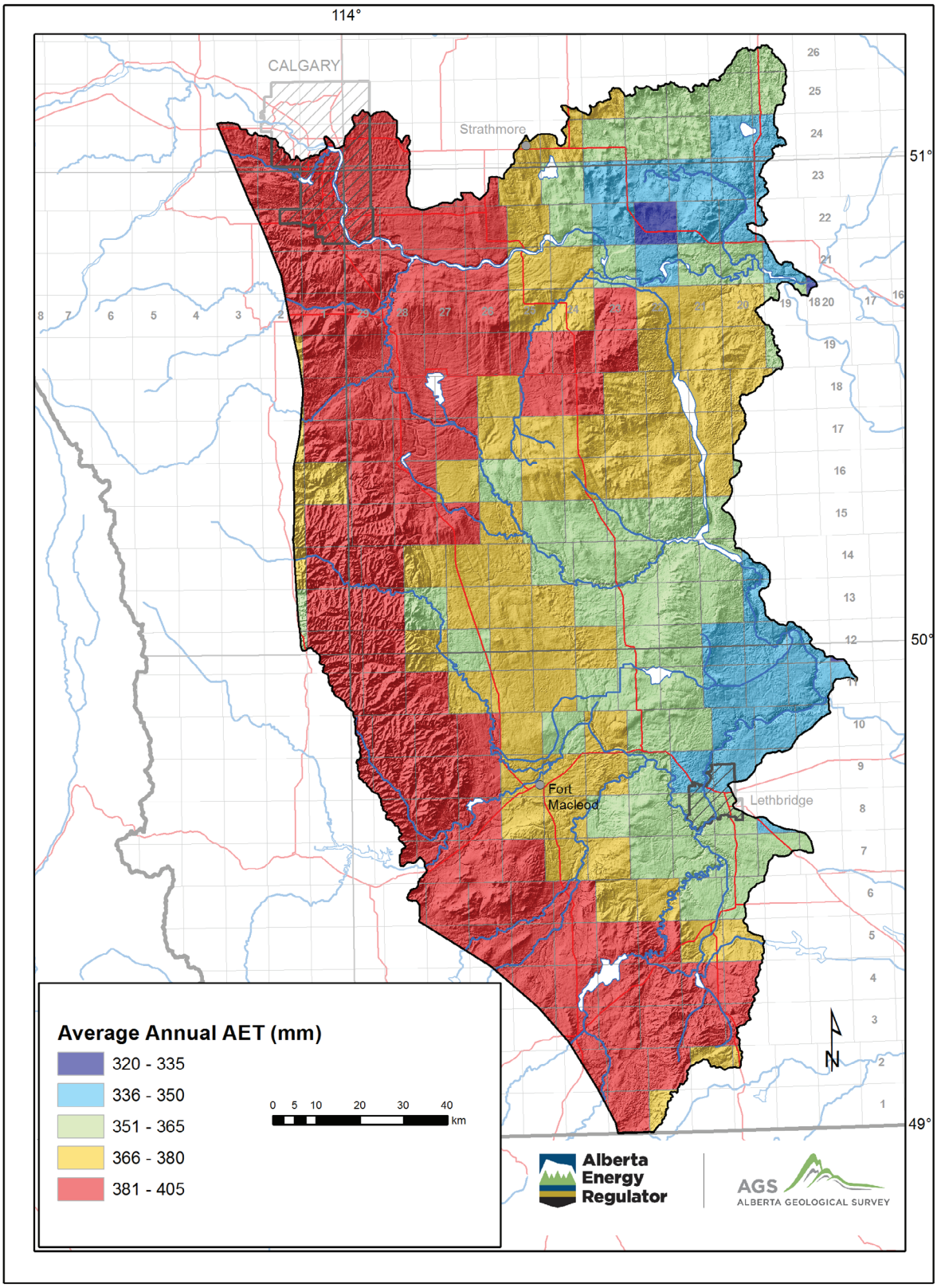

Figure 6. Average annual AET (30 year normal from 1981 through 2010) determined by ACIS for wheat crops.

3 Geological Setting

The interval of geological interest relating to the shallow subsurface hydrostratigraphy of the CLC comprises Upper Cretaceous–Paleogene bedrock overlain by Neogene–Quaternary sediments. Shallow permeable bedrock strata and overlying accumulations of coarse-grained deposits constitute potential aquifers in the CLC. To support the hydrogeological mapping initiatives in the shallow subsurface, a more thorough examination of the geological framework is required. The following sections provide an overview of the regional geological setting of the CLC 3D hydrostratigraphic model from land surface down to the Pakowki / upper Lea Park HSU, which acts as a regional confining unit and defines the base of the hydrostratigraphic model domain.

3.1 Regional Neogene–Quaternary Sediment Geology

The Neogene−Quaternary geological history of the CLC broadly includes (1) tectono-fluvial cycles of uplift, incision, and lateral planation, and (2) glaciation. This history is recognized in the physiography of the modern land surface (Figure 2) and that of the bedrock topography, as well as in the stratigraphy of Neogene–Quaternary sediments overlying bedrock.

Cycles of regional tectonic uplift and fluvial incision, interposed by tectonic quiescence and lateral fluvial planation, have operated throughout the Neogene and Quaternary. Lateral fluvial planation is indicated by broadly distributed, thin deposits of coarse-grained fluvial sediment (sand and gravel) mantling low-relief bedrock surfaces throughout the Interior Plains of Alberta and Montana (Osborn and du Toit, 1991). These coarse-grained deposits, being more erosion resistant than the underlying soft sedimentary bedrock (Section 3.2), partially protected planation surfaces during cycles of uplift, incision, and lateral planation, resulting in a stepped bedrock topography in which older surfaces are topographically higher than younger surfaces (Alden, 1932). Within or immediately adjacent to the CLC, Horberg (1954) and Edwards and Scafe (1994) recognize three planation surfaces that correlate with the No. 1, 2, and 3 benches described by Alden (1932; Figure 7). These surfaces consist of (from highest to lowest) isolated gravel-capped uplands above the plains surface, gravel-bearing bedrock plateaus coinciding with the plains surface, and incised paleovalleys buried beneath the plains surface (Figure 8).

During Late Wisconsinan glaciation, the CLC was covered by the Laurentide Ice Sheet (LIS) that coalesced with the Cordilleran Ice Sheet (CIS) along the Rocky Mountain Foothills, immediately west of the study area (Jackson et al., 2008, 2011). Advancing up the regional slope of the plains, the LIS blocked drainage within incised paleovalleys, causing them to be infilled with dominantly fine-grained glaciolacustrine sediment (buried paleovalleys on Figure 8). Glaciation of the CLC resulted in the deposition of an extensive, dominantly fine-grained till sheet that stratigraphically underlies glacial retreat-phase sediments including generally fine-grained glaciolacustrine and coarse-grained glaciofluvial deposits. Materials exposed at surface, and associated landforms, have been mapped as part of an updated surficial geology compilation in the CLC (Figure 9; Figure A1-1). As the LIS retreated to the northeast, it diverted drainage around its lobate margins and across the regional slope. In places, the modern drainage system is established within these diversions resulting in localized deviation between the positions of the pre- and post-glacial drainage systems. However, for the most part, modern major rivers within the CLC are superposed upon their paleovalley equivalents (e.g., Bow River and Calgary Valley, and Oldman River and Lethbridge Valley; Figure 8).

Neogene and Quaternary deposits within the CLC can be broadly categorized into three units based on depositional setting, texture, and relative position including: (1) a basal, dominantly coarse-grained, fluvial unit that overlies bedrock planation surfaces and the floors of buried valleys (Figure 8); (2) a fine-grained unit comprising till and glaciolacustrine sediment that overlies the basal fluvial unit or bedrock

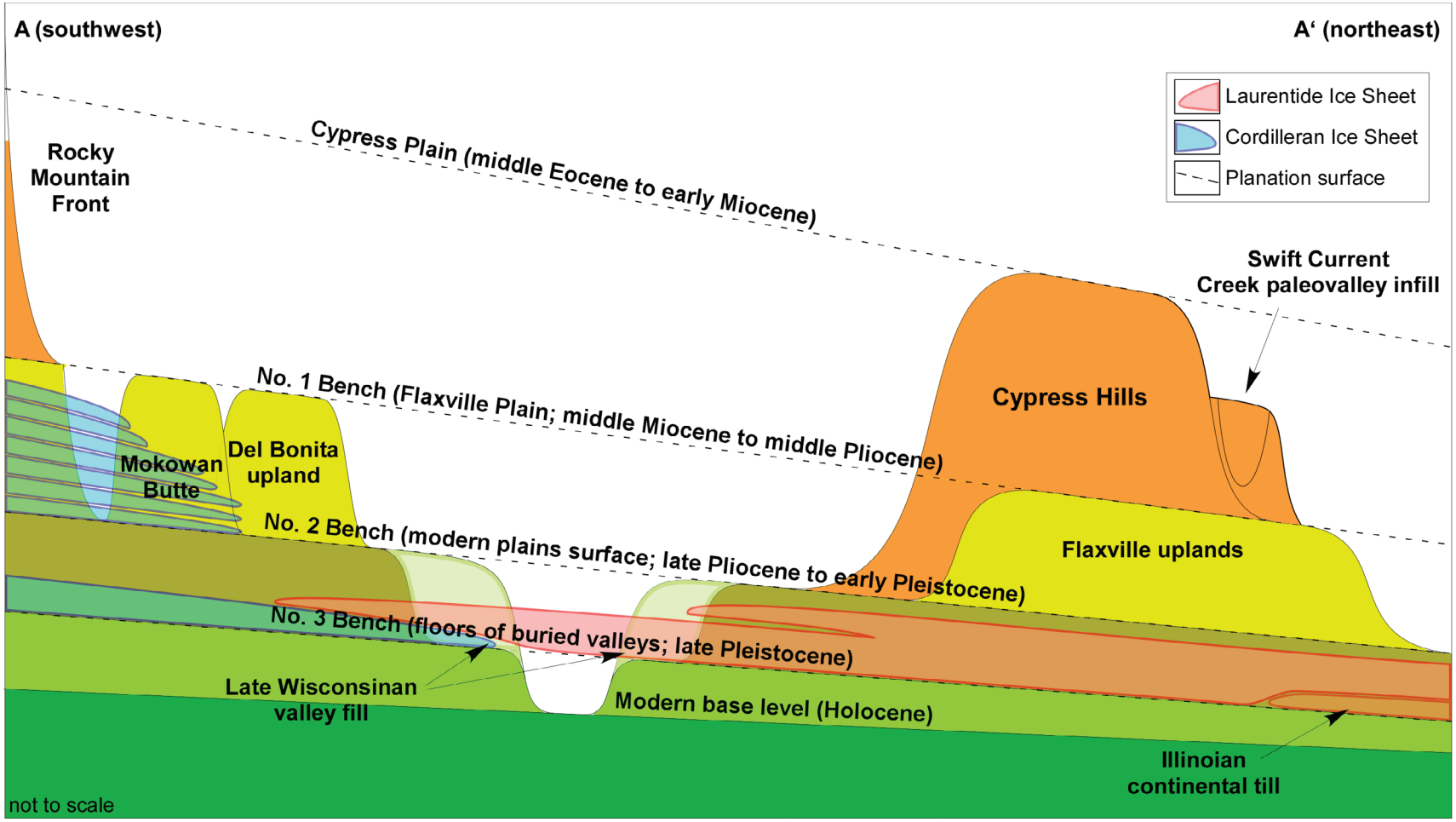

Figure 7. Southwest to northeast schematic cross-section showing the four tectono-fluvial cycles recognized in southern Alberta (from Hartman, 2015). Cumulative sediment removal resulting from these tectono-fluvial cycles totalled approximately 1000 m on the plains and up to 2000 m in the foothills (Nurkowski, 1984) and is illustrated on the cross-section by the dashed lines representing the vertical succession of erosional planation surfaces through geological time (age estimates from Edwards and Scafe, 1994).

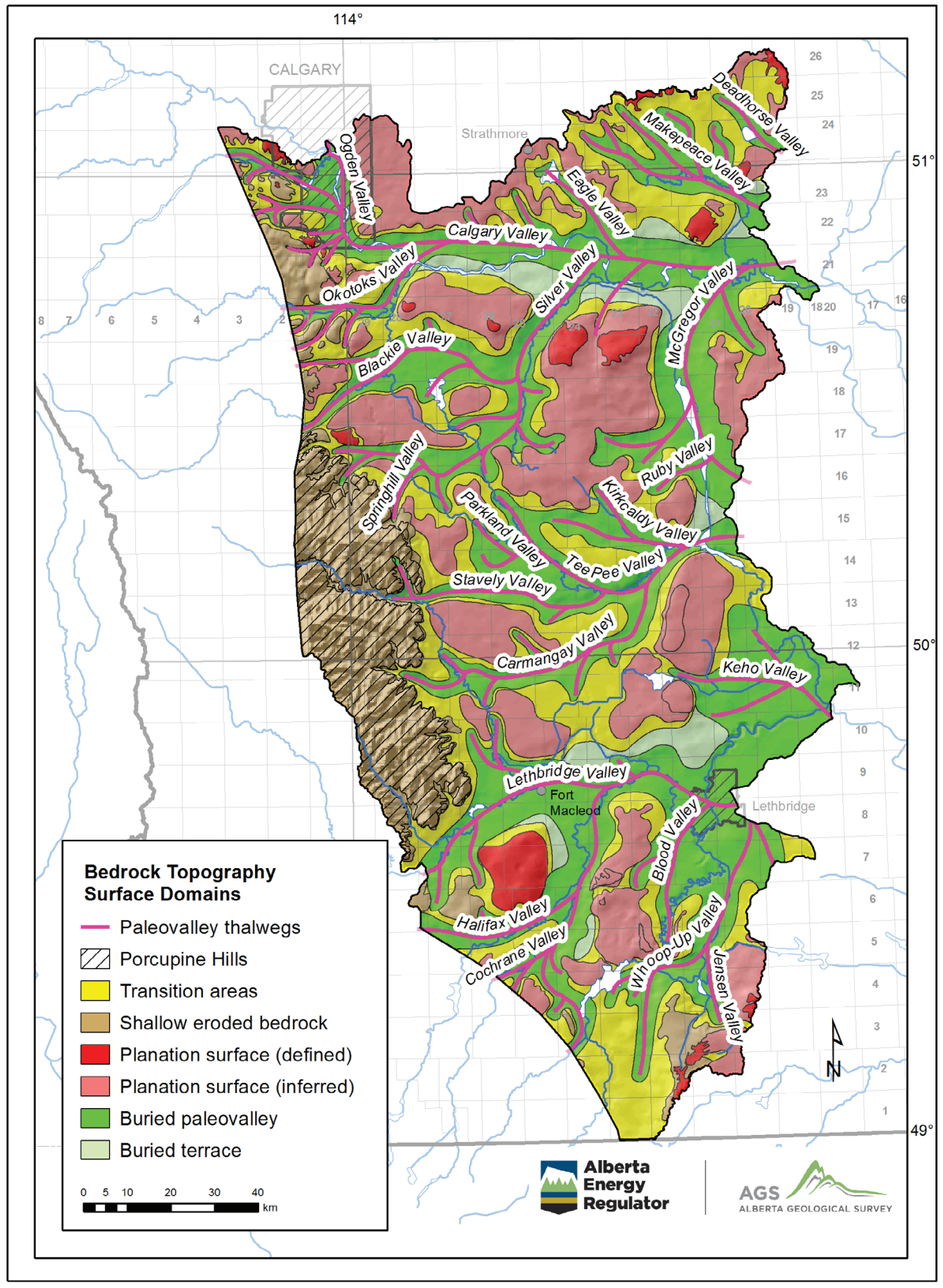

Bedrock Topographic Domains: Extended Legend

Planation surfaces: Low-relief bedrock surfaces resulting from lateral fluvial planation. Older surfaces are incised by younger surfaces forming a stepped bedrock topography. Planation surfaces are commonly overlain by a succession of coarse-grained Neogene fluvial sediments and Quaternary glaciogenic deposits. These surfaces are associated with the No. 1 and No. 2 benches illustrated in Figure 7. "Defined" versus "inferred" refers to the mapper's level of confidence in the boundary.

Shallow eroded bedrock: Portions of the Southern Alberta Uplands, including the Porcupine Hills and Milk River Ridge (Figure 2), characterized by eroded bedrock mantled by veneers of till and colluvium, typically less than 1 m thick.

Buried paleovalleys: Preglacial valleys are infilled with glaciogenic and modern sediments (Figure 16). The dominantly fine-grained sediments, glaciogenic, valley-fill sediments confine coarse fluvial sediments that typically line the valley floors. Re-incision by the postglacial drainage system may expose buried valleys where the two drainage systems intersect. These surfaces are associated with the No. 3 Bench illustrated in Figure 7.

Buried terraces: Buried planar bedrock benches adjacent to a wall of a buried valley. The features are directly overlain by coarse-grained fluvial sediment, which is in turn deeply buried beneath glaciogenic valley infill (Figure 16). These features are interpreted as terraces of the preglacial valley system and are associated with No. 3 Bench illustrated in Figure 7.

Transition areas: Transitional areas between the other four domains. Typically interpreted as eroded bedrock slopes.

Figure 8. Bedrock topography overlain by domains partitioned based on the interpretation of the topographic expression of the bedrock surface and the expected suite of sediments that lie within each domain (see extended legend and Section 4.1 for description of geological units overlying bedrock and associated with each domain).

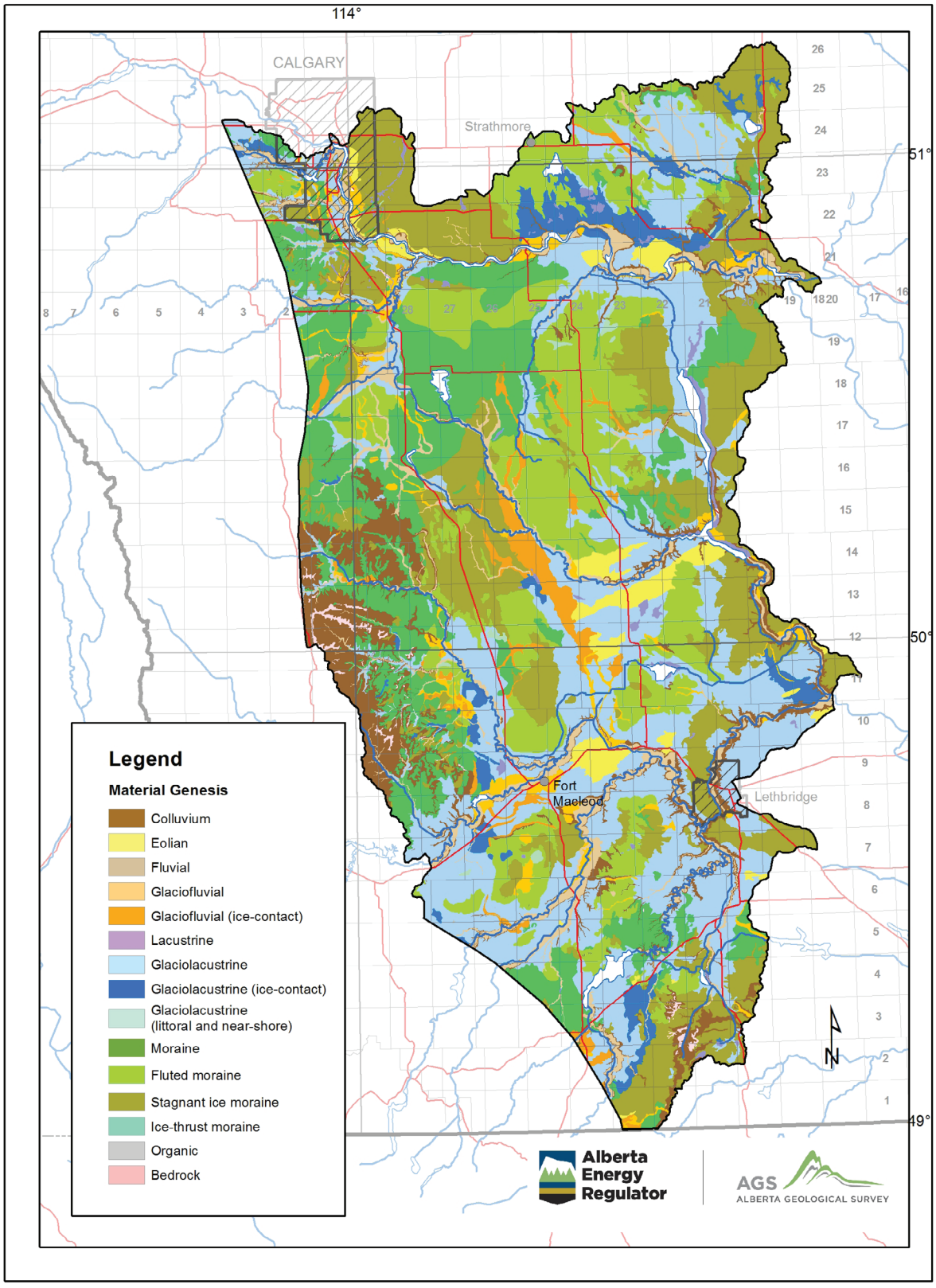

Figure 9. Updated surficial geology compilation in the CLC (adapted from Hartman, 2016). Sand and gravel units typically include eolian, fluvial, glaciofluvial, and glaciofluvial (ice-contact). All other sediment units are typically fine grained.

and which also can be exposed at surface where no overlying sediments have been deposited; and (3) a dominantly fine-to-coarse grained, glaciofluvial, fluvial, or eolian sand and/or gravel unit that is exposed at surface. These units are described further in Section 4.1.

3.2 Regional Upper Cretaceous–Paleogene Bedrock Geology

The Neogene–Quaternary succession is directly underlain by Late Cretaceous−Paleogene sedimentary rocks of the Western Canada Sedimentary Basin (WCSB). These bedrock units were derived from mountain-sourced sediment and deposited in a foreland basin adjacent to the mountain front in the southwestern part of the WCSB (Hamblin, 2004). The bedrock units of interest for this study include, in ascending order including lateral equivalents, Upper Cretaceous Pakowki / upper Lea Park formations, Belly River Group, Bearpaw Formation (including upper and lower tongues as per Eberth and Braman, 2012), Blood Reserve Formation, Horseshoe Canyon / St. Mary River formations (including the Strathmore Member of the Horseshoe Canyon Formation), uppermost Cretaceous and lowermost Paleogene Scollard / Willow Creek formations, and Paleogene Paskapoo / Porcupine Hills formations (Figure 10). These units modelled in the CLC collectively comprise the eastward-thinning wedge of mostly nonmarine strata; however, marine cycles did occur during the Late Cretaceous, resulting in large-scale intertonguing of marine and continental sediments (e.g., Bearpaw Formation; Jerzykiewicz and Norris, 1993). The study area is situated over the Alberta Syncline (Figure 11 and Figure 12), causing strata to gently dip to the west towards the deformation belt on the eastern limb of the Alberta Syncline and dip to the east on the western limb (Dawson et al., 1994), with increasing dip angles in deeper units.

4 CLC Hydrostratigraphic Model

The regional geology of the CLC (Section 3) supports the development of a regional hydrostratigraphic framework, described in more detail in Section 4.1. The hydrostratigraphic units (HSUs) that make up the framework are defined as units of similar texture, relative depositional position, geological history, and having lateral continuity. The delineation of HSUs in the unconsolidated Neogene–Quaternary sediments and the bedrock strata used different criteria, as described in Section 4.1. Using the regional hydrostratigraphic framework, 3D bounding grids for each HSU were interpolated to form a 3D gridded hydrostratigraphic model of the CLC, as described in Section 4.2.

Finally, in order to begin the process of refining HSUs in the bedrock strata from those used in this study, further analysis was performed to evaluate the spatial variability of potentially permeable rocks in the CLC (Section 4.3).

4.1 Development of a Regional Hydrostratigraphic Framework

The hydrostratigraphic framework informs the scale-appropriate selection of HSUs for a regional hydrogeological study. This phase of hydrostratigraphic modelling is necessary in order to group geological units into HSUs. In this study, different approaches were used to define unconsolidated HSUs in the Neogene–Quaternary sediments and bedrock HSUs in the bedrock strata due to the current state of geological knowledge and previous mapping in each of these successions.

As discussed in Section 3.1, the Neogene–Quaternary succession is a highly heterogeneous mix of sediments from tectono-fluvial and glacial processes. No previous 3D geological or hydrogeological mapping of this succession exists in the CLC in digital format. Therefore, three HSUs were developed and informally named as part of this study, based on an amalgamation and simplification of unconsolidated material overlying bedrock within the context of the regional geological history (Figure 13). The selection and mapping of the three unconsolidated HSUs displayed in Figure 13 was based on units that were

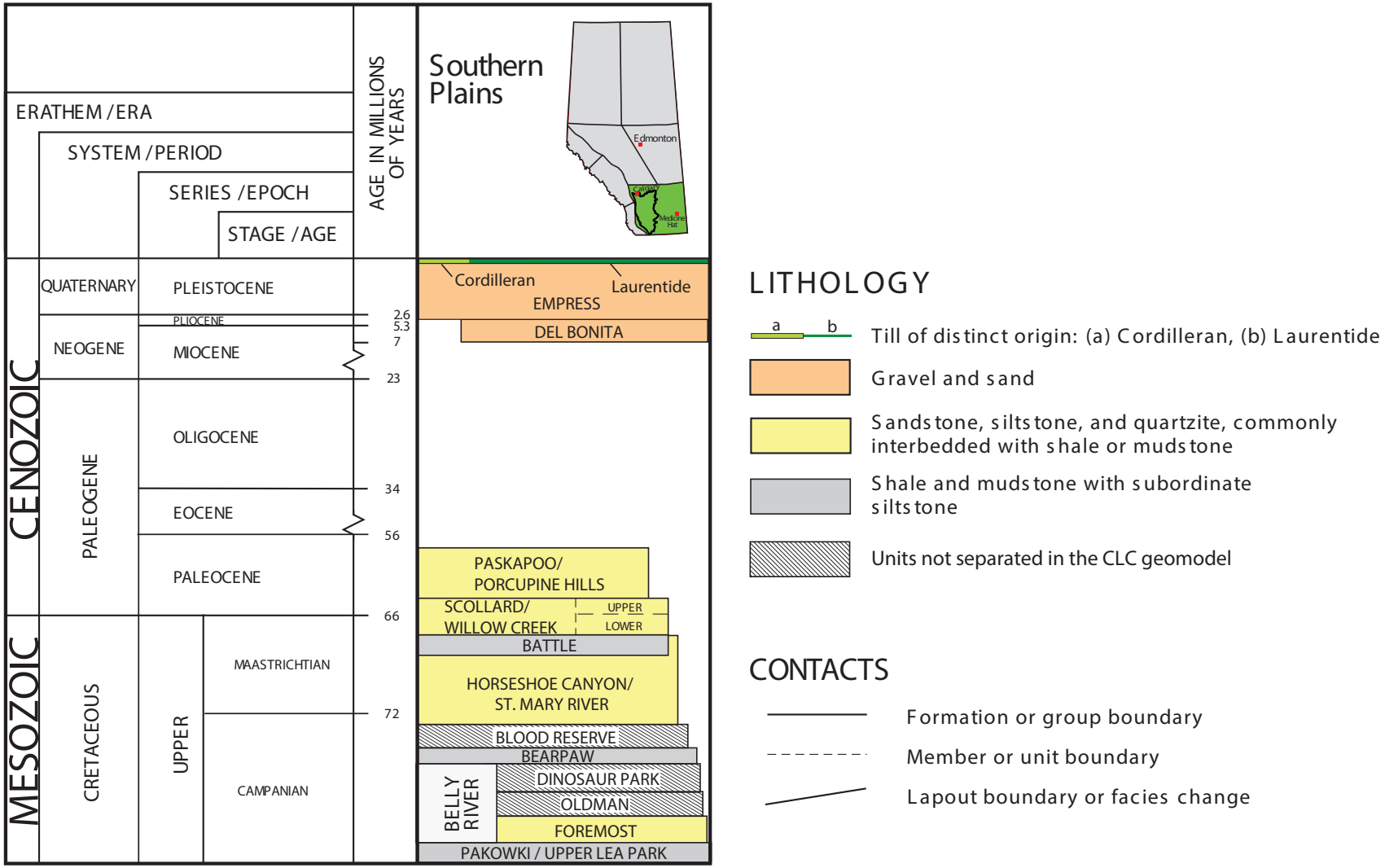

Figure 10. Stratigraphic column of bedrock units of the southwestern plains (modified from Alberta Geological Survey, 2015).

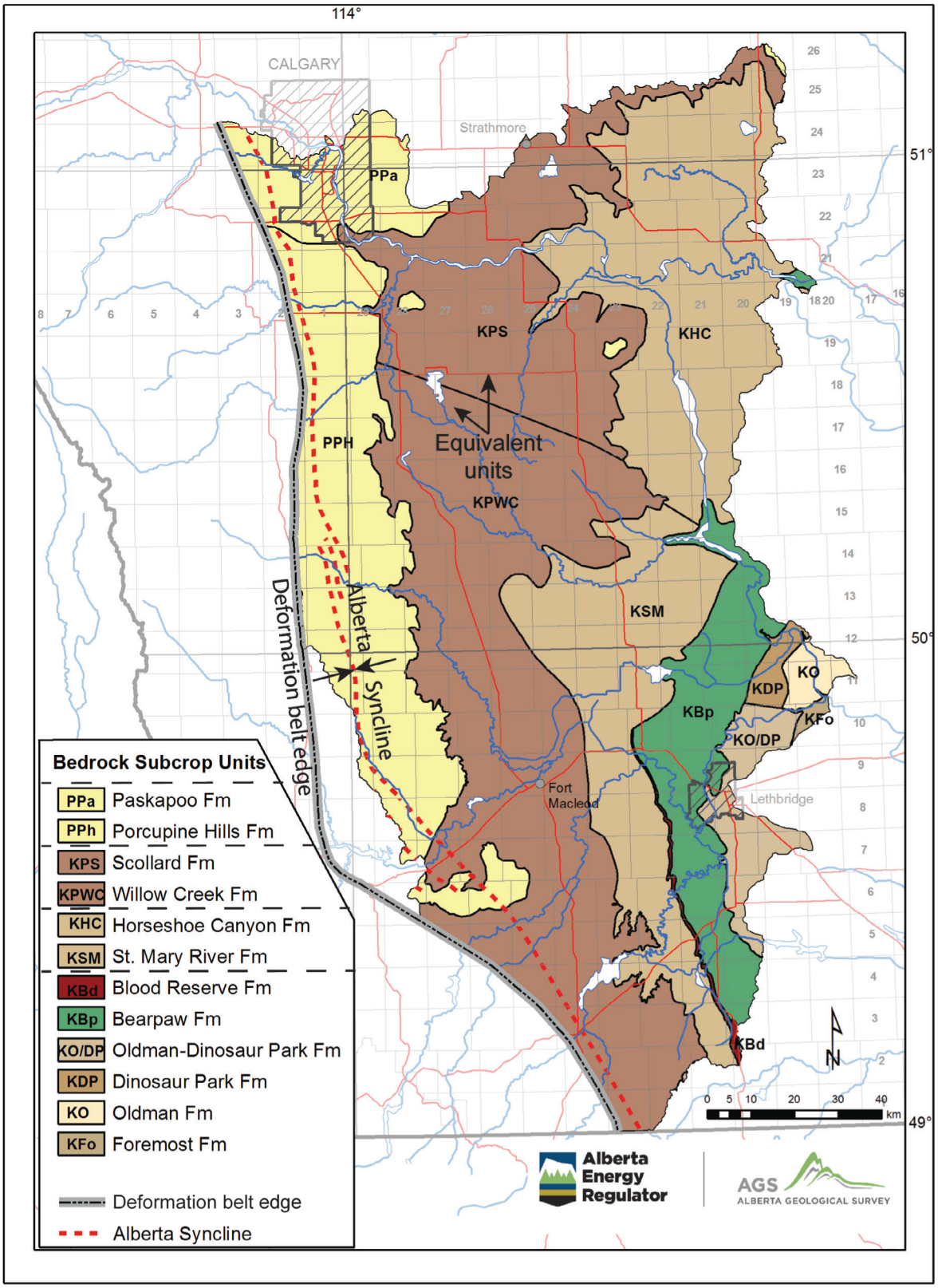

Figure 11. Bedrock units (modified from Prior et al., 2013) and their stratigraphic equivalents that subcrop in the CLC. Equivalent subcrop units are grouped by dashed lines in legend.

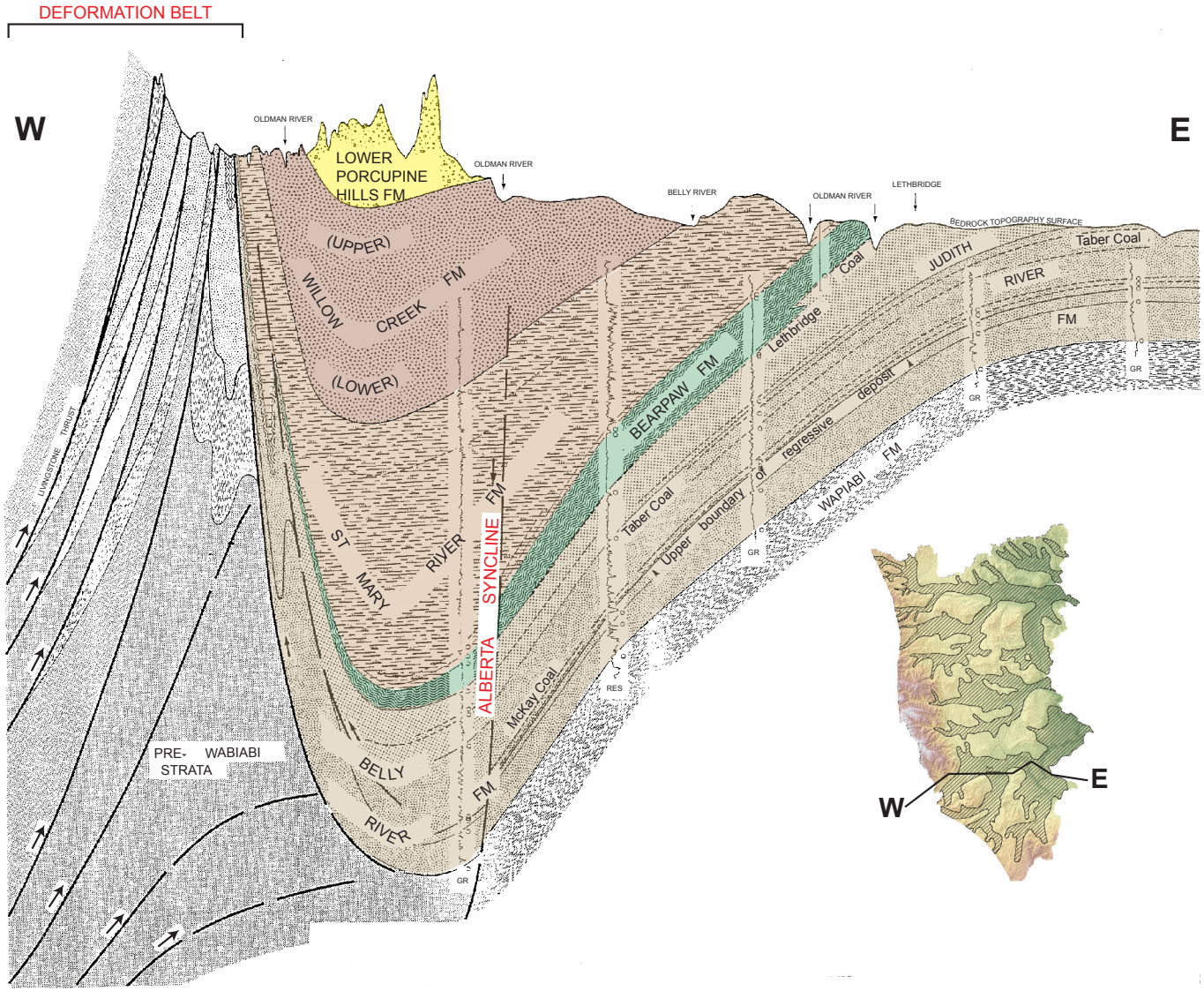

Figure 12. Schematic cross-section through the Upper Cretaceous−Paleogene bedrock strata showing the typical depth and lateral extent of bedrock units in the southern portion of the CLC. Schematic is not to scale, and arrows indicate direction of faulting (modified from Jerykiewicz and Norris, 1993).

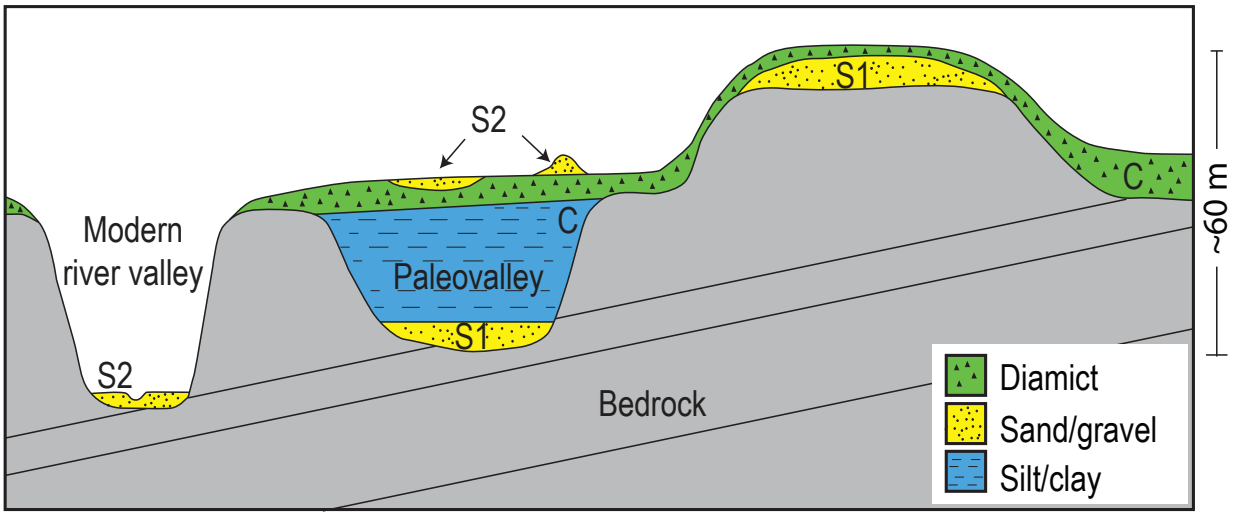

Figure 13. Schematic cross-section through Neogene–Quaternary HSUs S1, C, and S2. Units are discontinuous throughout the modelling domain, although they satisfy the definition of an HSU at the regional scale. Schematic is not to scale.

laterally extensive, mappable at a regional scale (1–100 km), and that had similar bulk physical material properties (e.g., texture) that are typically related to permeability. Although the unconsolidated HSUs are independent of geological history, delineation of them was also informed by their position on and stratigraphic relationship with the bedrock topography (Figure 8, Figure 13).

The bedrock topography surface domains described in Section 3.1 and Figure 8 facilitated correlation of subsurface HSUs from 2D well log observations (discussed in Section 4.2.1) by providing a plan view representation of the expected location of coarse-grained fluvial deposits and valley infill sediments. Information provided by the bedrock topography surface domains allowed for the identification of HSU S1, which includes sediments that are coarse-grained and constrained to buried valleys, terraces, and planation surfaces (Figure 13). This unit directly overlies bedrock and is covered by fine-grained sediments of HSU C. Fine-grained sediments of HSU C typically include diamicton or till and glaciolacustrine deposits (clay). Coarse-grained material may also occur as lenses, adding to the overall heterogeneity of HSU C; however, these lenses are typically thin and are not considered important for the regional hydrostratigraphic modelling. The distribution of glacial sediments across the landscape also includes coarse-grained glaciofluvial sediments, which potentially may act as surficial aquifers or function as recharge/discharge zones. These surface units are correlated to HSU S2 and also include postglacial coarse-grained fluvial deposits distributed throughout the modern drainage system (Figure 13).

Unlike the Neogene–Quaternary succession, formal, laterally extensive lithostratigraphic units have already been defined in the bedrock strata according to the North American Stratigraphic Code (NACSN, 2005; Alberta Geological Survey, 2015), dividing them into major formal bedrock groups, formations, or members, and informal tongues. Recent geological modelling work of bedrock lithostratigraphic units relevant for the regional hydrostratigraphic framework of the CLC includes that of Hamblin (2004), Glombick (2010), Eberth and Braman (2012) and Hathway (2011), as well as work completed at the AGS as part of the Geological Framework of Alberta Project (MacCormack, 2014; Glombick and Mumpy, 2014; Hathway, 2014; Hathway, 2016). While an established stratigraphic framework exists for the bedrock units in the CLC, no such hydrostratigraphic framework currently exists; therefore, in developing the regional hydrostratigraphic framework for the CLC in this study, the bedrock HSUs have been based generally on lithostratigraphic divisions and retain their established names (e.g., Scollard / Willow Creek HSU; Figure 14), because an established lithostratigraphic framework already exists. Although

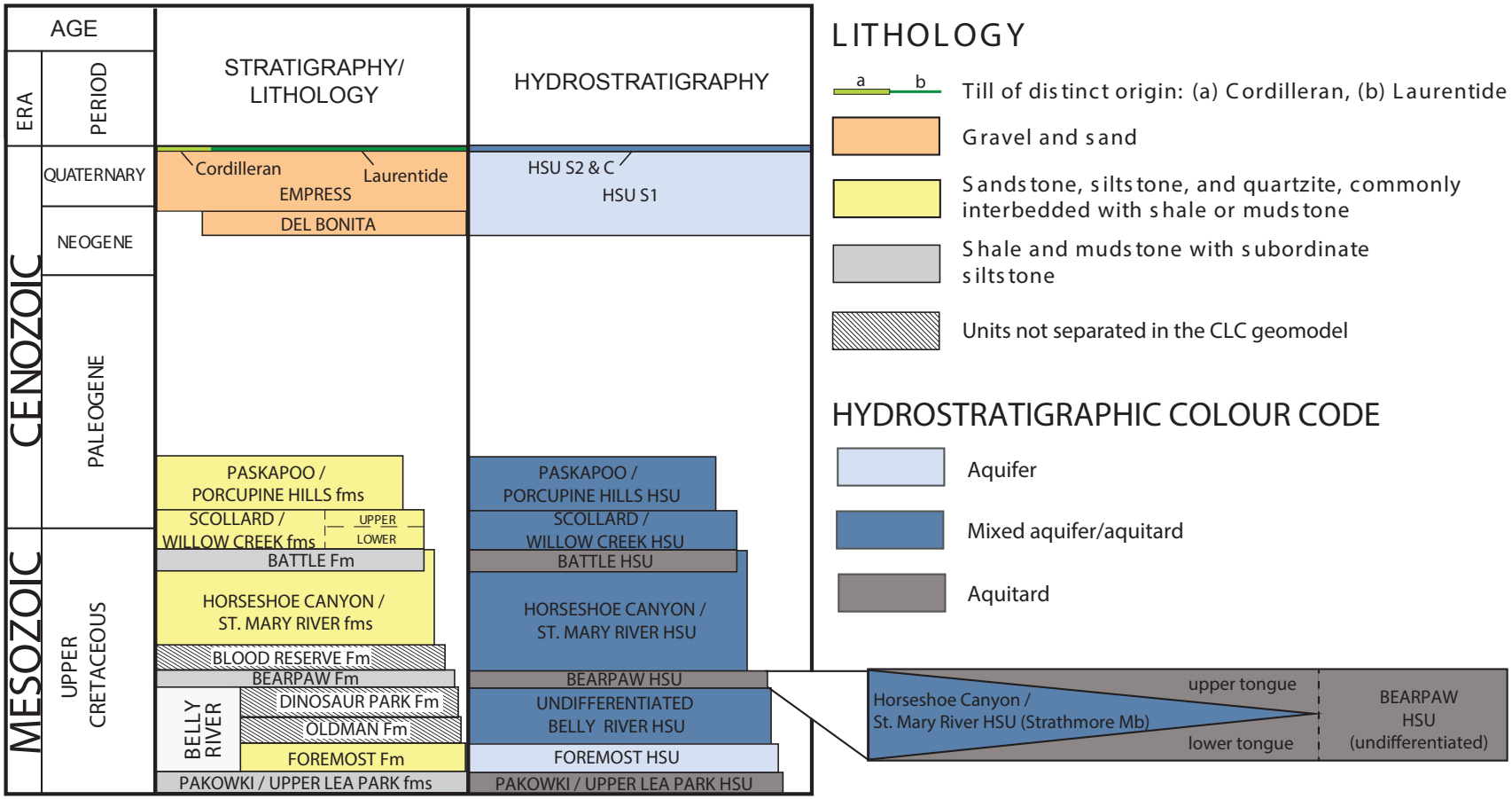

Figure 14. Summary of stratigraphy (modified from Alberta Geological Survey, 2015) and related hydrostratigraphy for the CLC study area. Inset of Bearpaw HSU shows how the Horseshoe Canyon / St. Mary River HSU (Strathmore Mb) separates the Bearpaw HSU into an upper and lower tongue. This occurs in the northern half of the CLC. Units not separated in the hydrostratigraphic model include the Blood Reserve Formation in the southern part of the CLC, which is grouped with the Horseshoe Canyon / St. Mary River HSU, and the Dinosaur Park and Oldman formations, which have similar hydraulic properties and are grouped together to form the undifferentiated portion of the Belly River HSU.

lithostratigraphic units may not always be directly equivalent to hydrostratigraphic units (the latter of which may cross lithostratigraphic boundaries or further subdivide lithostratigraphic units), this approach provides a starting point with which to map the regional hydrogeological properties of the CLC in this study. Further refinement of HSUs in the bedrock strata is discussed in Section 4.3 and 5.6.

The combination of three unconsolidated HSUs and ten bedrock HSUs forms the hydrostratigraphic framework for the CLC. Figure 14 shows a simplified diagram of the relationship between the lithostratigraphy and hydrostratigraphy of the CLC that is used in this study and Table 1 describes the geological characteristics of each of the thirteen HSUs.

4.2 Hydrostratigraphic Modelling

Both unconsolidated HSUs and bedrock HSUs are important for the regional hydrostratigraphy of the CLC and the mapping of associated hydrogeological parameters. Following the development of the regional hydrostratigraphic framework, a hydrostratigraphic model was developed for the CLC consisting of 3D grids representing the bounding surface of each particular HSU.

As outlined in Table 1, the hydrostratigraphic model includes

- three unconsolidated HSUs, defined as either dominantly coarse or fine grained and with specific depositional relationships to bedrock and surrounding sediments;
- ten distinct bedrock HSUs, defined by lithostratigraphic units with distinct lithological characteristics (all stratigraphic equivalents are modelled as one unit in this report; Figure 10; most bedrock HSUs subcrop at the bedrock topography interface); and
- two erosional surfaces: one to constrain the hydrostratigraphic model to the land surface topography, the other to act as a boundary between the unconsolidated HSUs and the underlying bedrock HSUs.

4.2.1 Input Data and Hydrostratigraphic Model Construction

Numerous data sources of varying quality and coverage were compiled for the construction of the hydrostratigraphic model. Each model HSU outlined in Table 1 was derived using a different suite of data to interpolate gridded surfaces representing the top elevation of each HSU. The following section provides an overview of the data and the preparation needed for each component of the hydrostratigraphic model.

1) Erosional Surfaces:
   Land surface topography: Gridded surface generated from the Sustainable Resource Development (SRD) digital elevation model (DEM; Figure 1; 25 m grid-cell size) was resampled to a 400 m grid-cell size (the required cell size for the CLC study) to constrain all gridded surfaces to the top of the hydrostratigraphic model domain. No major manipulations were performed on this surface.
   Bedrock topography: Gridded surface was assembled in conjunction with the creation of the overlying unconsolidated HSUs. Input data for the bedrock topography is outlined in Table 2, and all geospatial point data (x, y, and z coordinates) were compiled into ArcGIS for interpolation of the grid (Figure 15). In the Porcupine Hills upland (Figure A2-1), the number of point data was insufficient for interpolation of the bedrock surface. As an alternative to interpolation, the land surface DEM minus one metre was accepted as a proxy for the bedrock surface based on a geomorphological interpretation that suggests a veneer of Neogene–Quaternary sediment overlies bedrock in this upland (Figure 16).

Table 1. Geological description of thirteen unconsolidated and bedrock HSUs modelled within the CLC as well as the two erosional surfaces used to constrain the hydrostratigraphic model. Colours for each HSU correspond to those used in subsequent figures to identify each HSU. For the bedrock HSUs colours are modified from Prior et al. (2013).

HSU Age/Type	Model HSU	Overview
Erosional Surface	DEM (land surface)	• Erosional surface not used as a unit in the model • Used to constrain the model to the topography of the modern land surface
Neogene-Quaternary Unconsolidated HSUs	HSU S2	• Coarse-grained sediment exposed at surface (sand, gravel, silty sand) • Generally represented by fluvial and glaciofluvial sediments • Potential for functioning as a surficial aquifer or recharge/discharge area
	HSU C	• Fine-grained glaciogenic sediment including clay, silt, or diamicton • Generally represented by valley infill and all surficial sediments except those of fluvial or glaciofluvial genesis • Aquitard due to overall fine-grained lithologies but may include discontinuous sand lenses
	HSU S1	• Coarse-grained sediment (gravel and sand) directly overlying bedrock and underlying HSU C • Typically found overlying floors of buried valleys and capping planation surfaces (Figure 7) • Aquifer
Erosional Surface	Bedrock topography	• Erosional surface not used as a unit in the model • Used as the lower limit to constrain overlying unconsolidated HSUs • Used as an interface to include underlying Upper Cretaceous−Paleogene bedrock HSUs, which subcrop at the bedrock topography
Paleogene Bedrock HSUs	Paskapoo / Porcupine Hills HSU	• Eastward-thinning wedge of nonmarine sediments • Weathered mudstones and thick (>15 m), commonly stacked, cross-bedded sandstone beds (Dawson et al., 1994) • Calcareous cement produces prominent ridges (e.g., Porcupine Hills, Figure 1; Hamblin, 2004) • Mixed aquifer/aquitard
Late Cretaceous Bedrock HSUs	Scollard / Willow Creek HSU	• Deposited in a fluvial-dominant environment • Thick, gray to buff sandstone and siltstone units interbedded with thin, olive green mudstone beds and coal (Dawson et al., 1994) • The Scollard / Willow Creek HSU in southern Alberta contains red mudstones, characteristic of an arid environment (Jerzykiewicz and Sweet, 1988) • Mixed aquifer/aquitard
	Battle HSU	• Thin unit with an average thickness of approximately 10 m (Hathway, 2011) • Deposited in a prominently lacustrine environment • Dark purple-brown mudstone-dominated unit; minor siltstone, rare sandstone (Hathway, 2011) • Absent in paleovalleys (specifically in southeast-trending paleovalleys in the CLC), which are instead infilled with sand of the overlying Scollard / Willow Creek HSU in the northern part of the CLC (Hathway, 2011) • Regional aquitard

HSU Age/Type	Model HSU	Overview
	Horseshoe Canyon / St. Mary River HSU	• Nonmarine origin but intertongues with the marine Bearpaw HSU in central and southern Alberta (Hamblin, 2004; Eberth and Braman, 2012; Hathway, 2014) • Interbedded fine-grained sandstone, siltstone, shale, and coal (Hamblin, 2004) • Mixed aquifer/aquitard
	Bearpaw HSU (upper tongue)	• Dark grey marine shale, siltstone, and minor sandstone (Catuneanu et al., 1997) • Contains thin bentonite beds • Intertongues with the Horseshoe Canyon / St. Mary River HSU in the northern part of the CLC (Eberth and Braman, 2012; Hathway, 2014; Hathway, 2016) • Aquitard
	Horseshoe Canyon / St. Mary River HSU (Strathmore Mb)	• Present only in subsurface; does not subcrop in the CLC • Nonmarine origin • Thinly bedded sandstone, siltstone, and coal (Hamblin, 2004) of the Horseshoe Canyon / St. Mary River HSU in the northern part of the CLC • Separates the marine Bearpaw HSU into lower and upper tongues in central and southern Alberta (Hamblin, 2004; Eberth and Braman, 2012; Hathway, 2014; Hathway, 2016) • Mixed aquifer/aquitard
	Bearpaw HSU (lower tongue & undifferentiated portion)	• Dark grey marine shale, siltstone, and minor sandstone (Catuneanu et al., 1997) • Contains thin bentonite beds • Intertongues with the Horseshoe Canyon / St. Mary River HSU (Strathmore Mb) in the northern part of the CLC; outside of this area the Bearpaw HSU is undifferentiated • Aquitard
	undifferentiated Belly River HSU (excluding Foremost HSU)	• Nonmarine and dominantly fluvial (Hamblin and Abrahamson, 1996) • Interbedded sequence of siltstone, sandstone, carbonaceous mudstone, and coals (Glombick, 2010) • Heterogeneous sequence • Mixed aquifer/aquitard
	Foremost HSU	• Laterally stacked strata deposited in a fluvial coastal environment (Dawson et al., 1994) • Interbedded sandstone, siltstone, and coal (Hamblin and Abrahamson, 1996) • Intertonguing with the marine Pakowki / upper Lea Park HSU • Aquifer
	Pakowki / upper Lea Park HSU	• Present only in subsurface; does not subcrop in the CLC • Fine-grained marine shale (Dawson et al., 1994) • Overlies coarser-grained sediments of the Milk River Formation in southern Alberta • Regional aquitard

Table 2. Data input/quality for unconsolidated HSUs and the bedrock topography grid.

Data Type	Data Source	Quality
Boreholes	Calgary urban geology boreholes (Moran, 1986)	High
	AGS subsurface bedrock topography picks*	High
	High-quality well records (from AWWID)	High
	AGS borehole investigations (AER/AGS, 2014)	High
	Alberta Research Council / Alberta Environment and Sustainable Resource Development / Alberta Agriculture test holes (from AWWID)	Medium
	Medium-quality well records (from AWWID)	Medium
	Gamma-ray logs with associated litholog (well records from AWWID)	Medium
	Resistivity logs with associated litholog (well records from AWWID)	Medium
	AWWID well records with lithologs	Variable
	Resistivity logs without associated litholog (well records from AWWID)	Variable
Outcrops	Field sections logged by AGS (see field photos in Appendix 6)	High
	Observed outcrop (various sources)*	Medium
	Geological Survey of Canada Plains Outcrop (MacCormack et al., 2015)*	Medium
Gridded Surfaces	Digital Elevation Model (DEM)	High
	Airborne resistivity surveys	Variable
Map Information	Outcrop information from Map 600 (Prior et al., 2013)*	High
	Outcrop information from Map 601 (Fenton et al., 2013)*	High
	Till veneer information from Map 601 (Fenton et al., 2013)*	High
Contour Data	Bedrock topography information (various AGS sources)*	Low

* Input data for the bedrock topography grid only and not used for other grids created as part of this report.

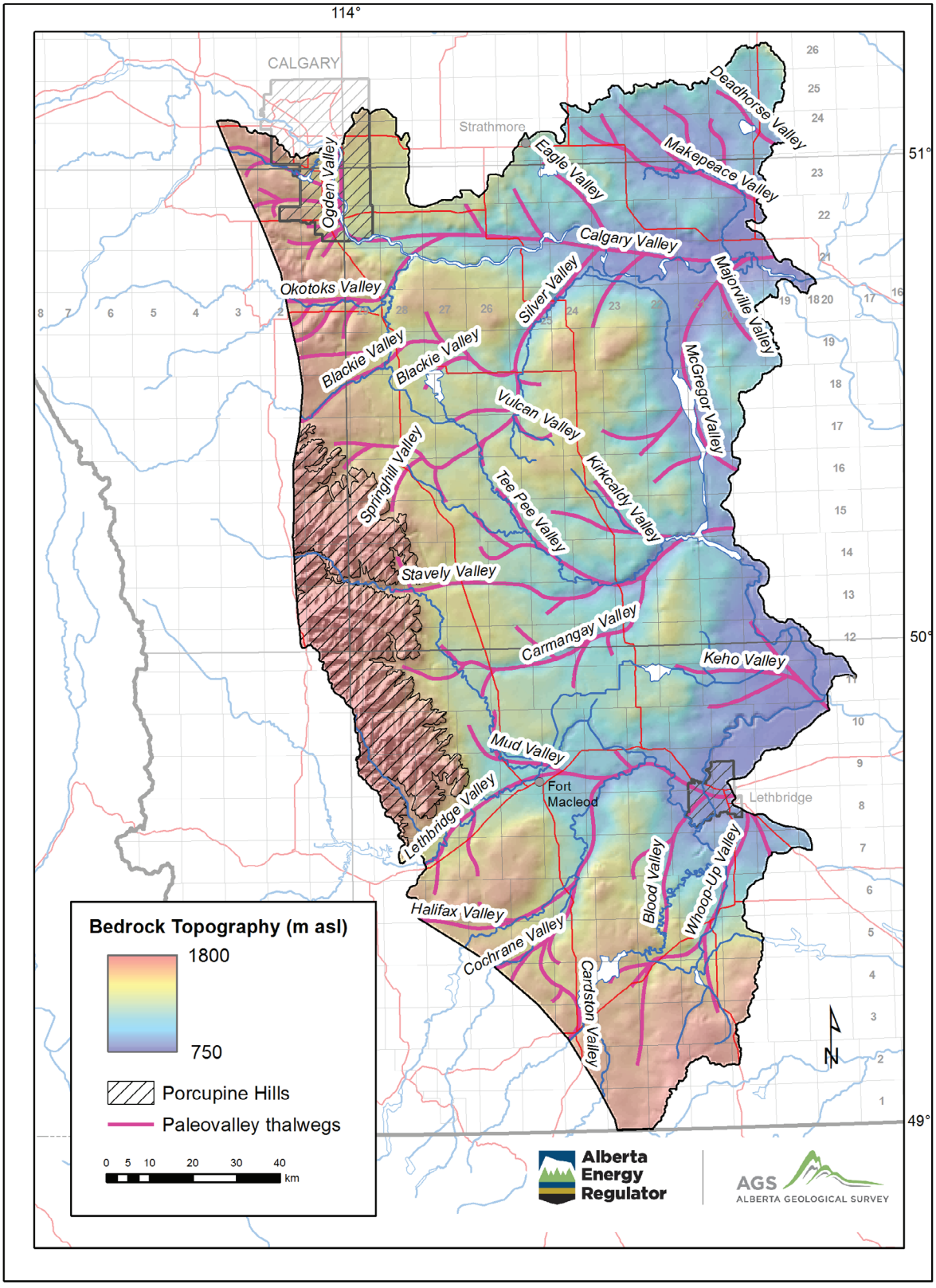

Figure 15. Updated bedrock topography and the location and names of paleovalley thalwegs (modified from Geiger, 1968).

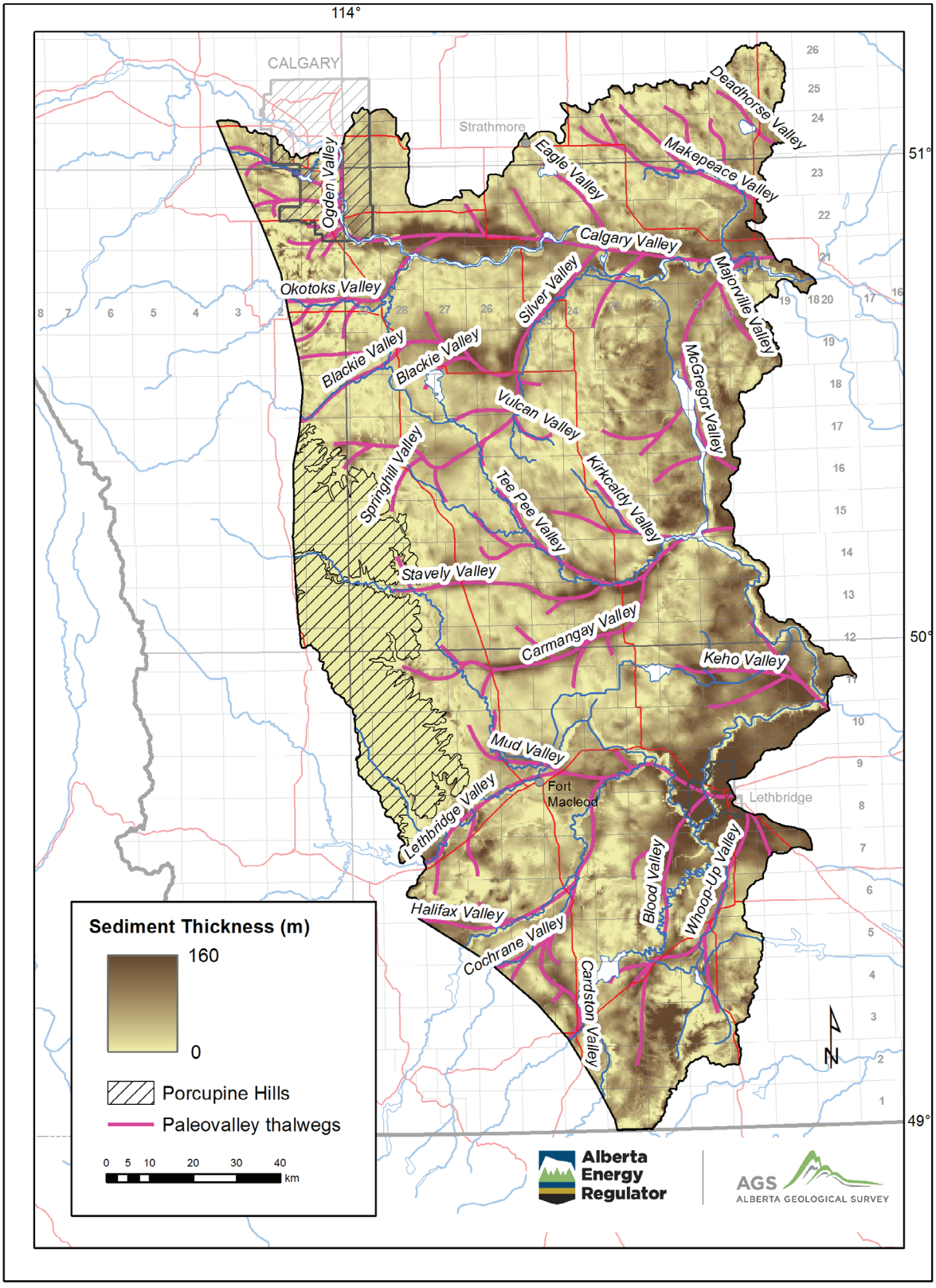

Figure 16. Sediment thickness created by subtracting the bedrock topography from the DEM.

2) Unconsolidated HSUs: Gridded surfaces were constructed from numerous geospatial data (x, y, and z coordinates) sources (see Table 2; Appendix 2). Well records from the March 2013 version of the Alberta Water Well Information Database (AWWID; http://groundwater.alberta.ca/WaterWells) with lithological data (n= 23 808) had the highest degree of coverage in the CLC and were used to identify either the top of bedrock or the three unconsolidated HSUs (i.e., S2, C, and S1) from litholog descriptions using cross-sections created in VIEWLOG. Where three or more wells were colocated in the database, the deepest and shallowest well logs were selected to include wells that were completed in bedrock and to also characterize the unconsolidated HSUs (final n=16 923). Low quality AWWID well data were constrained, where possible, by higher quality data (Table 2) and interpretive data products such as an inversion of airborne resistivity surveys (covering 53% of the study area); thematic maps including buried valleys (e.g., Geiger, 1968), provincial-scale bedrock geology (Prior et al., 2013), and provincial-scale surficial geology (Fenton et al., 2013); and a provincial-scale geostatistically rendered model of bedrock topography (MacCormack et al., 2015). All point data were coded with an x,y position and a corresponding surface elevation value representing the top elevation of a modelled HSU. Point data were then compiled in an ArcGIS project for interpolation irrespective of data quality (Appendix 2).

3) Bedrock HSUs: Gridded surfaces for each of the ten bedrock HSUs (Table 1) were obtained from the Geological Framework of Alberta, which is a provincial-scale 3D geological model (MacCormack et al., 2014), and then clipped to the CLC model domain. The bedrock grids for each unit were geostatistically interpolated from a series of stratigraphic picks. These stratigraphic picks include both published and unpublished high-quality AGS geologist stratigraphic picks (e.g., Glombick, 2010), as well as variable-quality stratigraphic picks from the AER corporate database (Table 3). The gridded surfaces were interpolated using geospatial data (x, y, and z coordinates) from the stratigraphic picks. The x and y coordinates provide spatial data on the geographic location of the geophysical log, and the z coordinate indicates the depth at which each formation top is encountered along the well. This data was geostatistically evaluated in ArcGIS to identify outliers, which could potentially represent erroneous data. All identified outliers were provided to an AGS geologist for further scrutiny and verification. Once both the geologist and modeller were satisfied that all erroneous data had been removed and the current dataset provided the most accurate representation of the geology possible, the data (Appendix 2) were imported into Petrel to generate 3D surfaces for each bedrock unit at a 500 m grid-cell size. These 3D grids were then integrated with one another to build a volumetrically sealed 3D geological model. Combining the grids into a 3D model ensured that bedrock grids were consistent with one another in 3D space to resolve regions of the model where surfaces were crossing over one another or where holes (gaps) in the model occurred. The grids for this project were extracted from the provincial 3D model, clipped to the CLC model study area, and then integrated with the unconsolidated HSUs in RockWorks16.

Table 3. Data input and quality for bedrock HSUs.

Data Type	Data Source	Quality
Boreholes	AGS geologist bedrock stratigraphic picks	High
	Oil and gas geophysical logs	High
	AER corporate database	Variable
	Provincial scale bedrock topography (MacCormack et al., 2015)	Variable

4.2.2 Hydrostratigraphic Model Compilation

The top of each HSU was interpolated separately using the ordinary kriging function of the ArcGIS Geostatistical Analyst extension to create 3D gridded surfaces representing the top elevation of each modelled HSU outlined in Table 1 (with the exception of the DEM). The surfaces, where necessary, were truncated by the erosional surfaces defined in Table 1.

The modelled unconsolidated HSUs were restricted to the CLC study area, while the bedrock HSUs were modelled across their entire provincial extent as part of the Geological Framework of Alberta Project (MacCormack, 2014). The 3D bedrock grids were clipped to the study area and combined with the unconsolidated HSU grids to create a full 3D model (Figure 17) using RockWorks16. Figure A1-2 describes the workflow to construct the 3D hydrostratigraphic model.

Several derivate products have been generated from the 3D hydrostratigraphic model, including an updated bedrock geology map, which shows where modelled bedrock HSUs subcrop at the bedrock topography interface (Figure 18), a cross-section (Figure 19), and 3D elevation grids and isopach maps for each model HSU. Results of the hydrostratigraphic model for each HSU are found in Appendix 3.

4.2.3 Limitations of the Hydrostratigraphic Model

Variable-quality data were used for the construction of unconsolidated HSUs (Table 2). The primary data source used to model the lateral extent and geometry of unconsolidated HSUs were well records from the AWWID. In some cases the AWWID includes inaccuracies in well location and material descriptions. However, the AWWID is an important data source to model laterally extensive HSUs within the CLC, as this database has the most widespread coverage across the study area. Where available, high-quality well records (Table 2) were used to constrain lower-quality data to improve the accuracy of modelled unconsolidated HSUs. However, as the high-quality data are not widespread in the CLC, lower-quality data were the primary data source used if no high-quality data were available.

Cross-sections were created across the CLC to evaluate the lithological descriptions provided in the variable-quality AWWID and other high-quality data sources (Table 1) and to group geological units into the three laterally extensive unconsolidated HSUs. It should be noted that the unconsolidated HSUs are a product of the main author's conceptual geological understanding and are considered important for input into hydrogeological mapping in the region. However, as the unconsolidated HSUs are a simplification of the lithostratigraphic units in the region, HSUs may be more complex or absent at the scale of a local investigation.

The bedrock stratigraphic units were used as a proxy for HSUs. The bedrock grids were clipped from the Geological Framework of Alberta model; therefore, the input data quality and associated provincial-scale statistics included in this report refer to the provincial-scale grids (e.g., Table 1 and Table A2-1). The primary source of data was from AGS geologists who made lithostratigraphic picks to define the stratigraphic top of each bedrock unit. These data are considered high quality because they have been verified by an AGS geologist, and the picks are typically made using quantitative information (e.g., differing suites of geophysical logs) to define each stratigraphic unit top. The location accuracy for this data is also very good considering that the wells are estimated to be within a 10 m radius of their actual locations.

Construction of the hydrostratigraphic model also introduces uncertainty during the interpolation of each HSU. To measure this error, the root mean square error (RMSE) was used (MacCormack et al., 2013). The RMSE is used to show how similar interpolated grid values are to the original input data for the entire grid. Further information about accuracy and location of input data for each HSU can be found

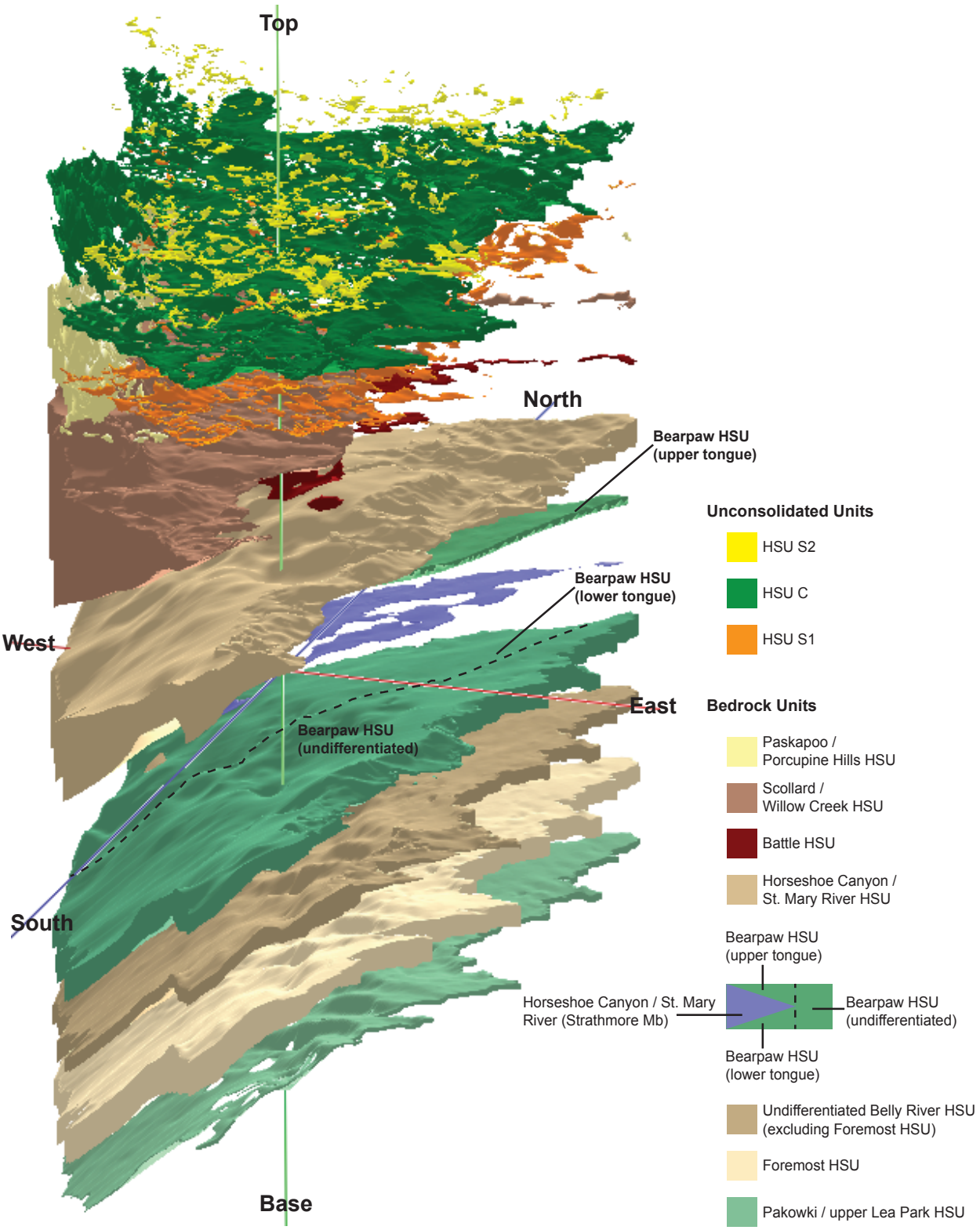

Figure 17. 3D hydrostratigraphic model of the CLC study area showing the thirteen unconsolidated and bedrock HSUs. HSUs are shown at 30× vertical exaggeration and a 500 m vertical offset between units for visualization purposes. Summary statistics for each modelled HSU is provided in Table A2-2.

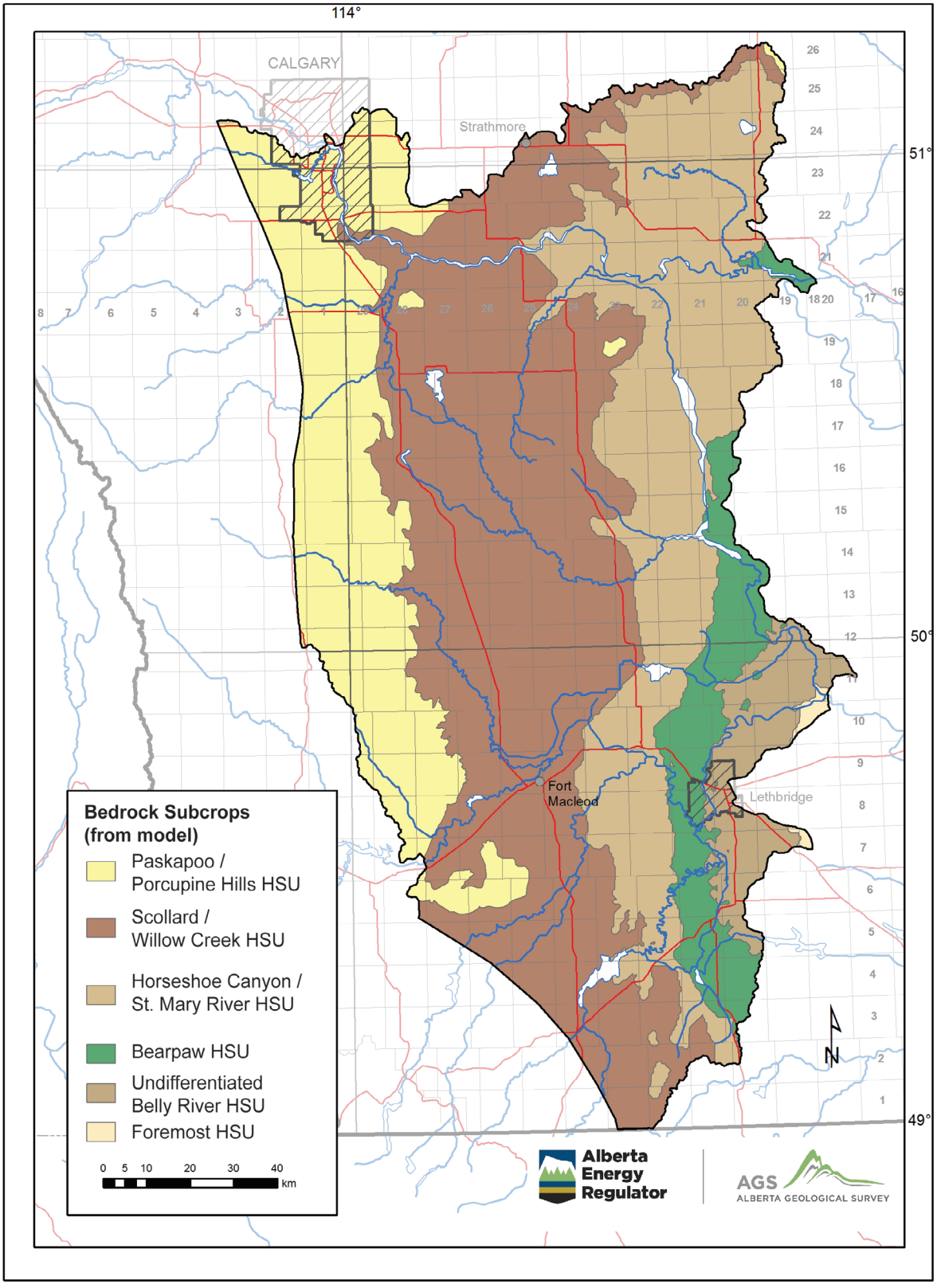

Figure 18. Bedrock geology map taken directly from the hydrostratigraphic model shown in Figure 17, where modelled bedrock units are truncated by the modelled bedrock topography grid.

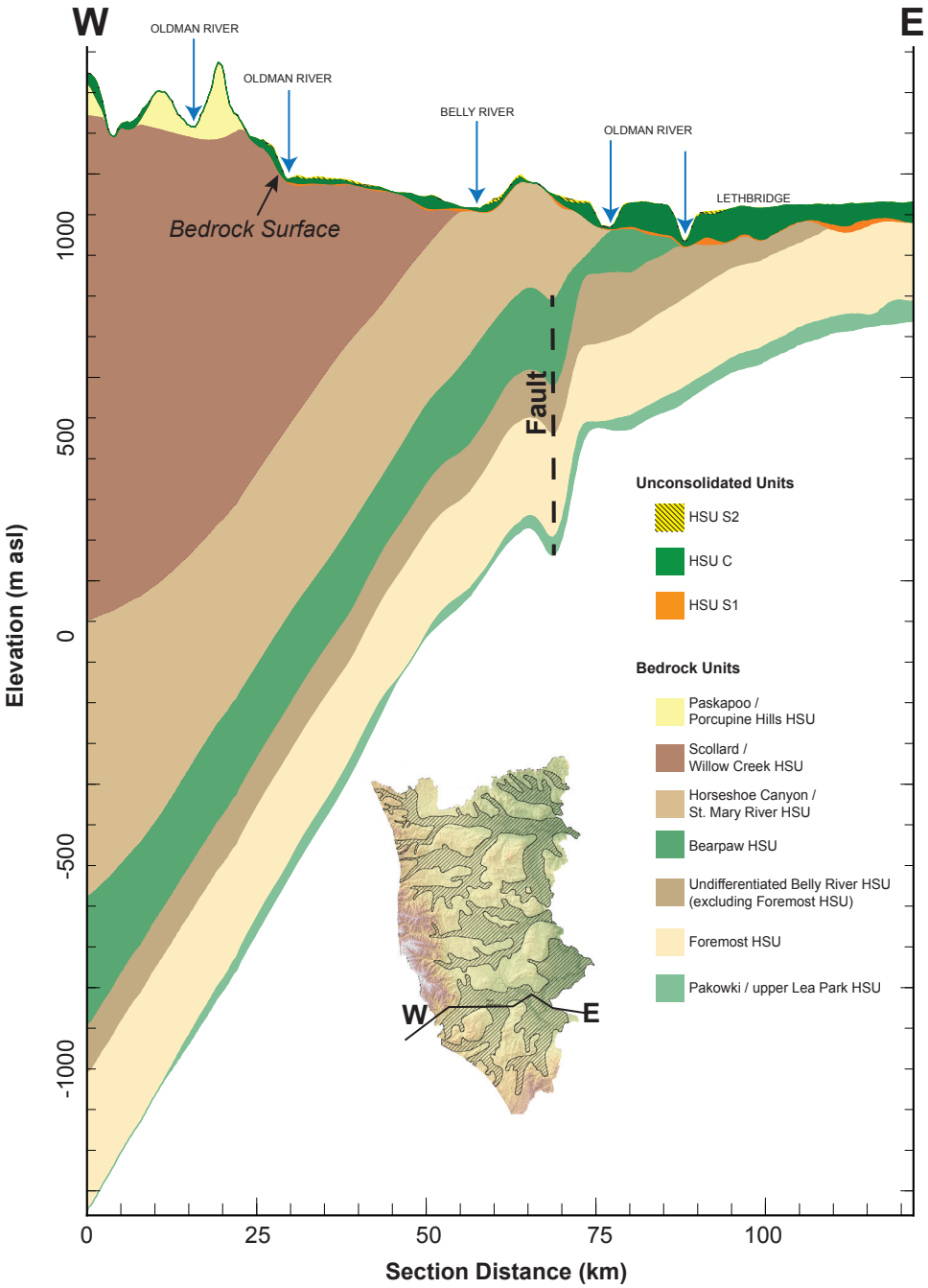

Figure 19. Cross-section through the southern part of the modelled area (see inset) showing the gridded surfaces from the hydrostratigraphic model. Cross-section location is the same as the schematic shown in Figure 12 to facilitate comparison between a conceptual model and the digital model, which excludes the deformation belt. Cross-section location does not include the Horseshoe Canyon / St. Mary River (Strathmore Mb) and Battle HSUs because these HSUs are not present in the southern half of the study area. A fault is also represented; however, faults were not included as input data for this study, rather stratigraphic picks were used to define the general orientation of a fault. Therefore, the fault orientation and offset on this cross-section may be shown at a greater magnitude than actually exists in the subsurface. Further information on faults in the study area is described in Mei et al. (2015). HSUs are shown at 60× vertical exaggeration.

in Appendix 2, and Table A2-2 specifically provides the RMSE for each 3D HSU grid where available. Finally, it should also be noted that due to the variable-quality input data and interpolation error, this model should only be used in regional-scale groundwater studies.

4.3 Analysis of the Distribution of Permeable Bedrock

Further analysis of bedrock HSUs included in the hydrostratigraphic model was performed by partitioning the subsurface into a series of slices (Figure 20), building on methodology described in Parks and Andriashek (2009) and Lyster and Andriashek (2012). The slices are used to evaluate major sandstone trends, which are likely to be more permeable than surrounding units, and thus have higher aquifer potential. This analysis will supplement available hydraulic data and provide insights on aquifer potential where hydraulic data is not available (discussed further in Section 5.6).

The maps of net sandstone to gross interval thickness (referred to in this report as net-to-gross ratio [NGR] sandstone maps) were derived from gamma-ray logs. A gamma-ray log shows a record of measurement of the natural emission of gamma rays in the rocks surrounding the logging tool within a borehole. The most common sources of natural gamma rays are potassium, thorium, and uranium, which are typically found in clay-rich clastic rocks. As a result, gamma-ray logs are commonly used to describe a sandstone-shale sequence because shale contains a high proportion of clays while clean sandstone does not. The bedrock strata of interest in the study area are composed of sandstone-siltstone-shale sequences with a small amount of coal and bentonite. Clean sandstone/siltstone and high-grade coal produce a low gamma-ray value. Conversely, shale/mudstone, bentonite, and low-grade coal yield a high gamma-ray value. In general the gamma-ray value, being proportional to the clay content, is inversely proportional to the porosity of the rock. A threshold gamma-ray value of ≥75 to 80 API was used to define sandstone-rich portions in a slice, and the NGR was calculated by dividing the cumulative thickness of the sandstone portion by the gross or total thickness of the slice (Figure 20). The resulting map is referred to as NGR sandstone map because the permeable portion in a slice is predominantly sandstone in our study area.

Nested within bounding surfaces that together form the hydrostratigraphic model shown in Figure 17, the subsurface was divided into a series of 81 stacked slices ranging in thickness from 1-20 m within three major intervals (Figure 20a). To create these intervals three stratigraphic surfaces interpreted to represent approximate timelines were used to initiate the slice geometry. The lowest surface used is the Milk River shoulder (Glombick and Mumpy, 2014), a log marker that defines the base of the Pakowki / upper Lea Park HSU. The middle surface is the maximum flooding surface (MFS) within the Bearpaw HSU. This Bearpaw MFS is close to, but slightly above the top of the Horseshoe Canyon / St. Mary River HSU (Strathmore Mb) (for details see Hathway, 2014) in the northern part of the CLC and within the lower part of the Bearpaw HSU (above the top of the undifferentiated Belly River HSU) in the southern part (Figure 20). The upper stratigraphic surface is the top of the Horseshoe Canyon / St. Mary River formations, which corresponds to the top of the Horseshoe Canyon / St. Mary River HSU. The use of these surfaces allowed for the subdivision of the lower two intervals into slices of variable thickness (1–20 m) but representing equal time. Due to the lack of a stratigraphic surface that could be used as a timeline to constrain the top of the bedrock succession, the uppermost interval was subdivided in slices of equal thickness of 20 m stacked upon its basal bounding surface and truncated by the bedrock topography surface. Each of the slices within these three intervals corresponds to a map showing the distribution of NGR (Figure 20b), as calculated from gamma-ray logs (see Figure A1-3 for full workflow to create NGR sandstone maps).

Merging of the 81 slices based on natural geological patterns, rather than the HSU boundaries in the hydrostratigraphic model, reduced the total number of slices to 13 (see Appendix 5) and established the geometry, orientation, and stacking arrangement of sandstone bodies. Figure 21 shows the NGR

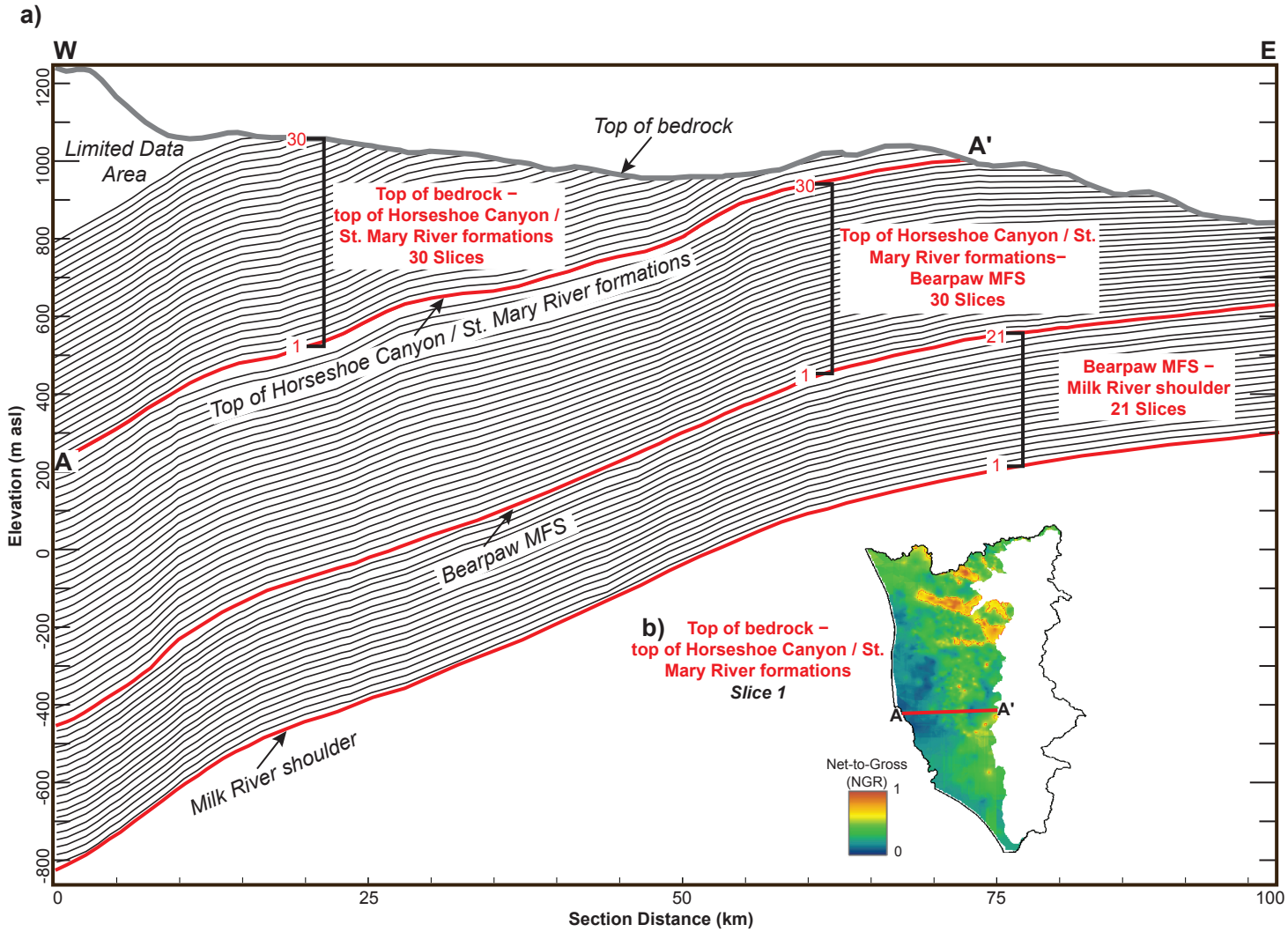

Figure 20. (a) West-east cross-section showing the 81 slices that were evaluated within three different intervals (i.e., top of bedrock – top of Horseshoe Canyon / St. Mary River formations; top of Horseshoe Canyon / St. Mary River formations – Bearpaw MFS; Bearpaw MFS – Milk River shoulder). Thick red coloured lines depict the three stratigraphic surfaces used to create the intervals. (b) Example NGR sandstone map of slice 1 of the top of bedrock – top of Horseshoe Canyon / St. Mary River formations interval. A similar NGR sandstone map was created for each of the 81 slices. Cross-section shown at 30× vertical exaggeration.

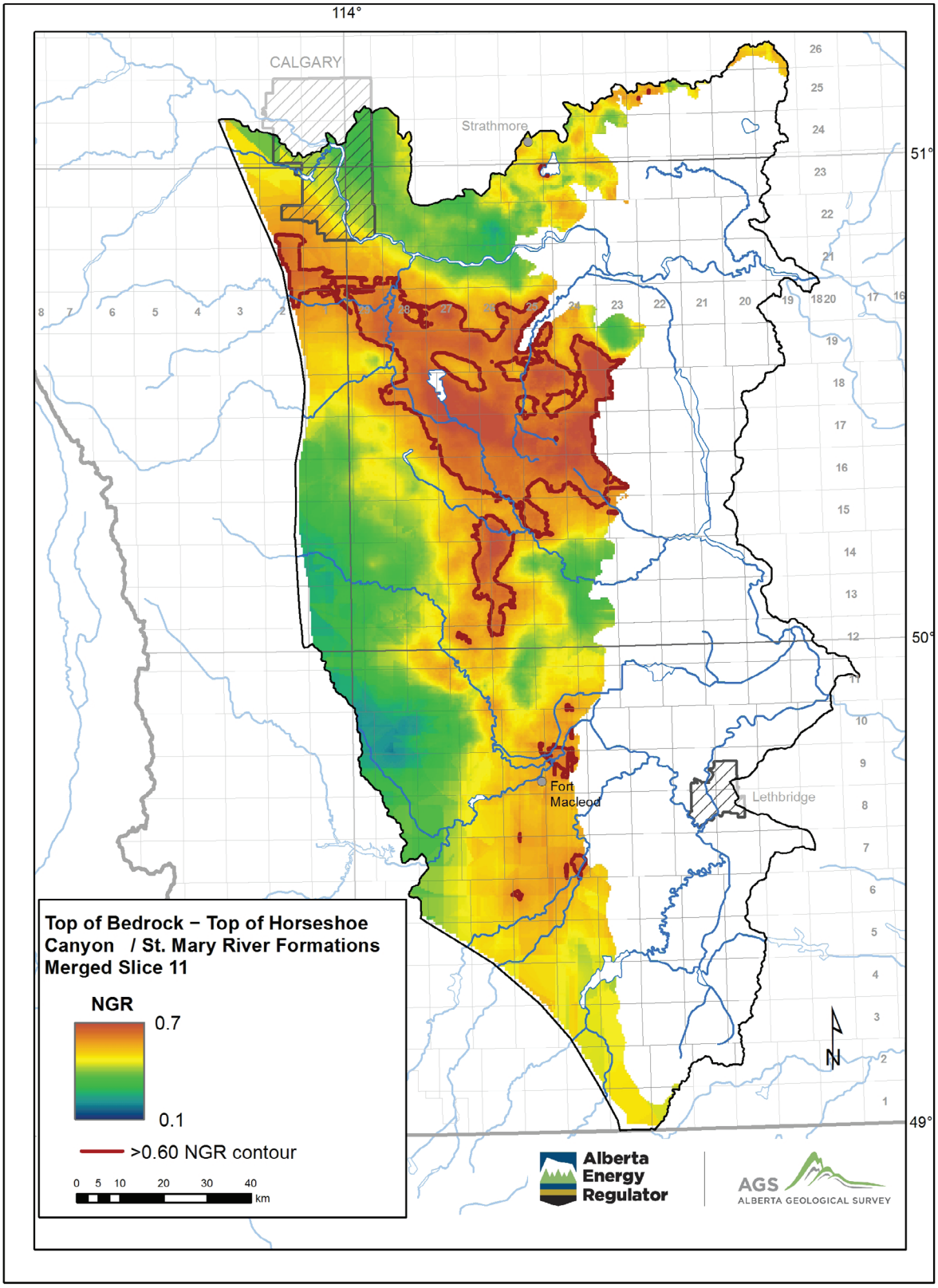

Figure 21. Merged slice 11 and the ≥0.60 NGR polygon.

sandstone map derived from merging slices in the interval from the top of bedrock to the top of Horseshoe Canyon / St. Mary River formations, which exhibit overall similar NGR patterns. When stacked together, these slices form a semicontinuous sandstone body outlined by a ≥0.60 NGR contour. Polygons delineating areas where a slice had ≥0.60 NGR values were produced for each slice and are interpreted to have potentially high permeability based on the connectivity and lateral extent of 2D sandstone-bodies in 2D. However, the accuracy of polygon traces and NGR sandstone maps differ with data density, despite the high-quality digital gamma-ray logs used to create the slices. For example, there is a paucity of data towards the western boundary of the CLC, which reduces the capacity to evaluate the uncertainty of NGR sandstone maps, especially in areas where there are no wells within a township (Figure 22). All merged slices within bedrock units analyzed using the slicing method are shown in Section 5.6 and in Appendix 5.

Gamma-ray logs for 15 340 wells were used in this study, and although gamma-ray logs are considered high quality, these data contain inherent uncertainties and errors. Borehole size, mud weight, tool type, and poor calibration affect the gamma-ray response of the rocks. Inconsistency also exists amongst logs that were recorded at different times and by different operators. In cased holes, the response of gamma-ray activity in the rock is also attenuated by the cement and casing thickness.

These uncertainties were managed and reduced in a number of ways. First, the recorded through-casing gamma-ray response was normalized using statistics obtained from the uncased interval for each well (after Quartero et al., 2014). Second, most of the errors, excluding the bias caused by casing, were randomly distributed across the study area and were therefore considerably reduced by the weighted average method of the interpolation technique. The reduction of error using ordinary kriging was appropriate, as the purpose of the NGR sandstone maps was to identify regional trends in the distribution of sandstone-rich, permeable rocks (Figure 21) rather than address the accuracy of the absolute NGR value at a specific location. Thirdly, geostatistical methods were used to identify systematic biases in the median gamma value of individual logs (i.e., a median gamma value that was too high or low) when compared to the median of the whole dataset for one of the three different intervals (Figure 20). These logs were treated as outliers and constitute only a fraction of the total number of logs; they were corrected by further normalization with the statistics derived from the corresponding interval to more closely match the median of the entire dataset. Normalization was not applied to the majority of the logs because it can mask natural geological variations that may have significance in understanding the distribution of aquifers across the study area.

5 Hydrogeology

The development of the hydrostratigraphic framework (Section 4.1), and modelling of 3D gridded surfaces of the unconsolidated and bedrock HSUs (Section 4.2), form the basis for the analysis of the regional hydrogeology in the CLC. Using the 3D gridded surfaces, well completions in the AWWID are allocated to an individual HSU, which is described either in the unconsolidated HSUs by similar bulk physical properties, or in the bedrock by lithostratigraphic formations (Section 4.1; Figure 13). Allocation of well completions is based on the HSU present at the same elevation as the middle of the screened interval (limitations of which are discussed in Section 5.4).

The following sections explore the hydrogeological data and properties of the individual HSUs from a regional perspective. The major steps in this analysis include the following:

- examine the spatial distribution and depths of water supply wells to provide information on groundwater use within the CLC (Section 5.1);

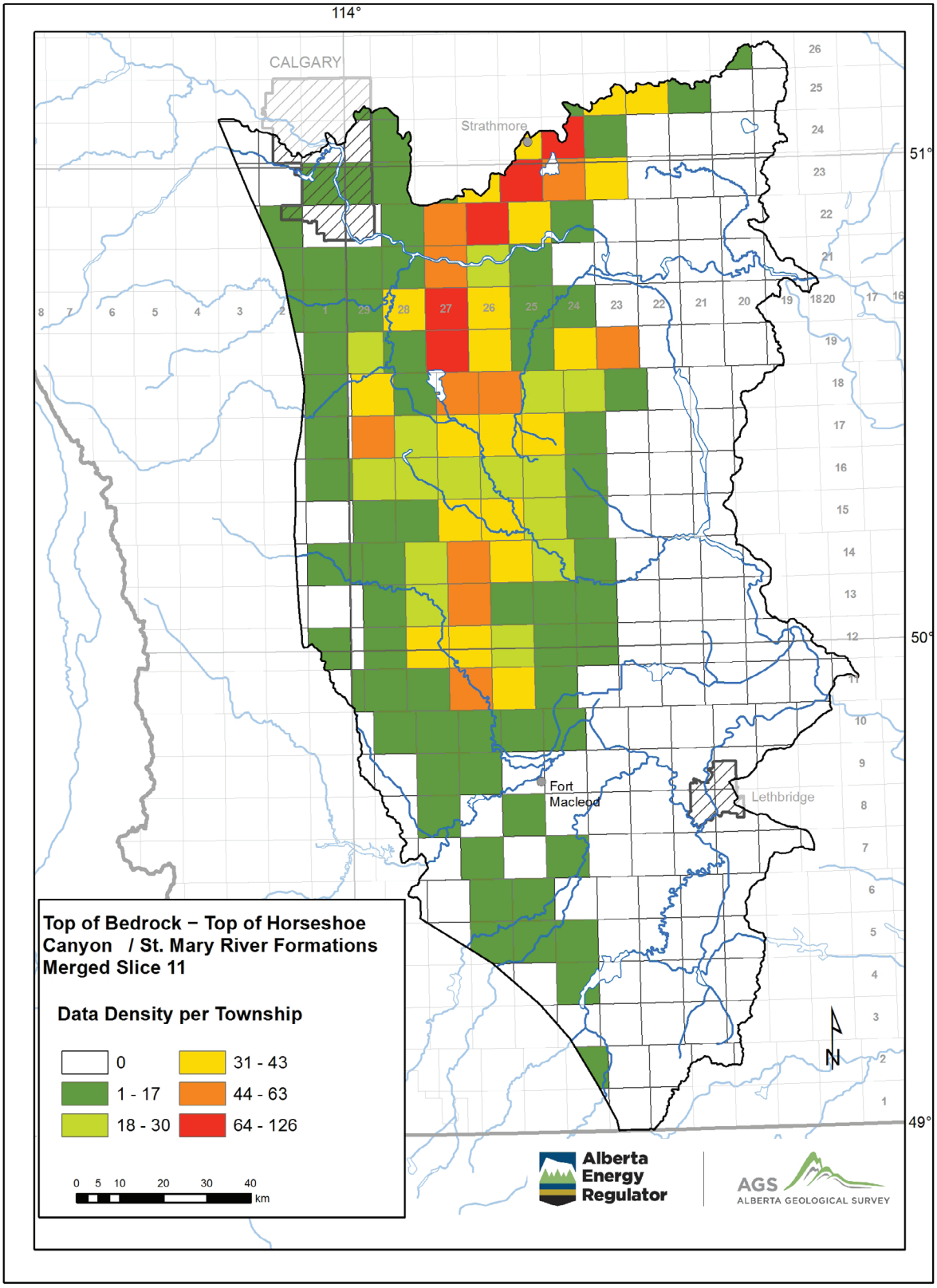

Figure 22. Data density map for merged slice 11.

- compile and interpolate hydraulic head data to produce potentiometric surface maps (where possible) to provide information on lateral hydraulic head gradients and groundwater flow potential (Section 5.2);
- compile and interpolate hydrochemical data of total dissolved solids (TDS) and generate maps of TDS (where possible) to provide information on groundwater quality (Section 5.3); and
- analyze regional recharge and discharge within the CLC, including 1D numerical recharge modelling and an analysis of vertical hydraulic gradients (Section 5.5).

5.1 CLC Wells and Water Supply

As of March 2013, there are 34 895 well records in the AWWID within the CLC. However, 15 112 of these wells are not used for water supply and instead are test holes, shot holes, dewatering wells, or monitoring wells. While these wells are important for their lithological and hydraulic information, they do not represent wells used for water supply in the CLC and were removed in Figure 23 through Figure 27. The complete list of well types and uses interpreted to identify wells supplying water from those not supplying water is found in Table A1-1. The remaining wells (i.e., water supply wells) were filtered based on the presence of screen information and allocated into individual HSUs based on the elevation of modelled unit tops (Section 4.2) and the elevation of the middle of the screened interval. The details of each stage in the filtering and allocation process are outlined in Table A1-2 along with the number of wells.

Figure 23 shows the location of 12 102 allocated water supply wells in the CLC (Table A1-2). This figure highlights that water supply wells are predominantly completed in bedrock (e.g., Little Bow Plain, Vulcan Upland areas) and areas where there is a mix of groundwater use from both unconsolidated and bedrock HSUs (e.g., Blackfoot Plain along Bow River and Three Rivers Plain by Fort Macleod). Note that this figure includes wells of all ages, including older wells that may no longer be in use.

Figure 24 and Figure 25 show the density of water supply wells per Alberta Township System (ATS) section (~1.6 × 1.6 km) completed into either the unconsolidated or bedrock HSUs, respectively. Figure 26 and Figure 27 show the average recommended pumping rate (as reported on water well drilling reports) per ATS section for wells completed in either the unconsolidated or bedrock HSUs, respectively. It is important to note that the recommended pumping rate is suggested by the driller and is based on a number of factors including a short duration pumping test, the well diameter, well use, length of screened interval, and geological formation. It may not reflect the long-term sustainable yield, the maximum possible yield, or the actual hydraulic conductivity of the aquifer.

5.2 Methodology for Mapping Potentiometric Surfaces

Hydraulic data from the AWWID were compiled for all HSUs included in the 3D hydrostratigraphic model with the exception of the upper and lower tongues of the Bearpaw HSU (hydraulic data is available in the undifferentiated portion), Horseshoe Canyon / St. Mary River HSU (Strathmore Mb), and Pakowki / upper Lea Park HSU. These HSUs are deeply buried in the subsurface and do not subcrop at the bedrock topography interface. As most AWWID wells are located in the shallow near-surface (i.e., ~150 m in total depth), these HSUs do not contain any wells with appropriate hydraulic information.

All AWWID wells went through a set of criteria to select wells with appropriate hydraulic information, irrespective of their water use type. These criteria focused on selecting wells with only one well record, a single screened interval, a single static water level, and not under flowing artesian conditions. Table A1-3 outlines the selection criteria in detail and the number of wells in each HSU that ultimately were used to interpolate potentiometric surfaces.

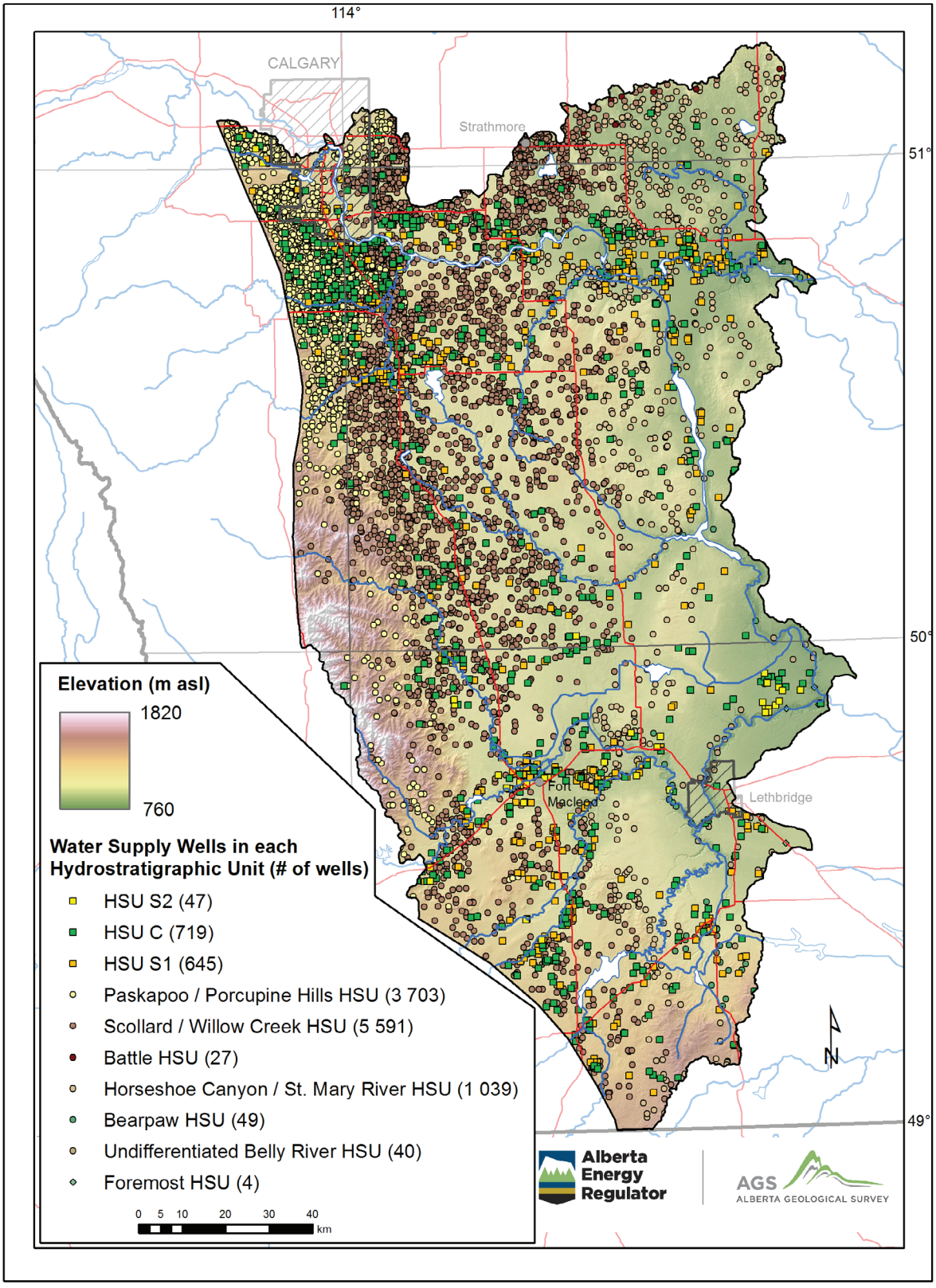

Figure 23. Allocation of water supply wells.

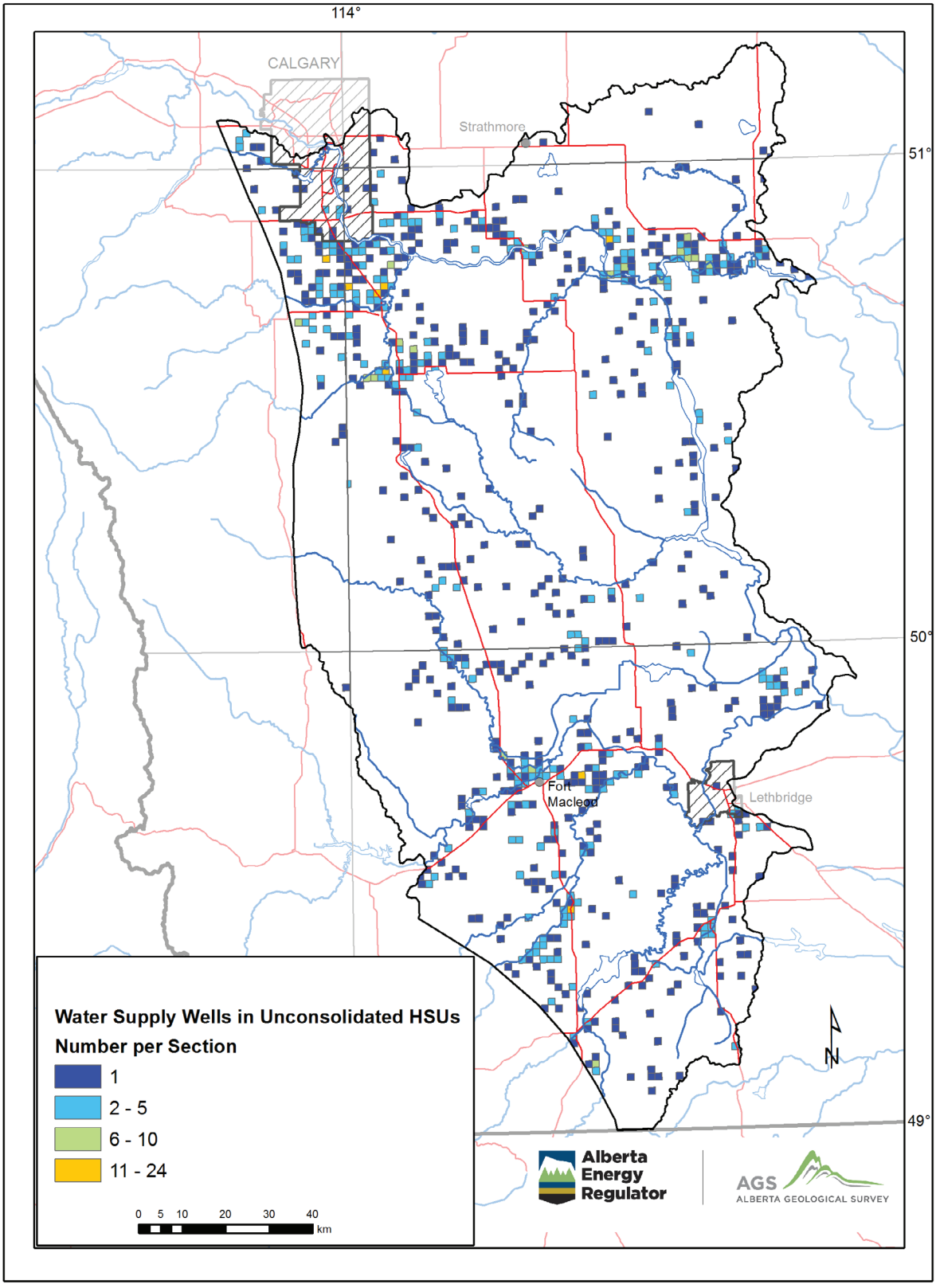

Figure 24. Water supply wells per ATS section in unconsolidated HSUs.

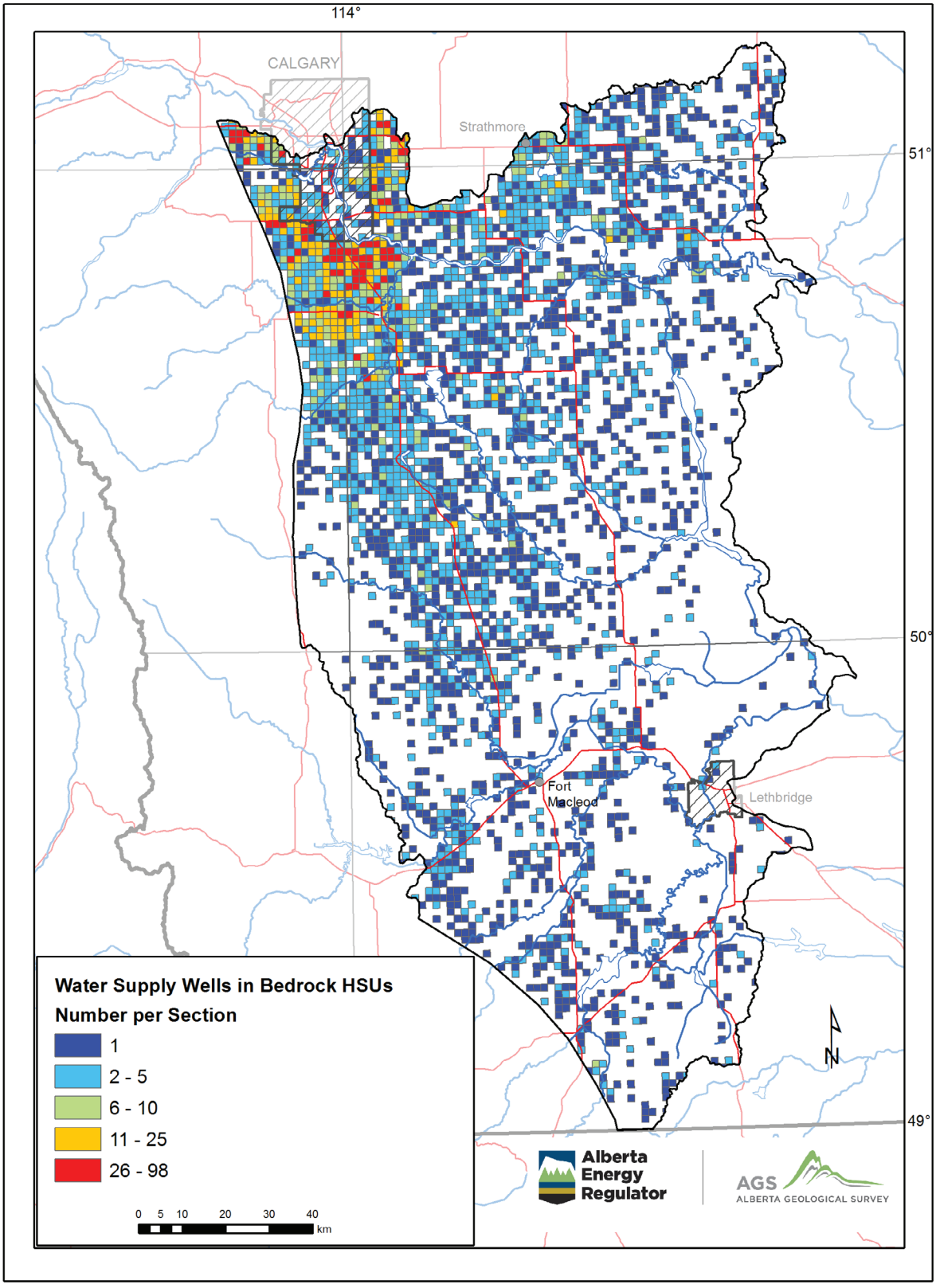

Figure 25. Water supply wells per ATS section in bedrock HSUs.

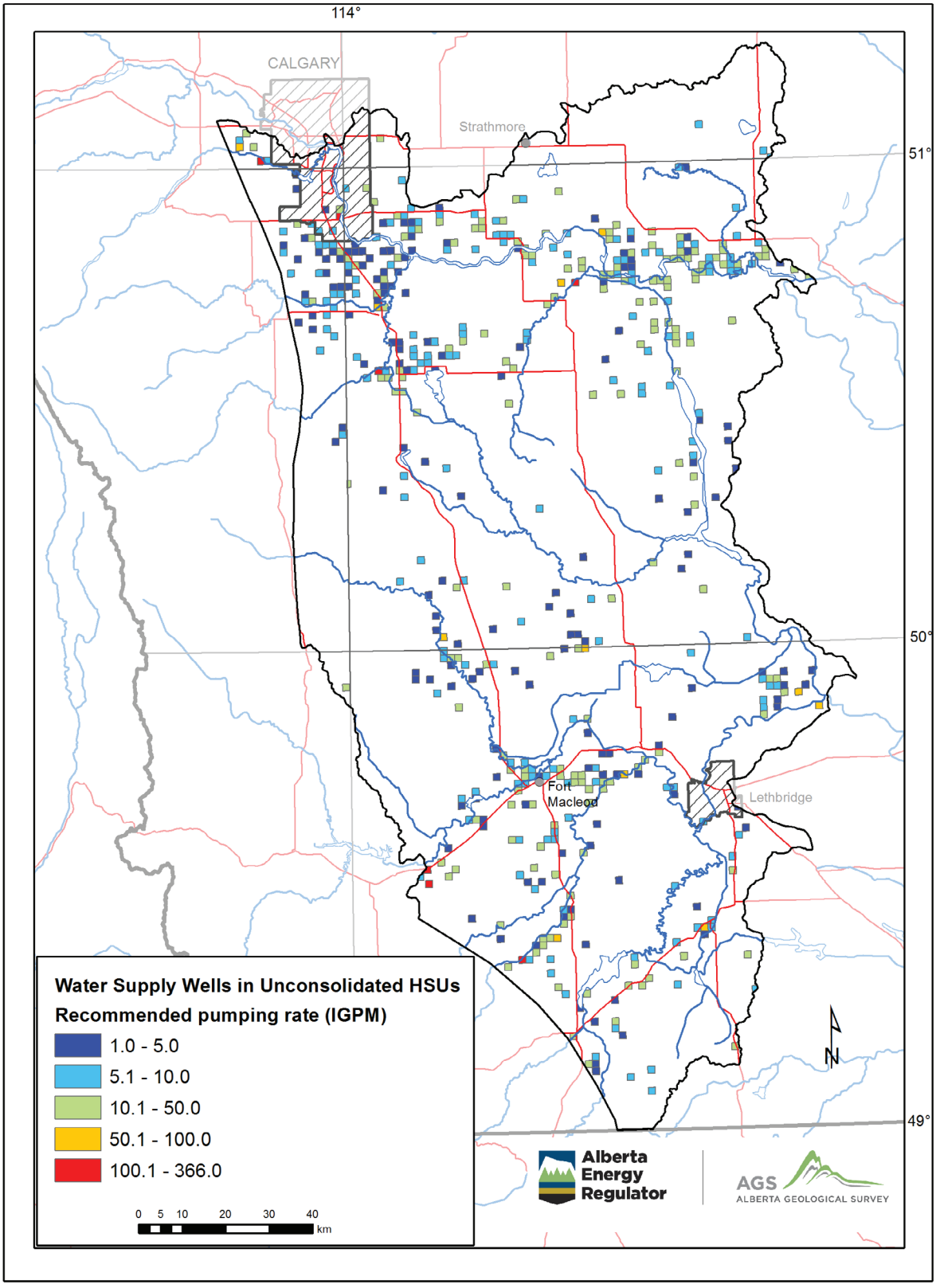

Figure 26. Average recommended pumping rate per section for water supply wells in unconsolidated HSUs.

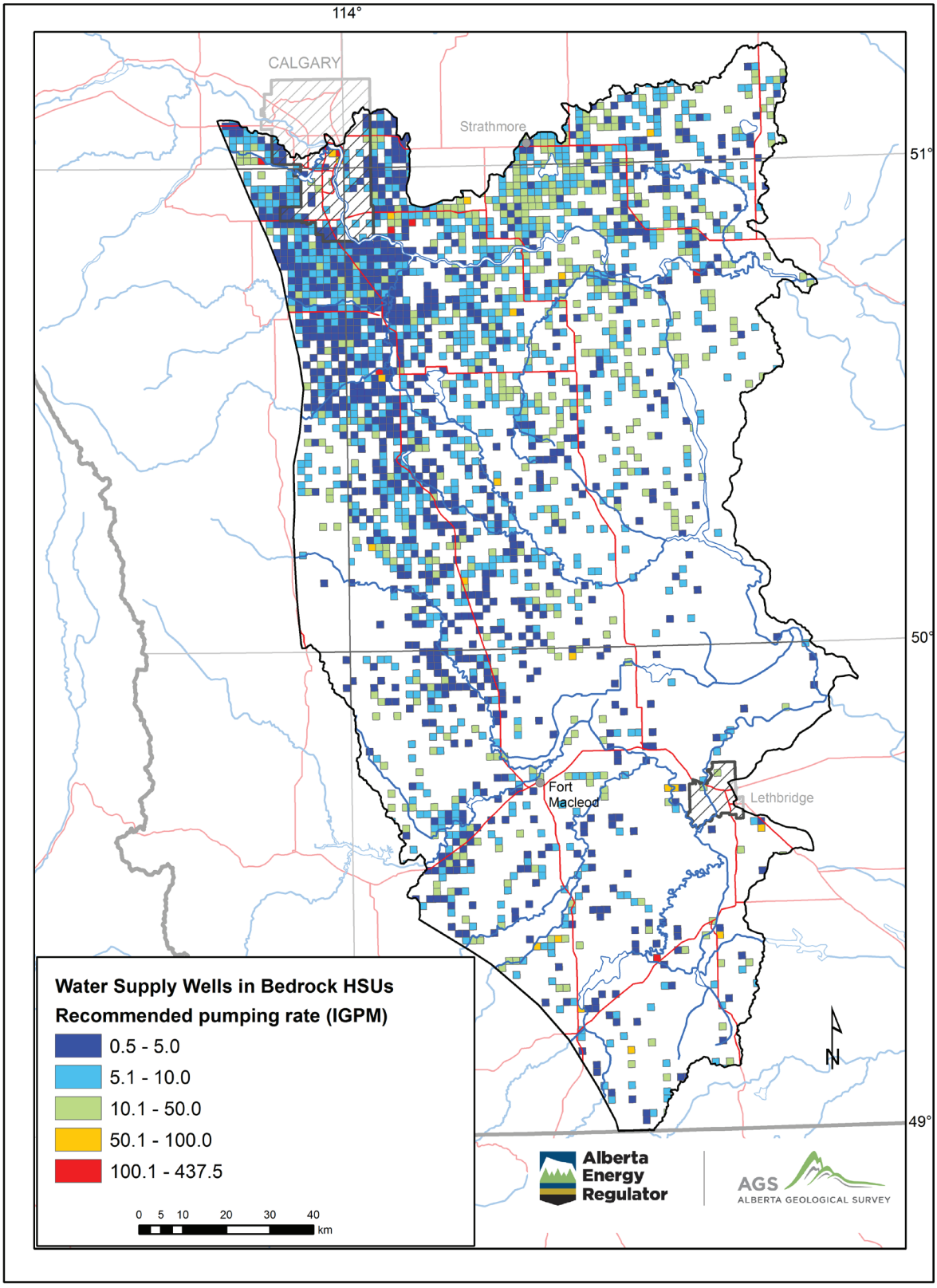

Figure 27. Average recommended pumping rate per section for water supply wells in bedrock HSUs.

Potentiometric surfaces were interpolated for all HSUs for which data were compiled, except HSU S2, Battle HSU, and Foremost HSU (Figure 13 and Table 1) because they have very little hydraulic data. In the remaining HSUs, potentiometric surfaces were interpolated in ArcGIS using the ordinary kriging function of the Geostatistical Analyst extension with a grid size of 400 m. The average hydraulic head was used to interpolate the potentiometric surface for all colocated data points. Outliers were removed manually (Step 8 in Table A1-3) during the interpolation process on the basis of the following criteria:

- mid-screen depth being much deeper (or shallower) than surrounding wells,
- static water level significantly different from surrounding wells and these differences could not be rectified,
- water well interpreted to be incorrectly located (e.g., on an upland versus a valley bottom in areas of slope breaks or well placement at the middle of the ATS quarter section) causing significant discrepancies in hydraulic data measured from land surface, and
- water well being located in the middle of the ATS quarter section where other adjacent wells had more accurate location coordinates (e.g., wells located within a legal subdivision (LSD) or a GPS was used to document location coordinates, especially for wells in the Scollard / Willow Creek HSU and Paskapoo / Porcupine Hills HSU).

In many HSUs, well data were sparse and insufficient to interpolate the potentiometric surface over the entire extent of the HSU. Therefore, a buffering approach (of the interpolated area) was taken to clip the potentiometric surface to areas where sufficient well data existed. First, a buffer was created around each well. Where buffers from individual wells intersected each other, the resulting merged polygon was used to clip the potentiometric surface. Wells with buffers that did not intersect another buffer were included in the potentiometric surface map as points rather than as part of the surface. A number of different buffer sizes were tested, and a final buffer size of 2 500 m was used for all HSUs. For the Scollard / Willow Creek HSU and Paskapoo / Porcupine Hills HSU, the potentiometric surfaces were not interpolated within the Porcupine Hills upland. This is because in the Porcupine Hills upland, topography is highly variable, well data is sparse, and well locations are often placed in the middle of the ATS quarter section. Finally, all surfaces were clipped to the extent of the particular HSU. Depth to potentiometric surface maps were created by subtracting the potentiometric surface elevation map from the resampled 400 m land surface DEM.

The AWWID wells provide data to map the hydrogeology of the upper 200 m of the subsurface. In order to examine the hydraulic heads in the deeper groundwater system, pressure data collected from drill stem tests (DSTs) of oil and gas wells was obtained from IHS Accumap in addition to internal data sources at the AGS. There are 18 235 DSTs in the CLC; however, many of these tests do not contain data on test interval or recorded pressure. Therefore, only 220 remain after this initial preselection step (Table A1-4). Following the preselection, these data were subject to further criteria to remove DSTs where the recorded pressure was not necessarily representative of the formation pressure. A number of parameters were assessed such as interval length, intervals that straddle HSUs, quality code, qualitative permeability, qualitative hydro factor, flow and shut-in times, and recovery and blow description. This procedure follows the criteria described by authors such as Khan (2006) and Melnik (2012). A method called the cumulative interference index (e.g., Tóth and Corbet, 1986; Alkalali, 2002) was also used to examine the influence of production and injection on the pressure recorded during the DST. After all the selection criteria were applied, 105 DSTs remained within the CLC study area and were allocated into the bedrock HSUs. Table A1-4 shows the steps in the selection process and number of DSTs allocated to each bedrock HSU.

From the selected DST data, potentiometric surfaces were interpolated for the undifferentiated Belly River HSU (Figure A3-36) and Foremost HSU (Figure A3-40) using ordinary kriging in ArcGIS, with a

grid size of 400 m. Unlike with the potentiometric surface mapping using the AWWID static water level data, buffers were not used to clip the potentiometric surfaces that used DST data. This is because the DST data is representative of the regional trend of hydraulic head in the deeper groundwater rather than the local-scale variations in shallow groundwater as obtained from the AWWID well data.

Results of the hydraulic head mapping are found in Section 5.4 and Appendix 3, and limitations of the mapping are discussed in Section 5.4.

5.3 Methodology for Mapping Total Dissolved Solids

Chemical analyses that included major-ion chemistry and TDS were exported from two sources: the AWWID and formation water analyses obtained during the drilling or completion of oil and gas wells (acquired from IHS AccuMap and internal AGS data sources). TDS was determined for each analysis by summing the concentration of major constituents. Acceptable charge balance error was constrained to ±10%. Chemical analyses from each source were subject to separate selection criteria to exclude chemical analyses from wells with no screen interval information, with multiple screen intervals, with screen intervals longer than 15 m, and with erroneous or incomplete chemical analyses. Chemical analyses from oil and gas wells were subjected to additional screening to identify potential contamination of the formation water by drilling fluids such as acid water, corrosion inhibitors, mud filtrates, and alcohols. This additional procedure is based on criteria set in previous studies (Hitchon and Brulotte, 1994; Hitchon, 1996; Palombi, 2008) and uses a series of calculations and true/false statements to identify if a sample is potentially contaminated. A numerical flag of 1 is given for true statements and 0 for false statements. The number of flags is summed, with high scores indicating potentially poor quality, contaminated samples, and low scores indicating that the sample is likely representative of formation water. Table A1-5 and Table A1-6 describe the selection criteria in more detail and the wells remaining after each step for the AWWID wells and oil and gas wells, respectively.

Chemical analyses from both data sources were merged and allocated into HSUs based on the 3D hydrostratigraphic model and elevation of the middle of the screened interval. Manual removal of outliers (Table A1-5 and Table A1-6) during the interpolation process was based on substantial difference in screen depth, potential for contamination (from oil and gas wells), and unexplained anomalous values.

Interpolated maps of TDS in mg/L were created for all HSUs except the HSU S2, Battle HSU, Bearpaw HSU (upper and lower tongues), Horseshoe Canyon / St. Mary River HSU (Strathmore Mb), undifferentiated Belly River HSU, and Foremost HSU (Figure 13 and Table 1), for which there are very few data. Maps of TDS were created in ArcGIS using the kriging function in the Geostatistical Analyst extension with a grid size of 400 m. The average TDS value was used to interpolate the potentiometric surface for all colocated data points.

In many HSUs, chemistry data were too sparse to interpolate over the entire extent of the HSU. Therefore, a buffering approach was taken to clip the interpolated surface to areas where sufficient data existed. A buffer of 5 000 m was created around each well, which was deemed appropriate given the distance between data points and the variability of the data. In areas where buffers from individual locations intersected each other, the resulting merged polygon was used to clip the interpolated surface. In cases where the spatial distribution of data allowed for a reasonable interpolation slightly beyond buffered areas, the interpolated surface was extended. Map areas where there were not enough data for interpolation are represented by the well location and TDS value. Finally, all interpolated surfaces were clipped to the extent of the particular HSU.

Results of the TDS mapping are found in Section 5.4 and Appendix 3, and limitations of the mapping are discussed in Section 5.4.

5.4 Analysis of Hydrostratigraphic Units

The thickness of each HSU and associated hydrogeological maps are presented in Appendix 3. They show (where possible) the following:

- thickness and extent of modelled HSUs (described in Section 4.2);
- the average depth of the middle of the well screens, per ATS section, for AWWID wells identified as providing water supply (Section 5.1, Table A1-2);
- AWWID wells in each HSU with appropriate static water levels and TDS measurements and provincial observation wells (GOWN wells), if present;
- potentiometric surface;
- depth to potentiometric surface and level of confinement compared to the location of flowing artesian wells; and
- TDS distribution.

The water supply well depths show the average depth interval per ATS section where groundwater is being extracted from each particular HSU. These maps can be used to identify patterns in groundwater extraction, including areas where groundwater may be coming from similar depths or areas where water use is more variable within the HSU.

The potentiometric surface maps show a strong link between hydraulic head and local-scale variations of the land surface and bedrock topography, with topographically high areas expressing high hydraulic head, and topographically low areas expressing lower hydraulic head. For the two potentiometric surfaces interpolated for the deeper Foremost HSU and undifferentiated Belly River HSU, the maps show a regional trend of lower hydraulic heads to the west and south. Note that the AWWID data provide information on the upper 200 m of the subsurface, whilst the DST data provide information from depths greater than 200 m and up to nearly 1 600 m.

On the maps of depth to potentiometric surface (Appendix 3), the stippled areas (e.g., Figure A3-20) show where the interpolated potentiometric surface is above the top of the mapped HSU. This indicates confined (or "artesian") conditions, and where this occurs one would need to penetrate the top of the HSU in order to obtain water from it (i.e., to a depth greater than shown within the stippled areas). For areas with a negative depth to potentiometric surface, the interpolated potentiometric surface lies above ground, indicating flowing artesian conditions. In some areas, this is a real physical possibility, and although flowing artesian wells were not included in the potentiometric surface mapping (due to a lack of pressure readings), there is good correlation between these wells and areas mapped as having a depth to potentiometric surface above or very near (within 5 m) of the land surface. Finally, unconfined conditions exist where the depth to potentiometric surface is below the top of the mapped HSU (e.g., nonstippled areas in Figure A3-20), and the depth shown corresponds directly to the depth to water in that HSU; however, there may be overlying low hydraulic conductivity materials restricting vertical flow into that HSU or that may support perched water tables. This is especially likely in the case of unconsolidated materials overlying bedrock HSUs. These unconfined areas may be potential recharge areas if located at potentiometric highs with a thin cover of overburden or higher-permeability overburden.

Figure 28 shows three cross-sections through the CLC: one along the thalweg of the Calgary Valley paleovalley (B–B′), which is generally followed by the modern-day Bow River; the second cross-cutting the Calgary Valley paleovalley (C–C′); and the third along the Lethbridge Valley paleovalley (D–D′). These cross-sections illustrate the modelled HSUs and the hydraulic heads for the HSU S1, Scollard / Willow Creek HSU, and Horseshoe Canyon / St. Mary River HSU, which are based on the potentiometric surfaces shown in Appendix 3. These cross-sections show the relationship between the potentiometric surfaces in the unconsolidated deposits and the bedrock, as well as with the land surface. Generally, the

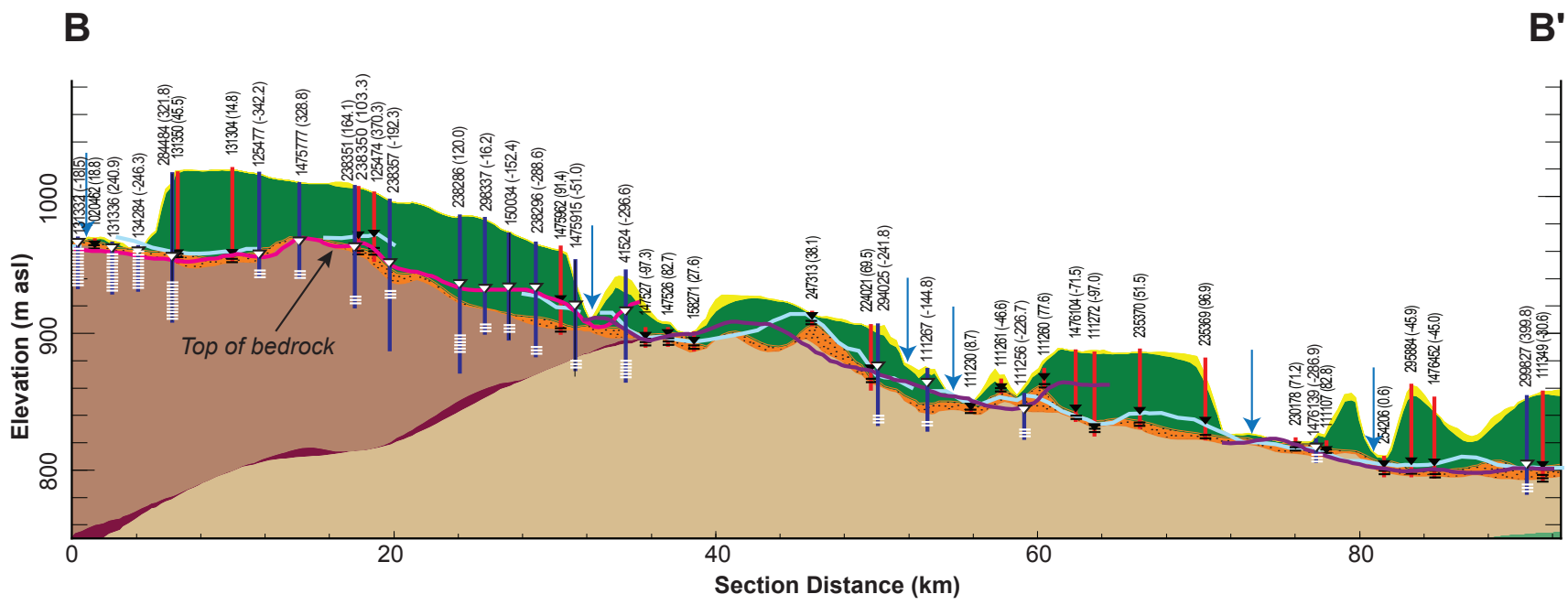

Figure 28. Three cross-sections showing the gridded surfaces from the hydrostratigraphic model: (a) along the thalweg of the Calgary Valley paleovalley (B-B'); (b) cross-cutting the Calgary Valley paleovalley (C-C'); and (c) along the Lethbridge Valley paleovalley (D-D'). See inset for location of cross-sections in the study area. Each cross-section includes the hydraulic head in HSU S1 and the Scollard / Willow Creek HSU or Horseshoe Canyon / St. Mary River HSU where data were available to map hydraulic properties and the HSU was present in the model. Blue arrows show where the cross-section intersects the modern-day Bow and Oldman rivers. The number in parentheses following the Groundwater Information Centre (GIC) Well ID is the distance of the well from the cross-section line, in metres. Cross-sections are shown at 100× vertical exaggeration.

potentiometric surface in HSU S1 is equal to or above the bedrock potentiometric surfaces, although there are some areas on cross-sections B–B′ and D–D′ that show the reverse. Figure 28 also shows the possible relationship and connection of the HSUs to the Bow and Oldman rivers and the associated hydraulic head; although, it should be noted that mapping was completed at a regional scale, and the interpolation of the potentiometric surface is not well constrained in the modern-day river valleys due to a lack of hydraulic data. The connection of surface water and groundwater in relation to the mapping is discussed in Section 5.4.

Most groundwater chemistry analyses from the unconsolidated HSUs come from wells with total depth ranging from 6 to 87 m and mainly located within buried valleys. Sparse data distribution in these HSUs was not conducive to creating continuous interpolated surfaces over the entire extent of the HSU. There is a large variability in TDS within the unconsolidated HSUs. Generally TDS varies between 300 and 4000 mg/L; however, there are a few samples in the southern region of the Vulcan Upland that show elevated TDS (7 000 to 22 000 mg/L) in HSUs S1 and C (Figure A3-7 and Figure A3-11). These samples are from piezometers installed for a study on the saline soils in the area known as Blackspring Ridge (Stein, 1987; Stein and Schwartz, 1990). This study found that the combination of thin unconsolidated material overlying highly fractured bedrock, local-scale groundwater flow systems, and evapoconcentration lead to high TDS groundwater being produced in the near-surface and transported to focused discharge areas (Stein, 1987; Stein and Schwartz, 1990). It is likely that this phenomenon of high TDS in the near surface is present in other areas of the CLC but is not represented on the maps in Appendix 3 because other areas may not have been intensely studied and would not be areas where one would install a water supply well.

The distribution of TDS data improves in the bedrock HSUs compared to the unconsolidated HSUs, although data are mainly within the extent of bedrock subcrop. Groundwater samples from bedrock HSUs come from wells with total depth ranging from 10 to 120 m, except in the undifferentiated Belly River HSU, where there are chemical analyses from oil and gas wells with deeper sampling intervals between 120 and 2 000 m.

A summary of the results of the hydrogeological mapping for each of the HSU's in the CLC is shown in Table 4.

The location information for the majority of the AWWID wells places them in the middle of an ATS quarter section (occasionally in the middle of a section) resulting in up to 400 m of error in the well location. This locational error may also introduce errors in the elevation of the top of the well, which was determined by taking the land surface elevation from the 25 m SRD DEM based on the location of the well. Any error in elevation may influence the allocation of the well into the modelled HSUs as well as the hydraulic head values, as the land surface elevation was used to calculate the mid-screen elevation and corresponding hydraulic head from measured "depth to" values. This is especially true where there are large changes in elevation within a quarter section, such as along the banks of rivers or in the Porcupine Hills and Okotoks Uplands. Additionally, most wells have a casing which sticks up above the land surface and where measurements of water level are usually recorded from. The calculation of hydraulic head in this study did not take into account casing stickup because the amount of stickup was not always recorded in the AWWID. These sources of error are not unique to the CLC and are encountered in any hydrogeological study that uses the AWWID unless further refinement of well locations is undertaken.

The allocation of wells into HSUs is based on the modelled 3D gridded surfaces and the elevation of the middle of the screen, rather than the lithology at the screen interval in a particular well. While there is generally good agreement between the lithology of the borehole at the mid-screen in the well for the allocated HSU, there are cases where the allocated HSU does not match the lithology of the associated borehole for the well. In spot checks, this appeared more common in areas where there was sparse data

Table 4. Hydrogeological summary of mapped HSUs in the CLC.

HSU Type	Model HSU	Figures	Hydrogeological Summary
Unconsolidated	HSU S2	A3-1, A3-2, A3-3	• Coarse-grained sediment exposed at surface (sand, gravel, silty sand) • Contains few wells, all of which are shallow (<20 m) • Extent is limited, although there are some larger connected deposits up to approximately 15 km long • Poorly used aquifer due to limited thickness and extent • May be important locally for groundwater recharge • Not enough data to interpolate potentiometric surface or TDS; therefore data are shown as single points in Appendix 3 • Measured TDS values range from 364 to 1636 mg/L
	HSU C	A3-4, A3-5, A3-6, A3-7	• Fine-grained glaciogenic sediment including clay, silt, or diamicton • Extensive throughout the CLC and can be up to 160 m thick • Regionally serves as an aquitard; however, thin, discontinuous coarse-grained lenses exist, which support local extraction of water • Mid-screen depths range from <5 to 70 m • Mostly unconfined with depth to water typically <25 m; however, it is likely that sand lenses which support water extraction are overlain by low hydraulic conductivity materials • Highly variable TDS, generally ranging from 300 to 4000 mg/L
	HSU S1	A3-8, A3-9, A3-10, A3-11	• Coarse-grained sediment (gravel and sand) directly overlying bedrock and underlying HSU C • Found mostly in the buried valley bedrock domain, although some areas have thick HSU S1 material on top of bedrock terraces and planation surfaces • Good aquifer unless intersected and drained by modern drainage system • Well used for water resources along the Bow River and on the Blackfoot Plain, around Fort Macleod, and northwest of Frank Lake. Other modelled HSU S1 areas do not appear well used for water supply at this time and may be potential areas of future water use • Mid-screen depths are typically greater than 5 m and up to 80 m • Hydraulic head increases westward and away from rivers • Most areas are under confined conditions (i.e., hydraulic head is above the top of the HSU) • Highly variable TDS, generally ranging from 300 to 4000 mg/L, but can be up to 6100 mg/L
Bedrock	Paskapoo / Porcupine Hills HSU	A3-12, A3-13, A3-14, A3-15, A3-16	• Weathered mudstones and thick cross-bedded sandstone beds in excess of 15 m and commonly stacked (Dawson et al., 1994) • Very high well density south of Calgary (Figure 25) • Mid screen depths are mostly <50 m, but can be up to 200 m deep • Mostly under unconfined conditions, except in the north of the subcrop area east of Calgary • Steep hydraulic gradients exist in the Okotoks Uplands, related to (bedrock) topography • Groundwater is generally fresh, with TDS mainly between 600 and 1000 mg/L, except in the northeastern part of the subcrop where TDS is up to 1800 mg/L • TDS is more variable in shallower samples (<60 m) than deeper

HSU Type	Model HSU	Figures	Hydrogeological Summary
Bedrock	Scollard / Willow Creek HSU	A3-17, A3-18, A3-19, A3-20, A3-21	• Thick, gray to buff sandstone and siltstone units interbedded with thin, olive-green mudstone beds and coal (Dawson et al., 1994) • Very high well density south of Calgary (Figure 25) • Most extensively used HSU for water in the CLC (also largest subcrop area) • Mid-screen depths are mostly <50 m, but there are areas of deeper water supply wells north of the Bow River on the Rosebud Plain, Northeast of Frank Lake, and south of Calgary in the Okotoks Upland • Mostly under confined conditions; notable unconfined areas include the Vulcan Uplands, along the Bow River, and south of Gladys Ridge • Good agreement between flowing artesian wells and areas where the interpolated potentiometric surface is at or near the land surface • Hydraulic heads follow bedrock topography (which is closely linked to the land surface topography) • TDS is generally between 700 and 2000 mg/L, except in few areas such as the northwestern and east-central part of the subcrop where TDS ranges from 2000 to 3000 mg/L
	Battle HSU	A3-22, A3-23, A3-24	• Thin HSU with an average thickness of approximately 10 m (Hathway, 2011) • Regional aquitard when present • 26 wells with hydraulic information are allocated to this HSU based on the middle of the screen; however, the Battle HSU is so thin that most of these wells actually have screens extending above or below the HSU; it is likely that these wells are actually drawing water from either the Scollard / Willow Creek HSU, or the Horseshoe Canyon / St. Mary River HSU • There is only one chemical analysis with TDS value of 933 mg/L
	Horseshoe Canyon / St. Mary River HSU	A3-25, A3-26, A3-27, A3-28, A3-29	• Interbedded fine-grained sandstone, siltstone, shale, and coal (Hamblin, 2004) • Depth to middle of the screen in water supply wells is highly spatially variable, but well density per section is lower than in the Paskapoo / Porcupine Hills HSU and Scollard / Willow Creek HSU subcrop areas • Mid-screen depths of water supply wells are generally <60 m • Hydraulic heads generally follow bedrock topography • Mostly under confined conditions; notable unconfined areas include the Vulcan Upland, Majorville Upland, and Crawling Valley Upland, with depths to water >40 m • Groundwater is fresher in the northern and southern part of the subcrop area, with TDS between 600 and 1600 mg/L; higher TDS are found in the central portion of the subcrop (2000 to 3200 mg/L)
	Bearpaw HSU (upper tongue)	A3-30	• Dark grey marine shale, siltstone, and minor sandstone (Catuneanu et al., 1997) • Aquitard • There are no AWWID wells with water supply or hydraulic information • Not enough chemistry data to interpolate a surface; there is only one chemical analysis with TDS value of 9324 mg/L
	Horseshoe Canyon / St. Mary River HSU (Strathmore Mb)	A3-31	• Thinly bedded sandstone, siltstone, and coal (Hamblin, 2004) of the Horseshoe Canyon / St. Mary River HSU; intertongues with the Bearpaw HSU in the northern part of the study area • There is no water supply, hydraulic, or chemistry information for this unit

HSU Type	Model HSU	Figures	Hydrogeological Summary
Bedrock	Bearpaw HSU (lower tongue & undifferentiated portion)	A3-32, A3-33, A3-34	• Dark grey marine shale, siltstone, and minor sandstone (Catuneanu et al., 1997) • Generally an aquitard, although some small sandstone layers can produce water • Only 51 AWWID wells with hydraulic information; as such, the mapped extents of the potentiometric surface and depth to potentiometric surface are limited • Mid-screen depths are generally less than 75 m • Mostly confined conditions except east of the Oldman River where depths to water up to 128 m; however, this area is at the edge of the interpolated surface where there is little data • Not enough chemistry data to interpolate a surface; TDS of available analyses range from 1591 to 2463 mg/L
	undifferentiated Belly River HSU (excluding Foremost HSU)	A3-35, A3-36, A3-37, A3-38	• Interbedded sequence of siltstone, sandstone, carbonaceous mudstone, and coals (Glombick, 2010) • Only 36 wells with hydraulic information • Many wells are located around the vicinity of the Oldman River north of Lethbridge • Wells in the river valley are generally shallower than wells on the main prairie, although placement of wells in the middle of the ATS quarter section and lack of well data around the river result in large errors in the potentiometric surface (Appendix 2) • Mostly confined conditions, except on the Enchant Plain • TDS ranges from 1500 mg/L in the southern portion of the subcrop (from AWWID wells) to 17 500 mg/L in the northern part of the CLC (from oil and gas wells)
	Foremost HSU	A3-39, A3-40, A3-41, A3-42	• Lower portion of Belly River Group • Interbedded sandstone, siltstone, and coal (Hamblin and Abrahamson, 1996) • Only 4 AWWID wells with hydraulic information are found in the CLC, hence no potentiometric surface was created from these wells; a potentiometric surface was created using the deeper oil and gas wells in the northern portion of the CLC. • 3 of 4 wells have a mid-screen depth of less than 20 m • Depth to potentiometric surface from the DST data is ≤15 m • TDS ranges from 3500 mg/L to 22 000 mg/L in the northern part of the CLC
	Pakowki / upper Lea Park HSU	Not shown	• Fine-grained marine shale (Dawson et al., 1994) • Regional aquitard • There are no AWWID wells with water supply, hydraulic, or chemistry information

with which to constrain the modelling of hydrostratigraphic surfaces, and in areas of variable elevation in the modelled surfaces (e.g., slope breaks in the bedrock topography). Errors in allocation will also be greater where the HSUs are thin (e.g., Battle HSU, HSU S1, at subcrop edges) or where the middle of the screen is located close to the boundary between two HSUs, thus the well screen may straddle multiple HSUs. Potential errors in the allocation will affect all maps that use those wells (e.g., water supply well maps, TDS maps, etc.).

The potentiometric surface maps include measured water levels from wells that have been drilled over many decades and in different seasons. As such, the resulting potentiometric and depth to potentiometric surfaces show the average conditions through time. Local and temporal variations are not captured in this analysis.

There is generally poor resolution of the potentiometric surfaces along modern-day river valleys. This is due to a lack of hydraulic data around river valleys and the imprecise placement of wells in the middle of the quarter section, which can make it difficult to determine the actual placement of the well in either the valley bottom or on the upland. Additionally, due to the regional scope of the current study, the local-scale hydraulic connection between rivers and individual HSUs has not been ascertained, and interpreting such connection from the products in this study should be done with caution. The degree of surface water–groundwater interaction will vary in space and time. For example, HSU S1 could be connected to a river if the river intersects it, but it may no longer be in direct connection if the river has eroded down below HSU S1. Likewise, bedrock HSUs might not be directly connected to the river if significant unconsolidated deposits lie between the bedrock topography interface and the river. Because of the uncertainty in surface water–groundwater connectivity, rivers, lakes, and other surface water bodies were not used to constrain any of the potentiometric surfaces.

The water table has not been mapped explicitly as part of this study for a number of reasons. First, the potentiometric surface and depth to potentiometric surface of each HSU has already been mapped. Second, water table maps are often interpolated with hydraulic data from shallow wells. However, there is a paucity of shallow (≤10 m) well data in the CLC (790 wells), and most are clustered either south of Calgary or along river valleys.

Even though the chemical analysis data were subjected to certain criteria in order to select the most representative groundwater samples, errors may still exist in reported concentration of constituents. Possible errors in reported values may come from the various techniques used for sample preservation, collection, and analysis. Also, data come from different sources and different laboratories, and the detection limits for parameters may be different or have changed over the years. Finally, vertical heterogeneity in sediments within a particular HSU may cause a substantial difference in the chemical composition of groundwater in these small-scale layers due to differences in permeability. When a well is sampled, turbulent flow in the well may mix water with different chemical compositions coming from different small-scale layers. Therefore, a water sample is usually a good indication of the average chemical composition of the well interval.

In general, all maps and analyses for this study have been completed at a regional scale and show generalized trends over the CLC. A more local-scale analysis of the hydrogeology and hydrochemistry would be required for site-specific studies. Finally, areas of discrete fracture or fault flow in the bedrock HSUs have not been identified.

5.5 Recharge, Discharge, and Vertical Gradients

Recharge and discharge to and from the groundwater system are important contributors to the groundwater balance of an area and provide important information on the sustainability of groundwater resources. This section provides a regional overview of possible recharge and discharge mechanisms within the CLC, including an analysis of the vertical gradients which drive the recharge and discharge potential.

5.5.1 Recharge

Recharge is the amount of precipitation that infiltrates into the ground and contributes to the groundwater system. Groundwater recharge can be highly variable, both spatially and temporally, and depends on a multitude of factors including climate, vegetation, slope, and the hydraulic properties of the unsaturated zone. There are many methods used to quantify recharge to the groundwater system at both regional and local scales (e.g., Scanlon et al., 2002).

One method of estimating regional recharge is by quantifying the regional water budget. Recharge is determined as the residual of inputs (e.g., precipitation), outputs (e.g., AET and surface runoff), and changes in storage (often assumed to be zero). Figure 29 shows the results of a simple version of a water budget for the CLC using the ACIS township-based data to determine the average annual difference between precipitation (the major input; Figure 4) and AET (the major output; Figure 6). This map estimates the average amount of precipitation that could potentially become recharge, although it does not account for other outputs such as surface runoff. While surface runoff can be estimated using river hydrographs, flow in the major CLC rivers is regulated by dams, weirs, and diversions for irrigation. Thus, surface runoff in the CLC was not determined by this study. Figure 29 shows that there is likely to be less than 50 mm/yr of recharge over most of the CLC and that areas of potentially higher recharge are restricted to the western portion of the study area that is higher in elevation and closer to the Rocky Mountains.

Previous estimates of areal recharge to regional aquifers in the Canadian and northern US prairies range from a few millimetres per year up to about 40 mm/yr and highlight the importance of depression-focused recharge (van der Kamp and Hayashi, 1998). A more recent study provided estimates of average annual recharge for the Oldman and Bow River sub-basins of 44 and 36 mm/yr, respectively, based on estimates of infiltration rates for various types of surficial material (Golder Associates Ltd., 2008). Farrow (2014) used the numerical Versatile Soil Moisture Budget (VSMB) model, modified to account for depression-focused recharge, to estimate recharge over four years from 2009 to 2012 at the Brocket AGDM climate station in the south of the CLC (Figure 29). Annual recharge at the Brocket station varied between 4 and 34 mm/yr, with an average of 22.5 mm/yr. North of Calgary (outside the CLC) at the Nier AARD climate station and West Nose Creek research station, simulated annual recharge over the four years varied between 2 and 26 mm/yr (average 16.5 mm/yr), and 4 and 41 mm/yr (average 20.5 mm/yr), respectively (Farrow, 2014).

Recharge is highly dependent on climate, vegetation, physical soil properties, and landscape characteristics. While Farrow (2014) modelled recharge at a number of locations within southern Alberta, he did not report on the sensitivity of the model to variations in soil type or ET parameters. Therefore, a numerical modelling exercise was undertaken to evaluate the sensitivity of recharge simulation to these parameters at three climate stations within the CLC (Figure 29).

Recharge was modelled using the 1D VSMB model (Baier and Robertson, 1966). This multilayer water balance model (Figure 30) determines potential recharge based on the residual between rainfall/snowmelt and runoff, the soil moisture budget, ET in each soil layer, and gravity drainage (Mohammed et al., 2013).

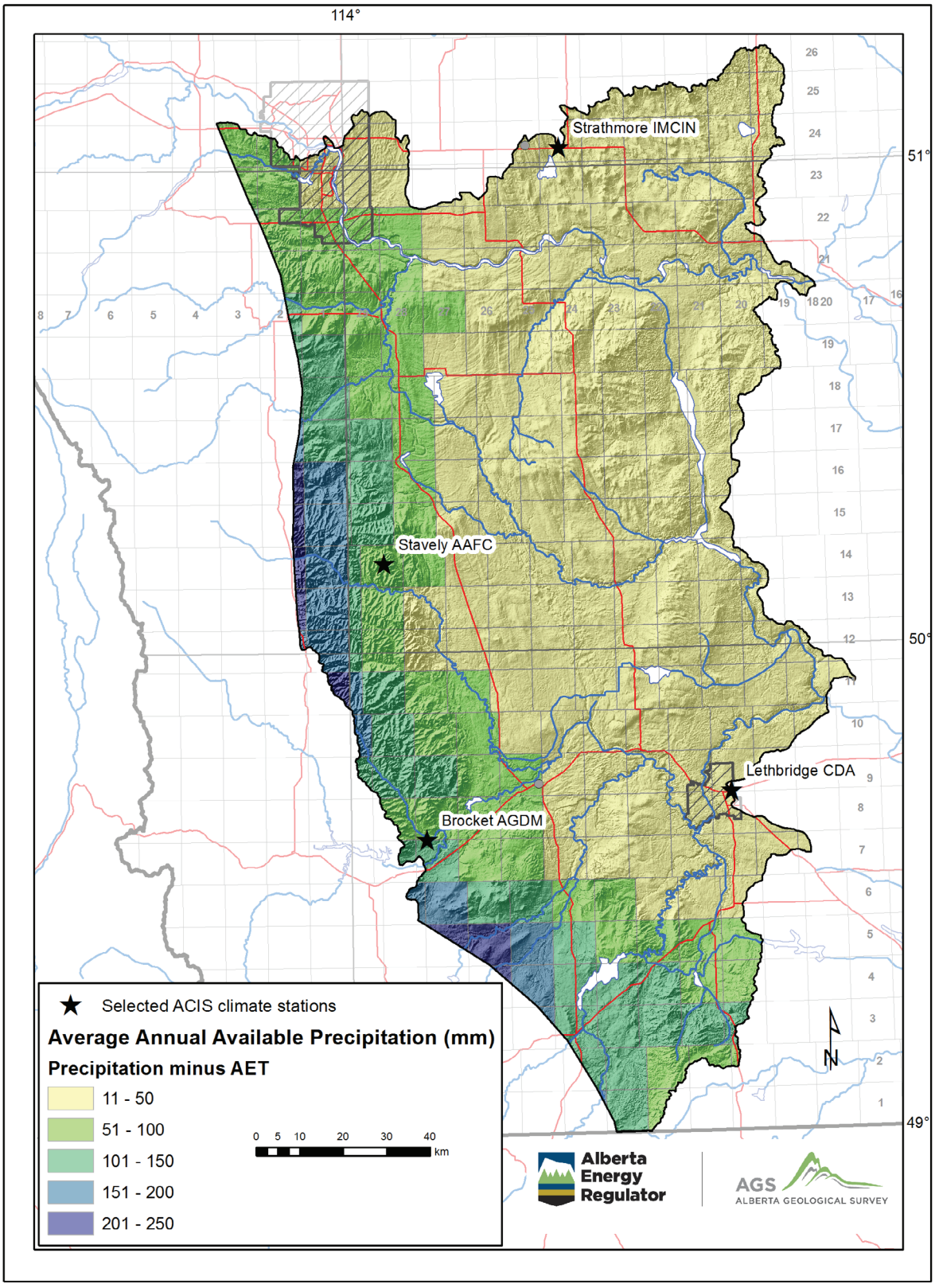

Figure 29. Estimate of potential recharge based on average available precipitation (precipitation minus AET). Also shown are the ACIS climate stations used in numerically modelling recharge in the CLC.

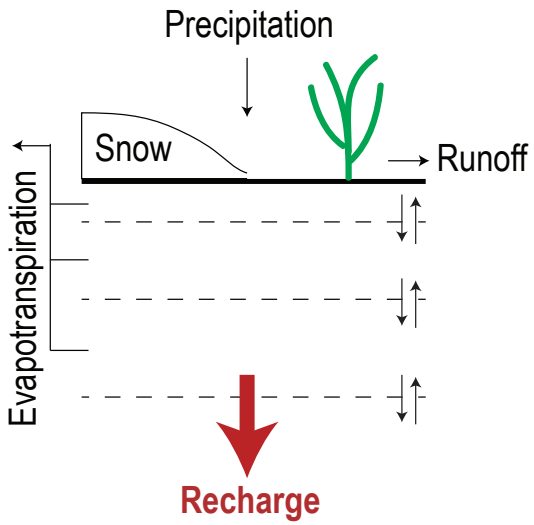

Figure 30. Schematic of the VSMB model with multiple soil layers.

Inputs to the model include climate data (e.g., precipitation, temperature, and relative humidity), soil material property data (e.g., layer wilting point and field capacity), and site information (e.g., slope and latitude). Details of all input variables can be found in Appendix 4.

The VSMB model has been widely used across the Canadian prairies, including by AARD for their mapping of soil moisture conditions (Mohammed et al., 2013). Modifications to the original VSMB model have occurred over time and include improvements to the simulation of ET and frozen soil processes (Akinremi et al., 1996; Mohammed et al., 2013) and accounting for depression-focused recharge (Farrow et al., 2014). The VSMB model version presented in Mohammed et al. (2013) was used in this study.

Recharge was estimated with a suite of simulations at four different weather stations (Figure 29, Figure A4-1) using two soil types (sandy loam and silty clay; Table A4-2). Additionally, because ET is highly influential in this area, three different sets of crop coefficients were tested (Table A4-3 and Table A4-4) along with three different drying curves (Table A4-5). This resulted in 36 simulations for each of the four climate stations: a total of 144 simulations.

Specific inputs to the recharge models can be found in Appendix 4. Initial soil moisture and temperature conditions were obtained by running a spin-up period before the simulation period. The spin-up period consisted of running the model with daily climate data from April 2, 2005, to April 1, 2013, repeated twice (i.e., 16 years of spin-up time). Results of this spin-up period were used as initial conditions for the simulation period, which utilised daily climate data from April 2, 2005, to July 31, 2014. Instead of compiling the recharge results according to calendar year, results reported are for hydrological years, which run from November 1 to October 31. Therefore, recharge results are for the eight hydrological years between November 1, 2005 and October 31, 2013 (although the simulation ran from April 2, 2005, to July 31, 2014).

Of 144 simulations performed with varying climate conditions, soil types, and ET parameters, only 70 produced any recharge over the eight hydrological years simulated (Table A4-7). Table 5 summarizes the results of the recharge modelling and shows that for the eight hydrological years the average annual recharge is 24 mm/y at the Brocket AGDM station, 10 mm/y at the Lethbridge CDA station, 58 mm/yr at the Stavely AAFC station, and 34 mm/yr at the Strathmore IMCIN station over the eight-year simulation period. These values fit within the range of previously published values for the region (Section 5.5.1). The Stavely AAFC station has a much higher average annual precipitation rate than the others; consequently, recharge results are the highest of the four stations, and 27 of the 36 simulations with varying combinations of soil type and ET parameters produced recharge (Table A4-7). Between the other three stations, only 18 of the different combinations produced recharge. In general, simulations with the coarse-grained sandy loam soil produce the most recharge (Table A4-7).

Although average annual recharge is low, recharge in any given year can be highly variable. Figure 31 shows all simulations with recharge for the Brocket ADGM climate station. Annual recharge varies from zero to nearly 140 mm within the same simulation. There is a strong correlation between precipitation and

Table 5. Summary of average annual results of the VSMB modelling for those simulations that resulted in groundwater recharge.

	Brocket AGDM				Lethbridge CDA				Stavely AAFC				Strathmore IMCIN			
	Precipitation (mm)*	AET (mm)	Recharge (mm)	Surface Runoff (mm)	Precipitation (mm)*	AET (mm)	Recharge (mm)	Surface Runoff (mm)	Precipitation (mm)*	AET (mm)	Recharge (mm)	Surface Runoff (mm)	Precipitation (mm)*	AET (mm)	Recharge (mm)	Surface Runoff (mm)
Average Annual (all simulations)	380	277	24	3	353	267	9	3	475	318	58	8	393	283	34	2
Minimum Average Annual (from any one simulation)	250	229	4	0	229	242	1	0	340	231	3	01	314	230	6	0
Maximum Average Annual (from any one simulation)	490	307	65	7	467	276	31	5	631	396	128	18	471	318	80	6

* Precipitation at each station is held constant across all simulations.

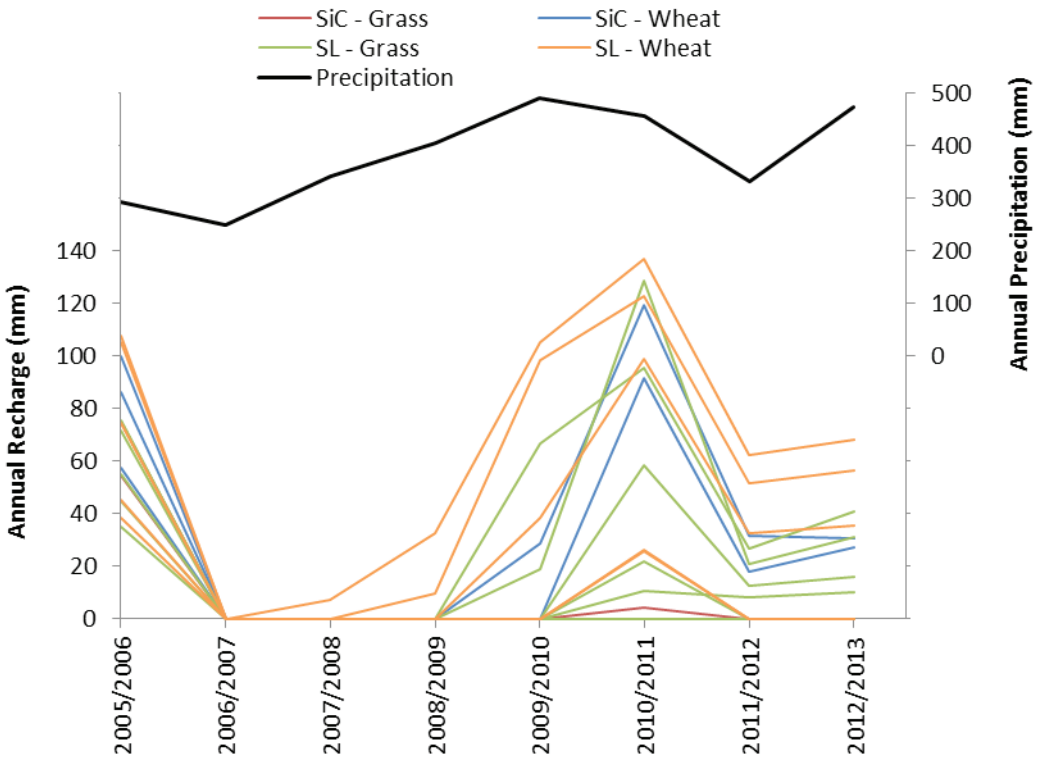

Figure 31. An example of the variation in annual recharge from the Brocket AGDM climate station (showing only those simulations with recharge). Simulations with the same line colour have the same soil and vegetation types shown in the legend but different crop coefficients and drying curves (i.e., ET parameters).

recharge, although actual timing of recharge to the groundwater system cannot be assessed from this study as the column depths were a standard 5 m and did not consider heterogeneity within the soil column.

Figure 32 shows that recharge is most likely to occur in the spring, when precipitation is high and ET is lower while vegetation is establishing itself. Again, the exact timing of delivery of water to the water table cannot be stated for certain from the current modelling study, which is possibly why small amounts of recharge are seen in the winter in Figure 32. Finally, the version of the VSMB model used in this study did not account for depression-focused recharge; therefore, it is possible that local-scale recharge may be higher than presented, although surface runoff (which would contribute to depression-focused recharge) was minimal (Table 5).

5.5.2 Discharge

Like recharge, discharge can also be highly variable both spatially and temporally. Figure 33 shows the location of springs (Stewart, 2014) and flowing artesian wells (from AWWID) in the CLC. The flowing artesian wells have been allocated, if possible, based on the elevation of the middle of the screen and the surfaces from the hydrostratigraphic model. Figure 33 shows a large occurrence of flowing wells present at the north end of Frank Lake. This feature is also present in the depth to potentiometric surface maps (Appendix 3) for the Scollard / Willow Creek HSU, HSU C, and HSU S1. Many flowing artesian wells are located at the bottom of upland areas (e.g., south of the Vulcan Upland).

The type and origin of the springs shown in Figure 33 are not included in the springs inventory by Stewart (2014), therefore these points represent springs of all types and of multiple origins. Some represent small springs from local-scale, shallow flow systems, while others likely represent water from deeper or bedrock sources on a more intermediate scale. Many of the springs are located along rivers or in the Porcupine Hills and Okotoks Uplands.

As explained in Section 5.4, a detailed analysis of the degree of connectivity of surface water bodies and groundwater in the CLC was not performed for this study, although it is expected that both recharge and discharge will occur in connection with surface water bodies.

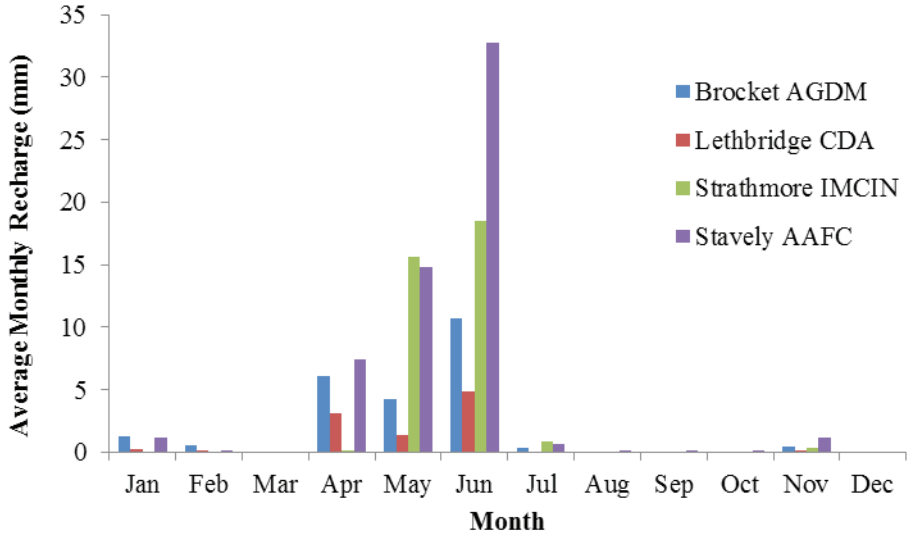

Figure 32. Average monthly recharge by climate station from those simulations with recharge.

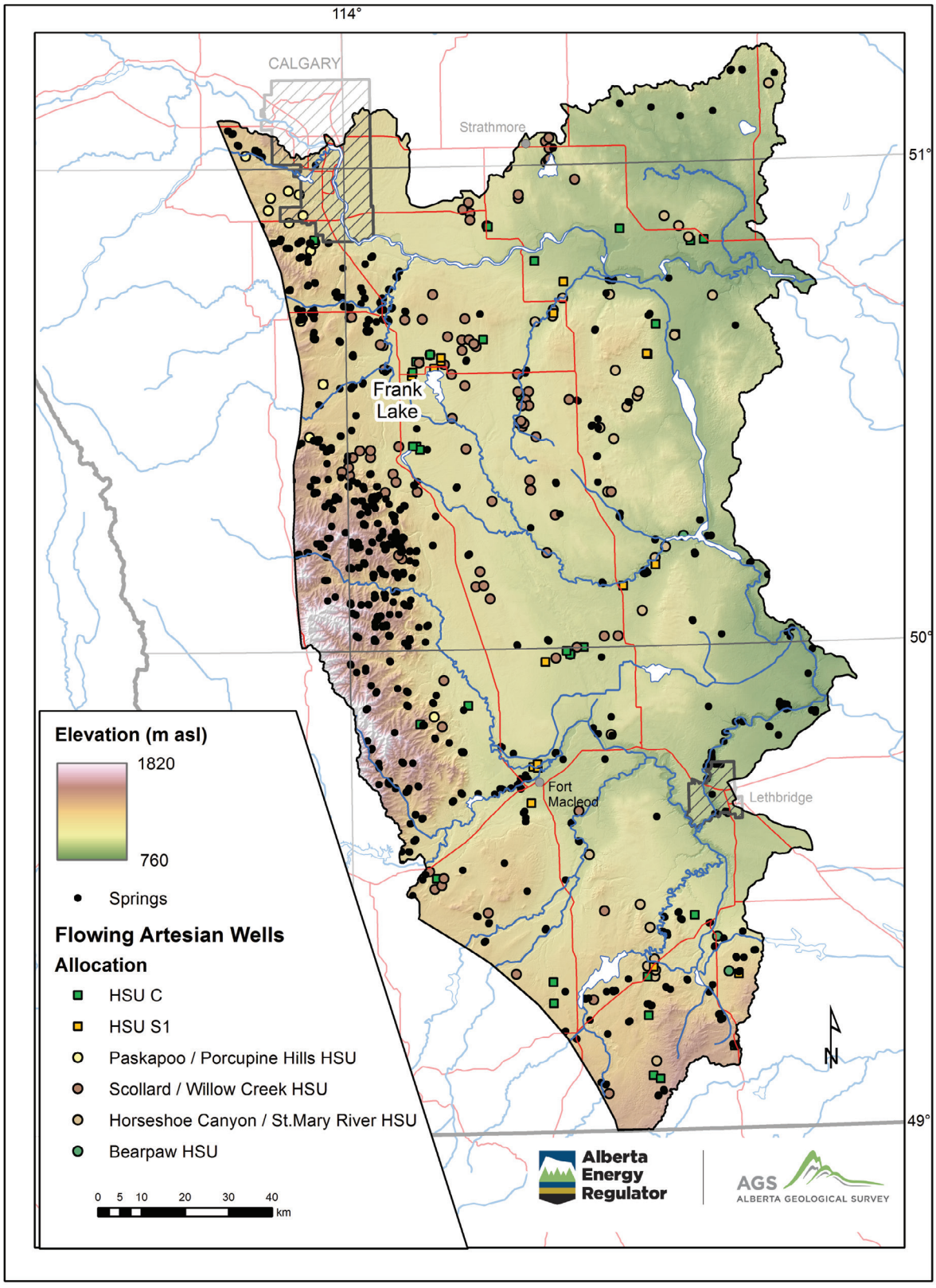

Figure 33. Springs (Stewart, 2014) and flowing artesian wells in the CLC.

5.5.3 Vertical Hydraulic Head Gradients

In order to assess the spatial distribution of recharge and discharge across the CLC, the vertical hydraulic head gradients were examined. The vertical gradient is defined by the difference in hydraulic head divided by the difference in elevation between where the hydraulic heads are measured. Two methods of mapping the vertical gradient were explored and in both cases the resulting vertical gradient is unitless.

The first approach to mapping regional vertical gradients was a tomographic-like approach (e.g., Tóth and Almási, 2001). A number of potentiometric surfaces are created using mid-screen depths from 20 m depth intervals from the land surface, which was a large enough interval to contain a sufficient amount of wells for interpolating but small enough to resolve meaningful vertical gradients. Two potentiometric surfaces from specific depth intervals are subtracted to determine where upwards or downwards gradients exist. Note that the results only show the head difference between the surfaces, not a true gradient, which would require division by the distance between the two surfaces (i.e., 20 m). Additionally, care must be taken in interpreting the results because this method involves interpreting the residual between two already interpolated surfaces, which each may have areas of high uncertainty where data are sparse. The Scollard / Willow Creek HSU was used to illustrate this tomographic approach because it covers a large portion of the CLC and has abundant well data.

Figure 34 shows the difference between potentiometric surfaces using two sets of wells in the Scollard / Willow Creek HSU: those with mid-screen depths of 0–20 m and 40–60 m, respectively. Only wells located within a legal subdivision (LSD) or where a GPS was used to document location coordinates were used in order to improve the accuracy of the elevation of the well, and thus calculation of hydraulic head. Additionally, similar to creating the potentiometric surfaces in Section 5.2, the potentiometric surface was clipped to areas of contiguous 2500 m buffers around wells. The resulting map in Figure 34 represents areas where both potentiometric surfaces from the two depth intervals overlap. Buffering the wells and clipping the potentiometric surfaces is important for this analysis to avoid subtracting interpolated surfaces in areas with sparse data, which may lead to erroneous interpretations of the results.

Figure 34 shows some expected results, with some high elevation areas (e.g., Vulcan Uplands, parts of Gladys Ridge) showing the potential for downwards water flow, and some low elevation areas (e.g., along the Bow River) showing potential for upwards flow. However, a comparison with spring locations and flowing artesian wells (Figure 35) shows limited correlation between areas of potential upwards flow and locations of springs and flowing artesian wells.

An alternate method of determining the vertical gradients uses the ATS grid. Within each ATS township (~9.6 km × 9.6 km), the hydraulic head versus mid-screen elevation was plotted for all wells in a particular HSU that were located within a legal subdivision (LSD) or where a GPS was used to document location coordinates (Figure 36). The slope of a linear best-fit line through these points is representative of the vertical gradient, with positive slopes indicating downwards flow potential and negative slopes indicating upwards flow potential. Larger magnitudes of the slope indicate larger gradients. The coefficient of determination (R^2) gives an indication of the goodness of the fit of the best-fit line to the data points. Low R^2 values indicate that the data do not strongly follow the trend of a linear hydraulic gradient, and high R^2 values indicate that the data do strongly follow the trend of a linear hydraulic gradient. Unlike the tomographic-like approach described above, the township-based approach does not interpolate data spatially. It merely shows an amalgamation of data within each township.

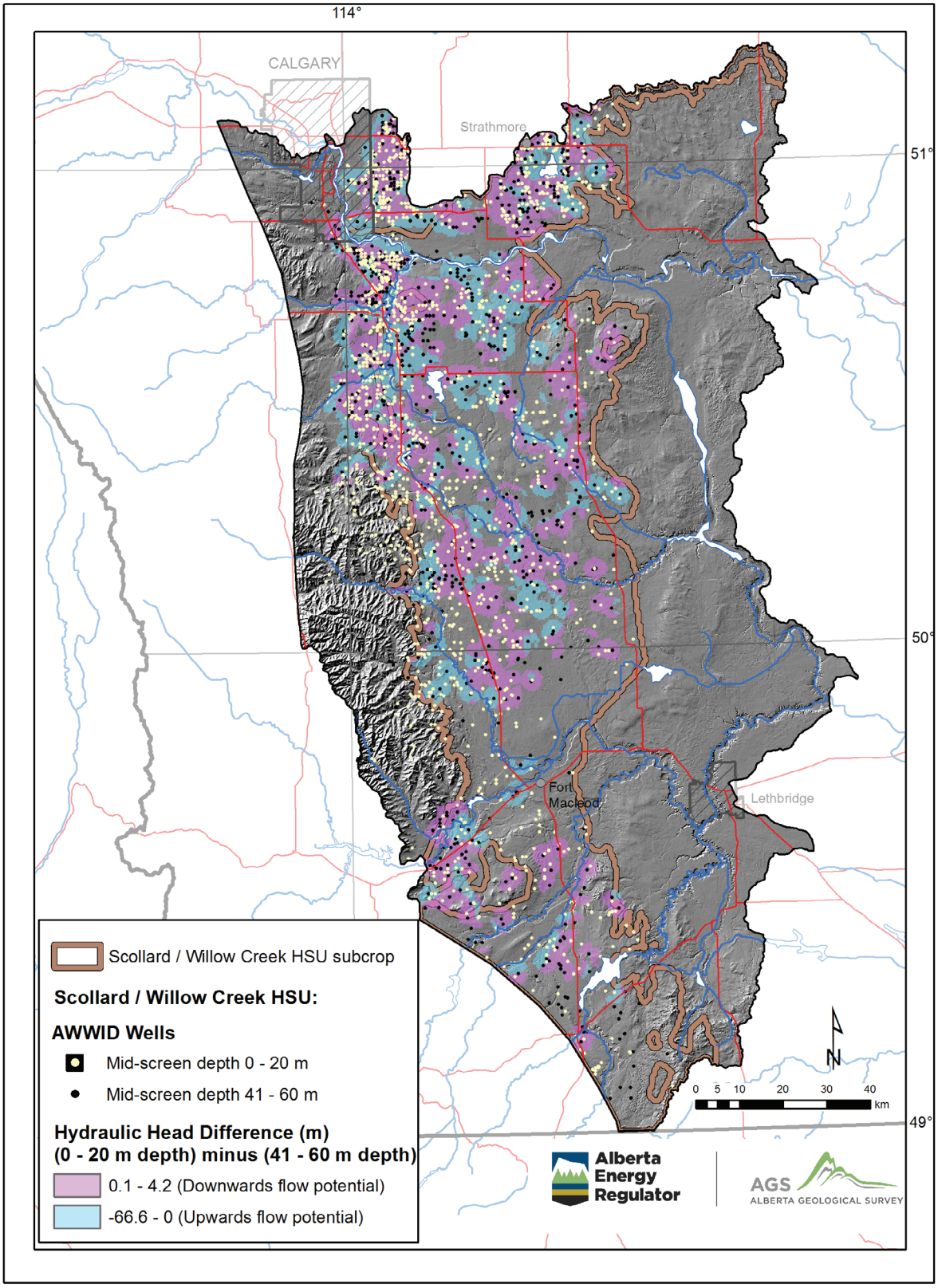

Figure 34. Hydraulic head difference between potentiometric surfaces from wells with mid-screen depths of 0–20 m and 40–60 m, respectively, showing upwards and downwards flow potential. Also shown is the well data used to create the surface at each depth interval.

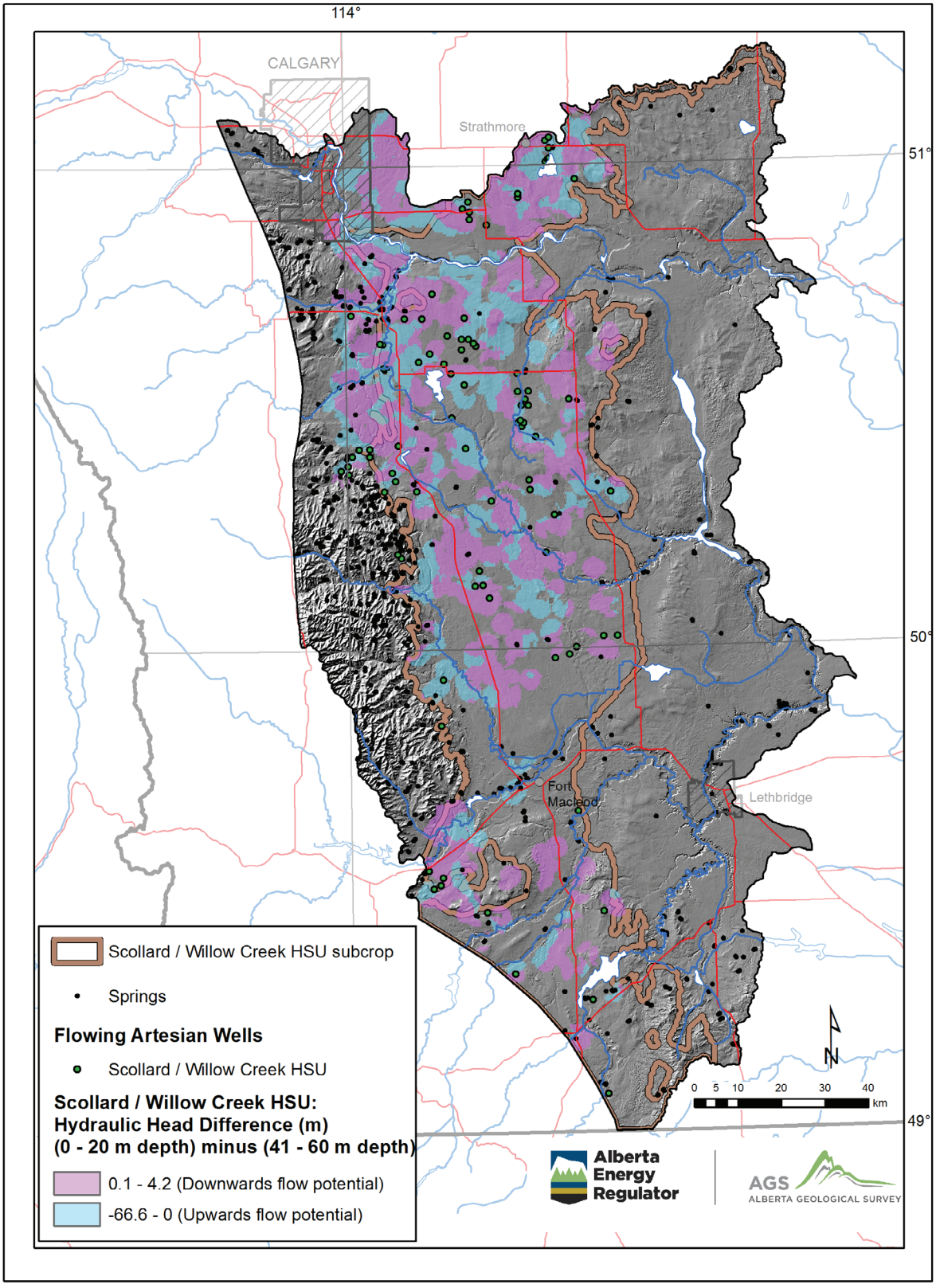

Figure 35. Hydraulic head difference between potentiometric surfaces from wells with mid-screen depths of 0–20 m and 40–60 m, respectively, showing upwards and downwards flow potential. Also shown are the locations of springs and flowing artesian wells.

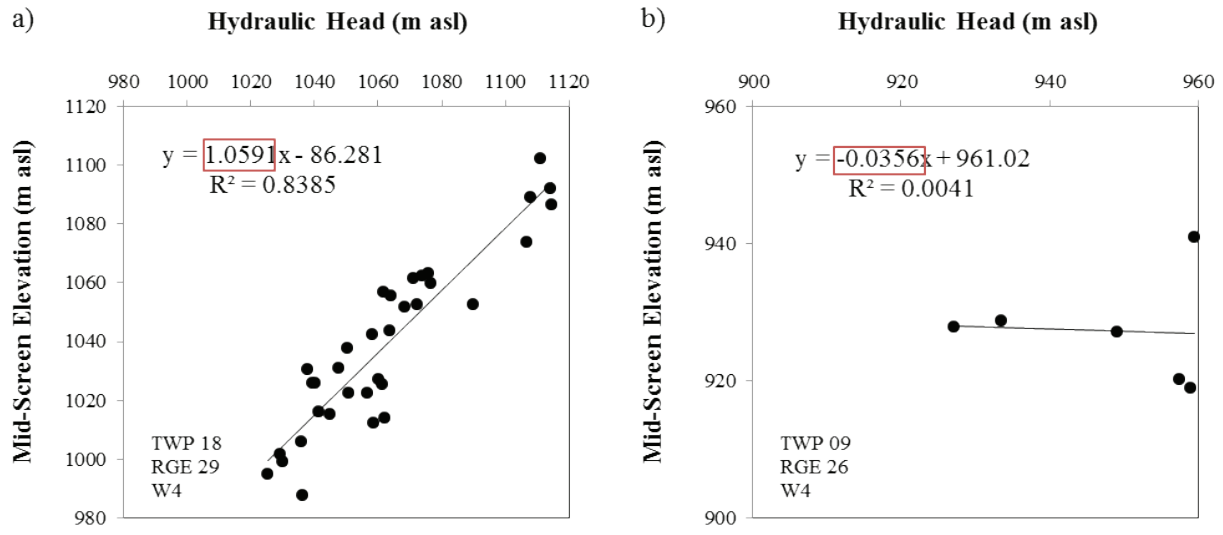

Figure 36. Hydraulic head versus elevation for two townships and wells in the Scollard / Willow Creek HSU. (a) Plot showing a strong positive slope/gradient (red box) indicating downwards flow potential and a good correlation of data points. (b) Plot showing a small negative slope/gradient (red box) and poor correlation of data points.

Figure 37 shows the vertical gradients per township for the Scollard / Willow Creek HSU. Since a township is a relatively large area, the vertical gradients were also determined on a per-section basis (Figure 37). Note that only townships and sections with more than one well and an R^2 greater than 0.6 are shown. The vertical gradients per township show, almost exclusively, the potential for downwards flow, which, on a regional-basis, is likely the case. Discharge is likely to occur on a much more localized scale around surface water bodies and at the bottom of upland areas. The vertical gradients per section show more localized areas of upwards flow potential but, similar to the tomographic-like approach, there is little correlation between these areas and known springs or flowing artesian wells within the extent of the Scollard / Willow Creek HSU (Figure 38). A comparison of the tomographic-like and section-based approaches directly shows little correlation between areas suspected of having upwards flow potential (Figure 38).

Because of the differences in the results between the methods and the lack of correlation with known springs and flowing artesian wells, the vertical gradient mapping was not extended to other HSUs in the CLC. Additionally, the Scollard / Willow Creek HSU is the most extensive and well-used HSU in the CLC, and other HSUs (except the Paskapoo / Porcupine Hills HSU) have much less well data. However, the results of this vertical gradient mapping may be used to give an indication of where to focus more local-scale studies of gradients and possible surface water-groundwater interaction.

It is important to note that these maps indicate the *potential* for water flow and not the *actual* water flow. The presence or absence of confining layers is not taken into account; for example, an area may show a large vertical gradient, but the actual amount of water flow between those depths may be minimal if low-permeability materials lie between them.

5.6 Hydrogeological Implications of the Distribution of Permeable Bedrock

In the absence of any previous hydrostratigraphic modelling in the CLC area, this study used established lithostratigraphic boundaries to define zones of hydrogeological interest (i.e., HSUs) in the bedrock strata (Section 4.1; Figure 14). Analysis of the hydrogeological parameters (Section 4.3) followed these stratigraphic divisions to provide a regional analysis of the hydrogeology of the CLC; however, this

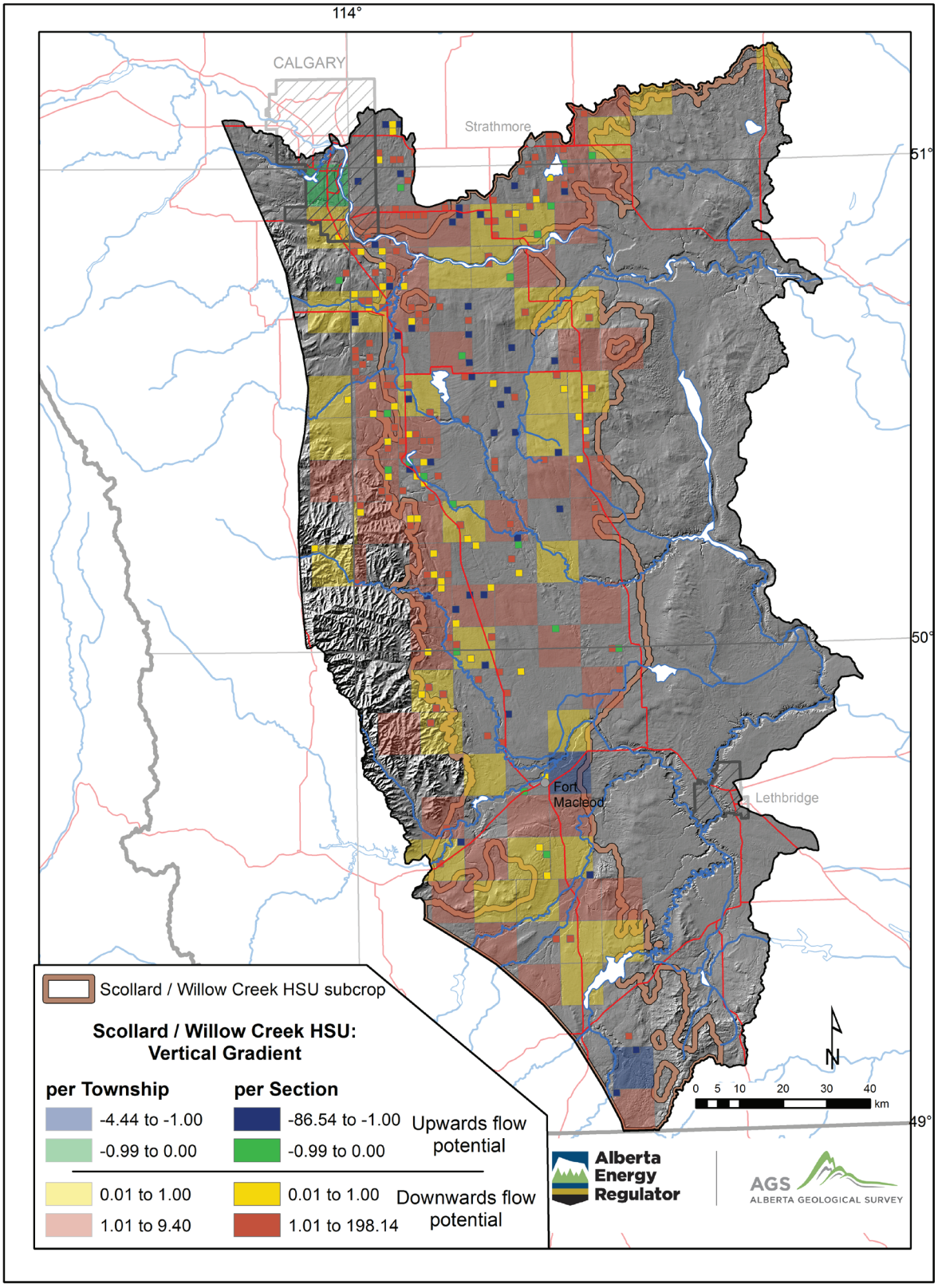

Figure 37. Vertical gradients for all GPS- or LSD-located wells per township (large squares) and per section (small squares).

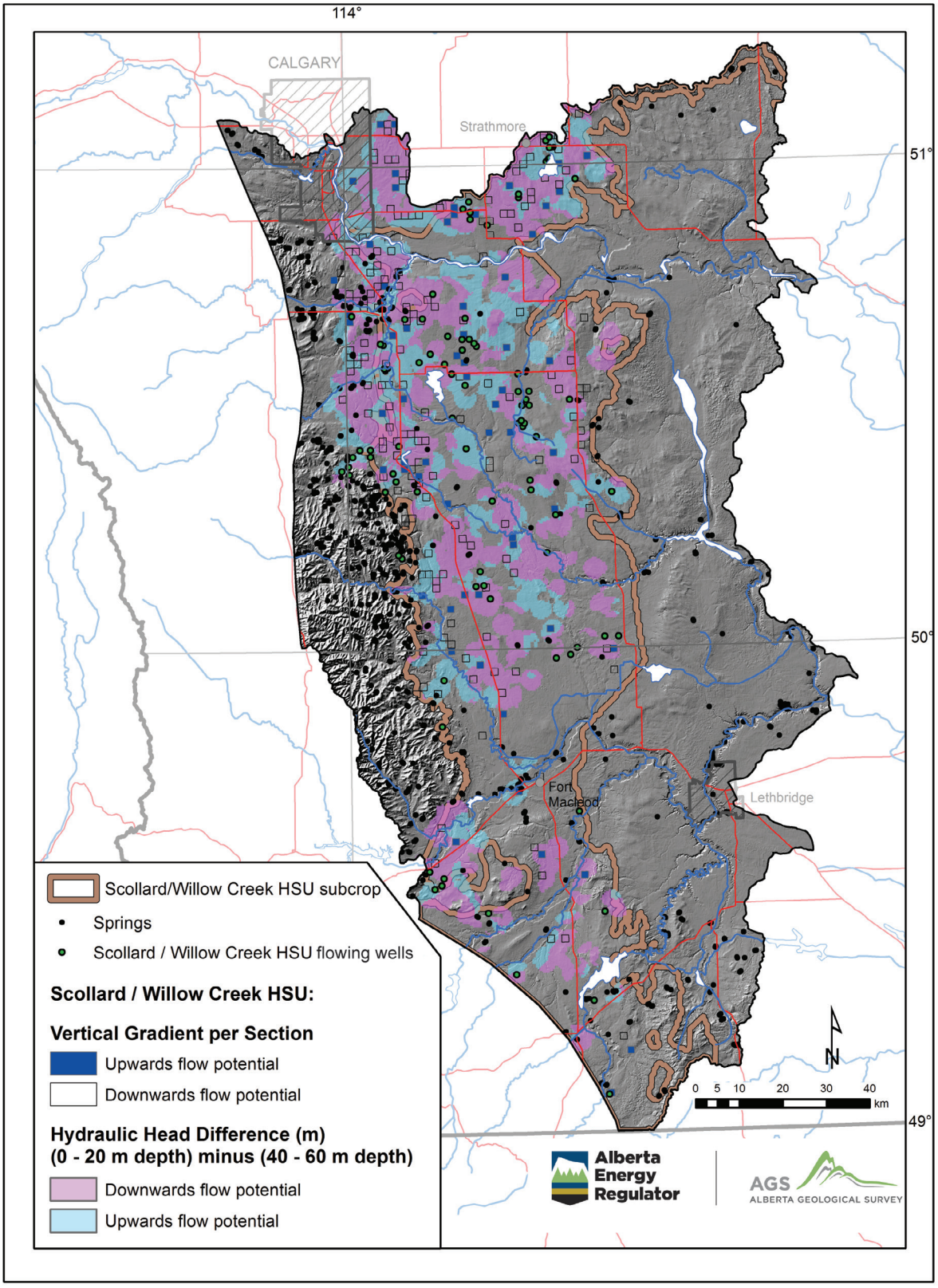

Figure 38. Comparison of flow potential directions for the tomographic-like approach and the section-based approach.

approach assumes the bedrock HSUs are homogeneous deposits that follow thick, laterally extensive stratigraphic divisions. Moving forward, the regional hydrostratigraphic framework presented in this study (Figure 14) can be refined as more detailed analysis of the heterogeneity and structure of the bedrock strata is performed.

Section 4.3 describes the slice mapping method used to evaluate major sandstone trends within the bedrock of the CLC. The results of the slice mapping in each of the 13 major slices are shown in Appendix 5. The slice mapping method highlights the spatial distribution of potentially permeable rock within the bedrock strata, which are the predominant source of water supply in the CLC (Figure 23). Areas with a high NGR are likely to be more permeable than surrounding sediments and thus have higher aquifer potential. This analysis represents an important step towards refining the hydrostratigraphic framework in the bedrock strata, rather than basing bedrock HSUs on regional stratigraphy alone. However, further refinement of the bedrock HSUs will also need to consider the purpose and scale of the study, for example, delineating aquifers for groundwater management.

The results obtained from slice mapping were evaluated within the context of current geological knowledge for the study area. Our results not only are in accordance with the previously published geology (e.g., Jerzykiewicz and Norris, 1993; Catuneanu et al., 1997; Hamblin, 2004; Glombick, 2010; Eberth and Braman, 2012; Prior et al., 2013) but also reveal more details on sedimentary depositional patterns, which provides direct insight for predicting and assessing the degree of connectivity of bedrock HSUs. Figure 39 provides a visualization of how the slices in the CLC fit together to give a pseudo-3D picture of the spatial distribution of NGR in the CLC. Regional trends in the CLC show

- large sandstone-bodies in the basal portion of the undifferentiated Belly River HSU and Foremost HSU,
- the Bearpaw HSU characterized by overall low NGR values,
- the Horseshoe Canyon / St. Mary River HSU characterized by small spatially distributed and discontinuous sandstone-bodies, and
- regionally higher NGR values within the Scollard / Willow Creek HSU.

Note that data paucity made it harder to evaluate much of the upper portion of the Scollard / Willow Creek HSU and Paskapoo / Porcupine Hills HSU in the far west of the CLC.

The top-most slice in Figure 39 shows the average NGR, 50 m below the top of the bedrock surface. This slice is also shown in Figure 40, along with the subcrop boundaries. Figure 41 shows the data density used to create the subcrop NGR sandstone map. The relatively high NGR in the Scollard / Willow Creek HSU and low NGR in the Horseshoe Canyon / St. Mary River and Bearpaw HSUs are apparent in Figure 40 (and Figure 39) and support the use of stratigraphic boundaries as an initial definition of regional HSUs in the CLC.

At shallow depths (<150 m), where a majority of water wells are completed, the slice mapping complements existing data on water use and hydraulic properties. Depending on groundwater management priorities and issues, focus areas may be chosen more selectively based on the geological and hydrogeological characteristics presented here. For example, the large area in the south of the Vulcan Upland has high NGR in the Scollard / Willow Creek HSU (Figure 40), is unconfined (Figure A3-20), lies within a topographic and potentiometric high (Figure A3-19), has a thin cover of unconsolidated material (Figure 16), and contains a substantial number of water supply wells (Figure 25).

At deeper depths (>150 m) there is a lack of well data. In these areas, the slice mapping provides important information on the potential distribution and connectivity of deep aquifers. While groundwater at these depths is not currently exploited much, knowledge of the deep groundwater system (quantity and

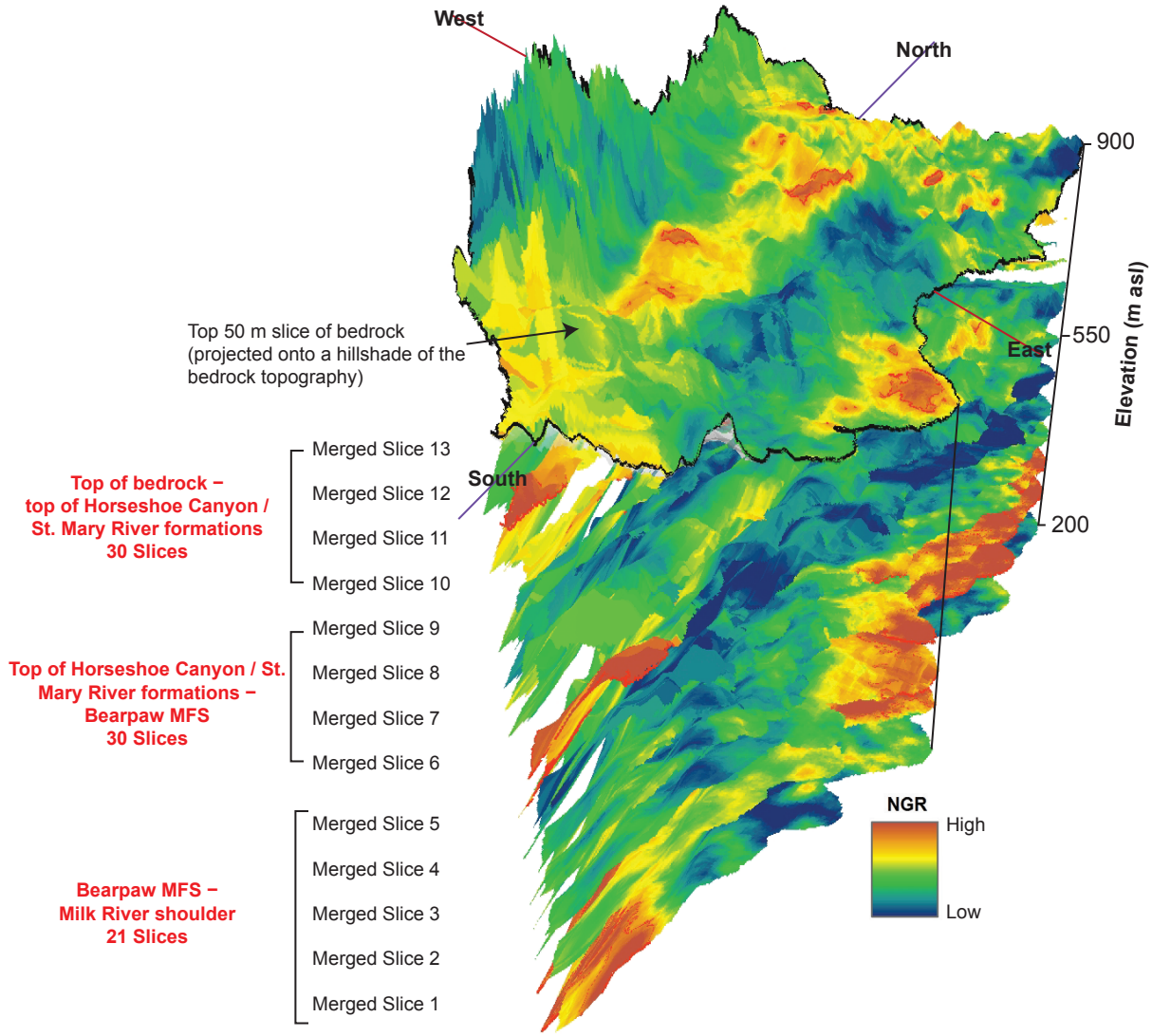

Figure 39. Pseudo-3D rendering of the 13 merged net-gross ratio (NGR) slices as well as the top 50 m depth slice below the bedrock surface in the CLC model. Each set of merged slices shows different sandstone trends laterally based on the distribution of NGR calculated from gamma-ray logs. NGR variation between separate merged slices is also apparent, as the merged slices partition different bedrock HSUs. The results of each merged slice can be found in Appendix 5.

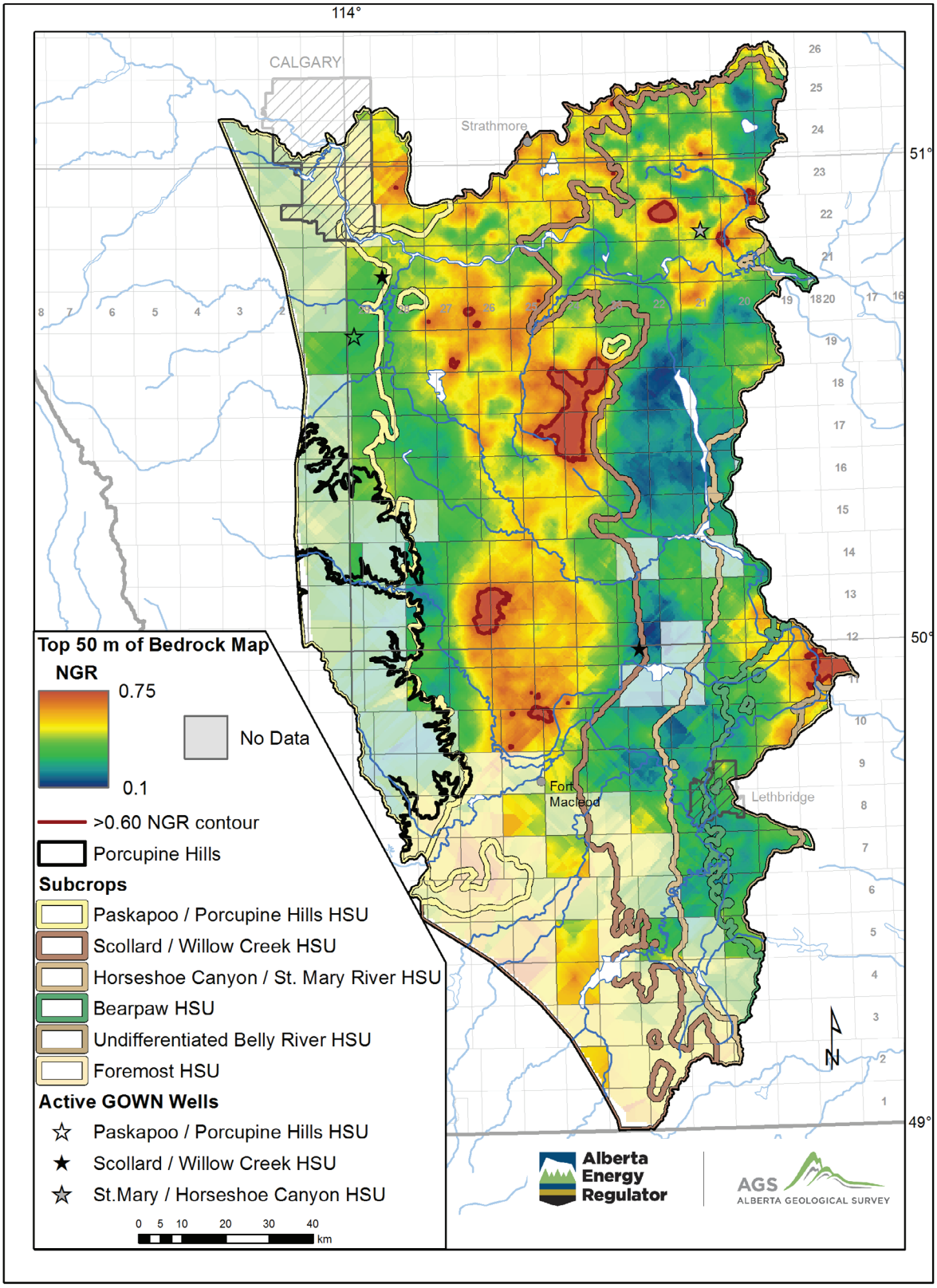

Figure 40. NGR subcrop map using averaged NGR data available within 50 m below the bedrock topography surface.

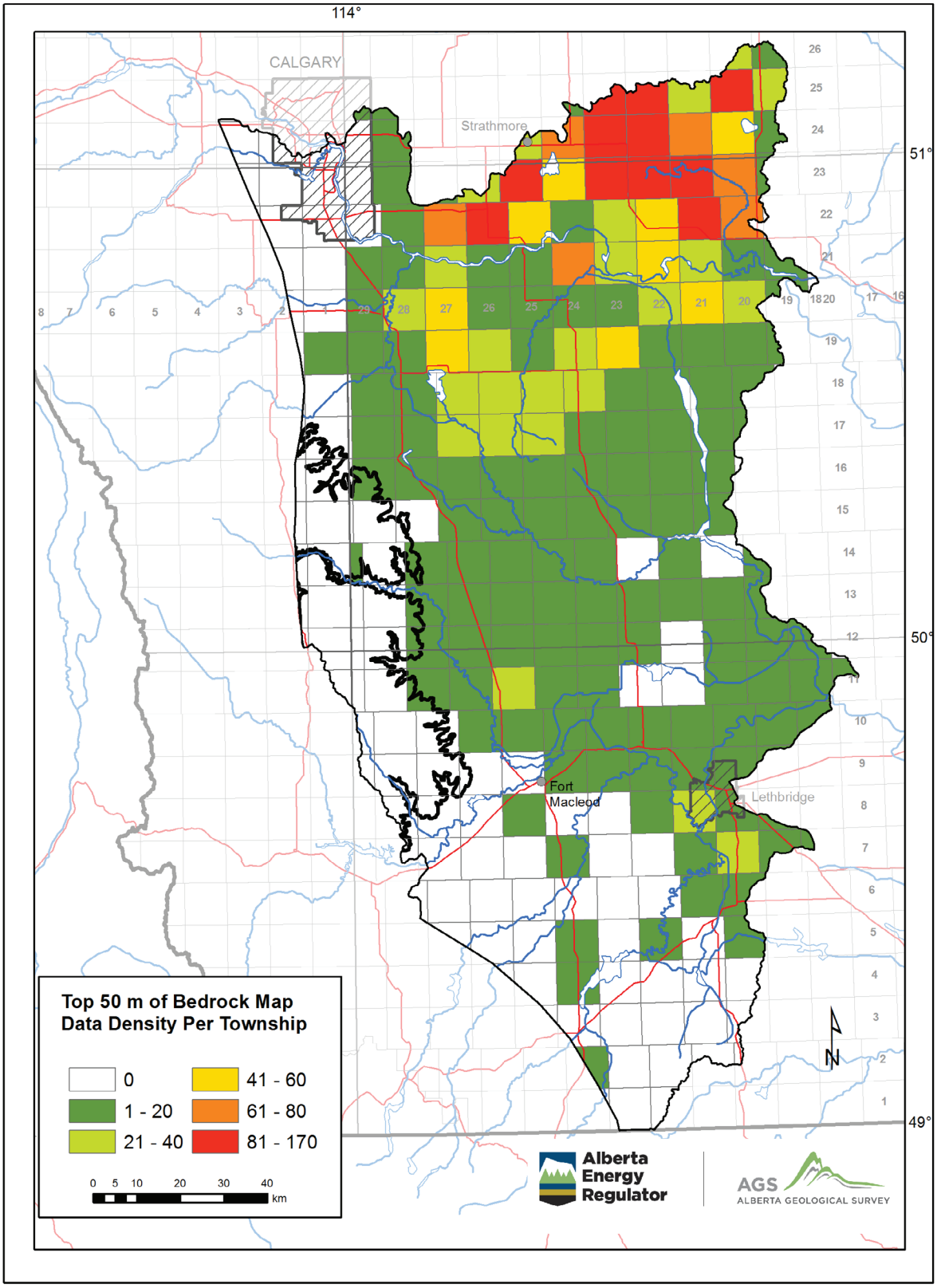

Figure 41. Data density map for the 50 m NGR subcrop map.

quality) and its connection with the shallow groundwater system is important for long-term management of potential future uses and demand for alternate sources of groundwater.

6 Provincial Observation Wells

There are a total of 288 observation wells in EP's Groundwater Observation Well Network (GOWN), only 17 of which are currently active in the CLC (as of February 2014). Most GOWN wells are inactive or have been reclaimed and are located around reservoirs such as Pine Coulee (217 wells), Twin Valley (28 wells), and Clear Lake (18 wells). Of the 17 active wells, the GOWN database reports that 6 are completed in bedrock HSUs and 11 are into unconsolidated HSUs (Table 6).

The allocation of GOWN well completions into HSUs based on the modelled surfaces shows some differences to their original allocation into formations or lithologies in the GOWN database (Table 6). This is due to two main factors: First, the modelled hydrostratigraphic surfaces have a degree of error, and this becomes more noticeable with the GOWN wells because they are often completed close to bedrock in HSU S1 or in thin sand lenses in HSU C. Second, there are significant differences in elevation (up to 170 m) between the top of casing recorded in the GOWN database and the ground surface elevation from the 25 m SRD DEM. Some of these differences may be explained by the location of the well in an area of variable topography, making accurate estimation of elevation more problematic; however, some wells in the GOWN database have an elevation that is conspicuously different from any nearby elevation when compared to the DEM. Additionally, we noticed differences in location between GOWN wells listed in both the GOWN and AWWID databases, and GOWN wells that appear to be in the AWWID based on location but have no AWWID well ID listed.

Table 6 shows the active GOWN wells in the CLC, the GOWN-listed formation or lithology, and any modifications to the HSU allocation made for this study. The location of the GOWN wells in each HSU is shown on the potentiometric surface map of the corresponding HSUs in Appendix 3. The GOWN wells in the bedrock HSUs are also shown on Figure 40. Most GOWN wells were not used directly in the potentiometric surface mapping because they have multiple water levels recorded and were filtered out in the well selection process (Table A1-3).

7 Summary

This work uses a new 3D hydrostratigraphic model in mapping the regional-scale hydrogeology of the CLC. The geology was divided into hydrostratigraphic units based on textural characteristics and stratigraphic position in the Neogene–Quaternary materials and formal lithostratigraphic units in the bedrock. In the unconsolidated succession, HSU S1 forms an important aquifer, confined by the dominantly fine-grained sediments of HSU C. Within HSU C, thin lenses of coarse-grained materials provide an important water source, although these lenses are not laterally-extensive. Thin, discontinuous, coarse-grained materials of HSU S2 occur at the modern land surface and are not readily used for water supply, although they could be important groundwater recharge areas. Within the bedrock, the Battle HSU, Pakowki / upper Lea Park HSU, and Bearpaw HSU (upper and lower tongues and undifferentiated portion) are important aquitards, although some permeable layers do exist in the Bearpaw HSU that provide water supply in the CLC. The remaining bedrock HSUs (Paskapoo / Porcupine Hills HSU, Scollard / Willow Creek HSU, Horseshoe Canyon / St. Mary River HSU, undifferentiated Belly River HSU, and Foremost HSU) generally act as aquifers, although additional slice mapping has identified areas that are likely to be less permeable based on the distribution of NGR sandstone maps. Of all the HSUs, the Scollard / Willow Creek HSU covers the largest portion of the CLC, including the most populous areas, and has an abundance of data. This analysis provides important insights for understanding

Table 6. Active GOWN wells in the CLC

GOWN Station Code	GOWN Station Name	AWWID GIC Well ID	GOWN Formation/ Lithology	Final HSU	Comment
117	Barons 615E_0117	194198	Bedrock - Horseshoe Canyon Fm	Scollard / Willow Creek HSU	Model puts well at edge of Scollard / Willow Creek HSU subcrop
218	Cluny 85-1_0218	196999	Bedrock - Horseshoe Canyon Fm	Horseshoe Canyon / St. Mary River HSU	Model allocation was HSU C, but well located in an area of highly variable bedrock topography
217	Okotoks Land Fill 2378E_0217	196892	Bedrock - Paskapoo/Willow Creek Fm	Paskapoo / Porcupine Hills HSU	
786	Okotoks 05-1 South_0786	1061144	Bedrock - Porcupine Hills Fm	Scollard / Willow Creek HSU	Model puts well at edge of Scollard / Willow Creek HSU subcrop
787	Okotoks 05-2 North_0787	1061160	Bedrock - Porcupine Hills Fm	Scollard / Willow Creek HSU	Model puts well at edge of Scollard / Willow Creek HSU subcrop
110	McNally_0110	154658	Channel - Sand & Gravel	HSU S1	Model allocation was Undifferentiated Belly River HSU, but the top of the screen is within HSU S1
113	Keho Lake 2019E_0113	196694	Channel - Gravel	HSU S1	
219	Cluny 85-2 South_0219	197015	Channel - Gravel	HSU S1	
220	Carseland 85-1_0220	197021	Channel - Gravel	HSU S1	Model allocation was Scollard / Willow Creek HSU, but the top of the screen is within HSU S1.
111	Orton 1514E_0111	205690	Channel - Sand & Gravel	HSU C	Might be in HSU S1, but hard to tell from GOWN description. No litholog in AWWID database.
112	Mud Lake 1537E_0112	1973544	Channel - Gravel	HSU S1	GOWN elevation for top of casing is 27 m higher than nearby land surface elevations from DEM, therefore the DEM elevation was used to determine the mid-screen elevation. Model allocation was Scollard / Willow Creek HSU, but the middle of the screen was at the bedrock surface and the top of screen was within HSU S1.
287	High River 2580E_0287	152302	Surficial - Sand	HSU C	
109	Lethbridge Airport_0109	196674	Surficial - Sand	HSU C	
793	Pine Coulee 23D_0793		Surficial - Till	HSU S1	

GOWN Station Code	GOWN Station Name	AWWID GIC Well ID	GOWN Formation/ Lithology	Final HSU	Comment
971	Rosebud #1_0971	1305192	Bedrock - Horseshoe Canyon Fm	Horseshoe Canyon / St. Mary River HSU	GOWN elevation for top of casing is 170 m lower than land surface elevation from DEM for the well location or anywhere in the surrounding area.
3010	Carmangay West_3010	42005	Surficial - Lacustrine	HSU S2	
3054	Mud Lake_3054	42018	Till - Sand & Gravel	Unallocated	No production interval. Total depth would put it just into top of HSU S1, but screen may be in HSU C

the distribution of potentially permeable bodies, particularly when no hydraulic data is available in the subsurface. The NGR sandstone map analysis represents an important step towards refining HSUs and delineating aquifers for the purposes of groundwater management, especially for deeper HSUs that are currently not being exploited and hence for which there is little hydrogeological information available.

Analysis of the hydrogeological information in the AWWID shows a very high density of water supply wells in the area south of Calgary, with upwards of 96 wells per section (~1.6 × 1.6 km). These water supply wells also show that groundwater is mainly sourced from bedrock HSUs in the CLC, although there are areas (generally along paleovalleys) where groundwater is sourced from a mixture of bedrock and unconsolidated HSUs. Potentiometric surface maps of each HSU show a strong link between hydraulic head and local-scale variations of the land surface and bedrock topography, with topographically high areas expressing high hydraulic head and topographically low areas expressing lower hydraulic head. The associated depth to potentiometric surface maps identify areas which, regionally, are likely under unconfined, confined ('artesian'), or flowing artesian conditions. Combining the maps of potentiometric surface, depth to potentiometric surface, total dissolved solids, thickness of sediment and bedrock HSUs, water supply wells, and the distribution of potential permeability from rock properties within modelled bedrock units can aid in identifying potential recharge areas or groundwater management units in the CLC.

Numerical modelling of recharge shows that annual recharge is highly variable, varying from 0 to more than 120 mm/yr. Average annual recharge varied between 10 and 58 mm/yr from simulations of climate conditions at four different weather stations throughout the CLC. These values are consistent with previously published estimates of groundwater recharge in the southern prairies. Mapping of vertical gradients using two different methods provided mixed results, but the maps can also be used to aid in interpretation of potential recharge and discharge areas.

Results of this work contribute to a better understanding of the regional hydrogeology of the CLC, which is required in order to focus future studies relating to land-use planning and groundwater monitoring. This study provides the foundation with which to begin identifying particular areas of interest for future local-scale studies, for specific aquifer-mapping endeavours, or for identifying gaps in current groundwater monitoring networks. Future work in the CLC should include

- collecting and analyzing existing pumping test data in the CLC to determine hydraulic properties of HSUs followed by field investigations to acquire new data where significant gaps exist (supporting future numerical modelling projects),
- more detailed mapping of groundwater chemistry,
- investigating the degree of influence of faults and fractures in bedrock HSUs,
- focused studying of surface water–groundwater connectivity around key rivers,
- refining HSUs in the bedrock strata, and
- delineating groundwater management units associated with mapped aquifers.

8 References

AER/AGS (Alberta Energy Regulator / Alberta Geological Survey) (2014): Compilation of Alberta Geological Survey borehole data (tabular data, tab delimited format, to accompany Open File Report 2014-06); Alberta Energy Regulator, AER/AGS Digital Dataset 2014-0012, URL<http://ags.aer.ca/publications/DIG_2014_0012.html> [March 2016].

AARD (Alberta Agriculture and Rural Development) (2013): Agricultural regions of Alberta soil inventory database version 4.0; Alberta Agriculture and Rural Development, URL <http://www1.agric.gov.ab.ca/$Department/deptdocs.nsf/All/sag14652> [March 2016].

Akinremi, O.O., McGinn, S.M. and Barr, A.G. (1996): Simulation of soil moisture and other components of the hydrological cycle using a water budget approach; Canadian Journal of Soil Science, v. 76, no. 2, p. 133–142.

Alberta Geological Survey (2015): Alberta table of formations; Alberta Energy Regulator, URL<http://ags.aer.ca/activities/table-of-formation.htm> [March 2016].

Alden, W.C. (1932): Physiography and glacial geology of eastern Montana and adjacent areas; United States Geological Survey, Professional Paper 174, 133 p.

Alkalali, A. (2002): Petroleum hydrogeology of the Nisku Aquifer; MSc thesis, University of Alberta, 165 p.

Allen, R.G., Pereira, L.S., Raes, D. and Smith, M. (1998): Crop evapotranspiration: guidelines for computing crop water requirements; Food and Agriculture Organization of the United Nations, Irrigation and Drainage Paper 56, 326 p., URL <http://www.fao.org/docrep/x0490e/x0490e00.htm> [March 2016].

Baier, W. and Robertson, G. W. (1966): A new versatile soil moisture budget; Canadian Journal of Plant Science, v. 46, p. 299–315.

Bostock, H.S., comp. (1967): Physiographic regions of Canada; Geological Survey of Canada, Map 1254A, scale 1:5M.

Bow River Basin Council (2010): Bow River Basin state of the watershed summary; Calgary, Alberta, 44 p., URL <http://wsow.brbc.ab.ca/index.php?option=com_content&view=article&id=102&Itemid=182> [March 2015].

Catuneanu, O., Sweet, A.R. and Miall, A.D. (1997): Reciprocal architecture of Bearpaw TR sequences, uppermost Cretaceous, Western Canada Sedimentary Basin; Canadian Society of Petroleum Geologists Bulletin, v. 45, no. 1, p. 75−94.

Dawson, F.M., Evans, C.G., Marsh, R. and Richardson, R. (1994): Uppermost Cretaceous and Tertiary strata of the Western Canada Sedimentary Basin; *in* Geological atlas of the Western Canada Sedimentary Basin, G.D. Mossop and I. Shetsen. (comp.), Canadian Society of Petroleum Geologists and Alberta Research Council, p. 387–406. URL<http://ags.aer.ca/publications/chapter-24-uppermost-cretaceous-and-tertiary-strata.htm> [March 2016].

Eberth, D.A. and Braman, D.R. (2012): A revised stratigraphy and depositional history for the Horseshoe Canyon Formation (Upper Cretaceous, southern Alberta plains; Canadian Journal of Earth Sciences, v. 49, p. 1053-1086.

Edwards, D.W.A. and Scafe, D. (1994): Mapping and resource evaluation of the Tertiary and preglacial sand and gravel formations of Alberta; Alberta Research Council, Alberta Geological Survey, Open File Report 1994-06, 246 p., URL <http://www.ags.aer.ca/publications/OFR_1994_06.html> [May 2016].

Farrow, C.R. (2014): Winter surficial processes and groundwater recharge in the southern Alberta Prairies; MSc thesis, University of Calgary, 195 p.

Fenton, M.M., Waters, E.J., Pawley, S.M., Atkinson, N., Utting, D.J. and Mckay, K. (2013): Surficial geology of Alberta; Alberta Energy Regulator, AER/AGS Map 601, scale 1:1 000 000, URL <http://ags.aer.ca/publications/MAP_601.html> [March 2016].

Geiger, K. (1968): Bedrock topography of the Gleichen map-area, Alberta; Alberta Research Council, Report 67-2, URL <http://ags.aer.ca/publications/ESR_1967_02.html> [March 2016].

Glombick, P. (2010): Top of the Belly River Group in the Alberta Plains: subsurface stratigraphic picks and modelled surface; Energy Resources Conservation Board, ERCB/AGS Open File Report 2010-10, 27 p., URL <http://ags.aer.ca/publications/OFR_2010_10.html> [March 2016].

Glombick, P. and Mumpy, A.J. (2014): Subsurface stratigraphic picks for the Milk River 'shoulder,' Alberta Plains: Including tops for the Milk River Formation and Alderson Member of the Lea Park Formation; Alberta Energy Regulator, AER/AGS Open File Report 2013-17, 23 p., URL <http://ags.aer.ca/publications/OFR_2013_17.html> [July 2016].

Golder Associates Ltd. (2008): Water for life: reliable, quality water supplies for a sustainable economy; water supply assessment for Alberta; Alberta Environment, 111 p., URL<http://environment.gov.ab.ca/info/posting.asp?assetid=8393&categoryid=5> [March 2015].

Government of Alberta (2014): South Saskatchewan regional plan; Government of Alberta, URL <https://landuse.alberta.ca/REGIONALPLANS/SOUTHSASKATCHEWANREGION/Pages/default.aspx> [March 2016].

Hamblin, A.P. (2004): The Horseshoe Canyon Formation in southern Alberta: surface and subsurface stratigraphic architecture, sedimentology, and resource potential; Geological Survey of Canada, GSC Bulletin 578.

Hamblin, A.P. and Abrahamson, B.W. (1996): Stratigraphic architecture of "Basal Belly River" cycles, Foremost Formation, Belly River Group, subsurface of southern Alberta and southwestern Saskatchewan; Canadian Society of Petroleum Geologists Bulletin, v. 44, no. 4, p. 654−673.

Hartman, G. (2016): Surficial geology of the Calgary-Lethbridge corridor (NTS 82O, 82P, 82J, 82I, 82G and 82H); Alberta Energy Regulator, AER/AGS Map 579, scale 1:250 000, URL <http://ags.aer.ca/publications/MAP_579.html> [April 2016]

Hartman, G. (2015): Synthesis of a post-Laramide stratigraphic framework of the South Saskatchewan River Basin, Alberta, in support of hydrostratigraphic modelling; Alberta Energy Regulator, AER/AGS Open File Report 2015-01, 36 p., URL <http://ags.aer.ca/publications/OFR_2015_01.html> [March 2016].

Hathway, B. (2016): Regional T-R sequence stratigraphy and lithostratigraphy of the Bearpaw Formation (Upper Campanian), west-central and southwestern Alberta plains; Bulletin Canadian Petroleum Geology, v. 64, no. 3, p. 449–466.

Hathway, B. (2014): 3rd-order sequence stratigraphy and lithostratigraphy of the Bearpaw–Horseshoe Canyon transition, Alberta plains. GeoConvention 2014 – Focus (Adapt, Refine, Sustain), Calgary; Canada; May 12-14, 2014, extended abstract, 7 p.

Hathway, B. (2011): Late Maastrichtian paleovalley systems in west-central Alberta: mapping the Battle Formation in the subsurface; Canadian Society of Petroleum Geologists Bulletin, v. 59, no. 3, p. 195–206.

Hayashi, M., Jackson, J.F. and Xu, L. (2010): Application of the Versatile Soil Moisture Budget model to estimate evaporation from prairie grassland; Canadian Water Resources Journal, v. 35, no. 2, p. 187–208.

Hitchon, B. (1996): Rapid evaluation of the hydrochemistry of a sedimentary basin using only "standard" formation water analyses: Example from the Canadian portion of the Williston Basin; Applied Geochemistry, v. 11, p.789–795.

Hitchon, B. and Brulotte, M. (1994): Culling criteria for "standard" formation water analyses; Applied Geochemistry, v. 9, p. 637–645.

Horberg, C.L. (1954): Rocky Mountain and continental Pleistocene deposits in the Waterton region, Alberta, Canada; Geological Society of America Bulletin, v. 65, no. 11, p. 1093–1150.

Jackson, L.E., Jr., Leboe, E.R., Little, E.C., Holme, P.J., Hicock, S.R., Shimamura, K. and Nelson, F.E.N. (2008): Quaternary stratigraphy and geology of the Rocky Mountain Foothills, southwestern Alberta; Geological Survey of Canada, Bulletin 583, 50 p.

Jackson, L.E., Jr., Andriashek, L.D. and Phillips, F.M. (2011): Limits of successive middle and late Pleistocene continental ice sheets, Interior Plains of southern and central Alberta and adjacent areas; *in* Quaternary glaciations: extent and chronology, J. Ehlers, P.L. Gibbard and P.D. Hughes. (ed.), Elsevier, Philadelphia, Pennsylvania, p. 575–589.

Jerzykiewicz, T. and Norris, D.K. (1993): Evolution of the Laramide foredeep and the adjacent thrust belt in southern Alberta; Geological Survey of Canada, GSC Open File Report 2663.

Jerzykiewicz, T. and Sweet, A.R. (1988): Sedimentological and palynological evidence of regional climatic changes in the Campanian to Paleocene sediments of the Rocky Mountain Foothills, Canada; Sedimentary Geology, v. 59, no. 1, p. 29−76.

Khan, D. K. (2006): Hydrogeological characterisation of the Weyburn CO2 project area and gradient-free inverse conditioning of heterogeneous aquifer models to hydraulic head data; PhD thesis, University of Alberta, 238 p.

Lyster, S. and Andriashek, L.D. (2012): Geostatistical rendering of the architecture of hydrostratigraphic units within the Paskapoo Formation, central Alberta; Energy Resources Conservation Board, ERCB/AGS Bulletin 66, 103 p., URL <http://www.ags.aer.ca/publications/BUL_066.html> [August 2016].

MacCormack, K.E. (2014): Developing a 3-dimensional geological framework model for Alberta; Geological Society of America Annual Meeting, October 19–22, 2014, Vancouver, British Columbia, Abstracts with Programs, v. 46, no. 7, 685 p. URL <https://gsa.confex.com/gsa/2014AM/webprogram/Paper249772.html> [February 2015].

MacCormack, K.E., Atkinson, N. and Lyster, S. (2015): Bedrock topography of Alberta, Canada; Alberta Energy Regulator, AER/AGS Map 602, scale 1:1 000 000, URL <http://ags.aer.ca/publications/MAP_602.html> [March 2016].

MacCormack, K.E., Brodeur, J.J. and Eyles, C.H. (2013): Evaluating the impact of data quantity, distribution and algorithm selection on the accuracy of 3D subsurface models using synthetic grid models of varying complexity; Journal of Geographical Systems, v. 15, no. 1, p. 71–88.

Mei, S., Pana, D. and Schultz, R. (2015): Mapping formation-top offsets in southwest Alberta, Canada: methodology and results; Canadian Society of Petroleum Geologists, Geoconvention 2015, Calgary, Alberta, 5 p., URL <http://www.geoconvention.com/archives/2015/349_GC2015_Mapping_Formation-Top_Offsets_in_SW_Alberta.pdf> [March 2016].

Melnik, A. (2012): Regional hydrogeology of southwestern Saskatchewan; MSc thesis, University of Alberta, 142 p.

Mohammed, G. A., Hayashi, M., Farrow, C.R. and Takano, Y. (2013): Improved characterization of frozen soil processes in the Versatile Soil Moisture Budget model; Canadian Journal of Soil Science, v. 93, p. 511–531.

Moran, S.R. (1986): Surficial geology of the Calgary urban area; Alberta Research Council, ARC Bulletin 53, URL <http://ags.aer.ca/publications/BUL_053.html> [March 2016].

NACSN (North American Commission on Stratigraphic Nomenclature) (2005): North American Stratigraphic Code; American Association of Petroleum Geologists Bulletin, v. 89, no. 11, p. 1547–1591.

Nurkowski, J.R. (1984): Coal quality, coal rank variation and its relation to reconstructed overburden, Upper Cretaceous and Tertiary plains coals, Alberta, Canada; American Association of Petroleum Geologists Bulletin, v. 68, no. 3, p. 285–295.

Oldman Watershed Council (2010): Oldman River state of the watershed report; Lethbridge, Alberta, 284 p., URL<http://oldmanbasin.org/teams-and-projects/state-of-the-watershed-report/> [March 2015].

Osborn, G. and du Toit, G. (1991): Lateral planation of rivers as a geomorphic agent; Geomorphology, v. 4, p. 249–260.

Palombi, D.D. (2008): Regional hydrogeological characterisation of the northeastern margin in the Williston Basin; MSc thesis, University of Alberta, 196 p.

Parks, K. and Andriashek, L.D. (2009): Preliminary investigation of potential, natural hydraulic pathways between the Scollard and Paskapoo formations in Alberta: implications for coalbed methane production; Energy Resources Conservation Board, ERCB/AGS Open File Report 2009-16, 66 p., <http://www.ags.aer.ca/publications/OFR_2009_16.html> [August 2016].

Pettapiece, W.W. (1986): Physiographic subdivisions of Alberta; Land Resource Research Centre, Research Branch, Agriculture Canada, Ottawa.

PFSRB (Partners for the Saskatchewan River Basin) (2009): From the mountains to the sea: the state of the Saskatchewan River Basin; Saskatoon, Saskatchewan, 166 p., URL<http://www.saskriverbasin.ca/pages/state_of_the_basin_report.html> [March 2016].

Prior, G.J., Hathway, B., Glombick, P.M., Pană, D.I., Banks, C.J., Hay, D.C., Schneider, C.L., Grobe, M., Elgr, R. and Weiss, J.A. (2013): Bedrock geology of Alberta; Alberta Energy Regulator, AER/AGS Map 600, scale 1:1 000 000. URL <http://ags.aer.ca/publications/MAP_600.html> [March 2016].

Quartero, E.M., Bechtel, D., Leier, A.L. and Bentley, L.R. (2014): Gamma-ray normalization of shallow well-log data with applications to the Paleocene Paskapoo Formation, Alberta; Canadian Journal of Earth Sciences, v. 51, no. 5, p. 452–465.

Rawls, W.J., Brakensiek, D.L. and Saxton, K.E. (1982): Estimation of soil water properties; Transactions of the American Society of Agricultural Engineers (ASAE), v. 25, no. 5, p. 1316–1320.

Scanlon, B. R., Healy, R. W. and Cook, P. G. (2002): Choosing appropriate techniques for quantifying groundwater recharge; Hydrogeology Journal, v. 10, no. 1, p.18–39.

Schroeder, P.R., Dozier, T.S., Zappi, P.A., McEnroe, B.M., Sjostrom, J.W. and Peyton, R.L. (1994): The hydrologic evaluation of landfill performance (HELP) model: engineering documentation for version 3; U.S. Environmental Protection Agency, Office of Research and Development, 126 p.

Stein, R. (1987): A hydrogeological investigation of the origin of saline soils at Blackspring Ridge, Southern Alberta; MSc thesis, University of Alberta, 124 p.

Stein, R., and Schwartz, F.W. (1990): On the origin of saline soils at Blackspring Ridge, Alberta, Canada; Journal of Hydrology, v. 117, p. 99–131.

Stewart, S. A. (2014): Alberta springs compilation (tabular data, tab-delimited format); Alberta Energy Regulator, AER/AGS Digital Dataset 2014-0025, URL <http://ags.aer.ca/publications/DIG_2014_0025.html> [March 2016].

Tóth, J. and Almási, I. (2001): Interpretation of observed fluid potential patterns in deep sedimentary basin under tectonic compression: Hungarian Great Plain, Pannonian Basin; Geofluids, v.1, no. 1, p. 11–36.

Tóth, J. and Corbet, T. F. (1986): Post-Paleocene evolution of regional groundwater flow-systems and their relation to petroleum accumulations, Taber area, southern Alberta, Canada; Bulletin of Canadian Petroleum Geology, v. 34, no. 3, p. 339–363.

USDA (United States Department of Agriculture) (1986): Urban hydrology for small watersheds; Technical Release 55 (TR-55), URL <http://www.nrcs.usda.gov/Internet/FSE_DOCUMENTS/stelprdb1044171.pdf> [March 2016].

van der Kamp, G. and Hyashi, M. (1998): The groundwater recharge function of small wetlands in the semi-arid northern prairies; Great Plains Research: A Journal of Natural and Social Sciences, v. 8, no. 1, p. 39–56.

Appendix 1 – Methodology Workflows

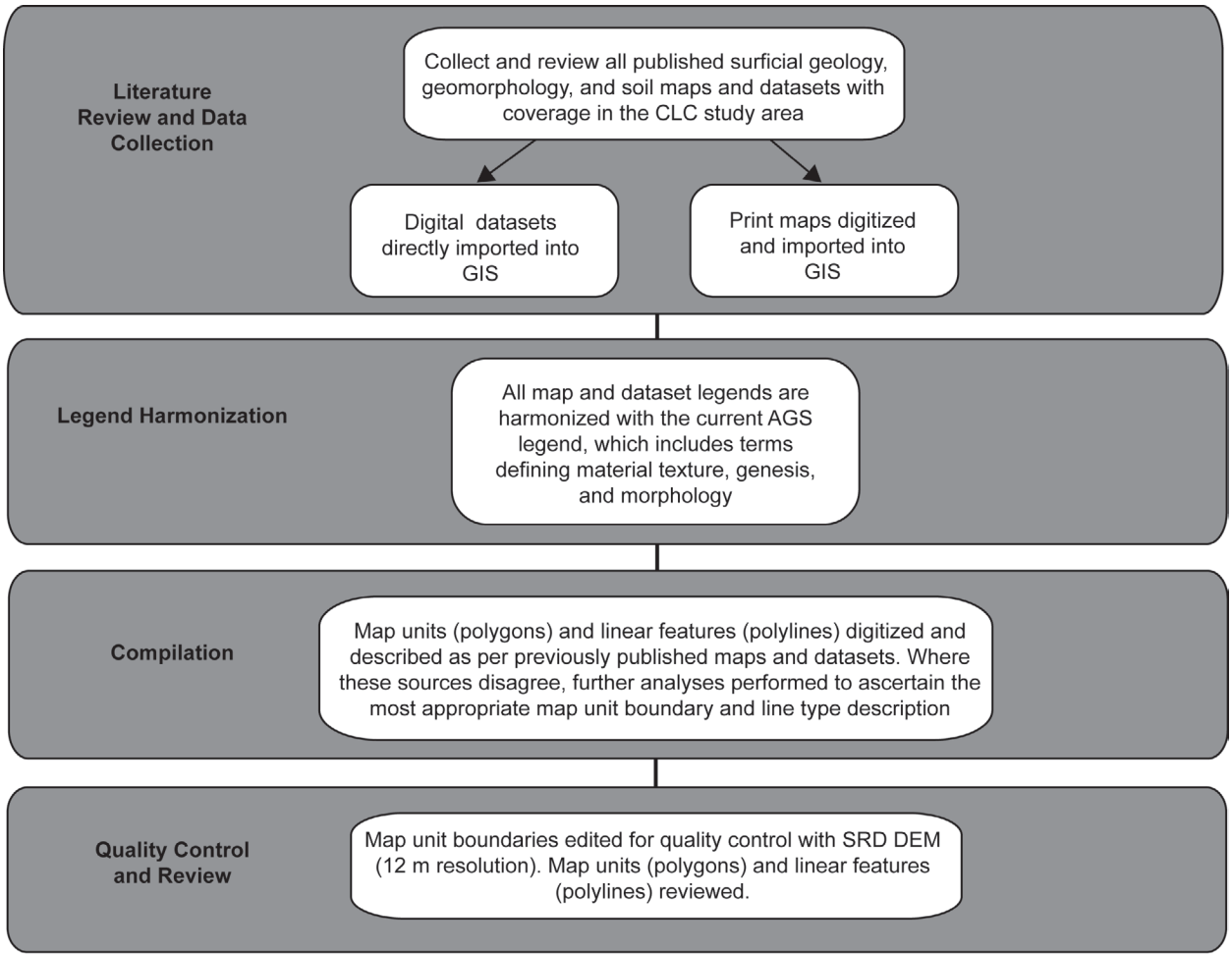

Figure A1-1. Workflow diagram for the updated surficial map compilation.

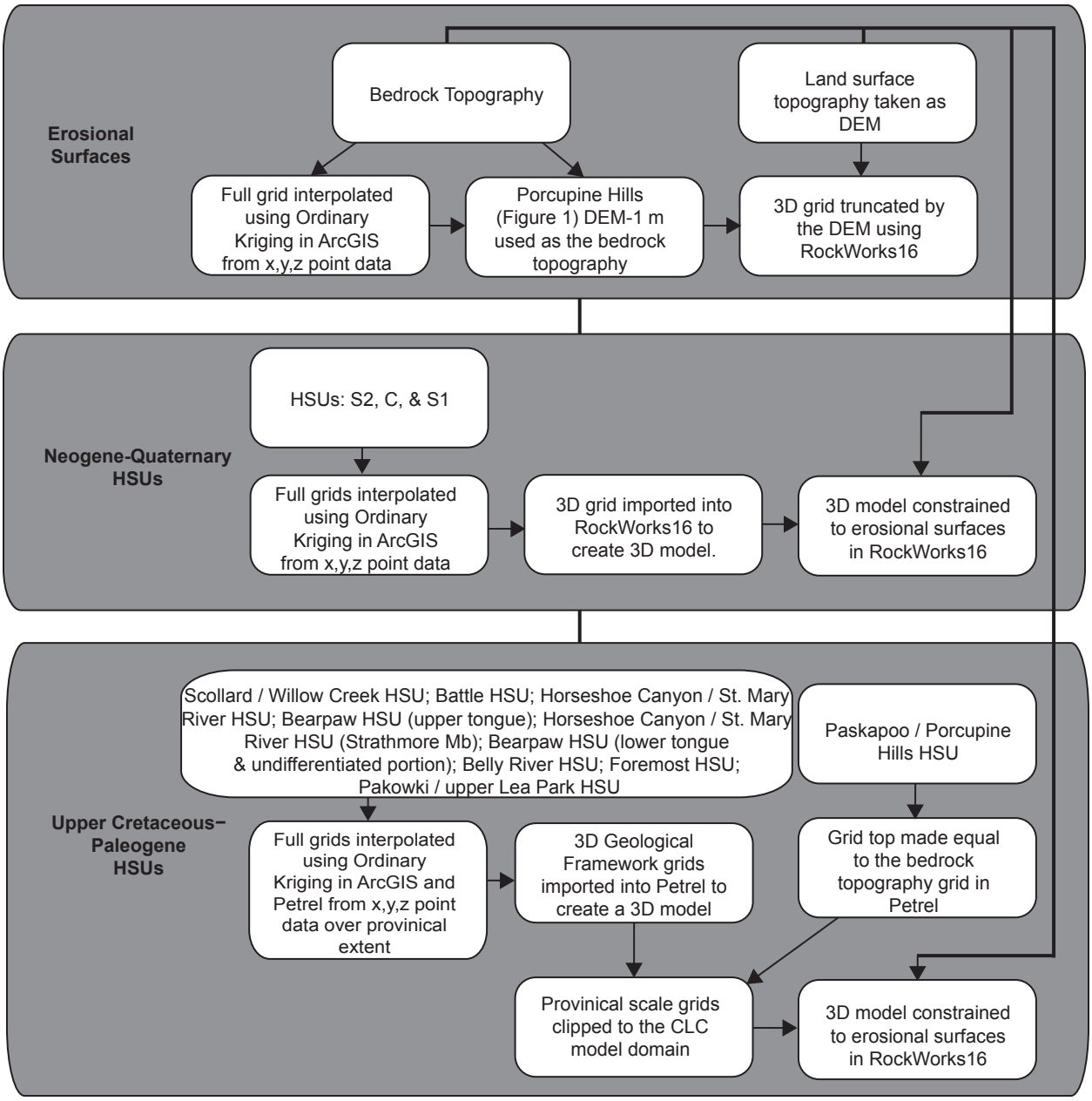

Figure A1-2. Workflow diagram for the construction of the hydrostratigraphic model.

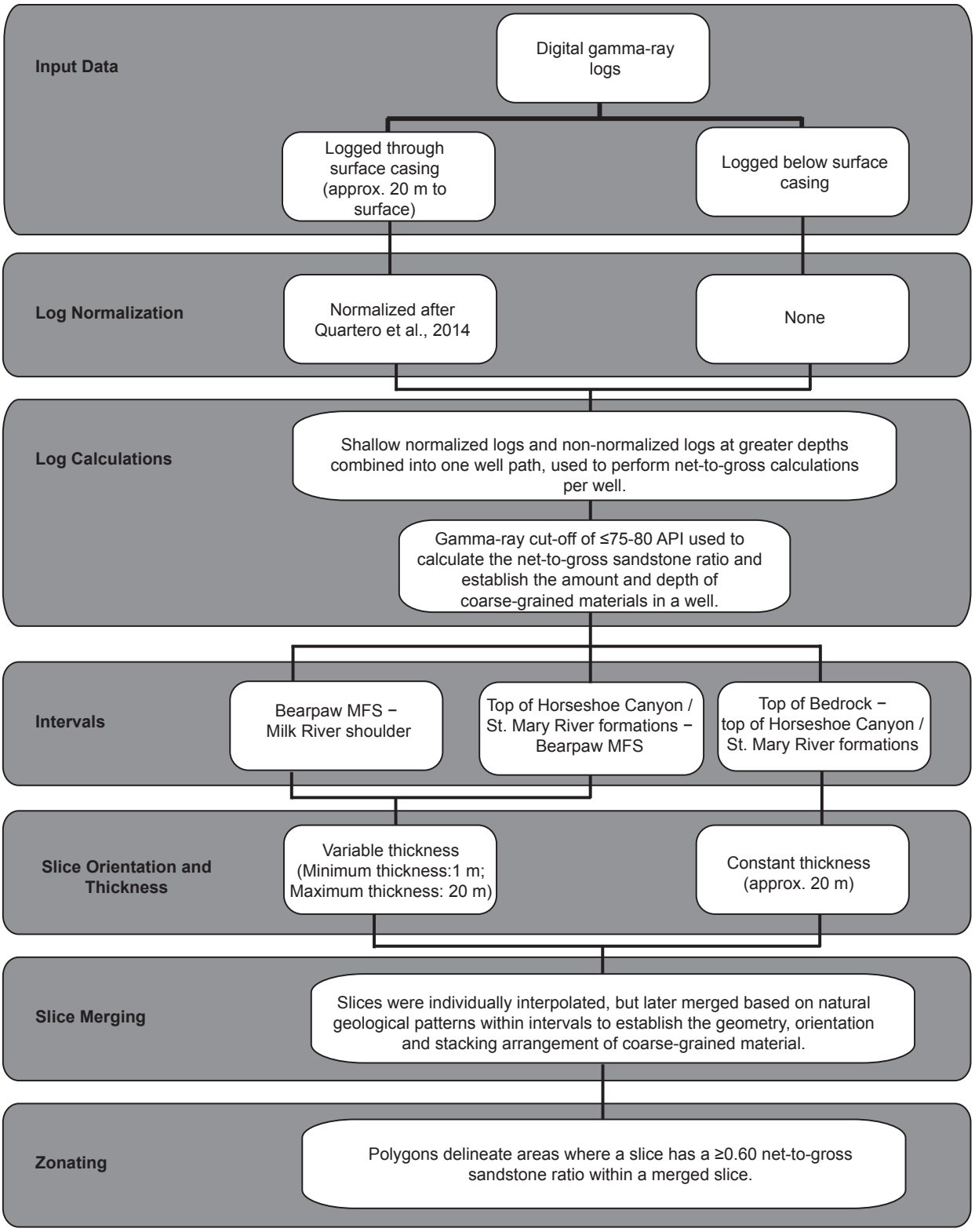

Figure A1-3. Workflow diagram for the net-to-gross sandstone slice map analysis.

Table A1-1. AWWID wells that are included or excluded as water supply wells.

Considered water supply wells	*Not* **considered water supply wells**
"Type of Work" field in AWWID	
New Well	Abandoned Holes (Test, New Well, Old Well)
Deepened	Cathodic Protection
Federal Well Survey	Chemistry
Old Well - Test	Coal Test Hole
Reconditioned	Core Hole
Reconstructed	Drill Stem Test Hole
Well Inventory	Dry Hole
Unknown	Flowing Shot Hole
Other	Oil Exploratory
	Piezometer
	Spring
	Seismic Shot Hole
	Structure Test Hole
	Test Hole
"Well Use" field in AWWID	
Commercial	Contaminant Investigation
Co-ops (Colonies)	Dewatering
Domestic (+ Industrial, + Irrigation, + Stock)	Dry Hole
Golf Courses	Geothermal
Industrial (+ Stock)	Heat Transfer
Industrial Camp	Hydrostatic Testing
Intensive Livestock Operation	Injection
Irrigation	Investigation
Municipal (+ Industrial)	Monitoring
New Well	Municipal + Observation
Old Well	Observation
Other	Piezometer
Rural Subdivision	
Standby	
Stock	
Unknown	
Water Hauling	
Well Inventory	

Table A1-2. Selection criteria for water supply wells and well counts after each step.

		Wells remaining after each step											
Step	**Action**	**F**	**BR**	**BP**	**HSC**	**BT**	**SC**	**PS**	**HSU S1**	**HSU C**	**HSU S2**	**UN**	**Total**
1	Total number of AWWID wells in CLC						34 895						
2	Removed wells not supplying water (see Table A1-1)						19 783						
3	Wells with multiple well records removed						19 268						
4	Wells with no screen information removed						14 222						
5	Wells with multiple screened intervals removed						12 189						
6	Final allocation into individual HSUs	4	40	49	1 039	27	5 591	3 703	645	719	47	325	11 864

F – Foremost HSU; BR – undifferentiated Belly River HSU; BP– Bearpaw HSU; HSC – Horseshoe Canyon / St. Mary River HSU; BT – Battle HSU; SC – Scollard / Willow Creek HSU; PS – Paskapoo / Porcupine Hills HSU; UN – unallocated (Most fall outside the coverage of the geomodel grids; some lie above the resampled 400 m HSU S2 grid, which represents the land surface)

Table A1-3. Selection criteria for AWWID wells with hydraulic information and well counts after each step.

		Wells remaining after each step											
Step	**Action**	**F**	**BR**	**BP**	**HSC**	**BT**	**SC**	**PS**	**HSU S1**	**HSU C**	**HSU S2**	**UN**	**Total**
1	Total number of AWWID wells in CLC						34 895						
2	Wells with multiple well records removed						34 504						
3	Wells with no screen information removed						14 823						
4	Wells with multiple screened intervals removed						12 764						
5	Wells without water level information removed	4	43	53	999	26	5 462	3 635	678	704	46	338	11 650
6	Wells with multiple water level readings differing by more than 1 m removed	4	43	53	992	26	5 397	3 607	678	696	46	—	11 542
7	Flowing artesian wells removed	4	43	51	979	26	5 351	3 598	671	684	46	—	11 453
8	Outliers removed during potentiometric surface mapping, (including wells located in the Porcupine Hills uplands for Scollard / Willow Creek HSU and Paskapoo / Porcupine Hills HSU)	4	36	51	938	26	4 640	2 546	666	670	46	—	9 623

F – Foremost HSU; BR – undifferentiated Belly River HSU; BP – Bearpaw HSU; HSC – Horseshoe Canyon / St. Mary River HSU; BT – Battle HSU; SC – Scollard / Willow Creek HSU; PS – Paskapoo / Porcupine Hills HSU; UN – unallocated (Most fall outside the coverage of the geomodel grids; some lie above the resampled 400 m HSU S2 grid, which represents the land surface)

Table A1-4. Selection criteria for DSTs from oil and gas wells and number of DSTs remaining after each step.

		Wells remaining after each step										
Step	**Action**	**F**	**BR**	**BP**	**HSC**	**BT**	**SC**	**PS**	**HSU S1**	**HSU C**	**HSU S2**	**Total**
1	Total number of CLC DSTs						18 235					
2	DSTs without intervals and those below the undifferentiated Belly River HSU removed						885					
3	DSTs without pressure maximum removed						330					
4	Wells straddling multiple HSUs, or having poor quality code (F), or large intervals removed	110	111	1	7	—	—	—	—	—	—	230
5	Manual assessment of specific DST parameters (e.g., flow and shut-in times, recovery and blow description) including application of cumulative interference index. DSTs interpreted to be not an adequate measure of formation pressure are removed.	49	51	1	3	—	—	—	—	—	—	105

F – Foremost HSU; BR – undifferentiated Belly River HSU; BP– Bearpaw HSU; HSC – Horseshoe Canyon / St. Mary River HSU; BT – Battle HSU; SC – Scollard / Willow Creek HSU; PS – Paskapoo / Porcupine Hills HSU

Table A1-5. Selection criteria for AWWID chemical analyses and number of analyses after each step.

		Wells remaining after each step											
Step	**Action**	**F**	**BR**	**BP**	**HSC**	**BT**	**SC**	**PS**	**HSU S1**	**HSU C**	**HSU S2**	**UN**	**Total**
1	Total number of AWWID chemical analysis in CLC						8 870						
2	Chemical analyses from wells without screen interval information removed						2 792						
3	Chemical analyses from wells with multiple screen intervals removed						1 470						
4	Chemical analyses from wells with screen interval >15 m removed						1 123						
5	Incomplete chemical analysis and ones that have charge balance error outside of ±10% removed						924						
6	Allocation of remaining chemical analysis	0	6	2	123	1	424	151	68	104	7	38	924
7	Exact duplicates and multiple samples per location removed	0	5	2	90	1	280	104	48	92	5	—	627
8	Outliers removed during mapping of each HSU	0	5	2	86	1	193	91	42	76	4	—	500

F – Foremost HSU; BR – undifferentiated Belly River HSU; BP– Bearpaw HSU; HSC – Horseshoe Canyon / St. Mary River HSU; BT – Battle HSU; SC – Scollard / Willow Creek HSU; PS – Paskapoo / Porcupine Hills HSU; UN – unallocated (Most fall outside the coverage of the geomodel grids; some lie above the resampled 400 m HSU C2 grid, which represents the land surface)

Table A1-6. Selection criteria for formation water from oil and gas wells and number of analyses after each step.

		Wells remaining after each step											
Step	**Action**	**PK**	**F**	**BR**	**BP**	**BP(U)**	**HSC**	**BT**	**SC**	**PS**	**HSU S2,C,S1**	**UN**	**Total**
1	Total number of raw chemical analysis from AccuMap in CLC						4 172						
2	Chemical analyses without test interval information removed						3758						
3	Chemical analyses with test interval >15m, removed						1634						
4	Chemical analyses with charge balance error outside of ±10% removed						758						
5	Identifying contaminated samples and allocation of remaining chemical analysis	29	241	176		5	26	0	5	0	0	276	758
6	Interactive culling, picking the best representative sample in multisample locations	0	175	128		5	20	0	2	0	0	—	330
7	Outliers removed during mapping of each HSU	0	12	9	1	1	0	0	2	0	0	—	25

PK – Pakowki / upper Lea Park HSU; F – Foremost HSU; BR – undifferentiated Belly River HSU; BP– Bearpaw HSU; BP(U) – Bearpaw HSU (upper tongue); HSC – Horseshoe Canyon / St. Mary River HSU; BT – Battle HSU; SC – Scollard / Willow Creek HSU; PS – Paskapoo / Porcupine Hills HSU; UN – unallocated (outside of CLC area and coverage of the geomodel grids)

Appendix 2 – Hydrostratigraphic Model Data Distribution and Gridded Surface Statistics

Table A2-1. Number of subsurface hydrostratigraphic assignments used in the CLC model.

Model HSU	Number of hydrostratigraphic assignments	Number of stratigraphic picks
S2	1 241	
C	15 134	
S1	3 595	
Bedrock Topography		17 252
Paskapoo / Porcupine Hills HSU		n/a*
Scollard / Willow Creek HSU		3 196†
Battle HSU		8 008†
Horseshoe Canyon / St. Mary River HSU		9 162†
Bearpaw HSU (upper tongue)		5 039†
Horseshoe Canyon / St. Mary River (Strathmore Mb)		3 557†
Bearpaw HSU (lower tongue & undifferentiated portion)		2 639†
Undifferentiated Belly River HSU (excluding Foremost HSU)		15 267†
Foremost HSU		12 303†
Pakowki / upper Lea Park HSU		19 445†

* The number of stratigraphic picks for Paskapoo / Porcupine Hills HSU is not reported because the top of the unit was made equal to the bedrock topography.

† The number of stratigraphic picks includes all picks used to create the top surface for this unit in the Geological Framework of Alberta model, which extends beyond the area of the CLC.

Table A2-2. Hydrostratigraphic model: grid elevation, thickness, and error statistics.*

	Elevation (m asl)			Thickness (m)			
Model HSU	**Min**	**Max**	**RMSE† (m)**	**Min**	**Max**	**Avg**	**Std. Dev**
DEM	768.0	1 800.0	0	n/a§	n/a§	n/a§	n/a§
S2	773.0	1 417.0	n/a‡	0	15.0	4.9	1.2
C	766.0	1 800.0	5.6	0	159.0	17.3	12.0
S1	753.0	1 400.0	3.9	0	45.0	5.4	2.1
Bedrock Topography	751.0	1 799.0	7.2	n/a§	n/a§	n/a§	n/a§
Paskapoo / Porcupine Hills HSU	962.0	1 799.0	n/a‡	0	602.0	103.4	28.4
Scollard / Willow Creek HSU	848.0	1 413.0	21.5	0	1 576.0	408.6	201.8
Battle HSU	460.0	1014.0	4.2	0	13.0	8.8	1.2
Horseshoe Canyon / St. Mary River HSU	−297.0	1 388.0	5.3	0	763.0	341.0	100.1
Bearpaw HSU (upper tongue)	−316.0	748.0	8.0	0	103.0	40.1	9.9
Horseshoe Canyon / St. Mary River (Strathmore Mb)	−343.0	635.0	4.7	0	138.0	39.6	11.3
Bearpaw HSU (lower tongue & undifferentiated portion)	−850.0	1267.0	5.0	0	367.0	144.4	48.2
undifferentiated Belly River HSU (excluding Foremost HSU)	−1 092.0	1 155.0	8.7	0	239.0	130.1	15.4
Foremost HSU	−1 254.0	915.0	8.0	101.0	420.0	208.8	26.9
Pakowki / upper Lea Park HSU	−1 426.0	805.0	9.7	0	134.0	36.8	9.4

* Grid statistics are for discrete grids and do not include nodes where the grid is equal to 0 m thick.

† The root mean square error (RMSE) is a global summary statistic value for a 3D grid used to compare how similar interpolated grid values are to the original input data. The RMSE values reported for the bedrock HSUs are for their provincial extent, which extend outside the CLC.

‡ The RMSE for HSU S2 and the Paskapoo / Porcupine Hills HSU is not reported because the top of HSU S2 was made equal to the DEM and the Paskapoo / Porcupine Hills HSU was made equal to the bedrock topography.

§ The thickness of the erosional surfaces (DEM and bedrock topography) is not reported because there is no unit base.

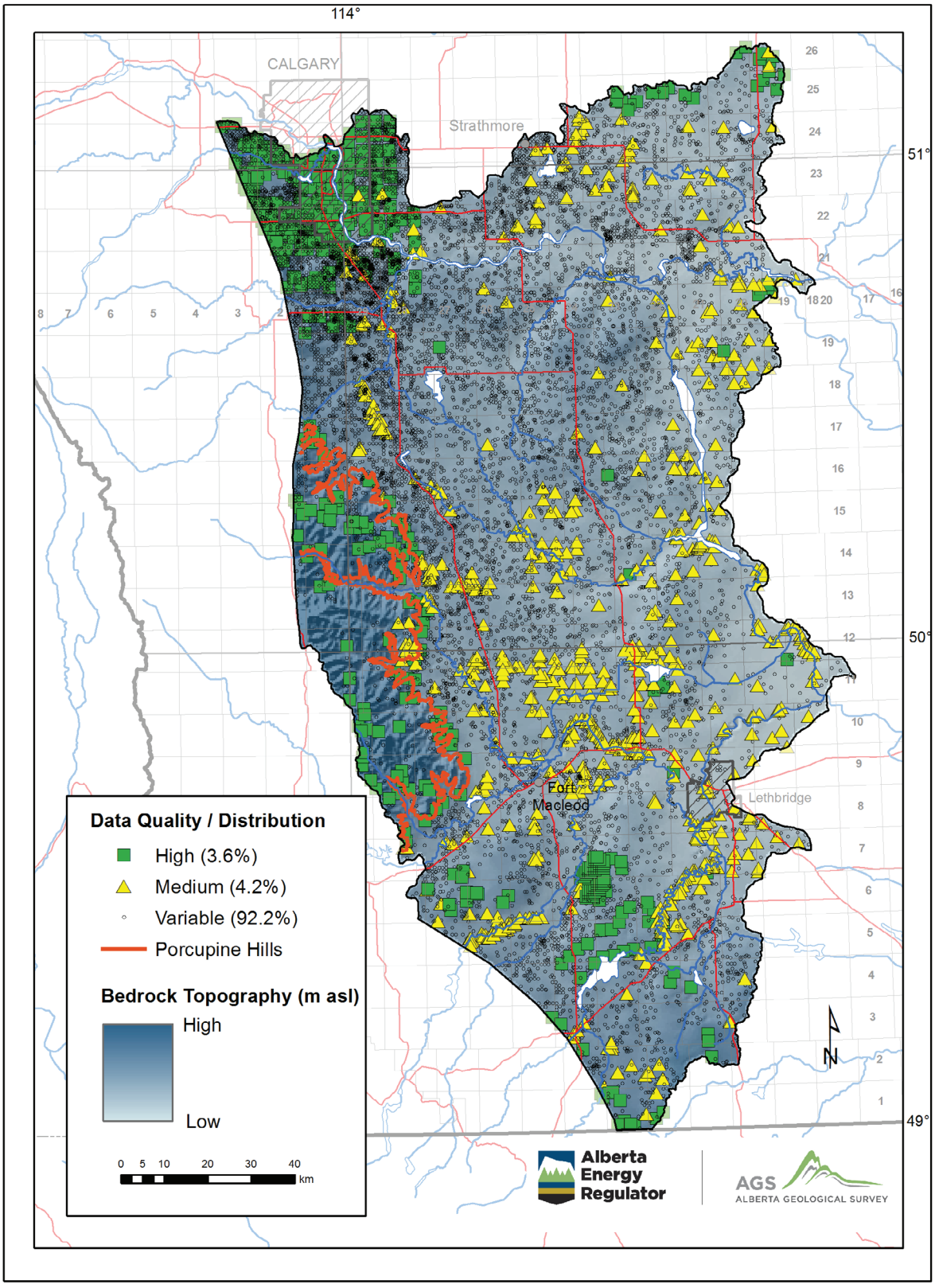

Figure A2-1. Data quality and distribution for the bedrock topography grid (blue).

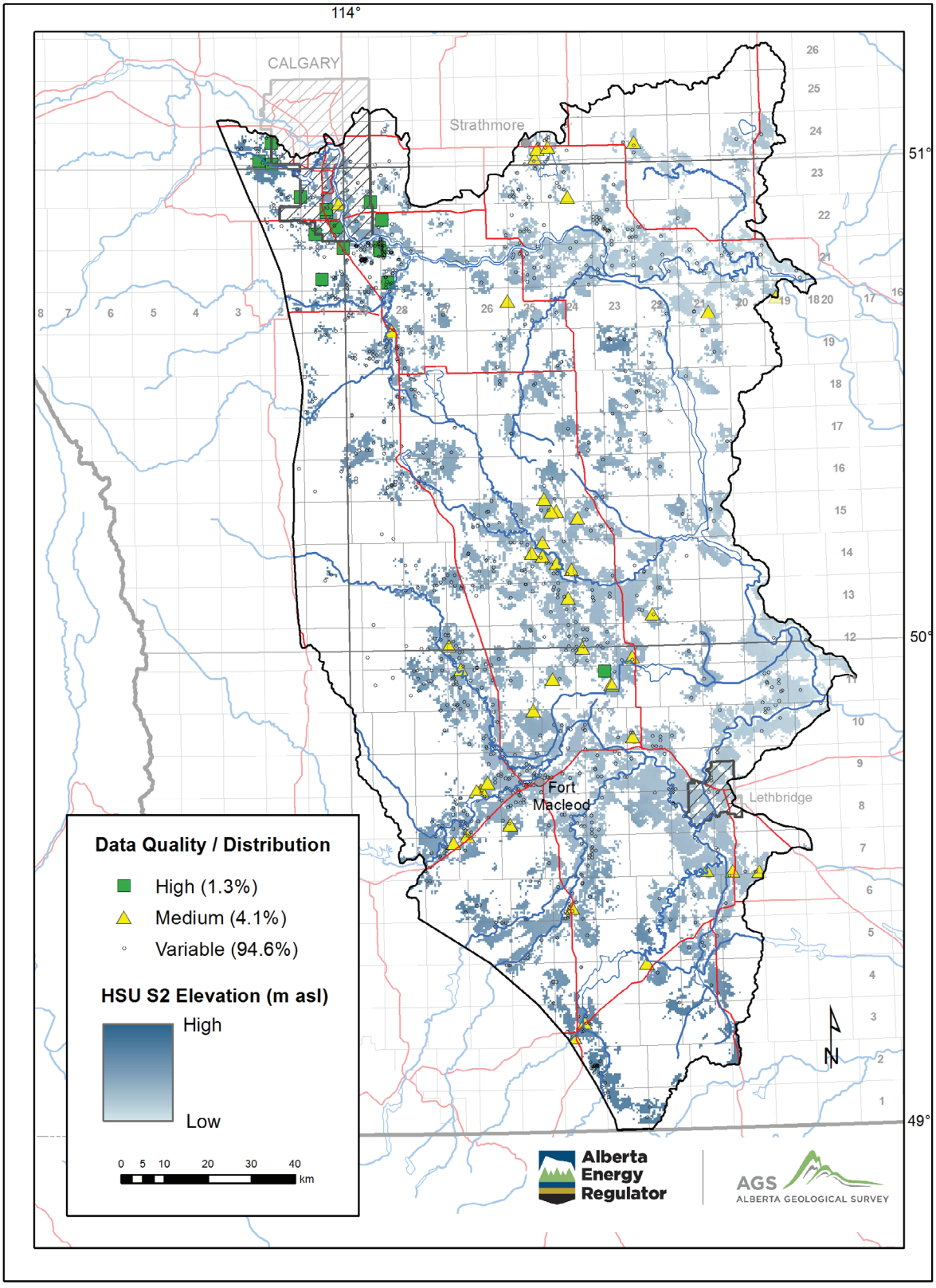

Figure A2-2. Data quality and distribution for the HSU S2 grid (blue).

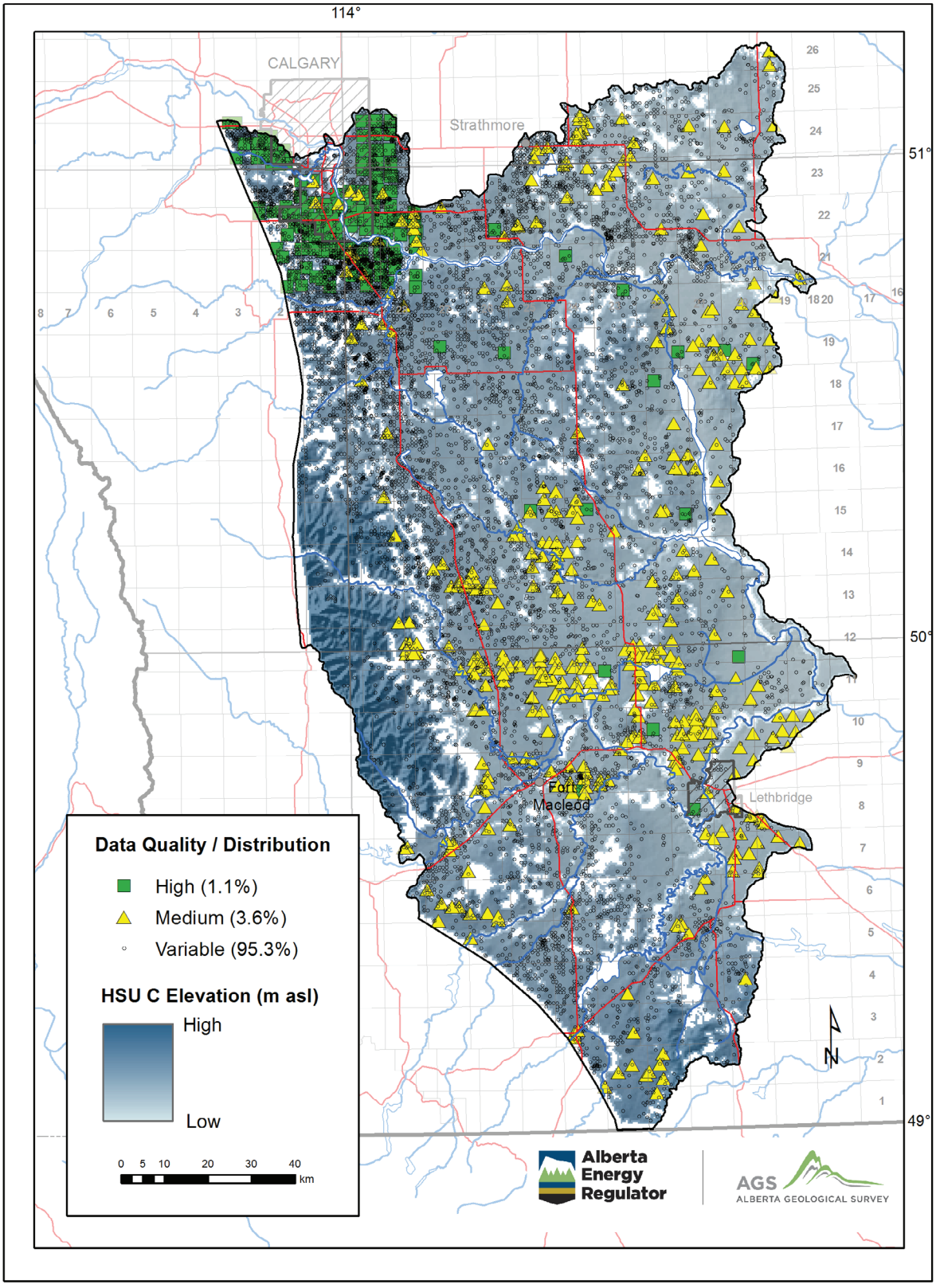

Figure A2-3. Data quality and distribution for the HSU C grid (blue).

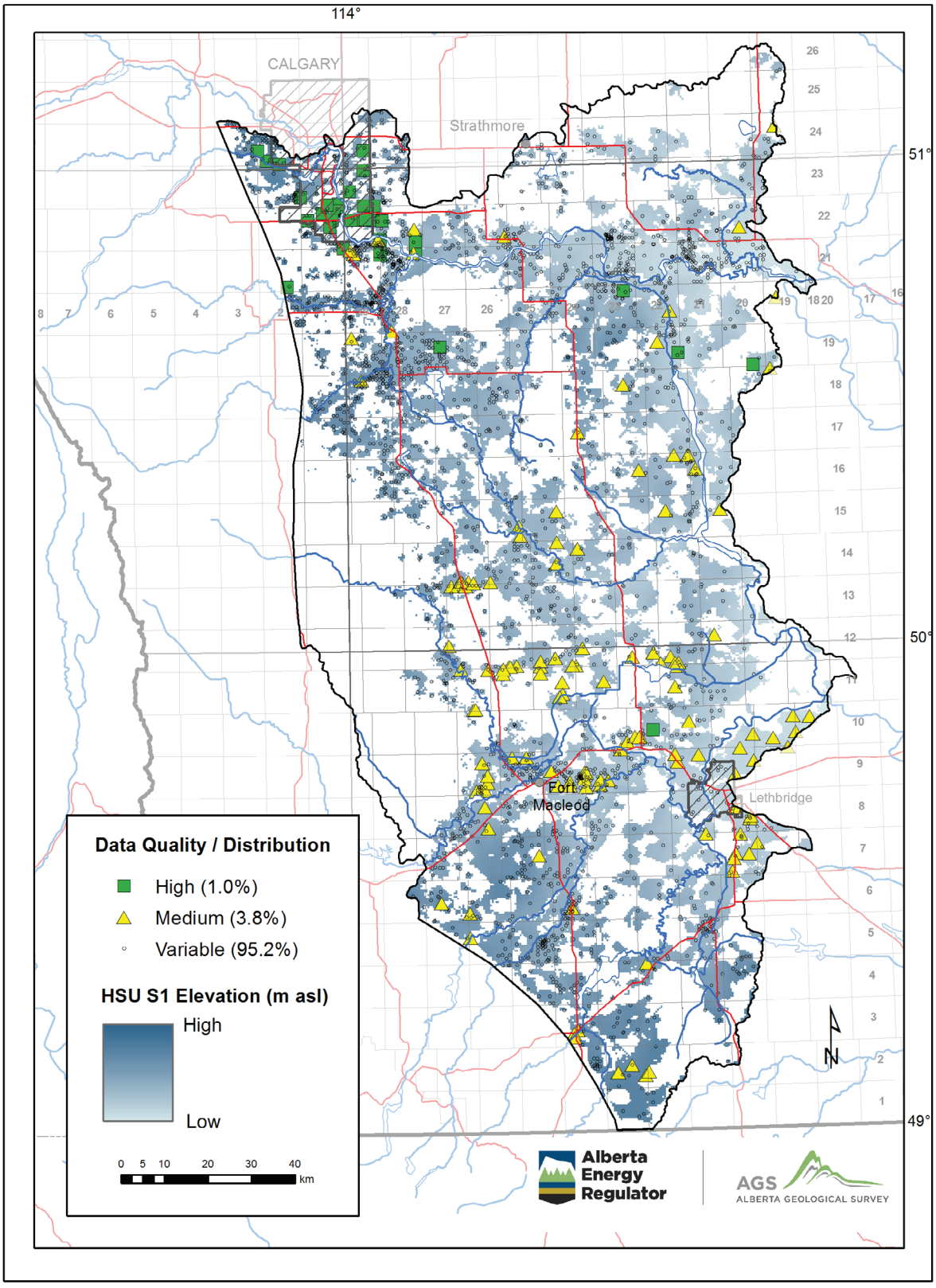

Figure A2-4. Data quality and distribution for the HSU S1 grid (blue).

Table A2-3. Grid errors between measured data points and interpolated potentiometric surface and maps of TDS concentration.

Model HSU	Potentiometric Surface RMSE (m)	TDS RMSE (mg/L)
S2	n/a*	n/a*
C	3.8	476
S1	1.5	46
Paskapoo / Porcupine Hills HSU	7.1	189
Scollard / Willow Creek HSU	3.8	442
Battle HSU	n/a*	n/a*
Horseshoe Canyon / St. Mary River HSU	3.5	644
Bearpaw HSU (upper tongue)	n/a*	n/a*
Horseshoe Canyon / St. Mary River (Strathmore Mb)	n/a*	n/a*
Bearpaw HSU (lower tongue) & Bearpaw HSU (undifferentiated)	2.4	n/a*
undifferentiated Belly River HSU (excluding Foremost HSU)	10.8 (surface from AWWID wells) 8.5 (surface from oil and gas wells)	n/a*
Foremost HSU	n/a* for AWWID wells 3.0 (surface from oil and gas wells)	n/a*
Pakowki / upper Lea Park HSU	n/a*	n/a*

* Surface not interpolated due to lack of data

Appendix 3 – Hydrostratigraphic and Hydrogeological Maps

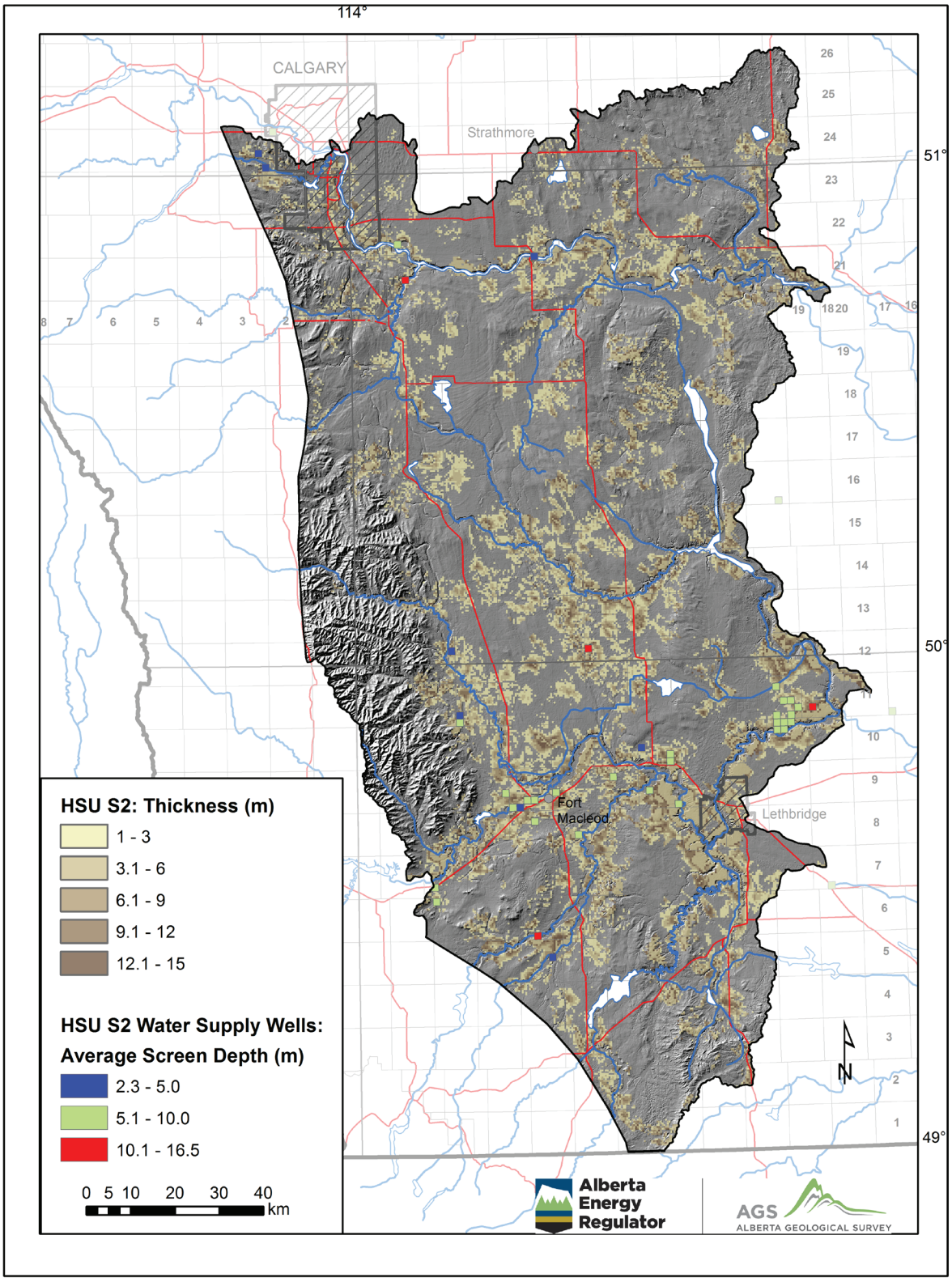

Figure A3-1. Thickness and extent of HSU S2 as well as average screen depth per ATS section for water supply wells.

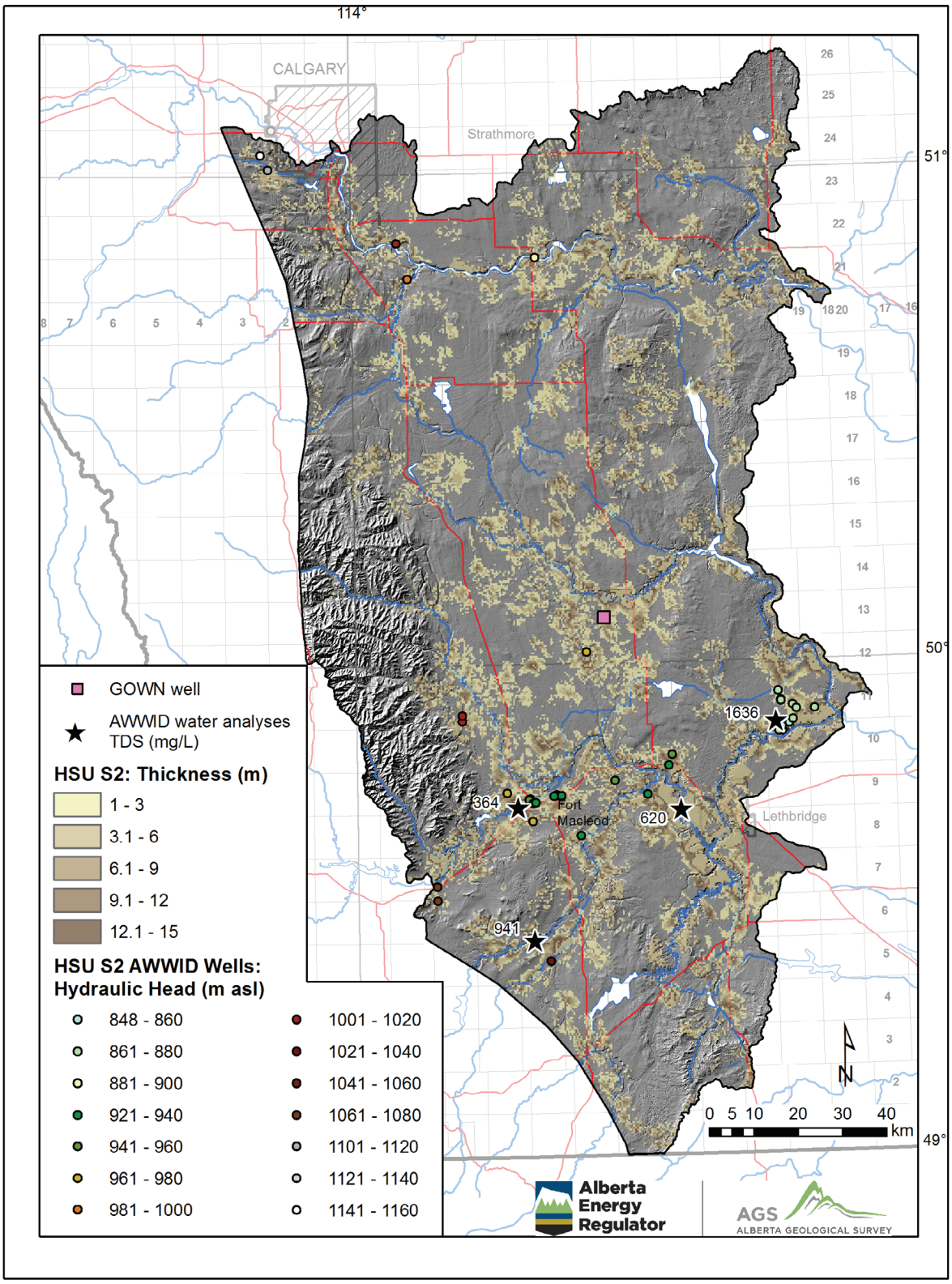

Figure A3-2. Hydraulic heads and chemical analyses from available HSU S2 wells. No potentiometric surface or map of TDS concentration was created for HSU S2 due to the lack of data.

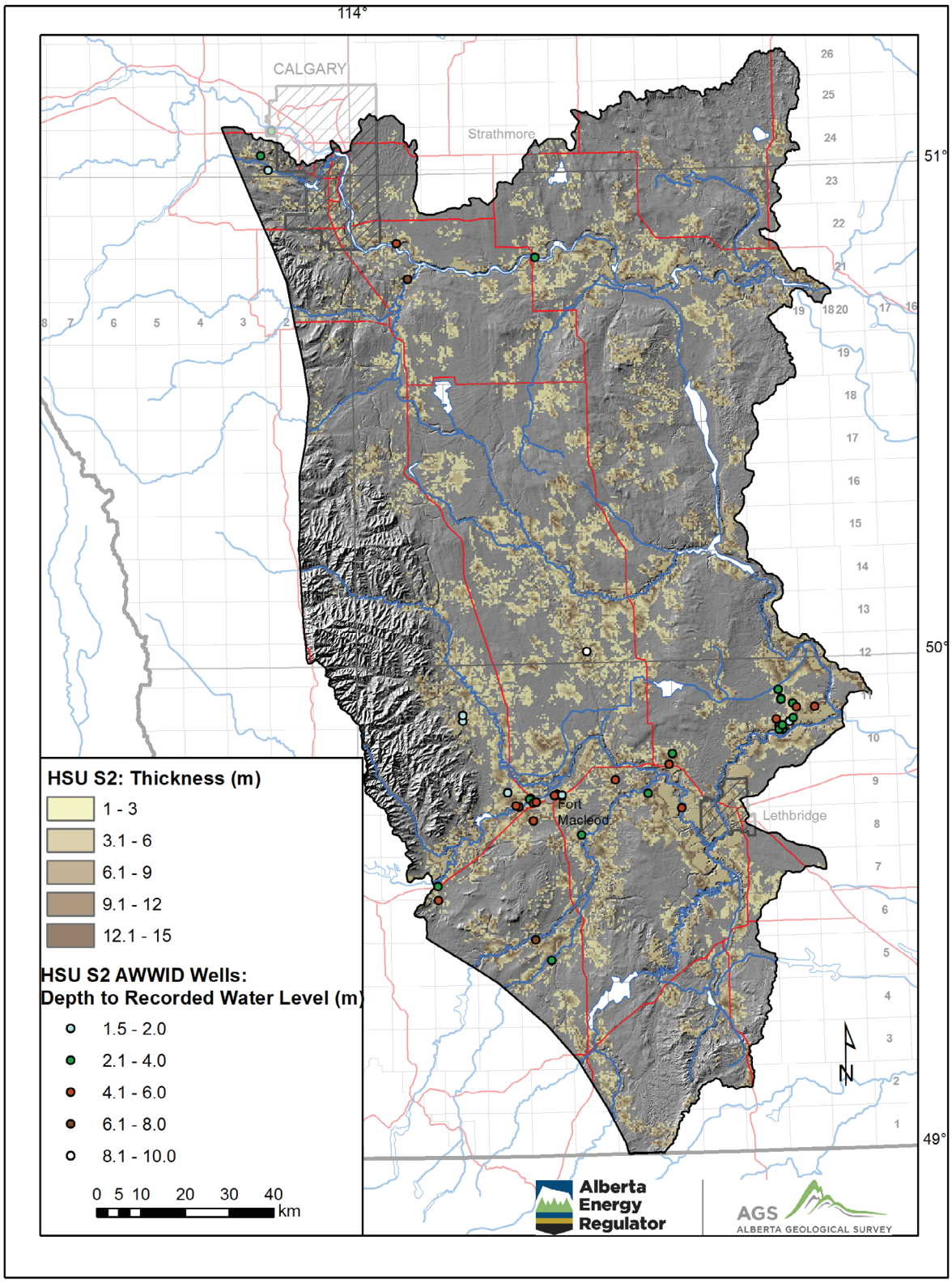

Figure A3-3. Depth to recorded water level from available HSU S2 wells.

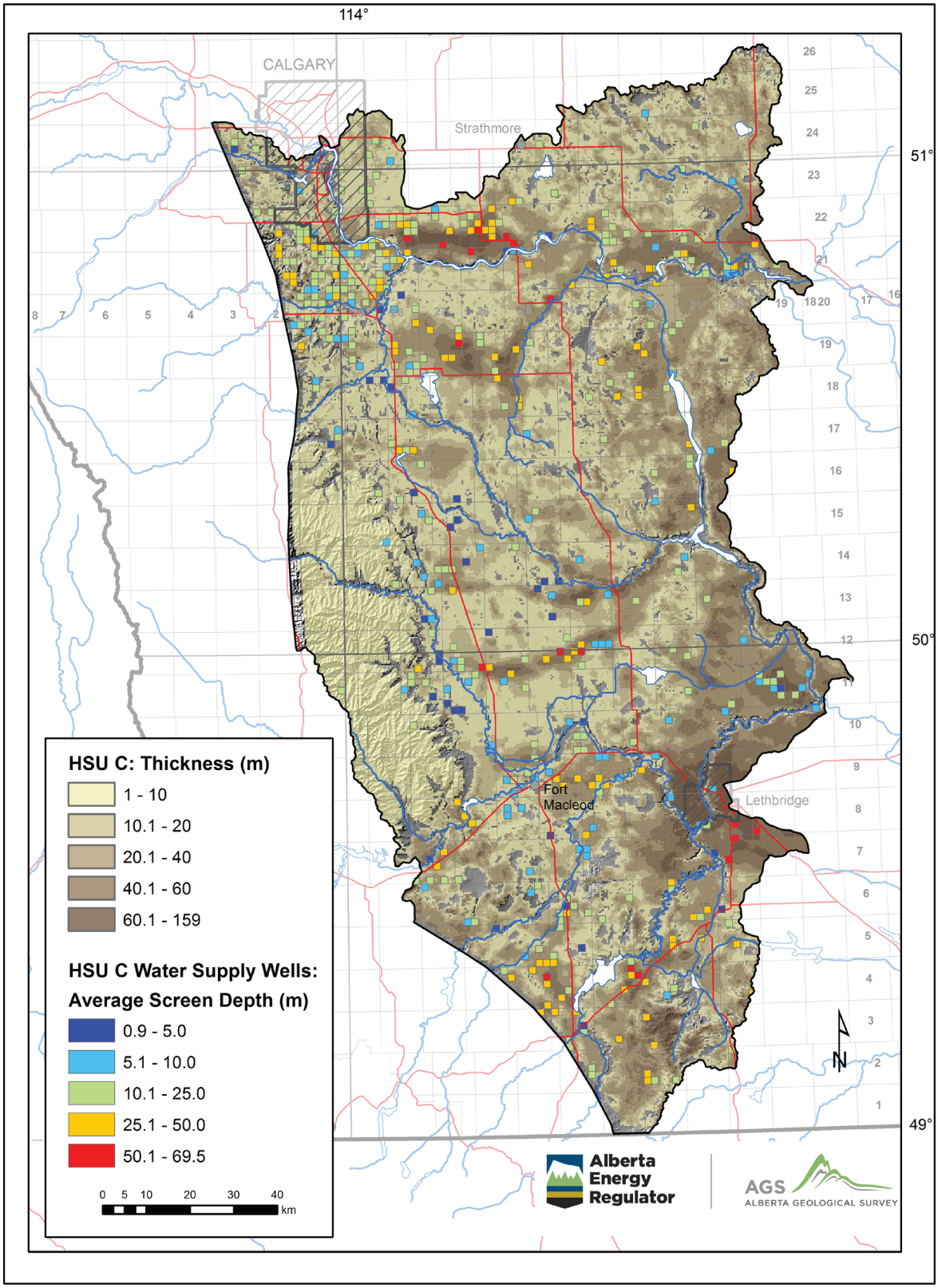

Figure A3-4. Thickness and extent of HSU C as well as average screen depth per ATS section for water supply wells. Dots represent wells where coarse-grained material was found within the HSU C. Most water supply wells in the HSU C are found in areas where inter-till material was recognized.

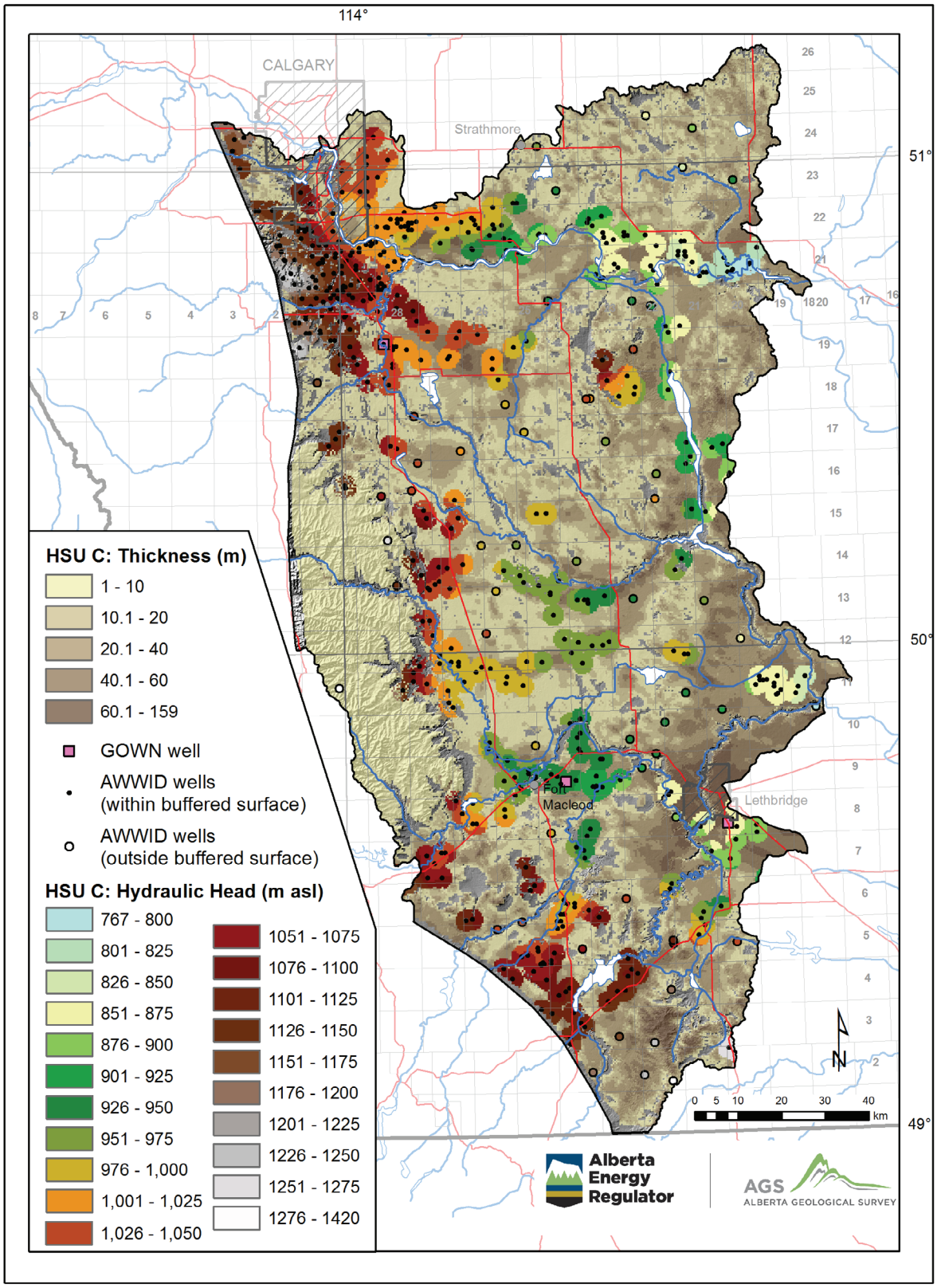

Figure A3-5. Potentiometric surface for HSU C. Note that the connection of the coarse-grained lenses was not mapped within HSU C.

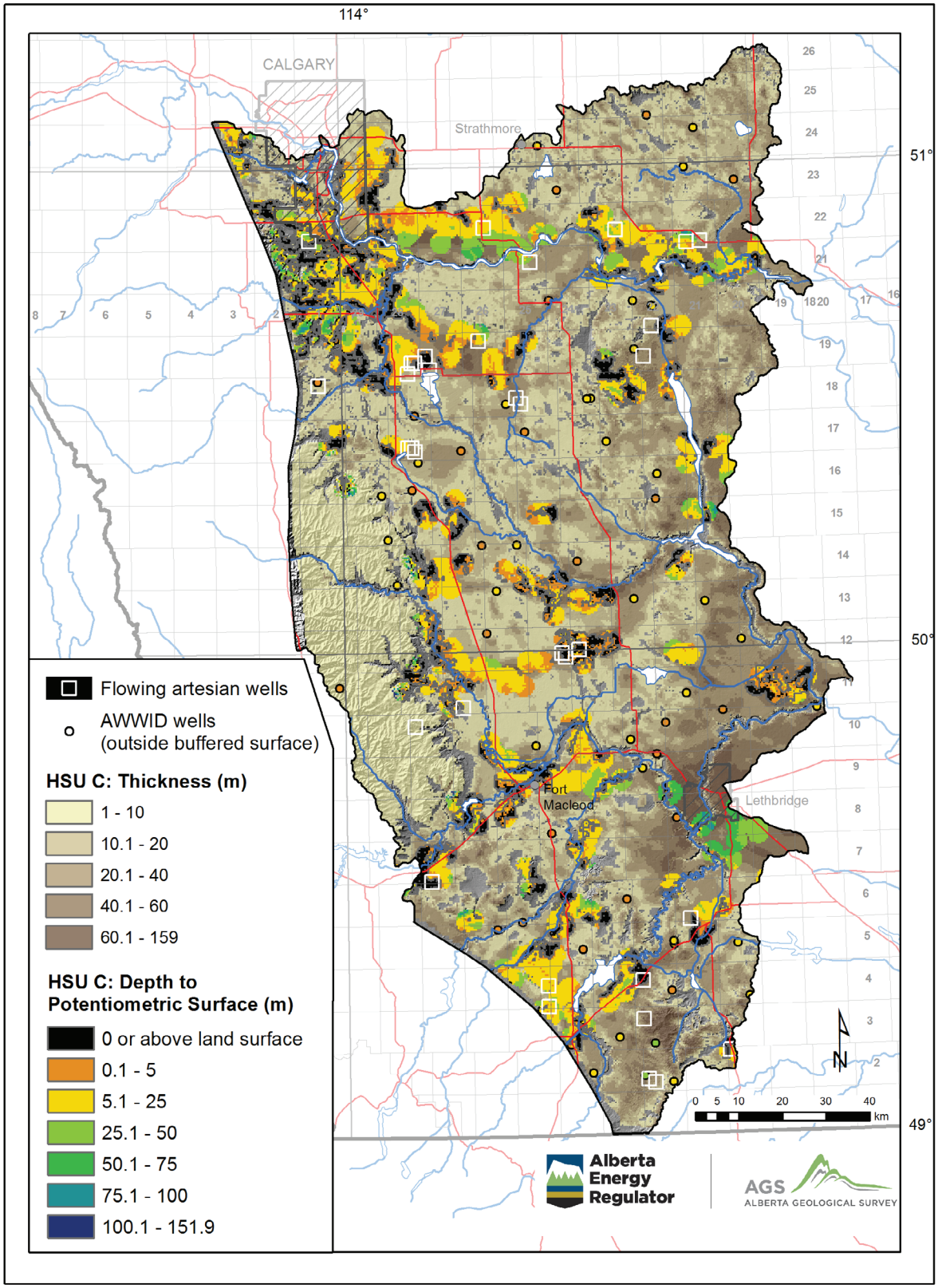

Figure A3-6. Depth to potentiometric surface for HSU C. Confined conditions are restricted primarily to those areas showing depth to potentiometric surface above the ground surface (i.e., black areas). Locations of flowing artesian wells are shown for comparison. Other areas are unconfined, with the potentiometric surface below the top of the unit.

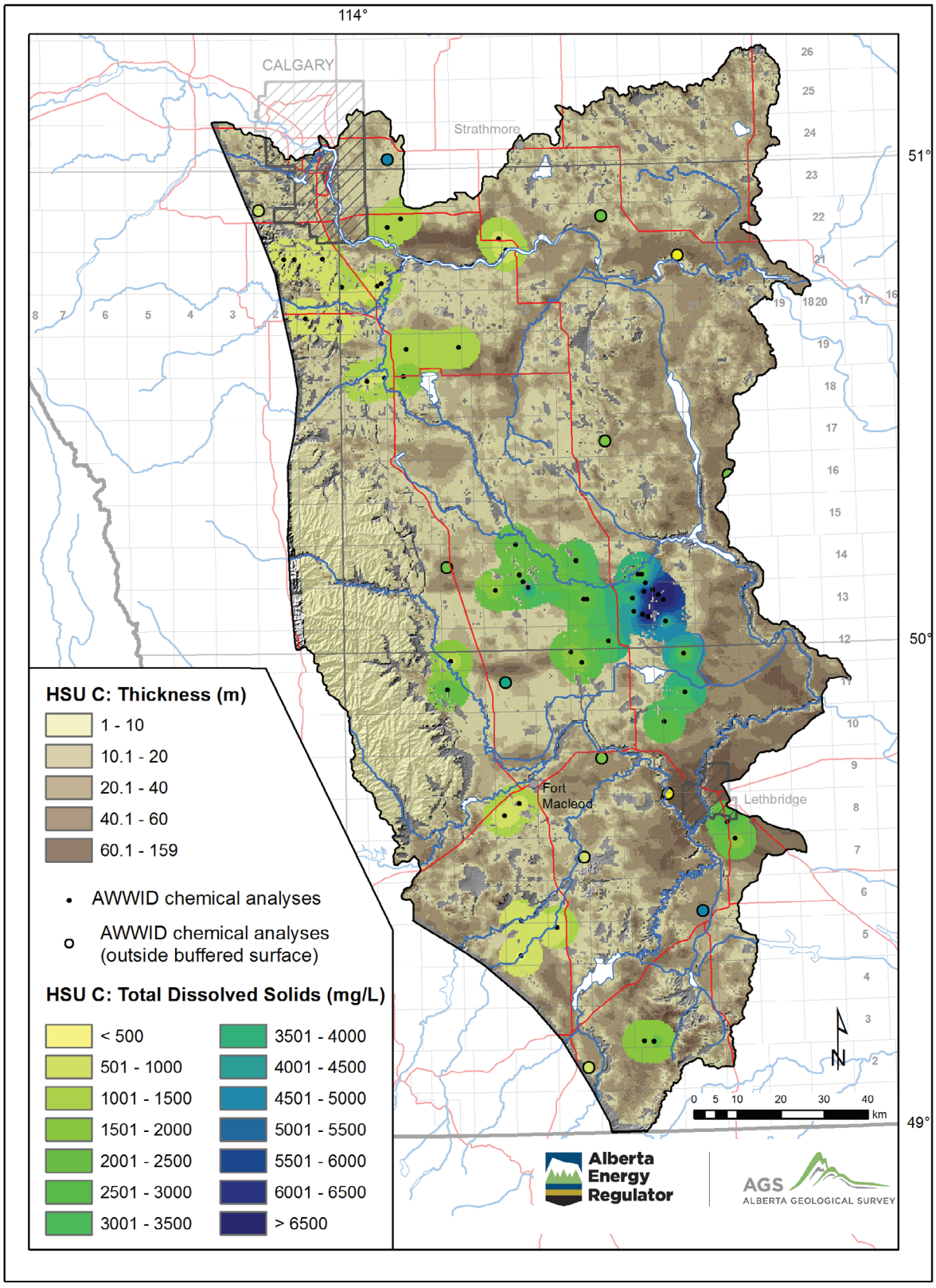

Figure A3-7. Concentration of TDS in HSU C.

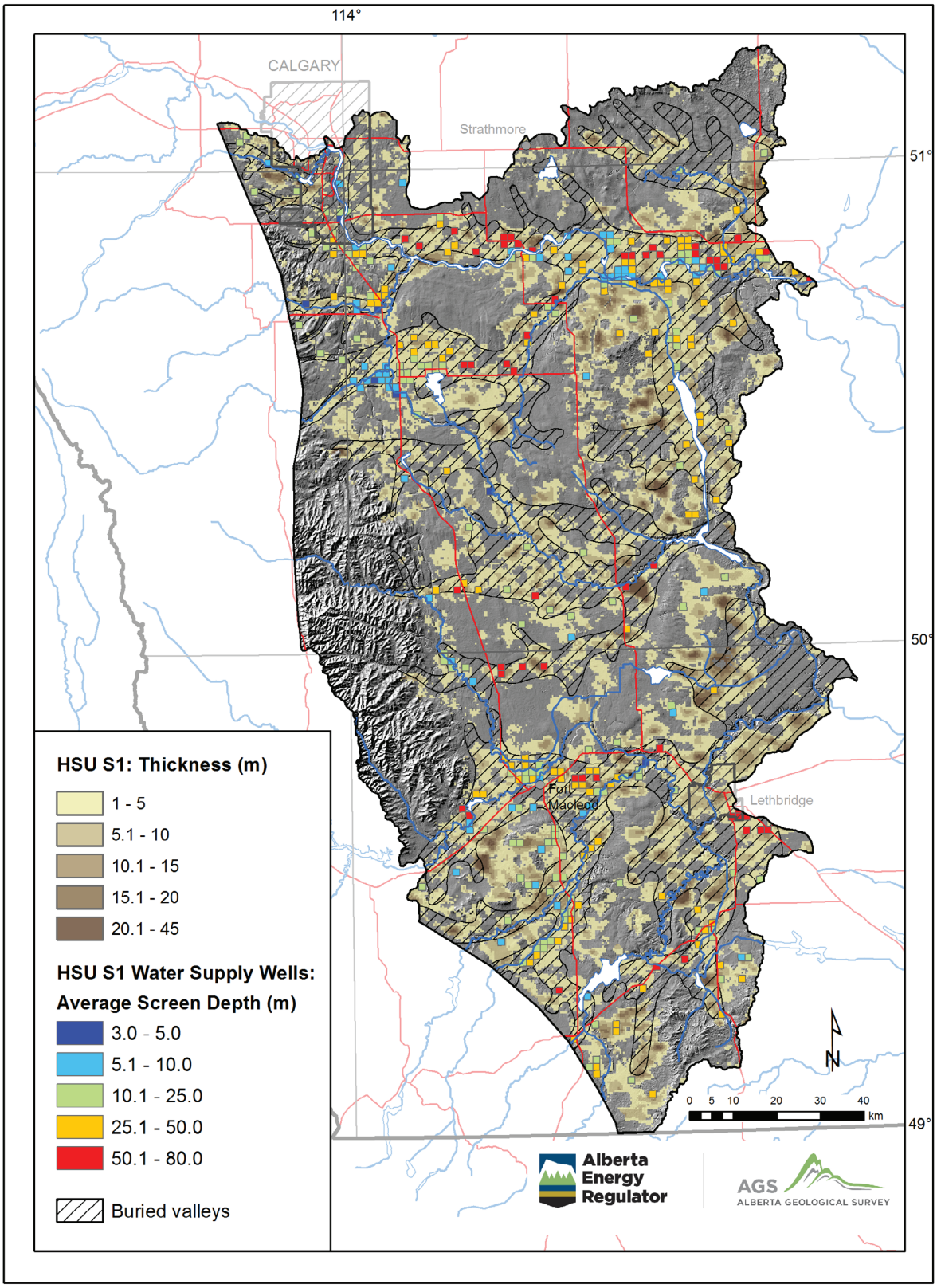

Figure A3-8. Thickness and extent of HSU S1 as well as average screen depth per ATS section for water supply wells.

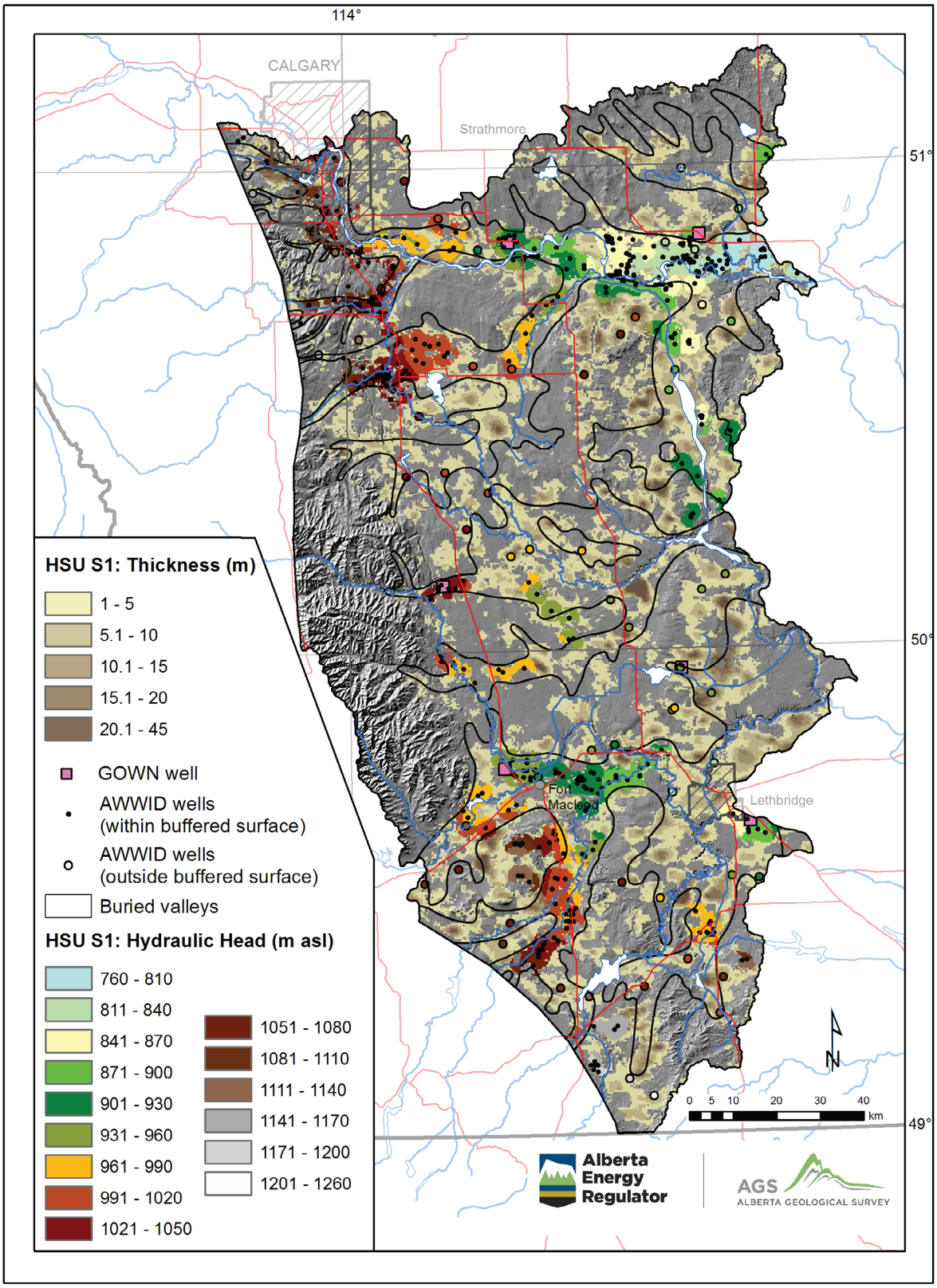

Figure A3-9. Potentiometric surface for HSU S1.

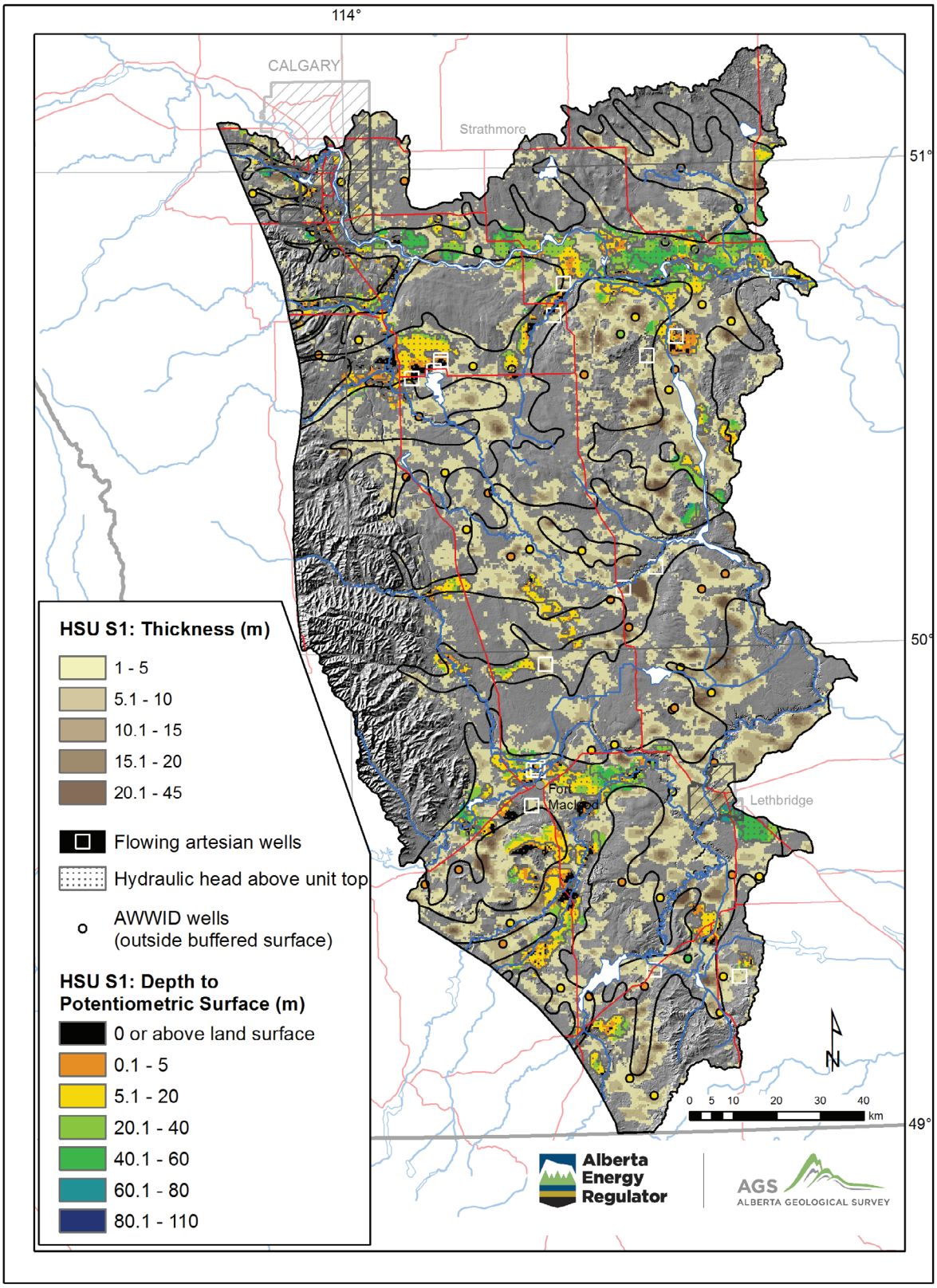

Figure A3-10. Depth to potentiometric surface for HSU S1. Black areas are where the interpolated surface is above ground. Locations of flowing artesian wells are shown for comparison.

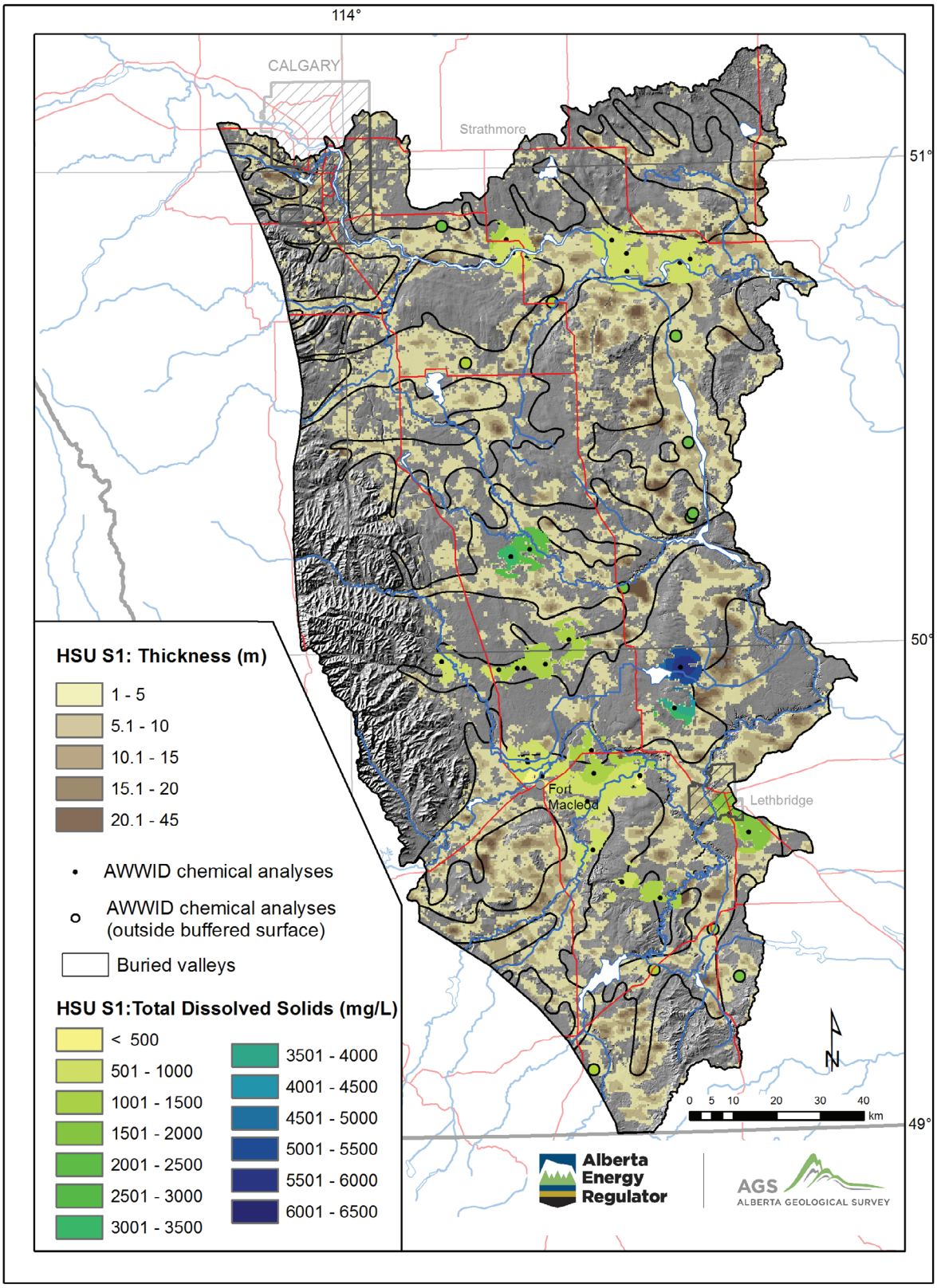

Figure A3-11. Concentration of TDS in HSU S1.

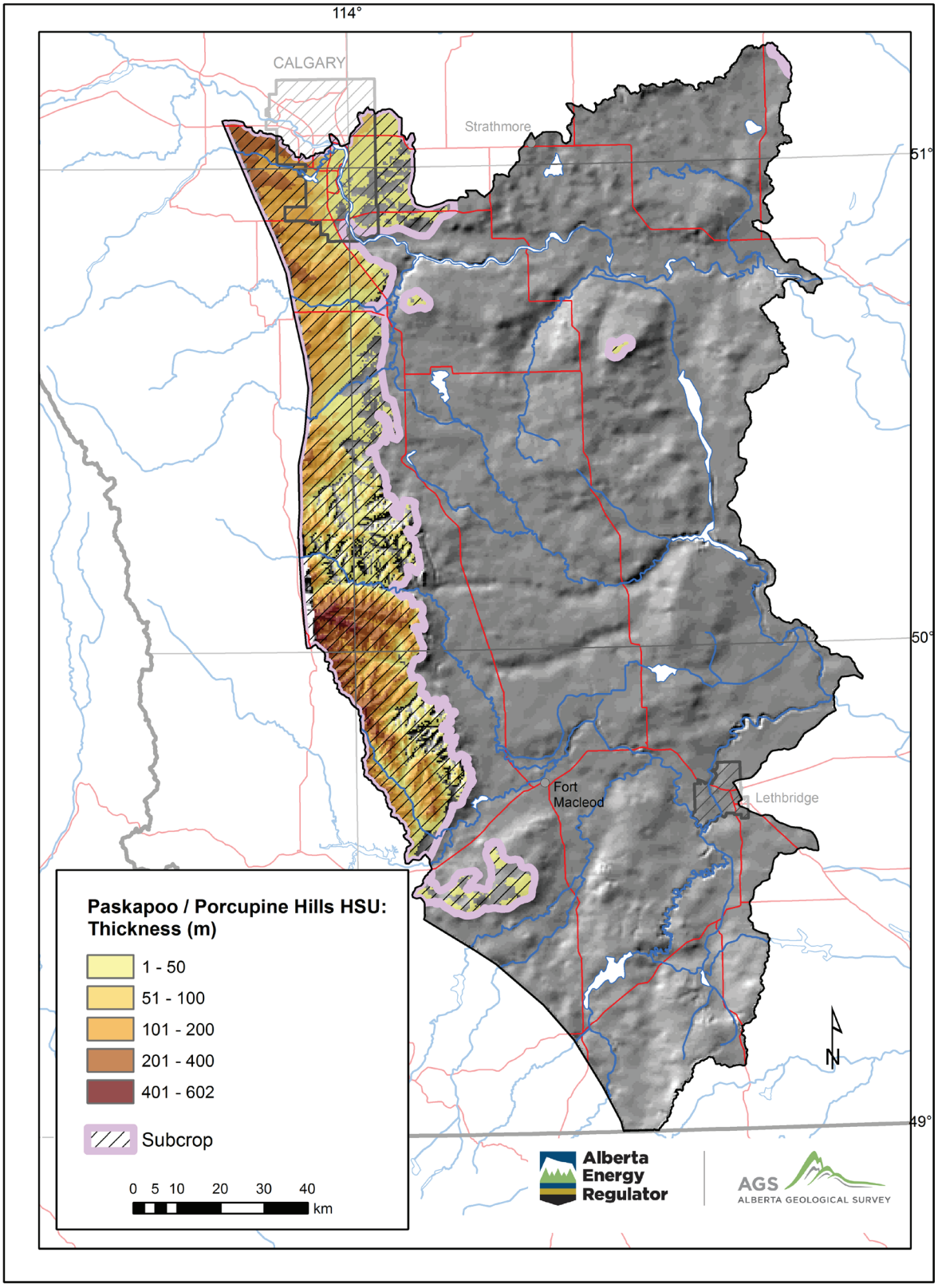

Figure A3-12. Thickness, extent, and subcrop of the Paskapoo / Porcupine Hills HSU. Hillshade is of the bedrock topography.

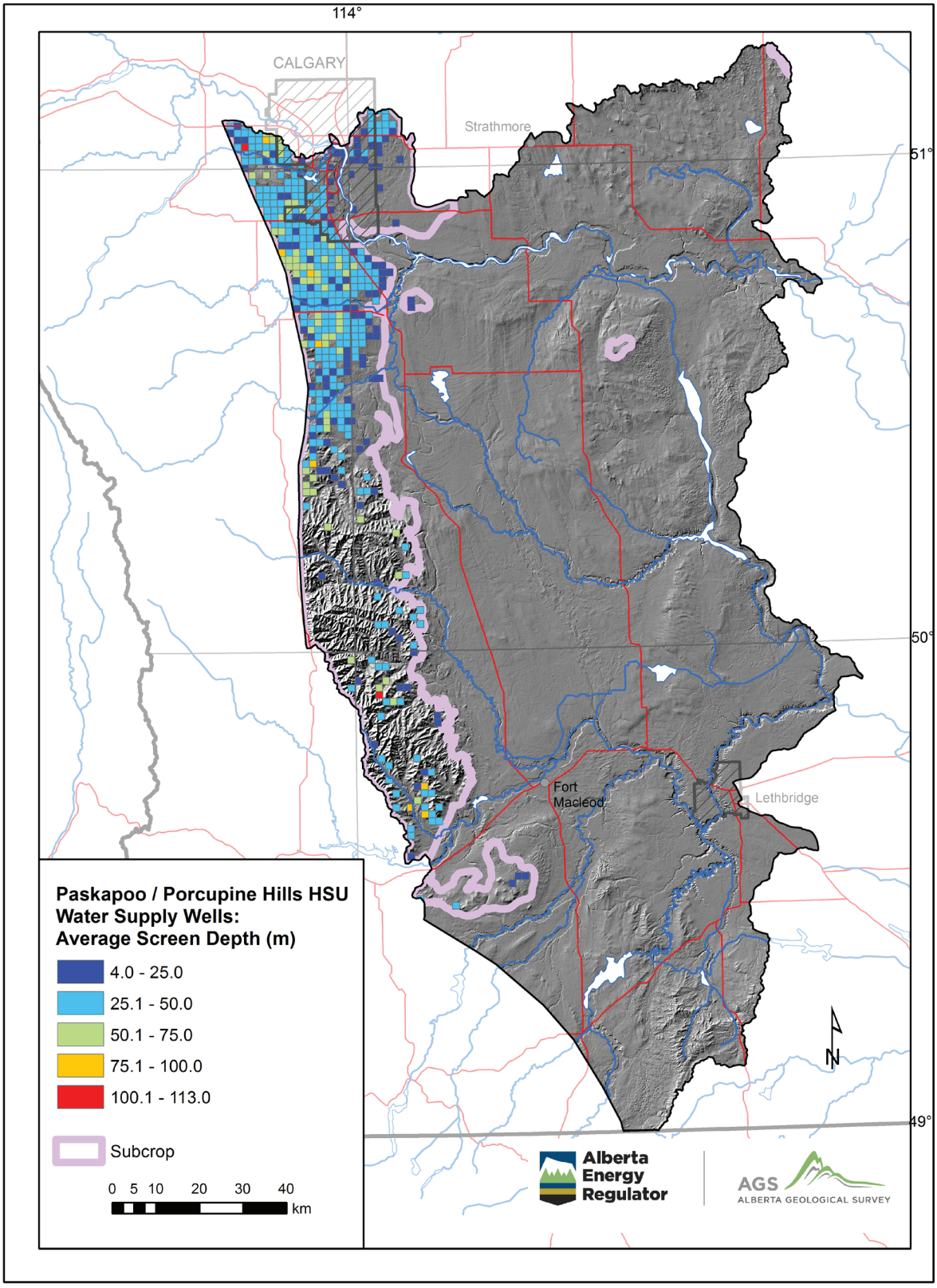

Figure A3-13. Average screen depth per ATS section for water supply wells in the Paskapoo / Porcupine Hills HSU. There is a very high density of water supply wells in the Okotoks Uplands south of Calgary (Figure 25).

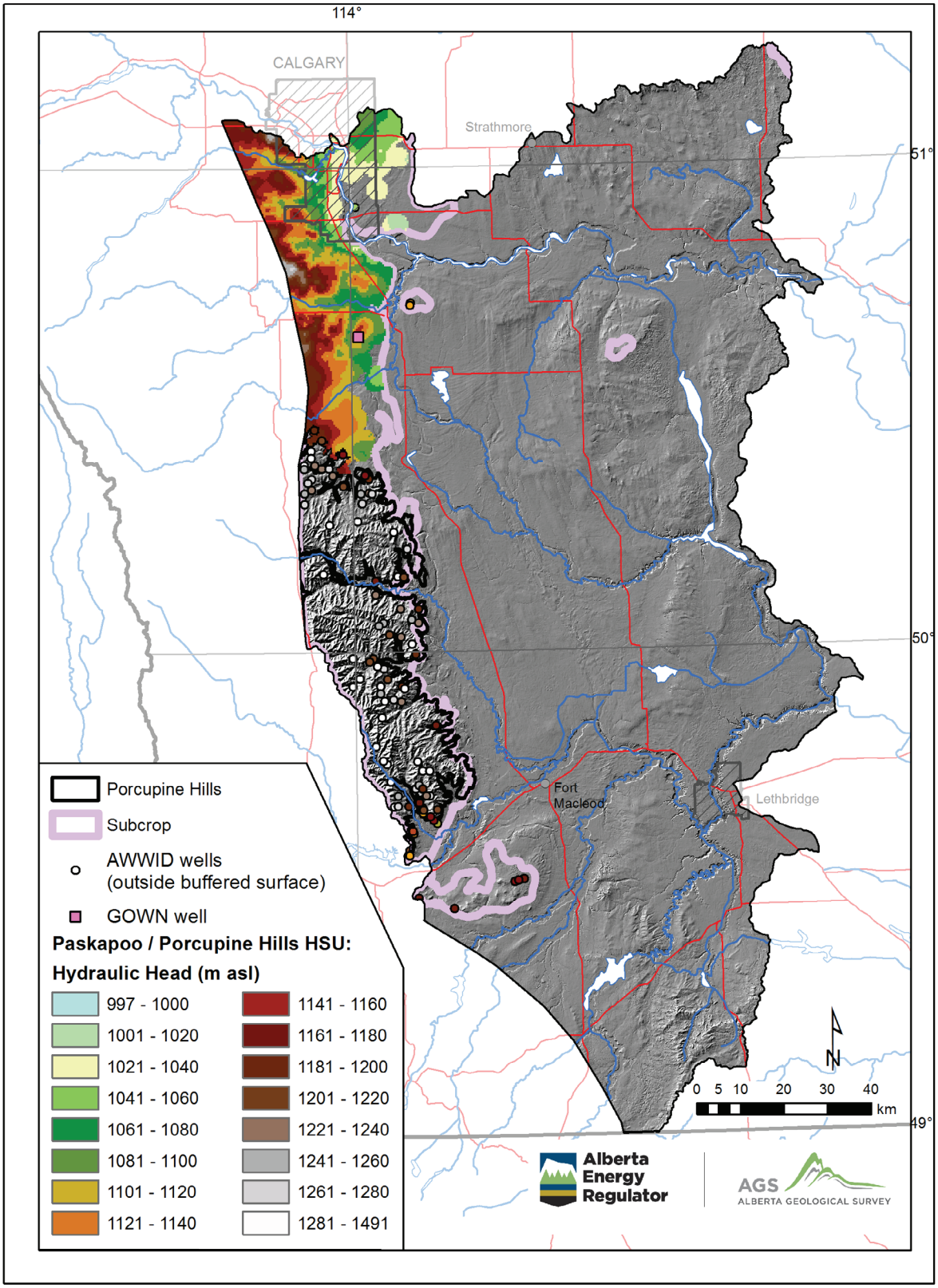

Figure A3-14. Potentiometric surface for the Paskapoo / Porcupine Hills HSU. Well density is so high where the potentiometric surface was interpolated that wells are not shown. Wells in the Porcupine Hills are shown although they were not included in the interpolation of the potentiometric surface.

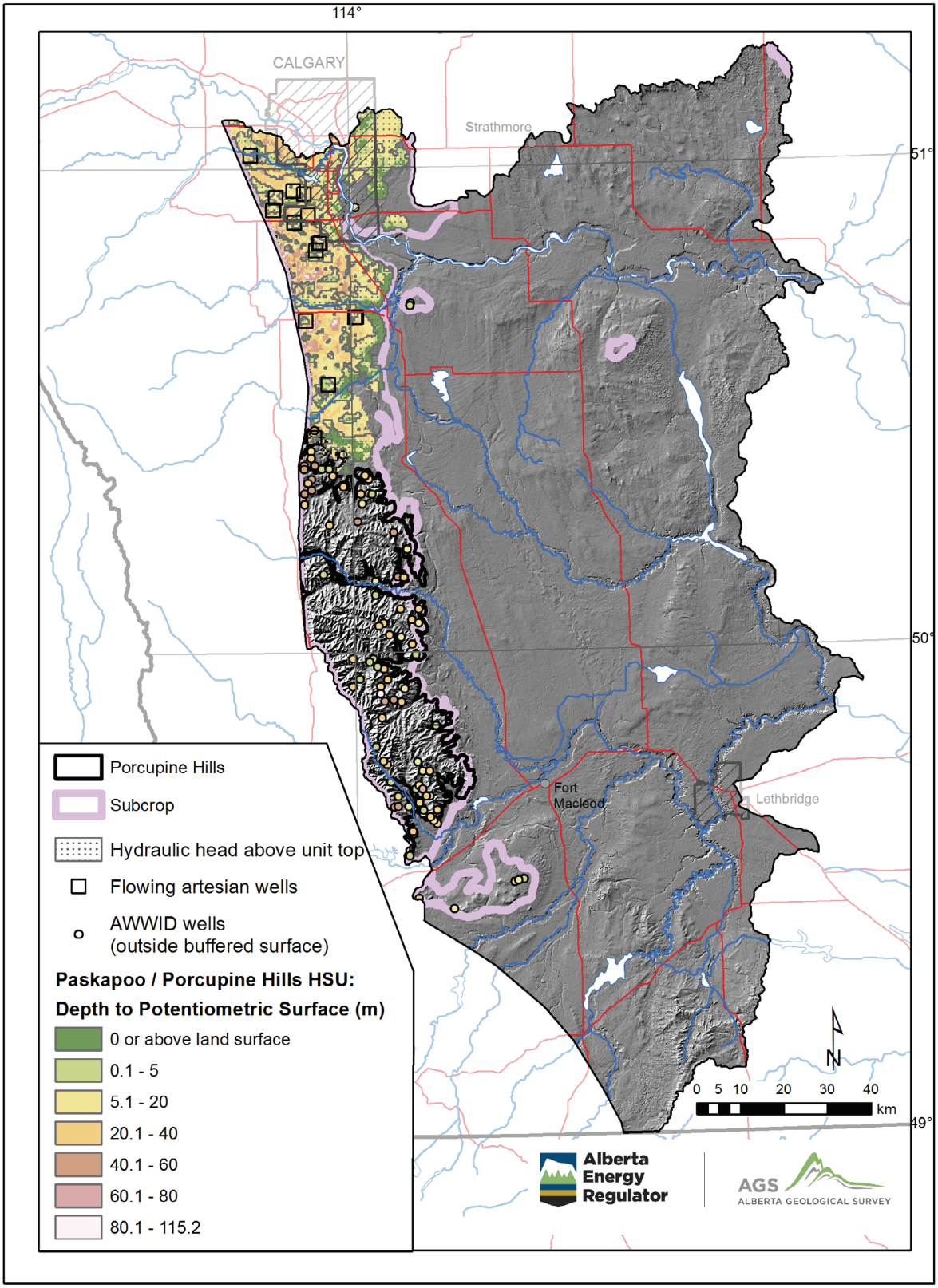

Figure A3-15. Depth to potentiometric surface for the Paskapoo / Porcupine Hills HSU. Green areas show where the interpolated potentiometric surface is above (dark green) or just below (light green) the land surface. Wells in the Porcupine Hills are shown although they were not included in the interpolation of the potentiometric surface.

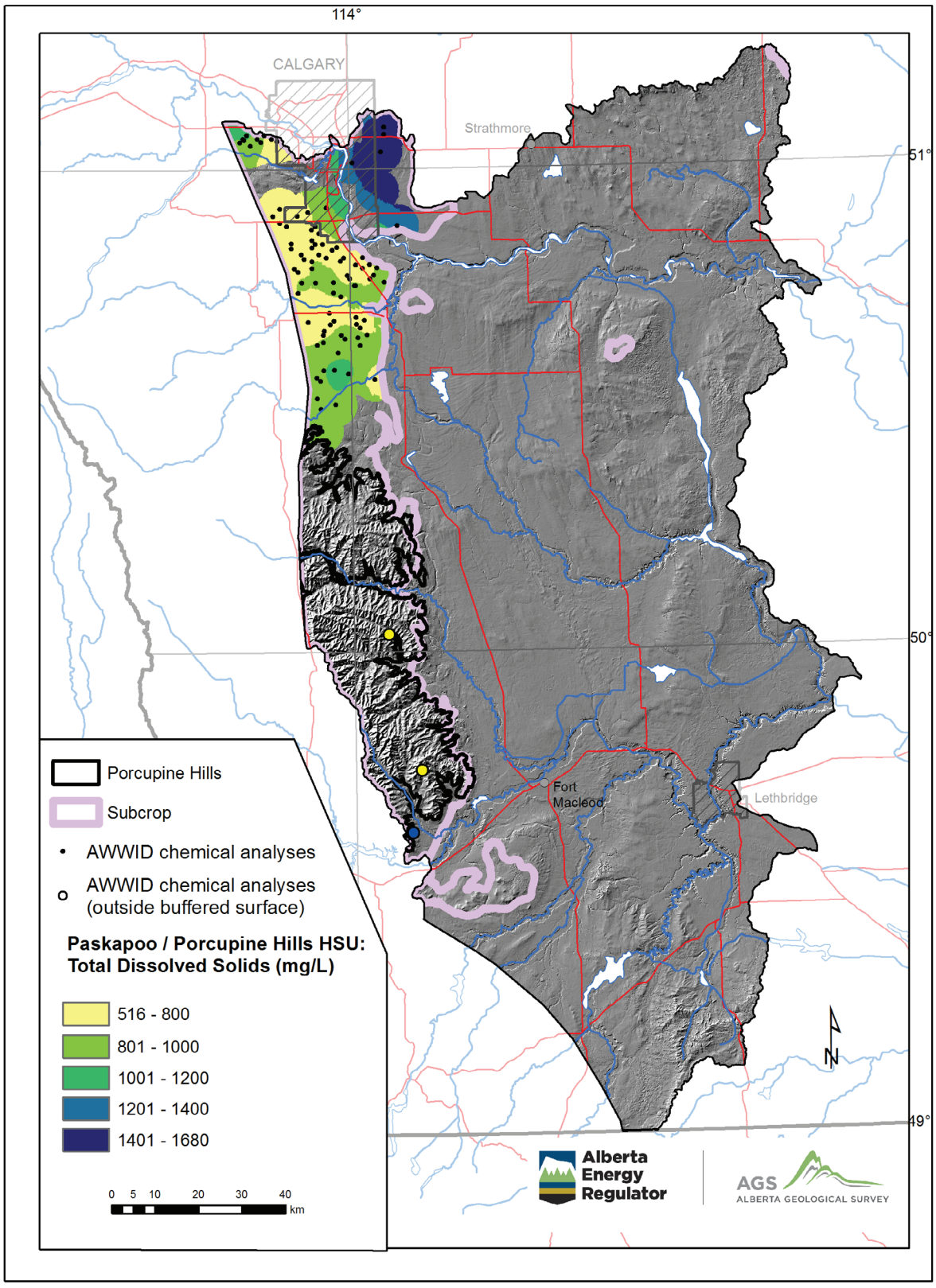

Figure A3-16. Concentration of TDS in the Paskapoo / Porcupine Hills HSU.

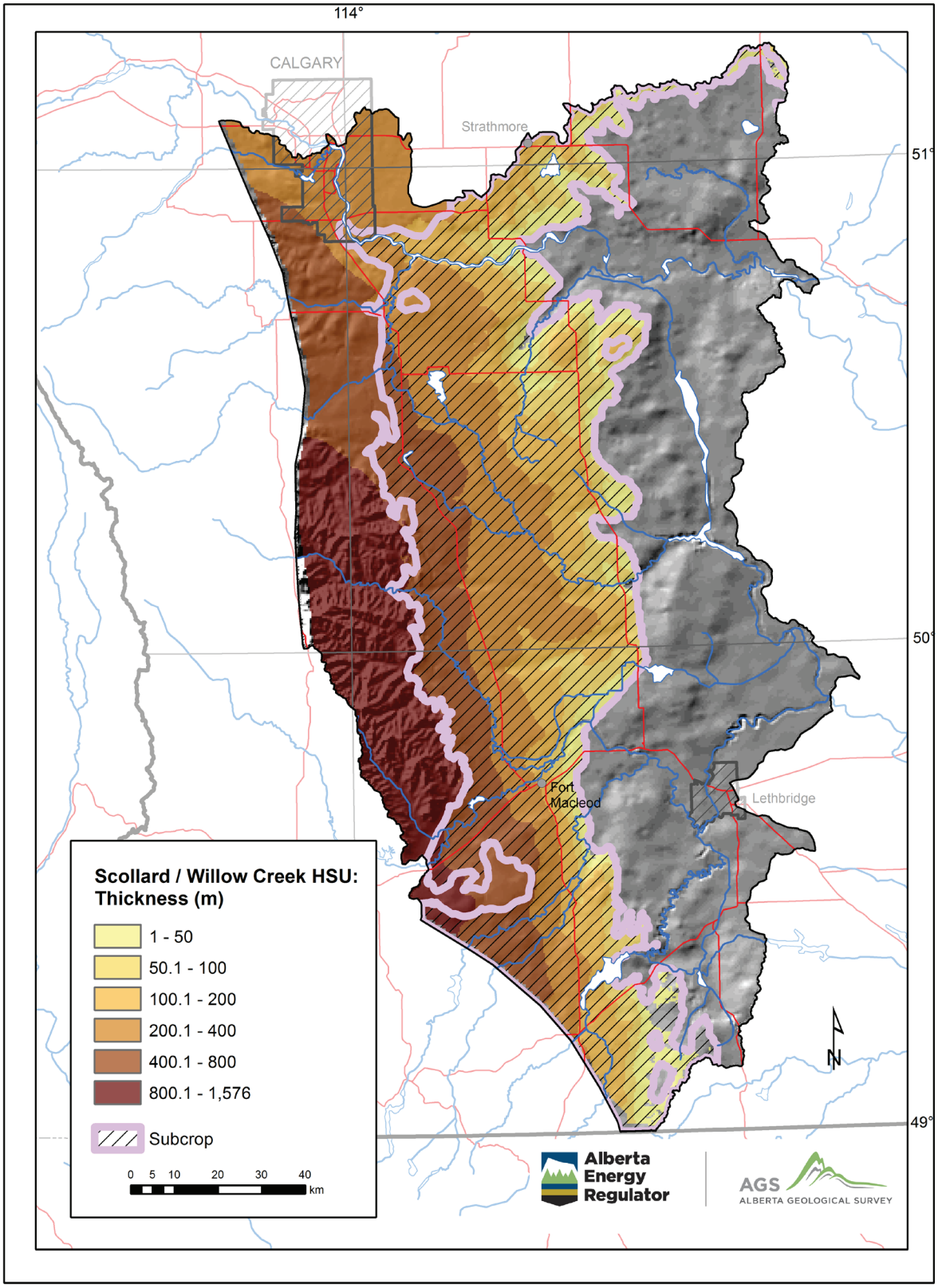

Figure A3-17. Thickness, extent, and subcrop area of the Scollard / Willow Creek HSU. Hillshade is bedrock topography.

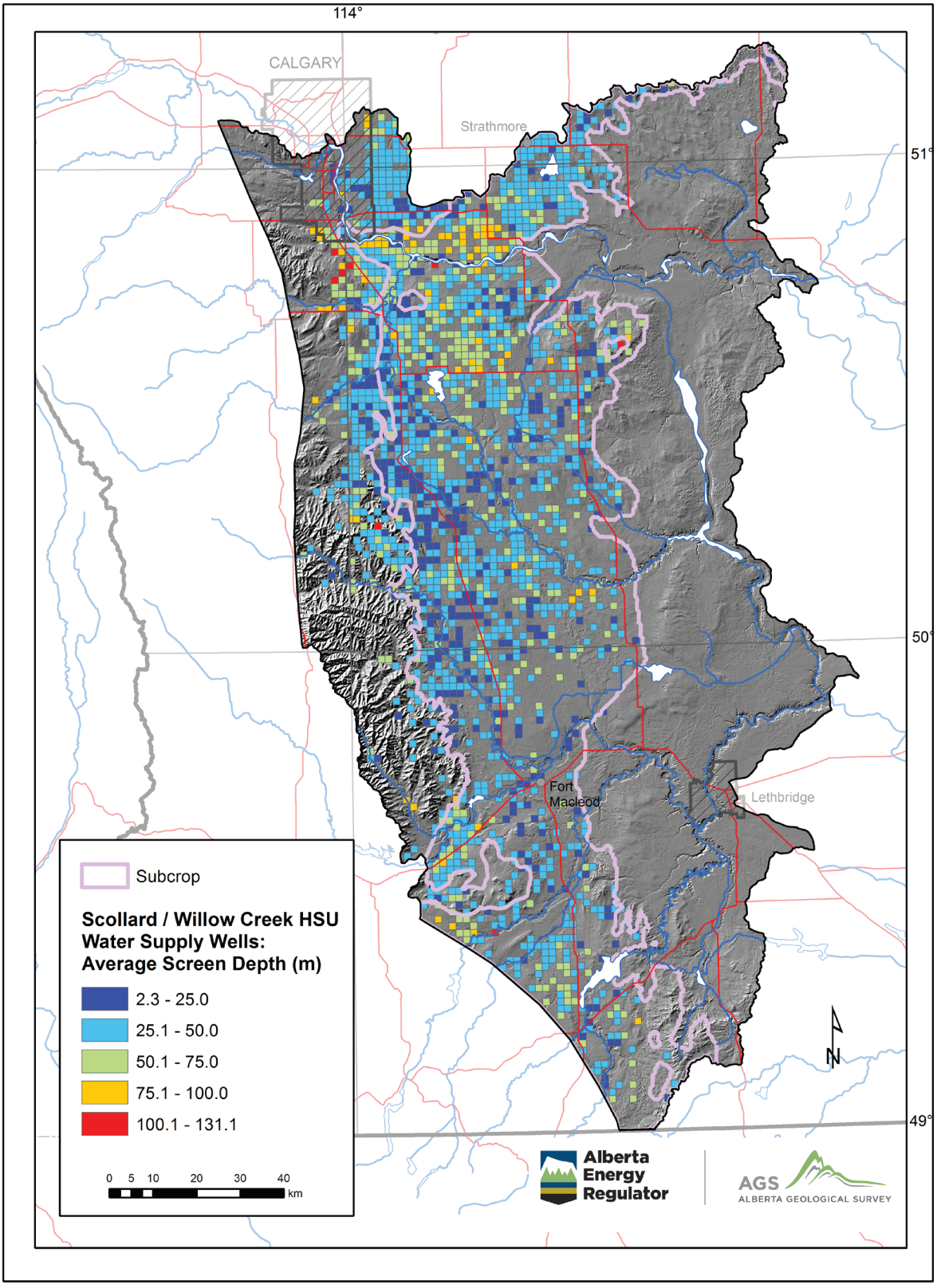

Figure A3-18. Average screen depth per ATS section for water supply wells in the Scollard / Willow Creek HSU. There is a very high density of water supply wells just south of Calgary, east of the highway and towards the Bow River.

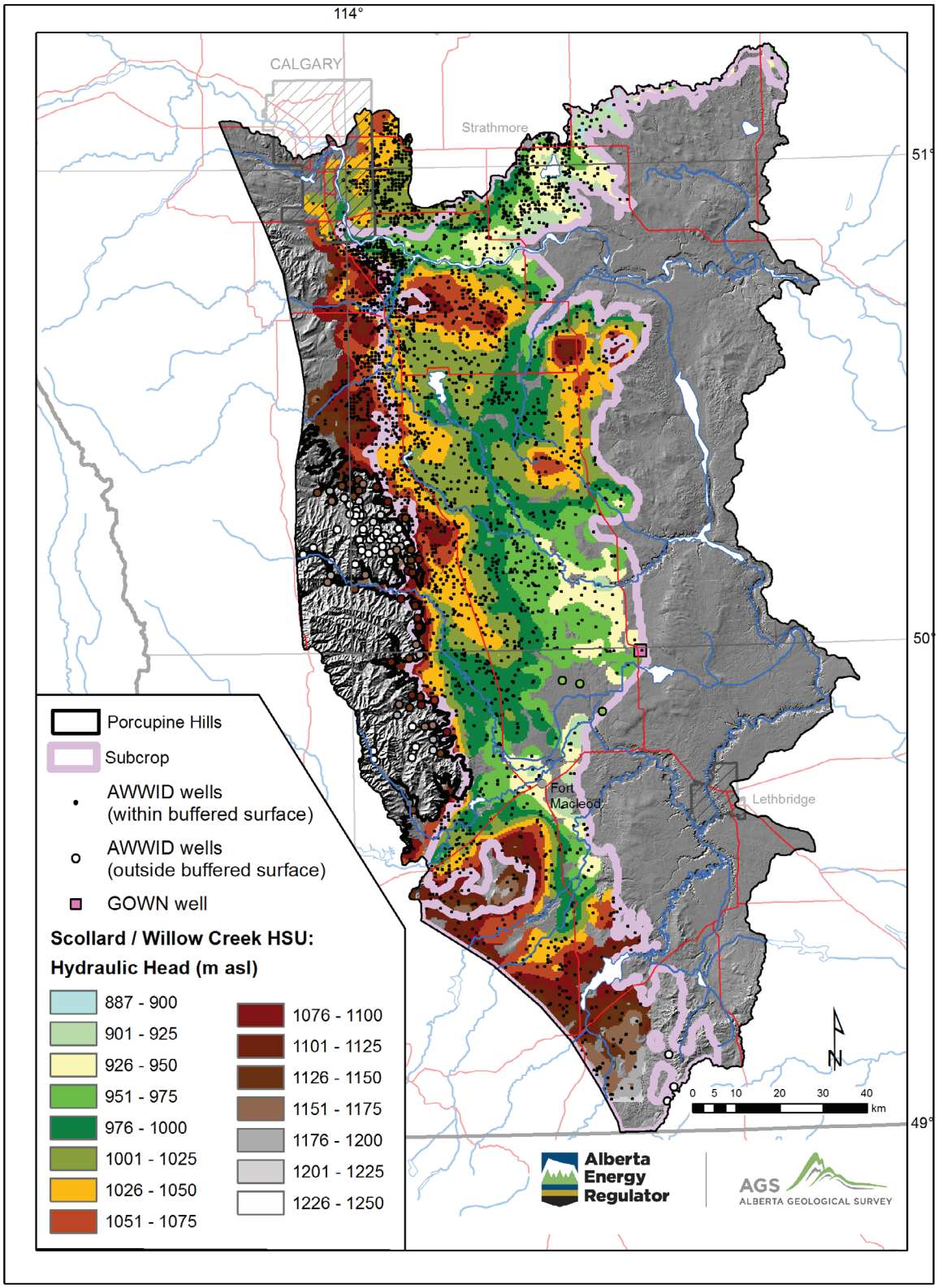

Figure A3-19. Potentiometric surface for the Scollard / Willow Creek HSU. Hydraulic gradients indicate primarily topographically driven groundwater flow. Wells in the Porcupine Hills are shown although they were not included in the interpolation of the potentiometric surface. There are three GOWN wells in this HSU, two of which are in the same location, south of the Bow River on the western edge of the subcrop area.

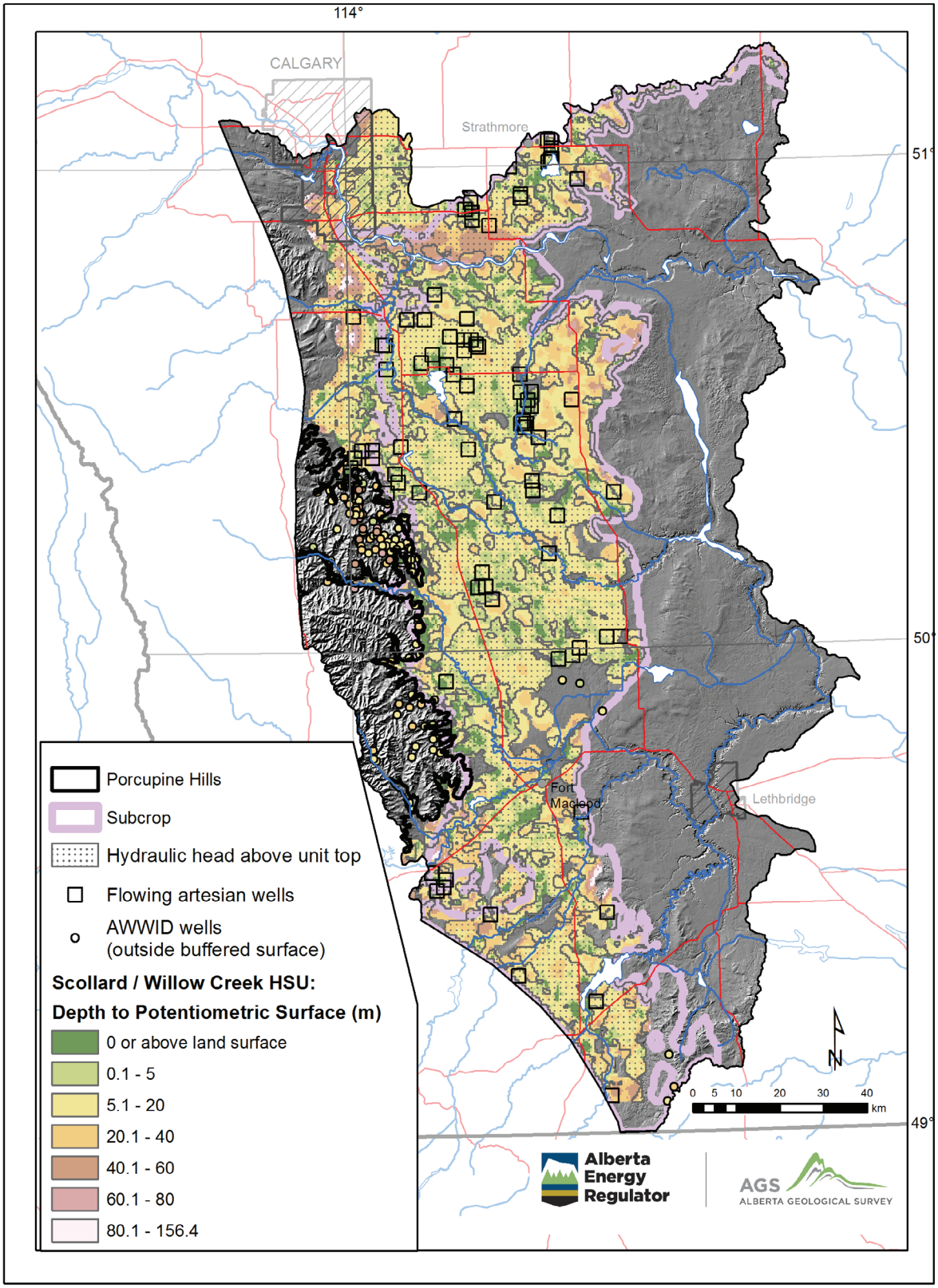

Figure A3-20. Depth to potentiometric surface for the Scollard / Willow Creek HSU. Green areas show where the interpolated potentiometric surface is above (dark green) or just below (light green) the land surface. Wells in the Porcupine Hills are shown although they were not included in the interpolation of the potentiometric surface.

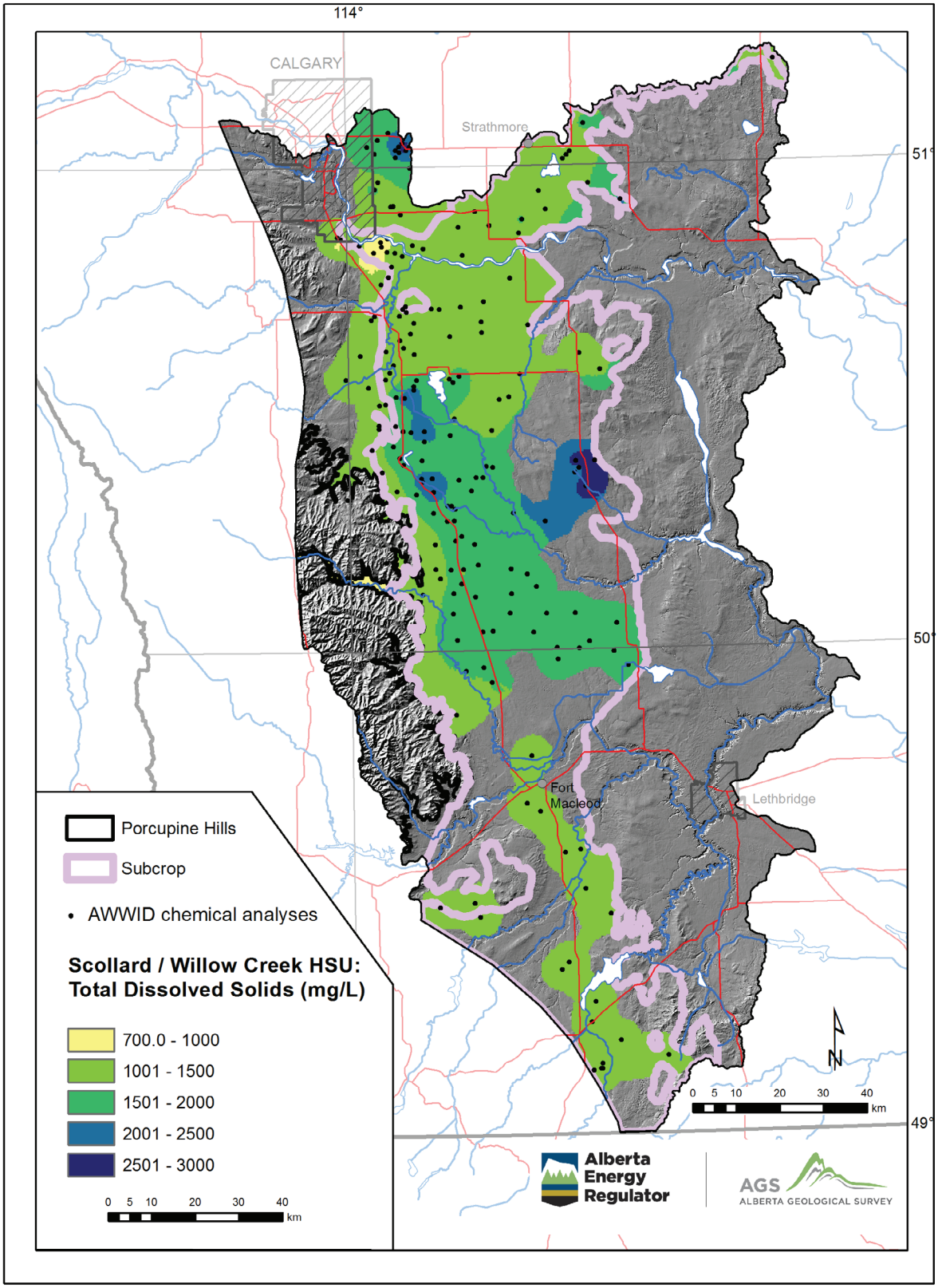

Figure A3-21. Concentration of TDS in the Scollard / Willow Creek HSU.

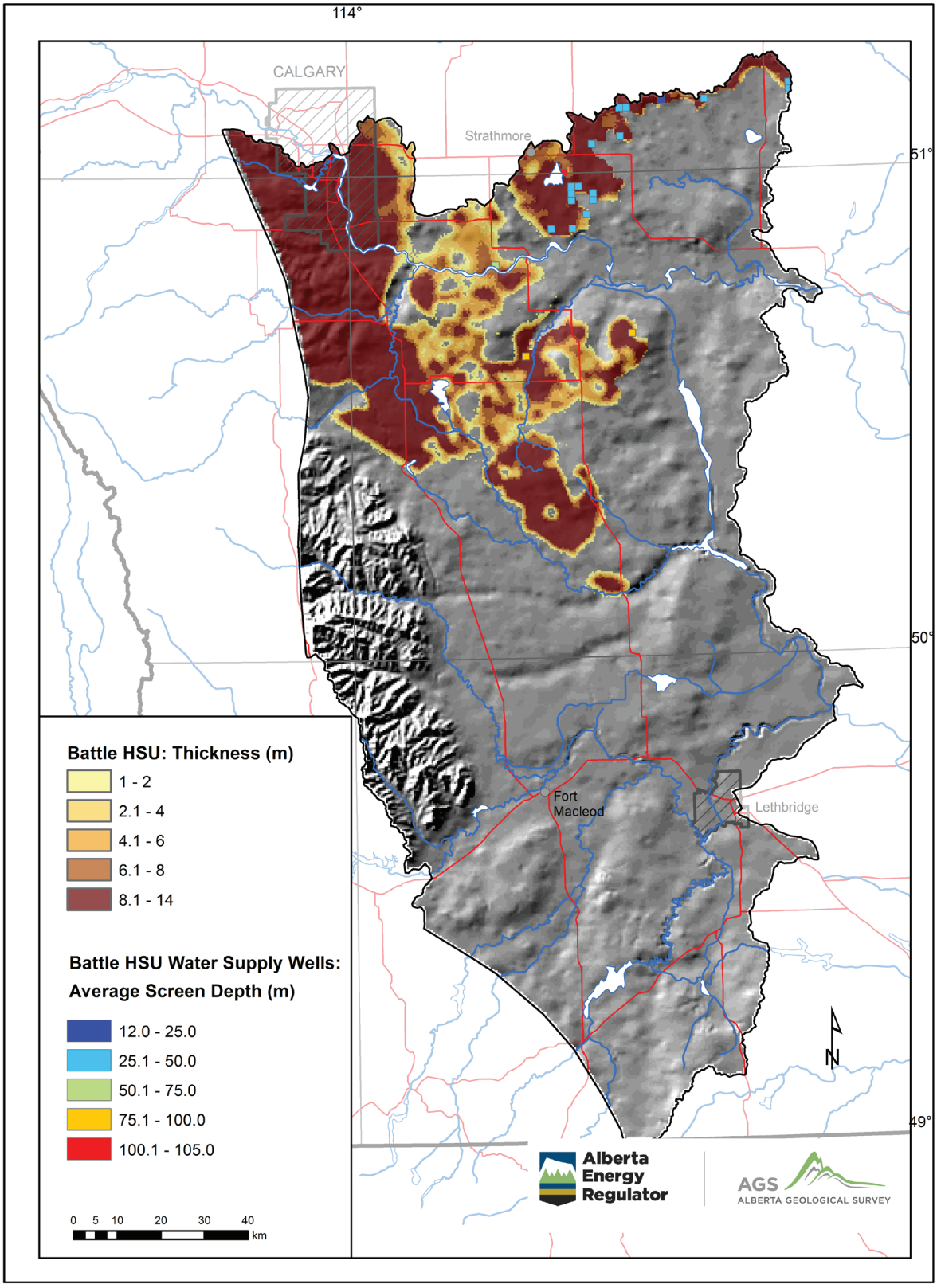

Figure A3-22. Thickness and extent of the Battle HSU. This HSU does not subcrop in the CLC. Average screen depth of water supply wells per section is also shown. Hillshade is for the bedrock topography.

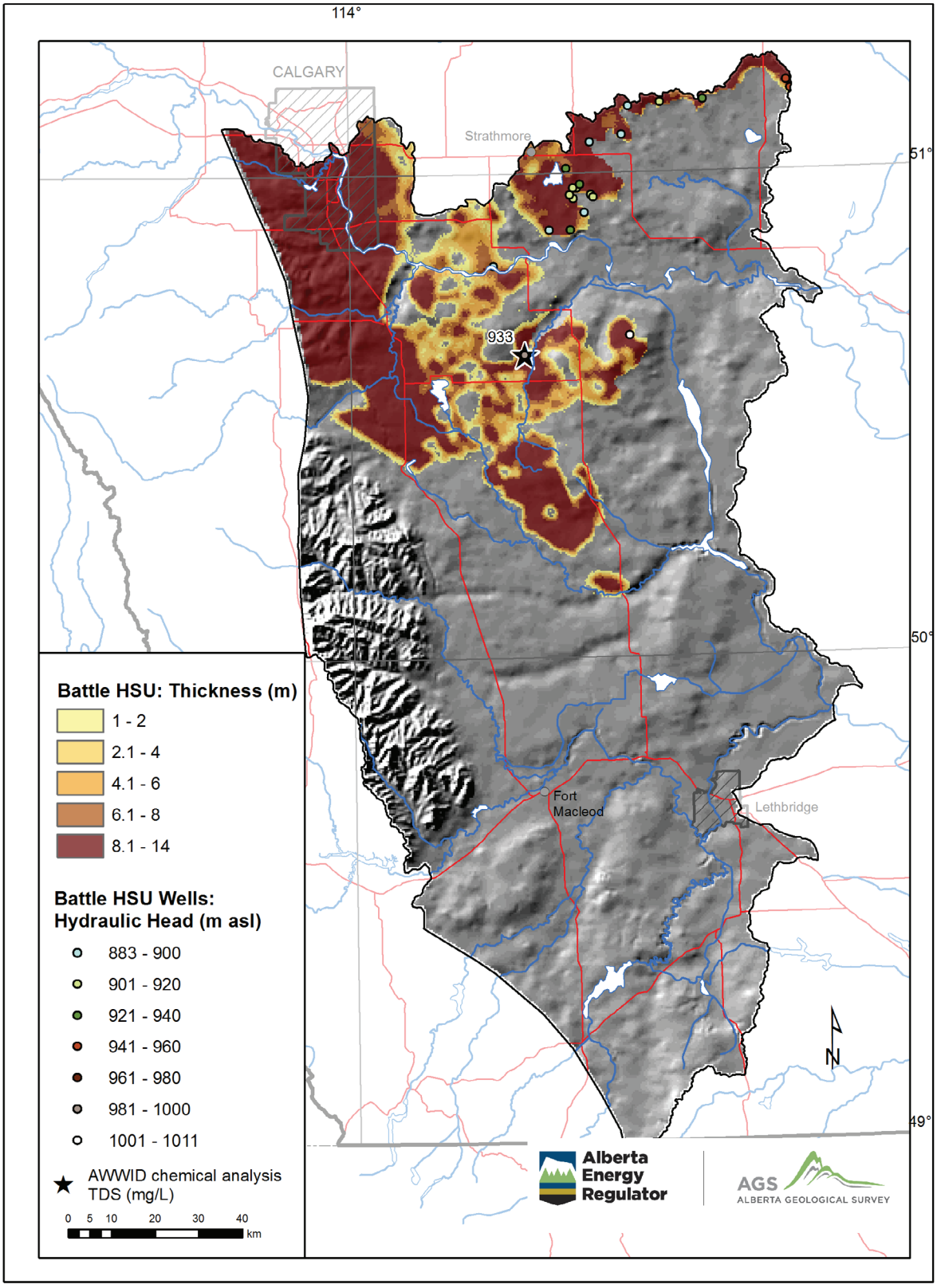

Figure A3-23. Hydraulic heads and TDS concentration from available Battle HSU wells. No potentiometric surface or TDS map was created for this HSU due to the lack of data.

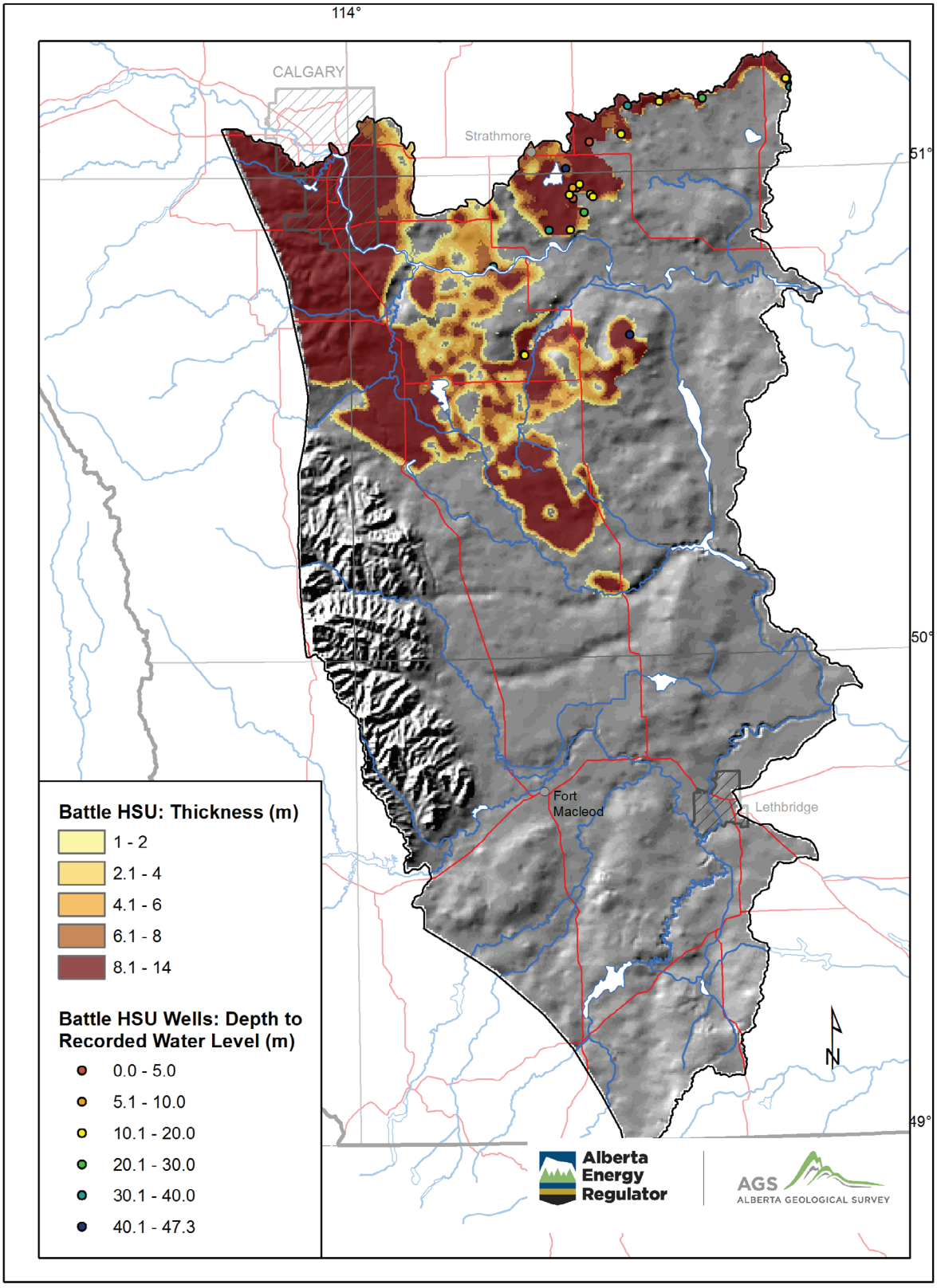

Figure A3-24. Depth to potentiometric surface in available wells for the Battle HSU.

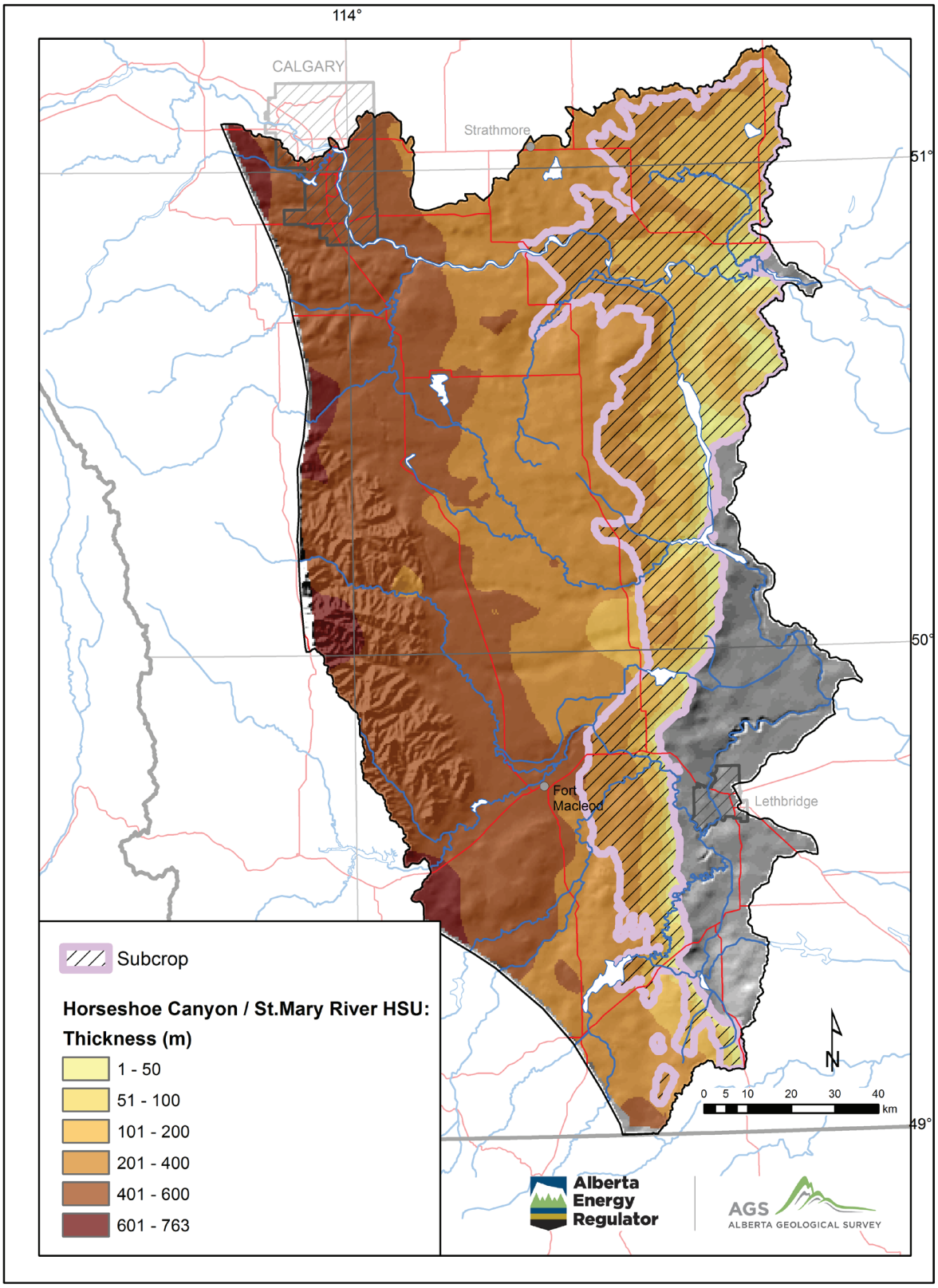

Figure A3-25. Thickness, extent, and subcrop area of the Horseshoe Canyon / St. Mary River HSU. Hillshade is bedrock topography.

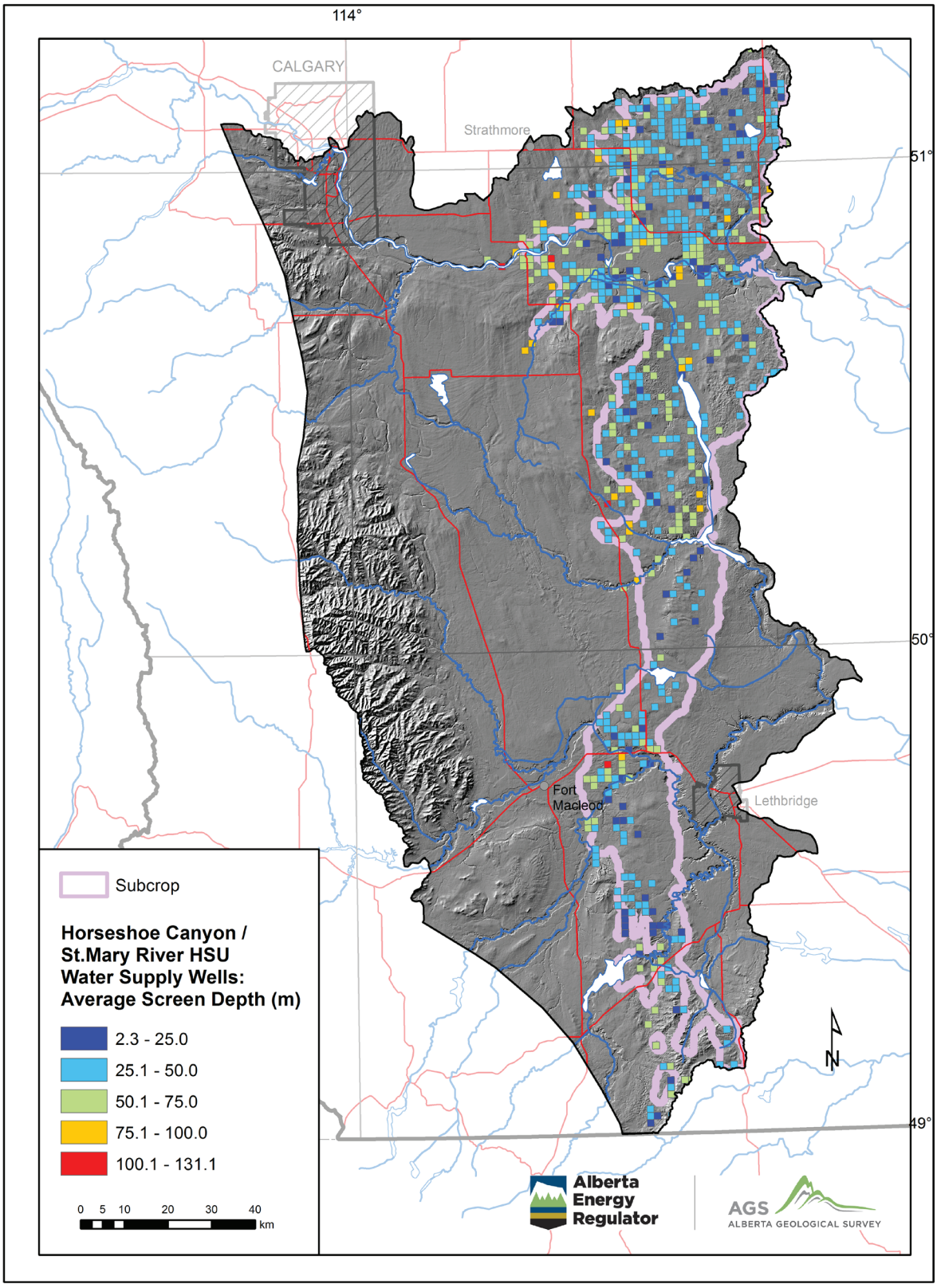

Figure A3-26. Average screen depth per ATS section for water supply wells in the Horseshoe Canyon / St. Mary River HSU.

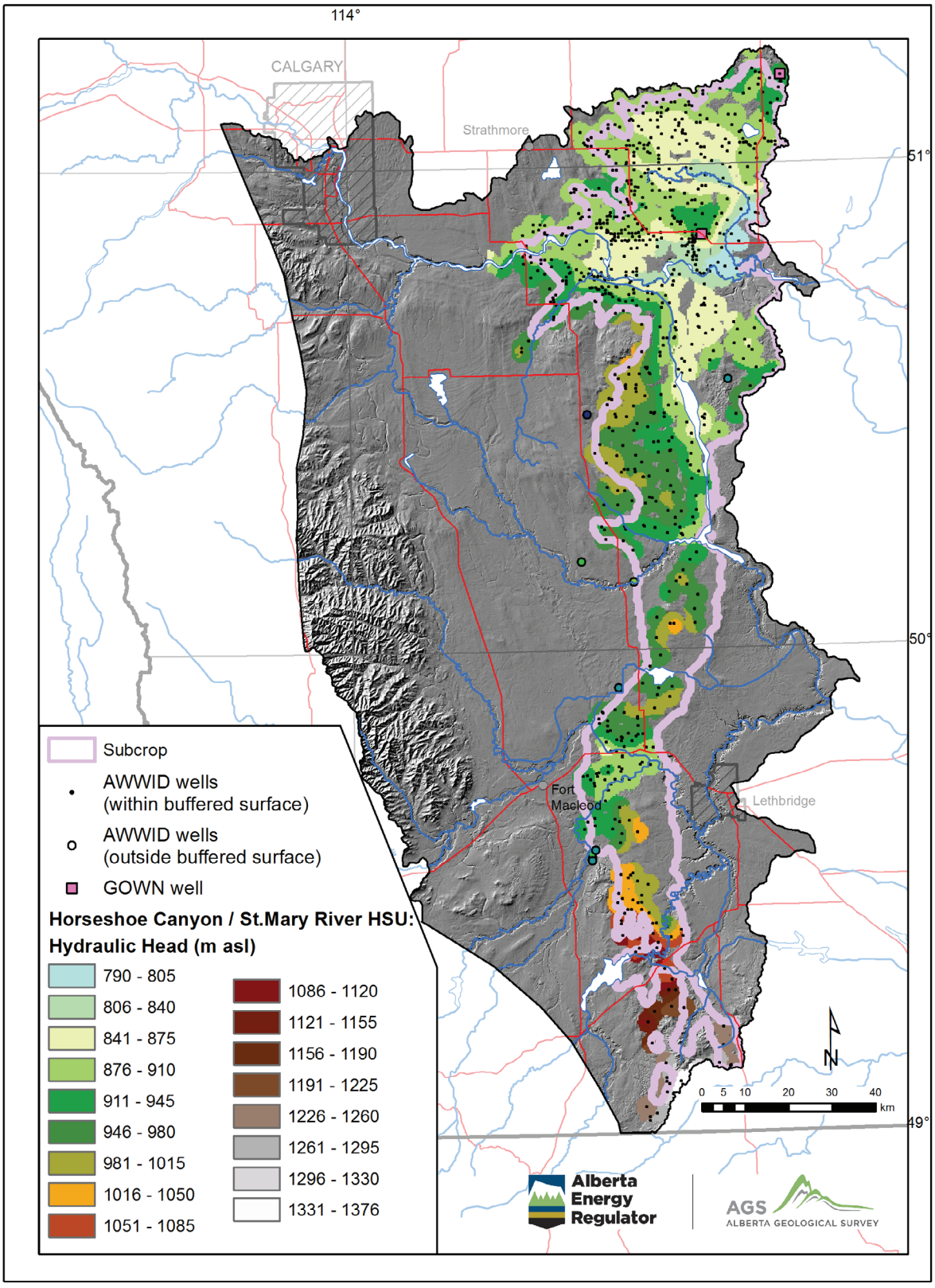

Figure A3-27. Potentiometric surface for the Horseshoe Canyon / St. Mary River HSU.

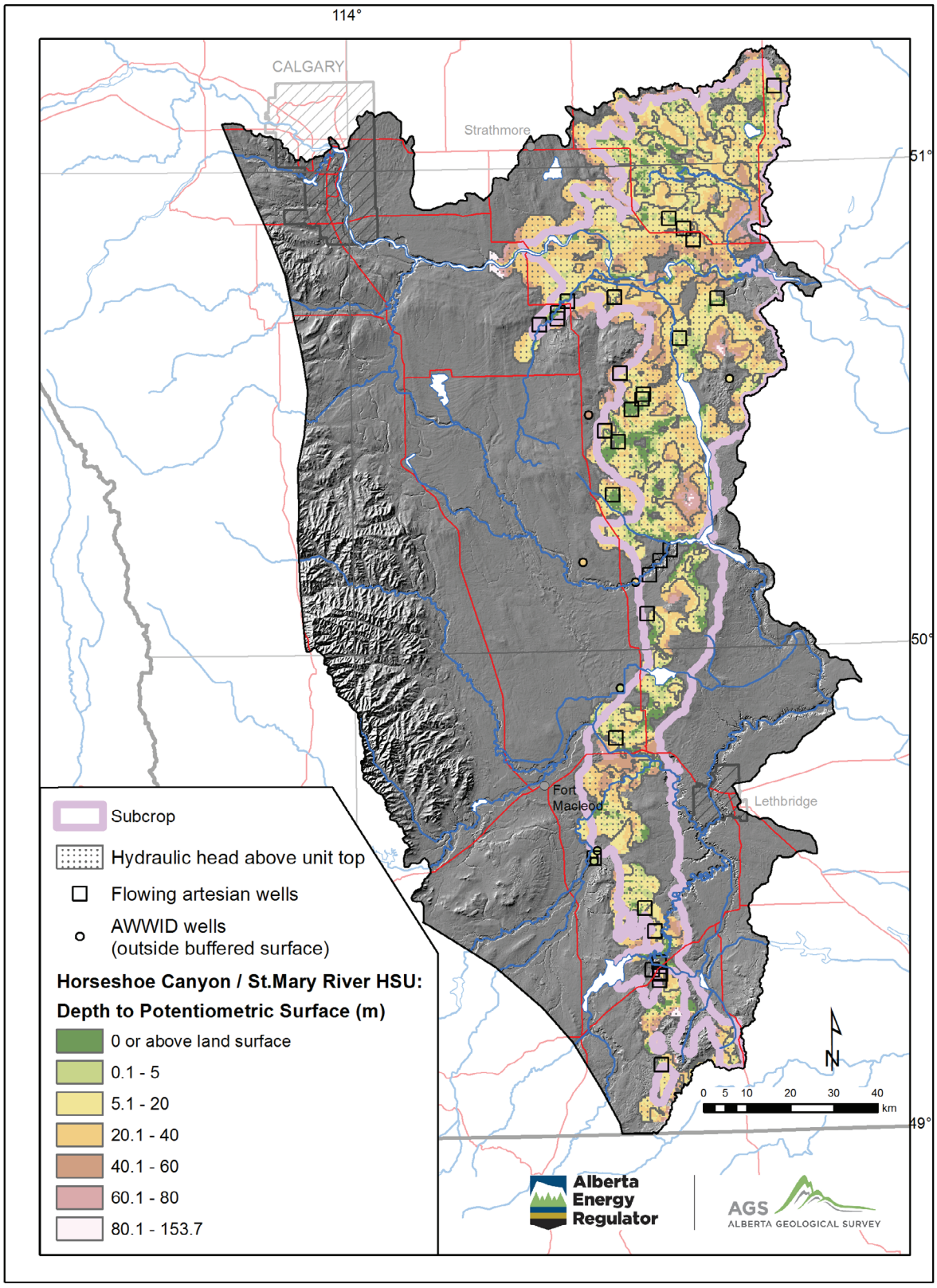

Figure A3-28. Depth to potentiometric surface for the Horseshoe Canyon / St. Mary River HSU. Green areas show where the interpolated potentiometric surface is above (dark green) or just below (light green) the land surface.

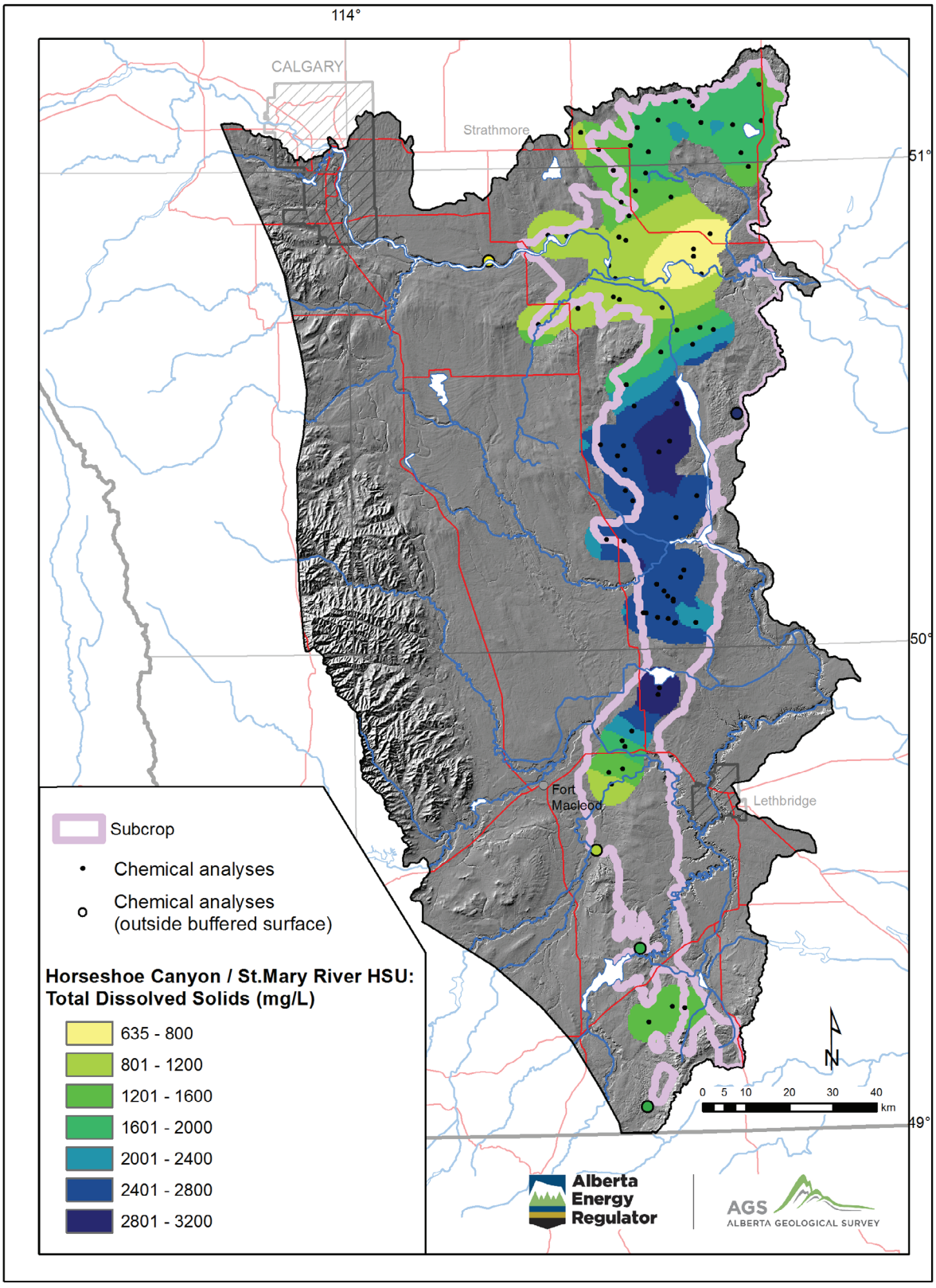

Figure A3-29. Concentration of TDS in the St. Mary River / Horseshoe Canyon HSU.

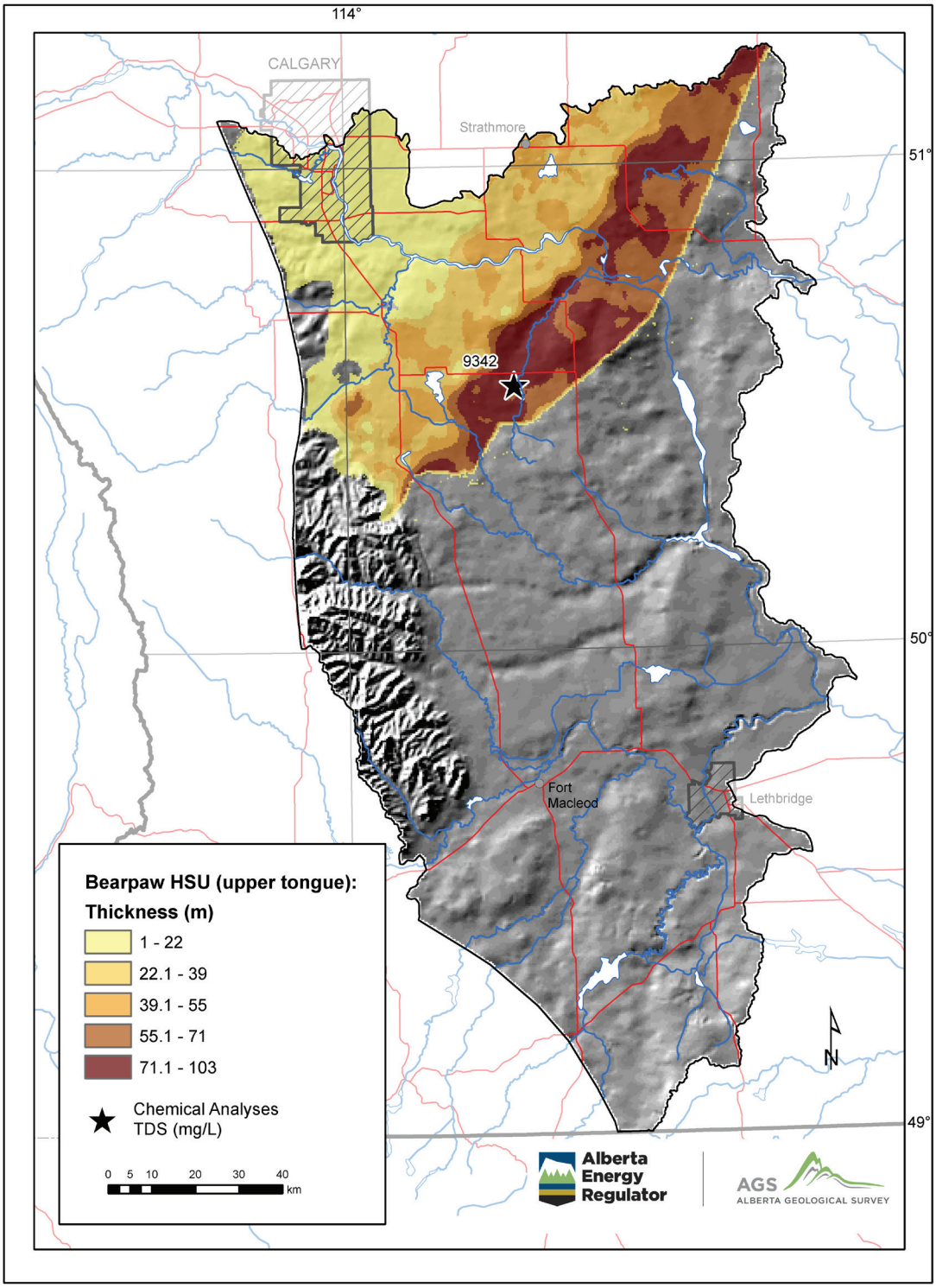

Figure A3-30. Thickness and extent of the upper tongue of the Bearpaw HSU. This HSU does not contain any AWWID wells with water supply or hydraulic information. There is only one chemical analysis from oil and gas wells. The Horseshoe Canyon / St. Mary River HSU (Strathmore Mb) (Figure A3-31) separates the upper and lower tongues of the Bearpaw HSU; however, to the east and south of the extent of the Bearpaw HSU (upper tongues) shown above, the Horseshoe Canyon / St. Mary River (Strathmore Mb) is not present, and there is no distinction between the upper and lower Bearpaw HSU tongues. Hillshade shown is of bedrock topography.

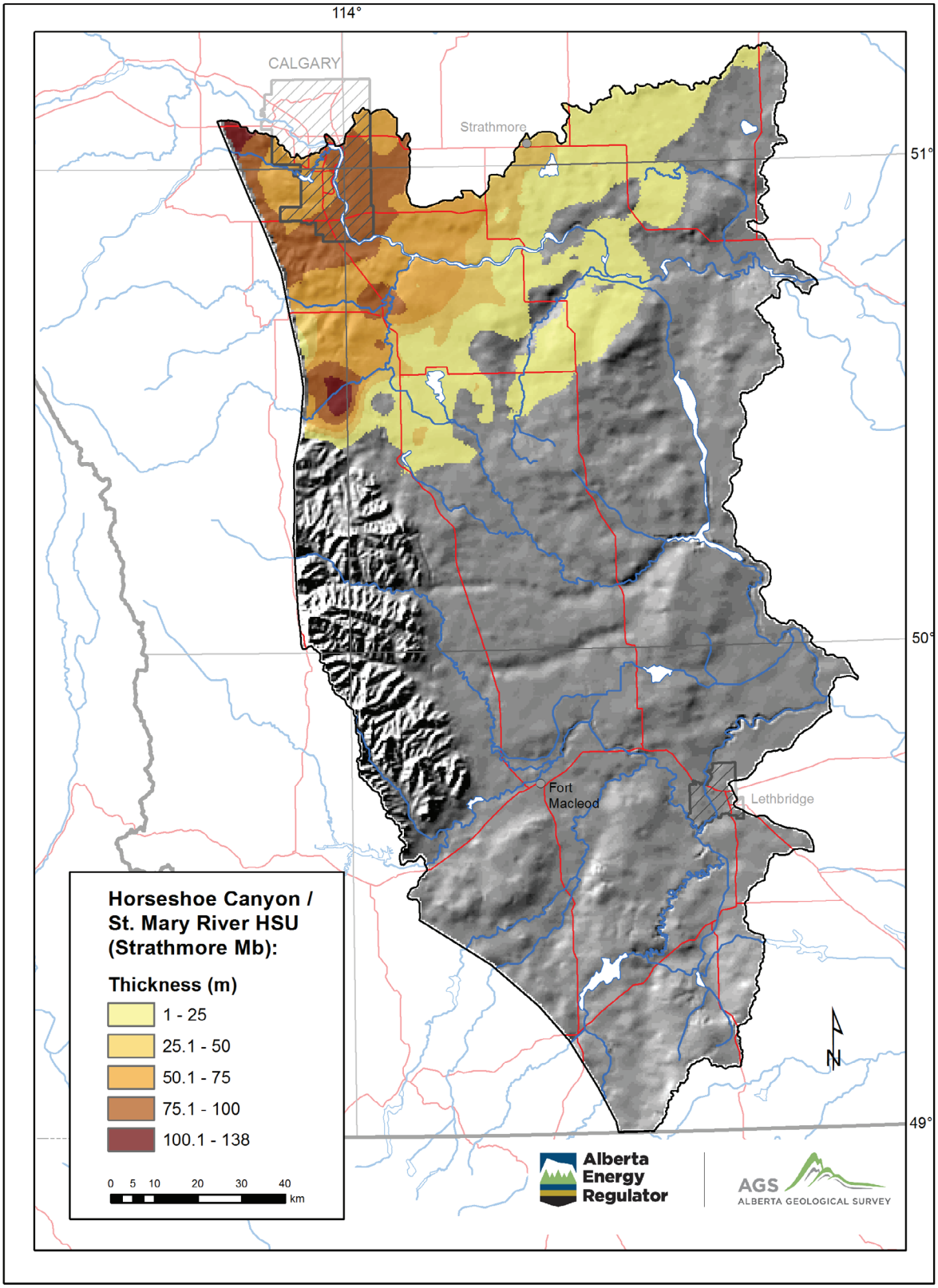

Figure A3-31. Thickness and extent of the Horseshoe Canyon / St. Mary River HSU (Strathmore Mb), which separates the upper and lower tongues of the Bearpaw HSU. This HSU does not subcrop in the study area and contains no AWWID or oil and gas wells with hydrogeological or hydrochemical information. Hillshade is of bedrock topography.

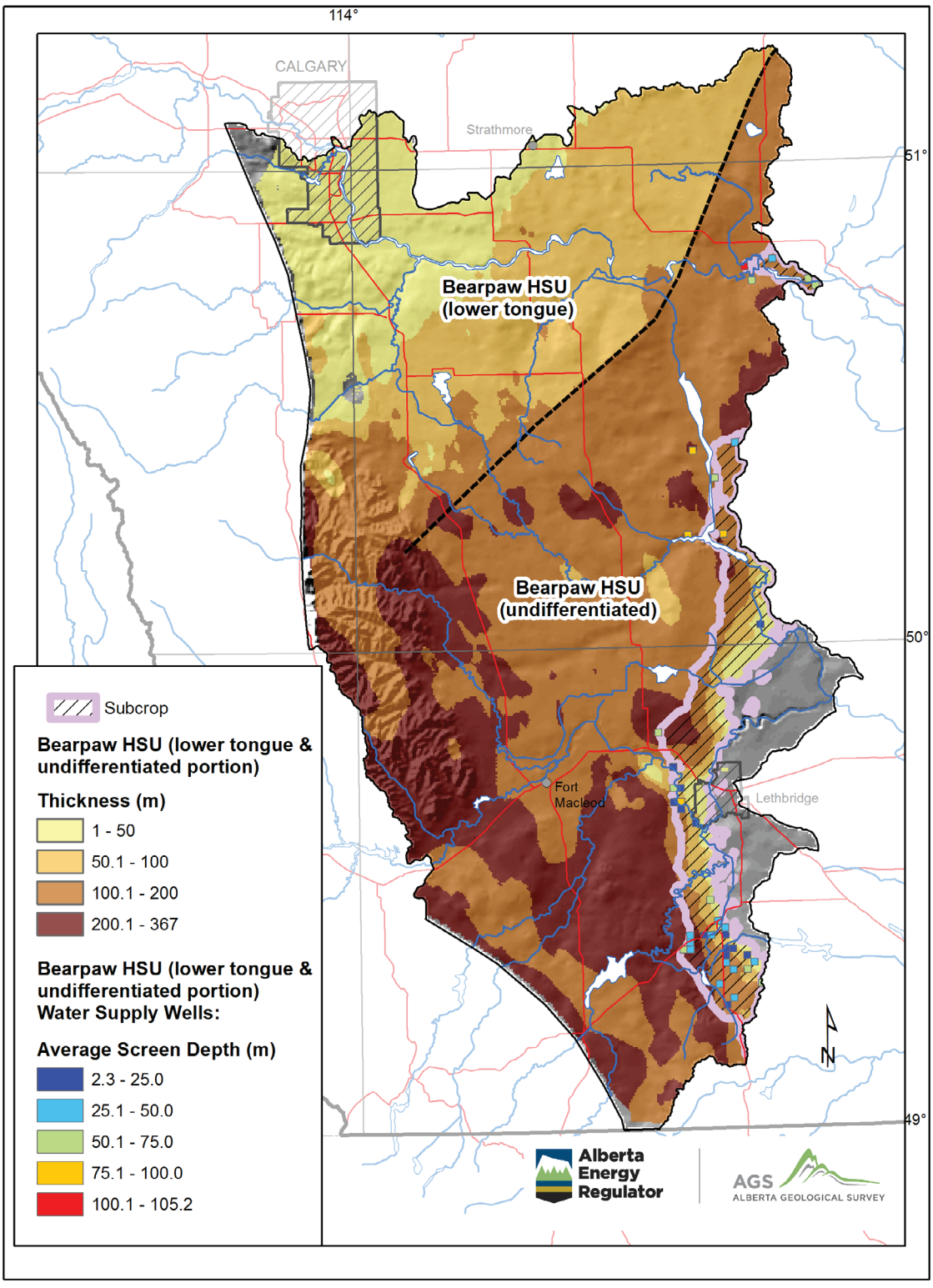

Figure A3-32. Thickness, extent, and subcrop of the Bearpaw HSU (lower tongue and undifferentiated portion). The Bearpaw HSU is undifferentiated outside of the extent of the Horseshoe Canyon / St. Mary River HSU (Strathmore Mb), where it is not separated into a lower and upper tongue. Also shown is the average screen depth per ATS section for water supply wells. Hillshade is of bedrock topography.

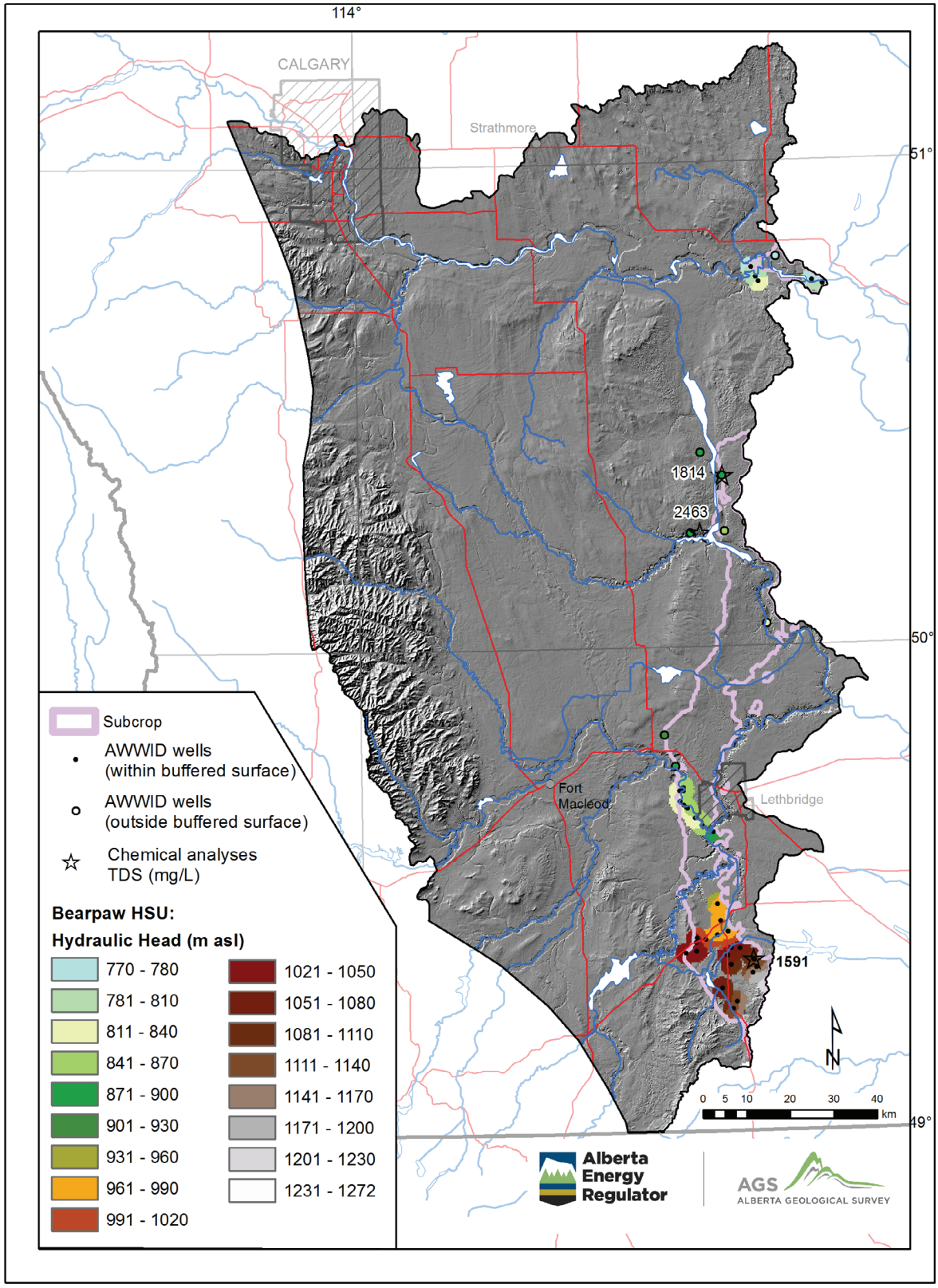

Figure A3-33. Potentiometric surface, hydraulic heads, and TDS for the Bearpaw HSU.

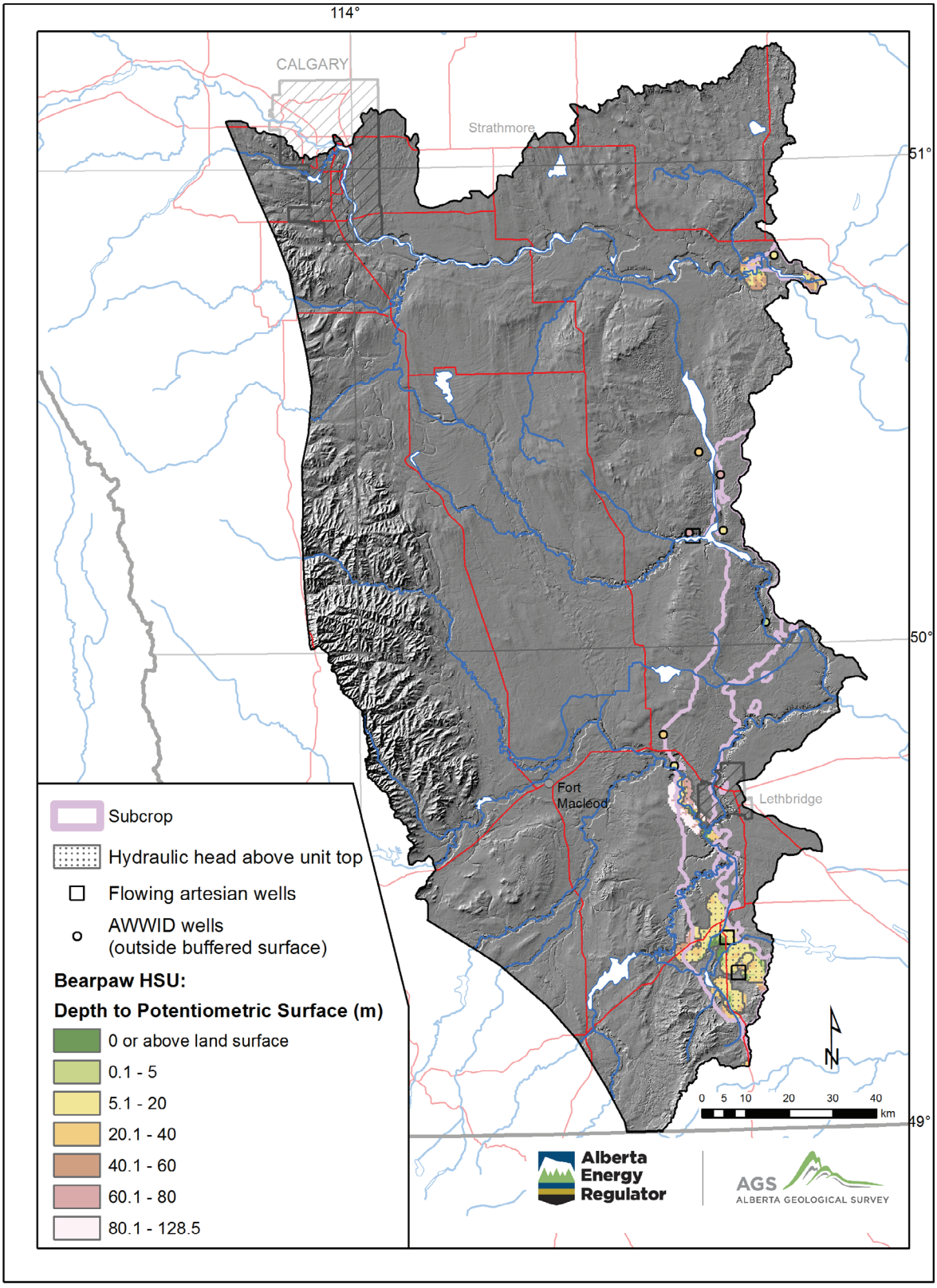

Figure A3-34. Depth to potentiometric surface for the Bearpaw HSU. Green areas show where the interpolated potentiometric surface is above (dark green) or just below (light green) the land surface.

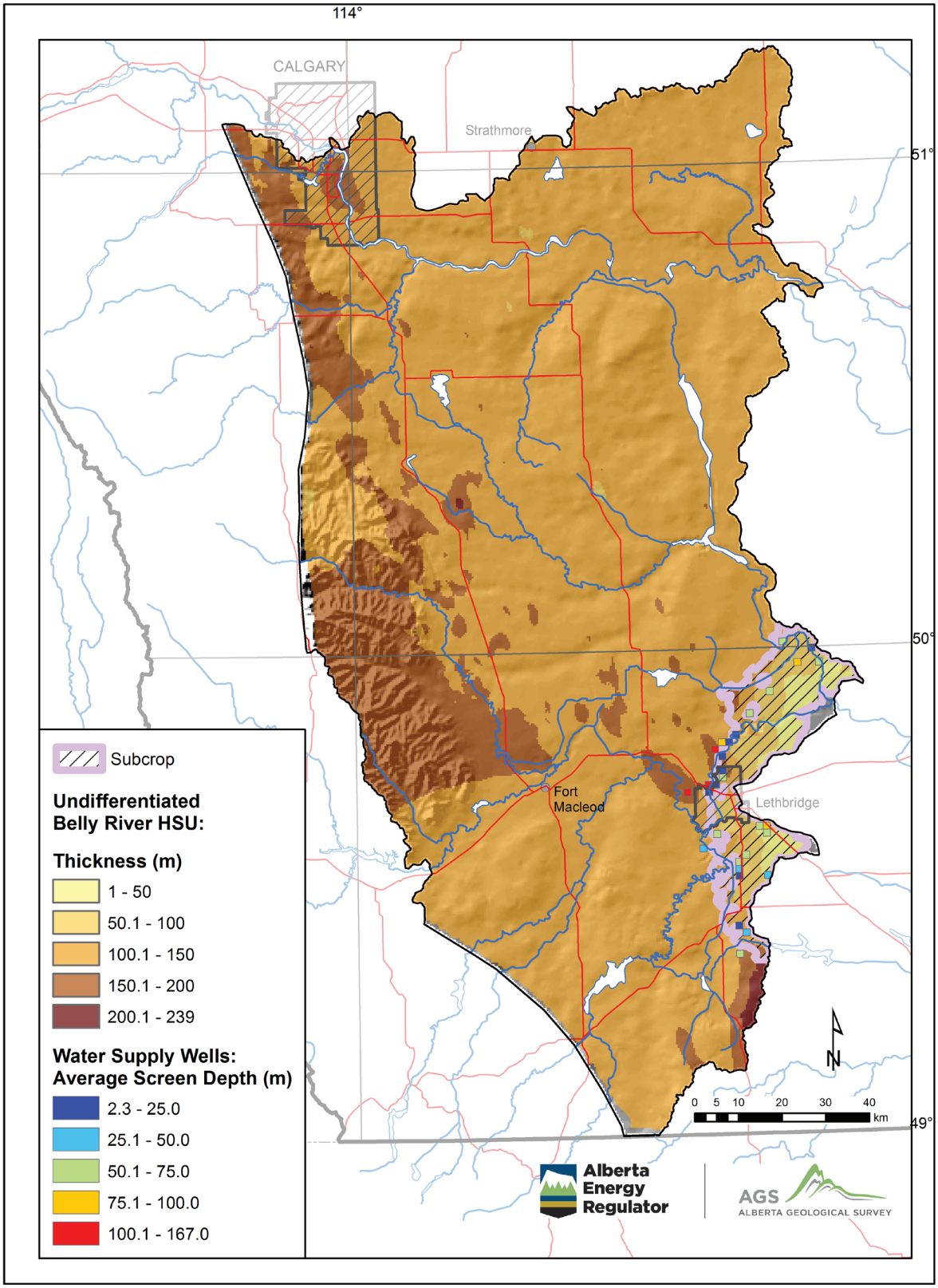

Figure A3-35. Thickness, extent, and subcrop of the undifferentiated Belly River HSU. Also shown is the average screen depth per ATS section for water supply wells. Hillshade is of bedrock topography.

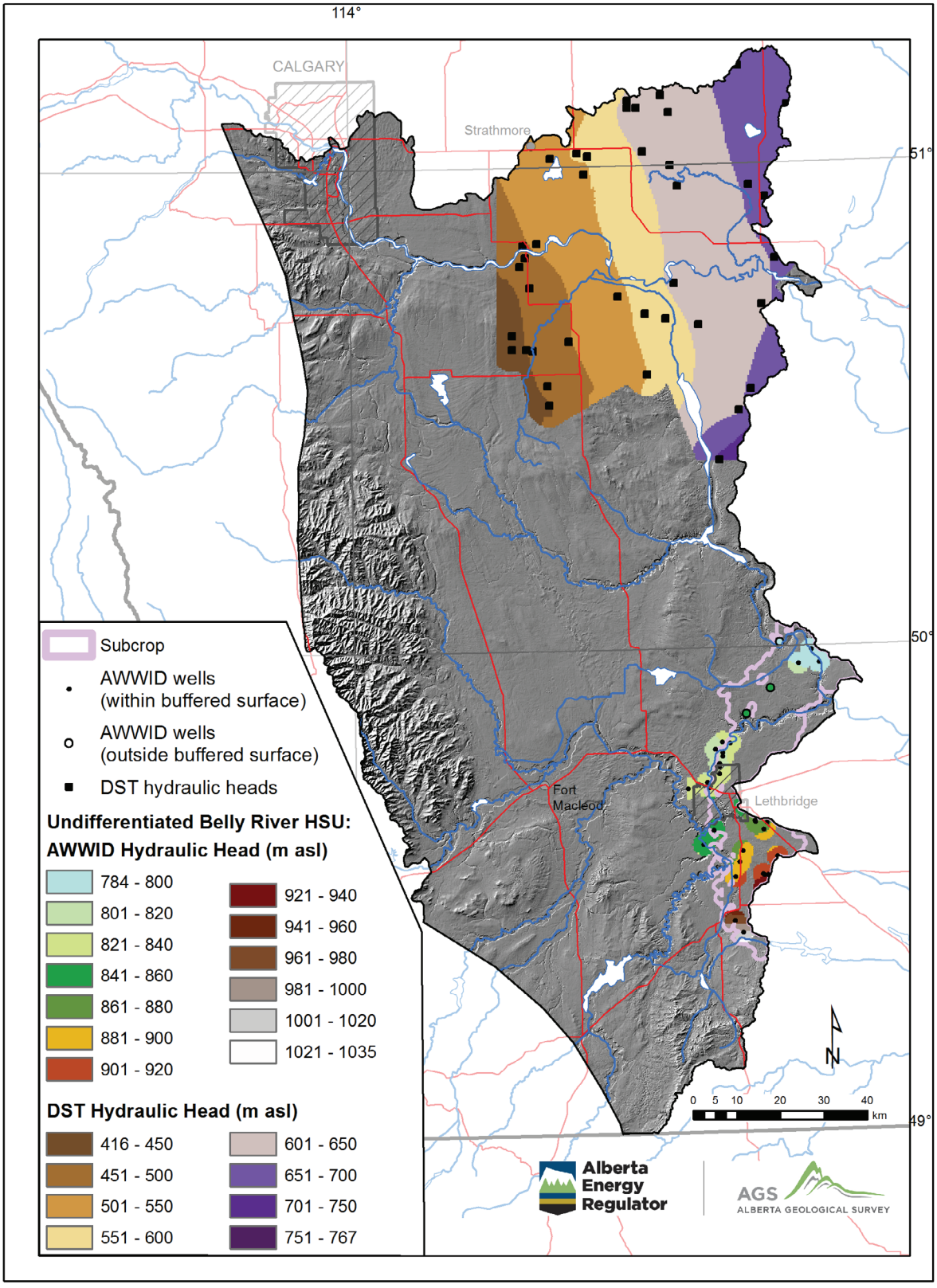

Figure A3-36. Potentiometric surfaces of the undifferentiated Belly River HSU.

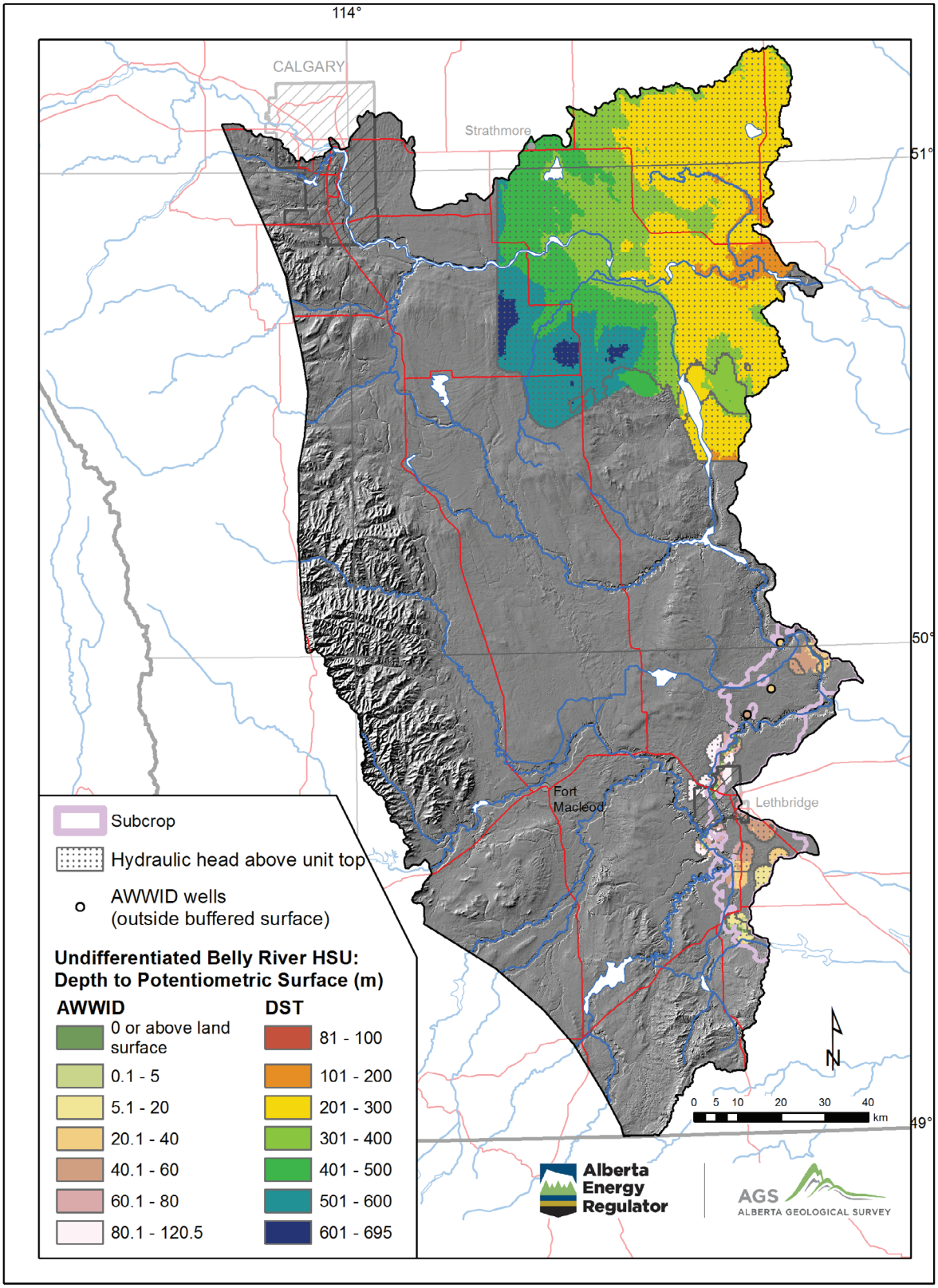

Figure A3-37. Depth to potentiometric surface for the undifferentiated Belly River HSU. There are no flowing artesian wells within the CLC in this HSU.

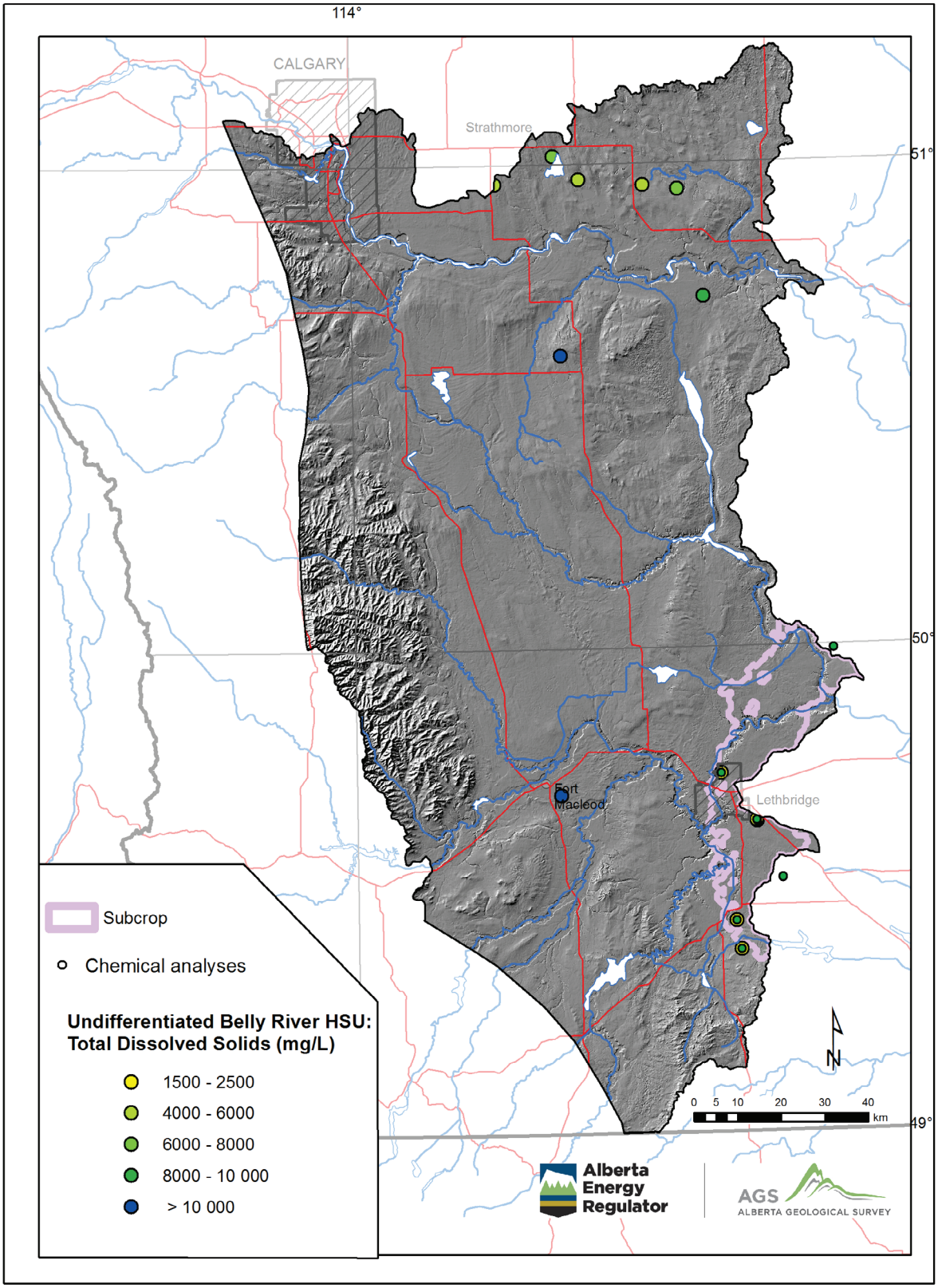

Figure A3-38. Concentration of TDS in the undifferentiated Belly River HSU. Chemical analyses in the vicinity of the subcrop area are from AWWID wells, and chemical analyses in the northern part of the CLC are from deeper oil and gas wells.

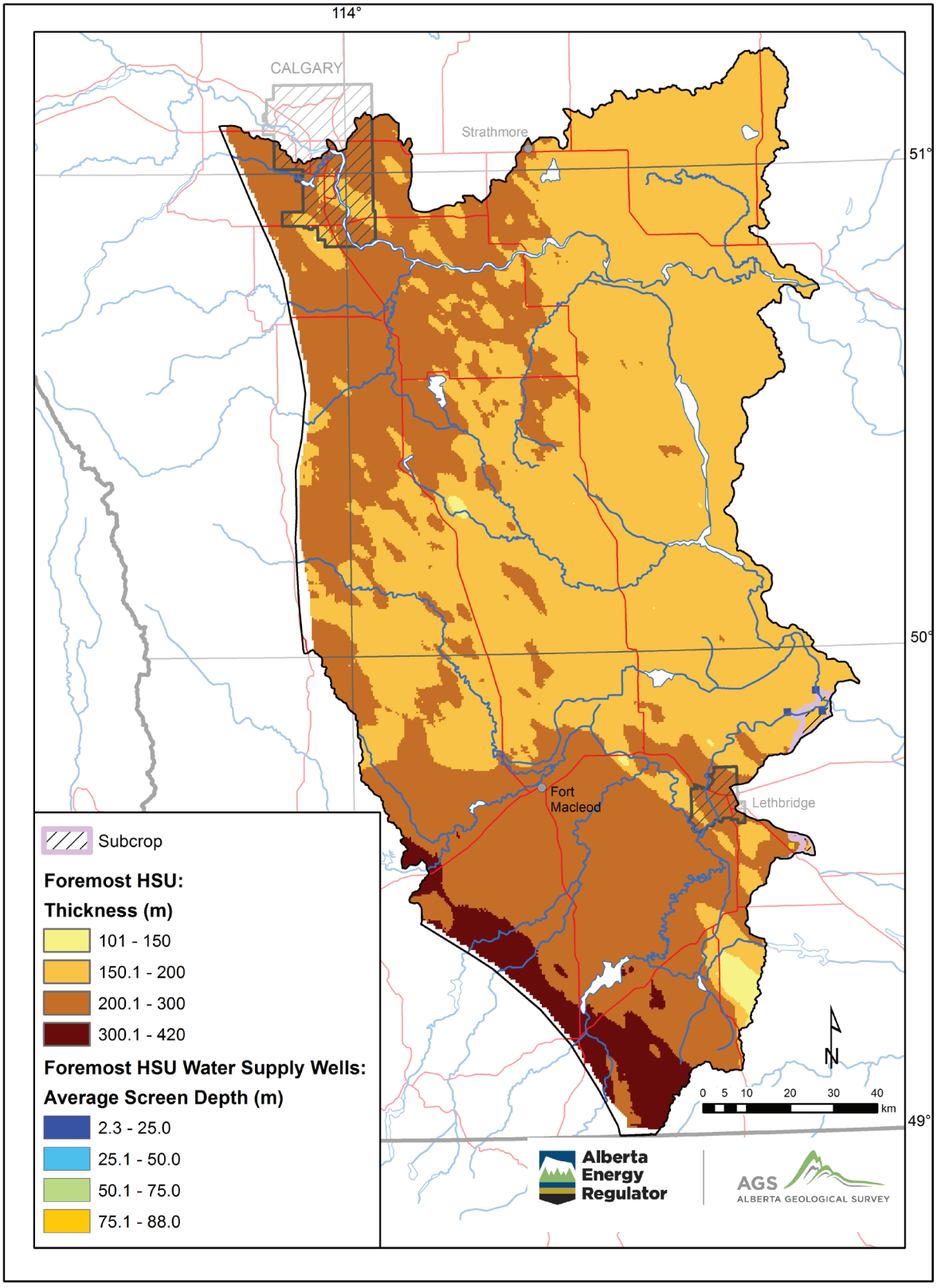

Figure A3-39. Thickness and extent of the Foremost HSU. There is a very small area of subcrop to the extreme east of the CLC near Lethbridge.

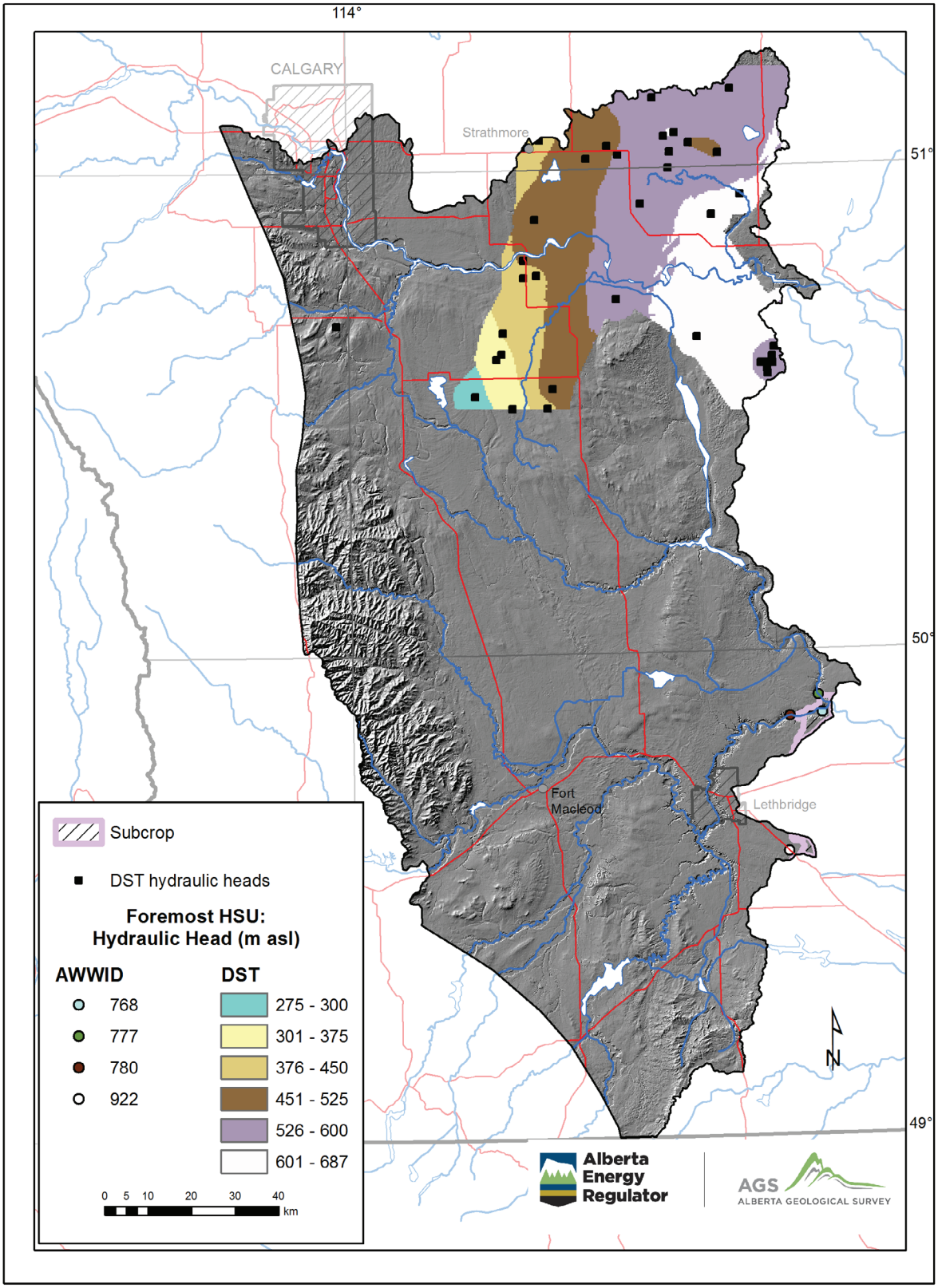

Figure A3-40. Hydraulic heads in available wells in the Foremost HSU. Only four AWWID wells with hydraulic information lie within the Foremost HSU in the CLC, hence the potentiometric surface was not interpolated. In the northern portion of the CLC, the hydraulic head was interpolated from oil and gas well DST data.

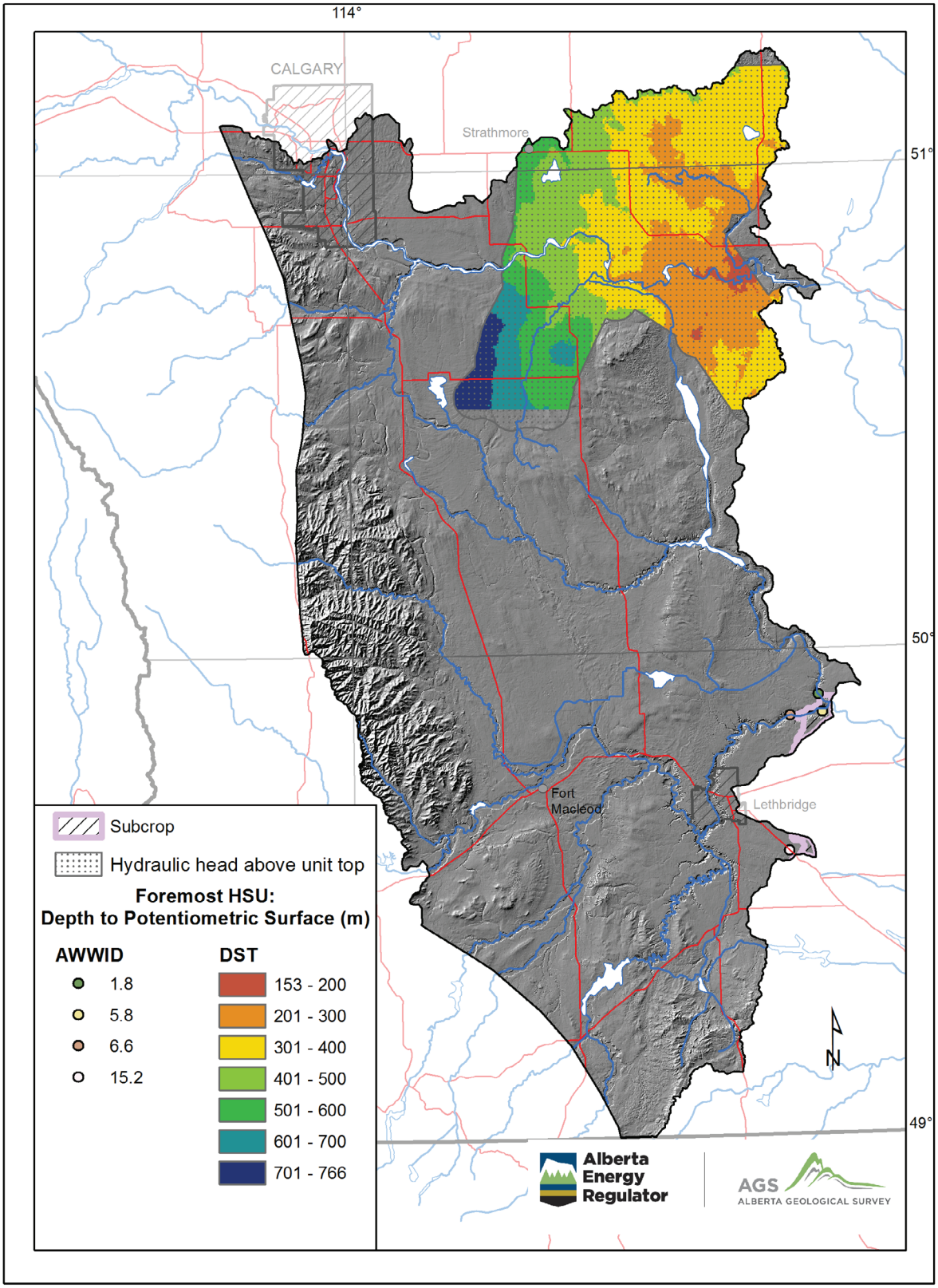

Figure A3-41. Depth to potentiometric surface in available wells in the Foremost HSU. No flowing artesian wells are present within the CLC in this HSU.

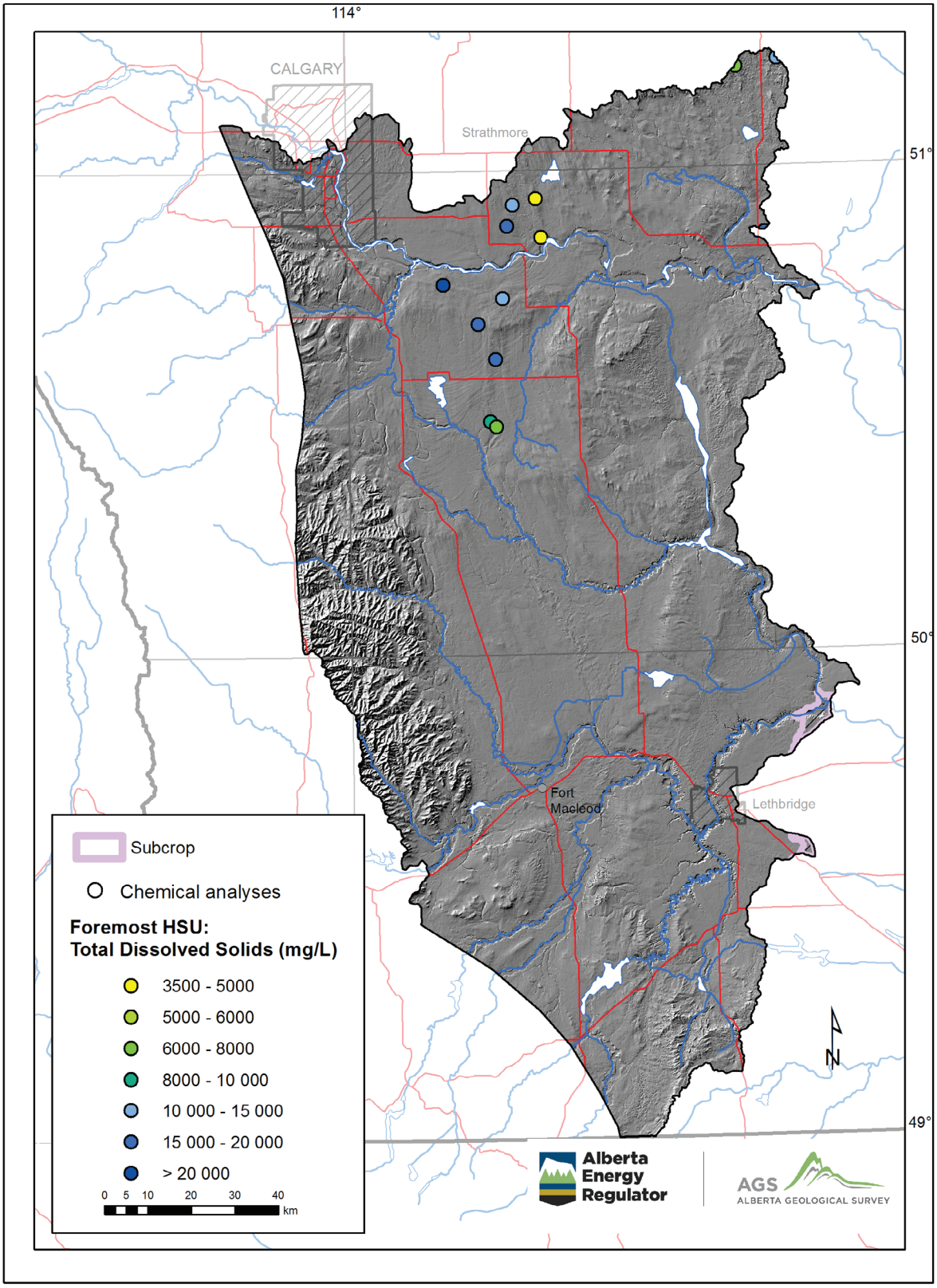

Figure A3-42. Concentration of TDS in the Foremost HSU. All chemical analyses are from deeper oil and gas wells.

Appendix 4 – Recharge Modelling

Table A4-1. Four climate stations were used in the VSMB modelling and their individual characteristics for model input. These stations were selected because they have all the required VSMB input variables (daily average temperature, precipitation, wind speed, relative humidity, and shortwave radiation) over a long period of time. The climate stations are also distributed across the CLC. Average air pressure was calculated from Allen et al. (1998, Equation 7). Location of the climate stations is displayed in Figure A4-1.

	Latitude (°)	Elevation (m asl)	Air Pressure (Pa)
#1 - Brocket ADGM	49.6107	1 073	89 243
#2 - Lethbridge CDA	49.7	921	90 877
#3 - Strathmore IMCIN	51.0387	976	90 283
#4 - Stavely AAFC	50.1833	1 364	86 182

Table A4-2. Two different soil properties were used for the VSMB simulations: SL – sandy loam, SiC – silty clay. All soil columns were homogeneous. Soil types were selected based on soil distributions in AARD (2013; see Figure A4-1 and Figure A4-2). The goal was to span the range of soil types in the CLC. Soil property information is based on Rawls et al. (1982) and Schroeder et al. (1994). Curve numbers based on USDA (1986). All soil properties are unitless.

	Soil Properties				Curve Number	
Soil Type	Field Capacity	Permanent Wilting Point	Saturated Water Content	Residual Liquid Water Content	Wheat	Grass
#1 - SL	0.2	0.11	0.45	0.04	63	39
#2 SiC	0.43	0.27	0.53	0.12	83	74

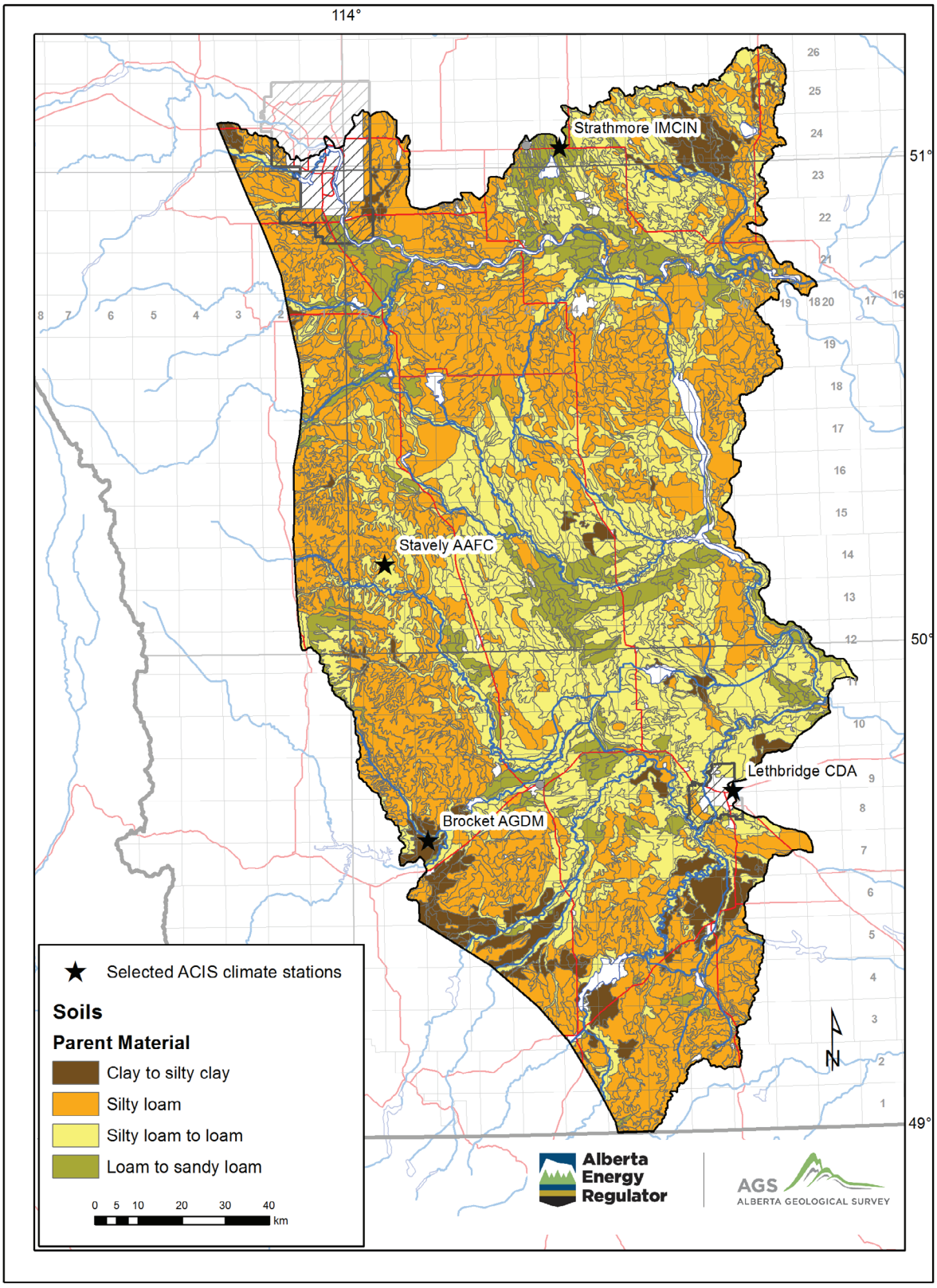

Figure A4-1. Texture of the parent material of the dominant soil type in each soils polygon in the CLC. Soil information from AARD (2013). The three climate stations used in the modelling are also shown.

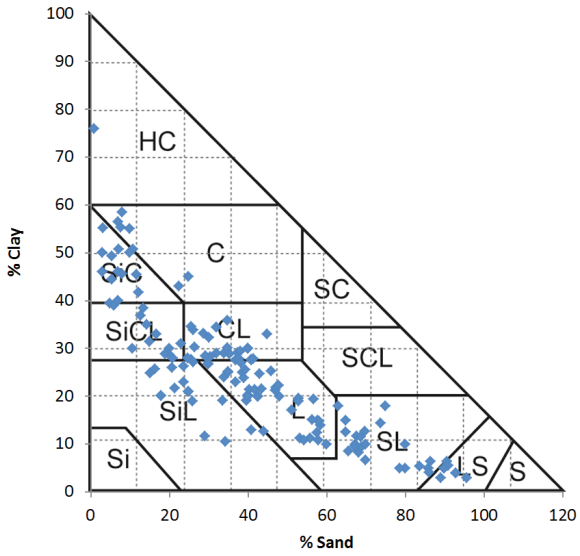

Figure A4-2. Plot of C horizon texture of the dominant soil type in each soils polygon. Data from AARD (2013).

Table A4-3. Three crop coefficient inputs used for wheat.

	Depth (cm)	0–20	20–40	40–80	80–120	120–200	200–400
	Layer #	1	2	3	4	5	6
#1 - Default	Stage 1	0.45	0.275	0.08	0.05	0.02	0.03
	Stage 2	0.4875	0.325	0.12	0.1	0.025	0.0375
	Stage 3	0.4375	0.475	0.2	0.13	0.125	0.1875
	Stage 4	0.425	0.525	0.25	0.15	0.15	0.225
	Stage 5	0.425	0.525	0.25	0.15	0.15	0.225
#2 - Modified from Akinremi et al. (1996)	Stage 1	0.5	0.05	0.05	0.01	0.01	0
	Stage 2	0.55	0.1	0.1	0.02	0.01	0
	Stage 3	0.75	0.2	0.2	0.1	0.05	0
	Stage 4	0.8	0.25	0.25	0.15	0.05	0
	Stage 5	0.8	0.25	0.25	0.15	0.05	0
#3	Stage 1	0.2	0.12	0.04	0.012	0.012	0.012
	Stage 2	0.3	0.18	0.06	0.018	0.018	0.018
	Stage 3	0.45	0.27	0.09	0.027	0.027	0.027
	Stage 4	0.6	0.36	0.12	0.036	0.036	0.036
	Stage 5	0.5	0.3	0.1	0.03	0.03	0.03

Table A4-4. Three crop coefficient inputs used for grass.

	Depth (cm)	0–20	20–40	40–80	80–120	120–200	200–400
	Layer #	1	2	3	4	5	6
#1 - Default	**Stage 1**	0.50	0.2	0.12	0.04	0.01	0.01
	Stage 2	0.64	0.2	0.2	0.05	0.01	0.025
	Stage 3	0.57	0.3	0.2	0.08	0.03	0.075
#2 – Modified from Hayashi et al. (2010)	**Stage 1**	0.22	0.063	0.012	0.005	0.005	0.005
	Stage 2	0.68	0.142	0.038	0.005	0.005	0.005
	Stage 3	0.68	0.215	0.095	0.015	0.015	0.015
#3	**Stage 1**	0.20	0.12	0.04	0.012	0.012	0.012
	Stage 2	0.50	0.3	0.1	0.03	0.03	0.03
	Stage 3	0.43	0.255	0.085	0.0255	0.0255	0.0255

Table A4-5. Three drying curve coefficients for VSMB. Drying curves #2 and #3 are the same for both grass and wheat.

Drying Curve Coefficients	#1 (Moderate ET; Default)		#2 (Low ET; DC1 from Hayashi et al. 2010)	#3 (High ET; DC4 from Hayashi et al. 2010)
	Grass	Wheat		
C_m	0.5	0.27	0.5	0.11
C_n	0.9	0.9	0.72	0.95
C_h	0.05	0.3	0.05	0.05
C_r	1	1.58	1.2	1

Table A4-6. Parameters common to all VSMB simulations.

Description and Units*	Value
Slope (°)	0
Aspect (°)	180
Forest cover fraction (–)	0
Drift factor (–)	1
Thermal conductivity (W/m/K)	
- Water	0.57
- Ice	2.2
- Soil material	2.9
Volumetric heat capacity ($J/m^3/K$)	
- Water	4200000
- Ice	1900000
- Soil material	2000000
Latent heat of fusion (J/Kg/K)	335000
Density of water (Kg/m^3)	1000
Distance between centre of last soil layer and bottom imaginary boundary (m)	5
Temperature of bottom (°C)	7

Description and Units*	Value
Frozen runoff coefficient (–)	0.02
Vegetation resistance (m^2/K/W)	0.2
Allowable water flux for frozen-saturated soil (mm/d)	10
Number of soil layers (–)	6
Thickness of each soil layer (top to bottom) (m)	200, 200, 400, 400, 800, 2000
Coefficient to modify field capacity of layer (–)	1
Temperature above which all is rain (°C)	2
Temperature below which all is snow (°C)	1.99
Emissivity of snow (–)	0.99
Ground heat capacity (KJ/Kg/°C)	1.5
Nominal measurement height for air temperature and humidity (m)	2
Surface aerodynamic roughness (m)	0.001 (grass), 0.003 (wheat)
Snow density (kg/m^3)	190
Soil density (kg/m^3)	1400
Liquid holding capacity of snow (–)	0.05
Snow saturated hydraulic conductivity (m/s)	0.00556
Bare ground albedo (–)	0.19
Visual new snow albedo (–)	0.85
NIR new snow albedo (–)	0.65
Thermal conductivity of fresh (dry) snow (KJ/m/K/hr)	0.54
Low frequency fluctuation in deep snow/soil layer (–)	0.0654
Amplitude correction coefficient of heat conduction (–)	1.5
Stability correction control parameter	1
Threshold depth for new snow (m)	0.002
The fraction of surface melt that runs off (e.g., from a glacier)	0
Albedo extinction parameter (m)	0.1
Bristow-Campbell coefficient A	0.8
Bristow-Campbell coefficient C	2.4
Snow surface modelling option	1

* Some parameters are unitless, expressed as (–).

Table A4-7. Average annual recharge (AET) and surface runoff from the VSMB simulation of eight hydrological years (November 1, 2005, to October 31, 2013). Highlighted cells are those simulations that produced recharge. First portion of simulation ID is soil type (sandy loam [SL] or silty clay [SiC]), second portion is vegetation type (grass [g] or wheat [w]), third part is the crop coefficient values (#1,2,3 from Table A4-3 and Table A4-4), and last part is the drying curve coefficient values (#1,2,3 from Table A4-5).

	Brocket AGDM			Lethbridge CDA			Stavely AAFC			Strathmore IMCIN		
Simulation ID	Recharge (mm)	AET (mm)	Surface Run-off (mm)	Recharge (mm)	AET (mm)	Surface Run-off (mm)	Recharge (mm)	AET (mm)	Surface Run-off (mm)	Recharge (mm)	AET (mm)	Surface Run-off (mm)
SiC_g_1_1	0	308	0.9	0	280	0.0	0	402	2.0	0	322	0.6
SiC_g_1_2	0	309	0.9	0	281	0.0	0	401	2.0	0	324	0.9
SiC_g_1_3	0	307	0.9	0	279	0.0	0	402	2.0	0	323	0.5
SiC_g_2_1	0	320	1.3	0	282	0.0	38	348	2.9	0	330	0.8
SiC_g_2_2	7	301	1.1	0	283	0.0	70	311	3.4	16	305	0.7
SiC_g_2_3	0	326	1.1	0	279	0.0	22	365	2.9	0	335	0.7
SiC_g_3_1	0	318	1.2	0	283	0.0	45	338	2.9	6	318	0.8
SiC_g_3_2	10	295	1.5	0	283	0.4	83	295	3.5	40	280	1.2
SiC_g_3_3	0	314	1.2	0	282	0.0	24	361	2.9	0	335	0.9
SiC_w_1_1	0	300	2.5	0	277	1.8	0	375	11.6	0	316	2.1
SiC_w_1_2	0	300	2.6	0	275	3.5	0	375	11.7	0	316	2.8
SiC_w_1_3	0	299	2.4	0	276	1.8	0	378	9.3	0	316	1.4
SiC_w_2_1	0	303	2.6	0	277	3.5	11	366	11.4	0	318	1.9
SiC_w_2_2	0	303	2.7	0	277	3.5	11	361	11.5	0	319	1.9
SiC_w_2_3	0	302	2.4	0	277	1.8	3	374	11.4	0	318	1.9
SiC_w_3_1	28	268	5.5	0	275	4.3	95	266	17.7	51	262	5.7
SiC_w_3_2	39	255	7.0	9	267	4.8	107	252	17.7	64	249	5.7
SiC_w_3_3	7	293	5.3	0	277	4.1	73	291	17.6	26	286	3.4
SL_g_1_1	0	311	0.0	0	280	0.0	7	393	0.9	0	322	0.0
SL_g_1_2	0	311	0.1	0	281	0.2	10	381	1.5	0	324	0.0
SL_g_1_3	0	310	0.0	0	278	0.0	4	396	0.9	0	322	0.0
SL_g_2_1	18	284	0.1	0	282	0.2	77	304	2.0	23	296	0.0
SL_g_2_2	38	263	0.1	10	269	0.2	102	276	2.2	45	272	0.0
SL_g_2_3	9	293	0.0	0	283	0.0	67	315	1.9	16	303	0.0

Simulation ID	Brocket AGDM			Lethbridge CDA			Stavely AAFC			Strathmore IMCIN		
	Recharge (mm)	AET (mm)	Surface Run-off (mm)	Recharge (mm)	AET (mm)	Surface Run-off (mm)	Recharge (mm)	AET (mm)	Surface Run-off (mm)	Recharge (mm)	AET (mm)	Surface Run-off (mm)
SL_g_3_1	12	292	0.1	0	284	0.2	75	304	2.6	26	294	0.0
SL_g_3_2	34	266	0.1	6	276	0.2	108	269	2.5	58	260	0.0
SL_g_3_3	4	307	0.1	0	284	0.0	56	325	2.0	11	313	0.0
SL_w_1_1	0	299	2.2	0	275	3.5	0	374	12.9	0	316	2.0
SL_w_1_2	0	299	2.3	0	275	3.6	0	374	12.9	0	316	2.0
SL_w_1_3	0	298	2.0	0	277	1.9	0	377	10.5	0	317	1.2
SL_w_2_1	8	293	2.4	2	274	3.5	48	321	13.0	12	305	1.9
SL_w_2_2	9	291	3.0	2	274	3.6	52	316	13.0	14	303	2.0
SL_w_2_3	0	298	2.4	1	275	3.3	37	332	12.7	6	309	1.2
SL_w_3_1	56	240	4.6	22	252	4.1	118	243	16.3	69	243	4.3
SL_w_3_2	65	229	4.7	31	242	4.1	128	231	16.3	80	230	4.4
SL_w_3_3	35	259	4.5	6	272	4.1	100	263	16.1	47	265	4.3
Average Annual*	24	277	3	10	267	3	58	318	8	34	283	2
Minimum Average Annual*	4	229	0	1	242	0	3	231	1	6	230	0
Maximum Average Annual*	65	307	7	31	276	5	128	396	18	80	318	6

* Of those simulations which produced recharge (i.e., highlighted cells)

Appendix 5 – Slice Mapping Results

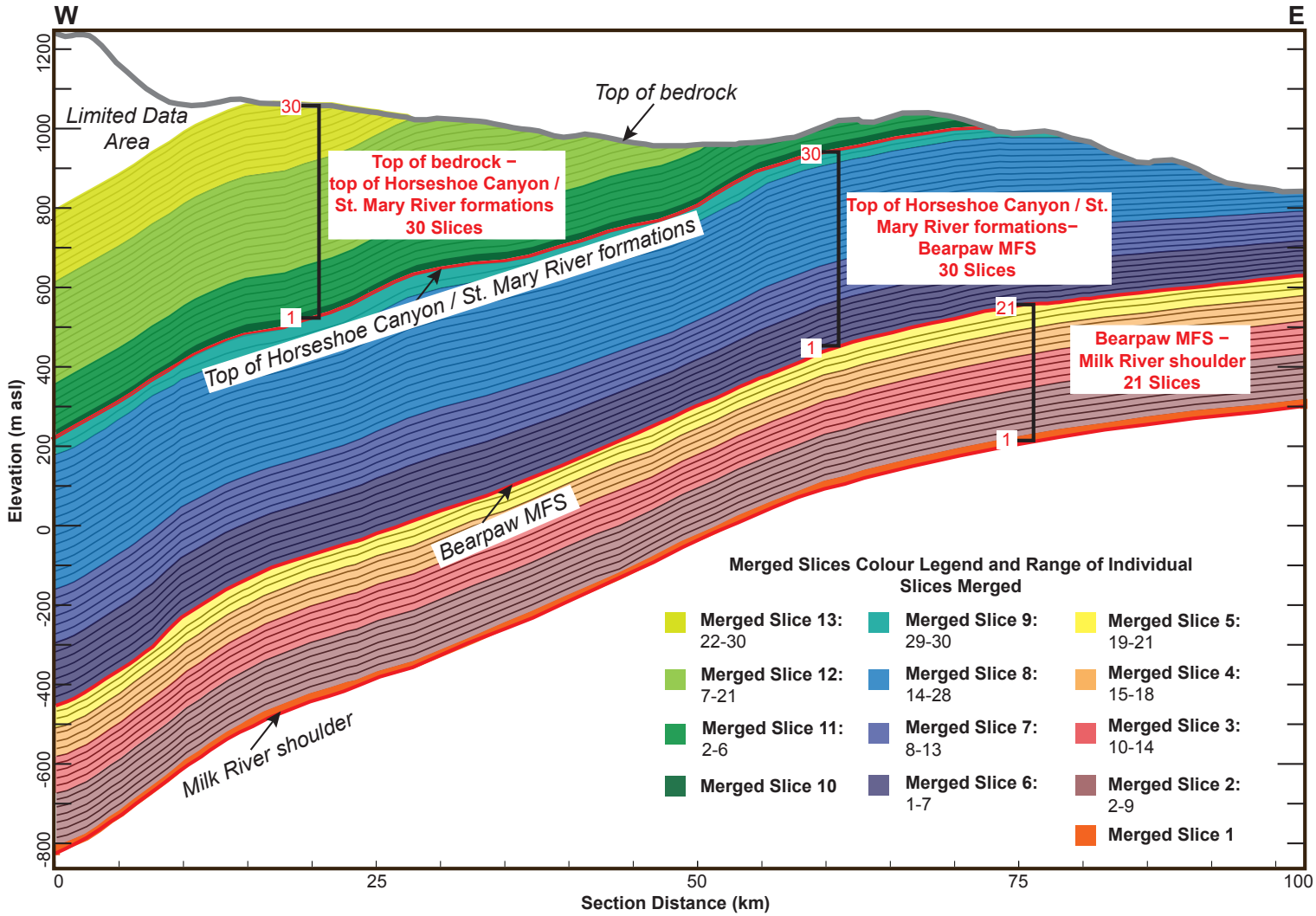

Figure A5-1. West–east cross-section showing the 81 slices that were evaluated within three different intervals (i.e., top of bedrock – top of Horseshoe Canyon / St. Mary River formations; top of Horseshoe Canyon / St. Mary River formations – Bearpaw MFS; Bearpaw MFS – Milk River shoulder). The 81 slices were merged based on natural geological patterns and are displayed on the cross-section using different colours to show the slices that have been grouped together.

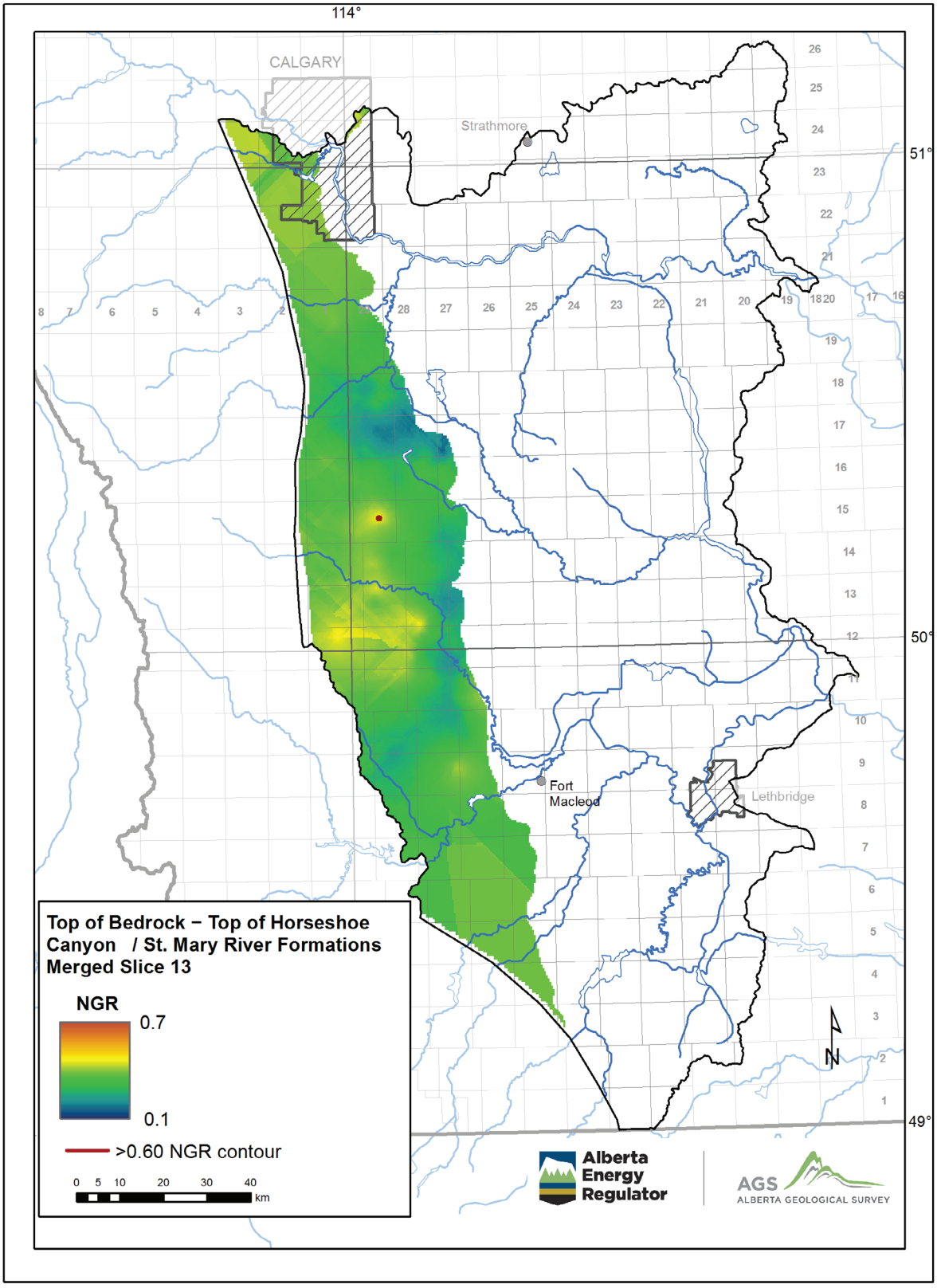

Figure A5-2. Merged slice 13 and the ≥0.60 NGR polygon.

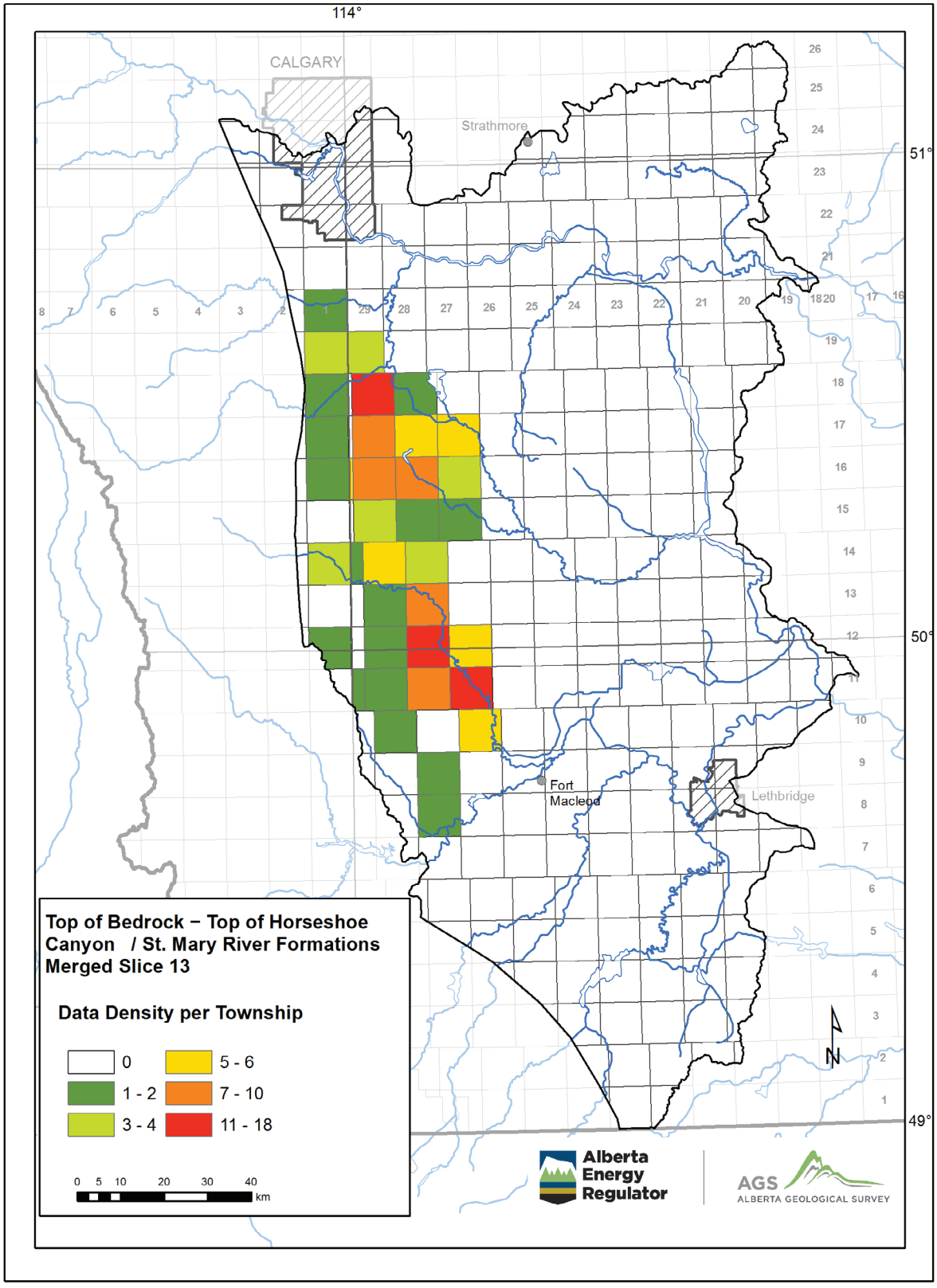

Figure A5-3. Data density map for merged slice 13.

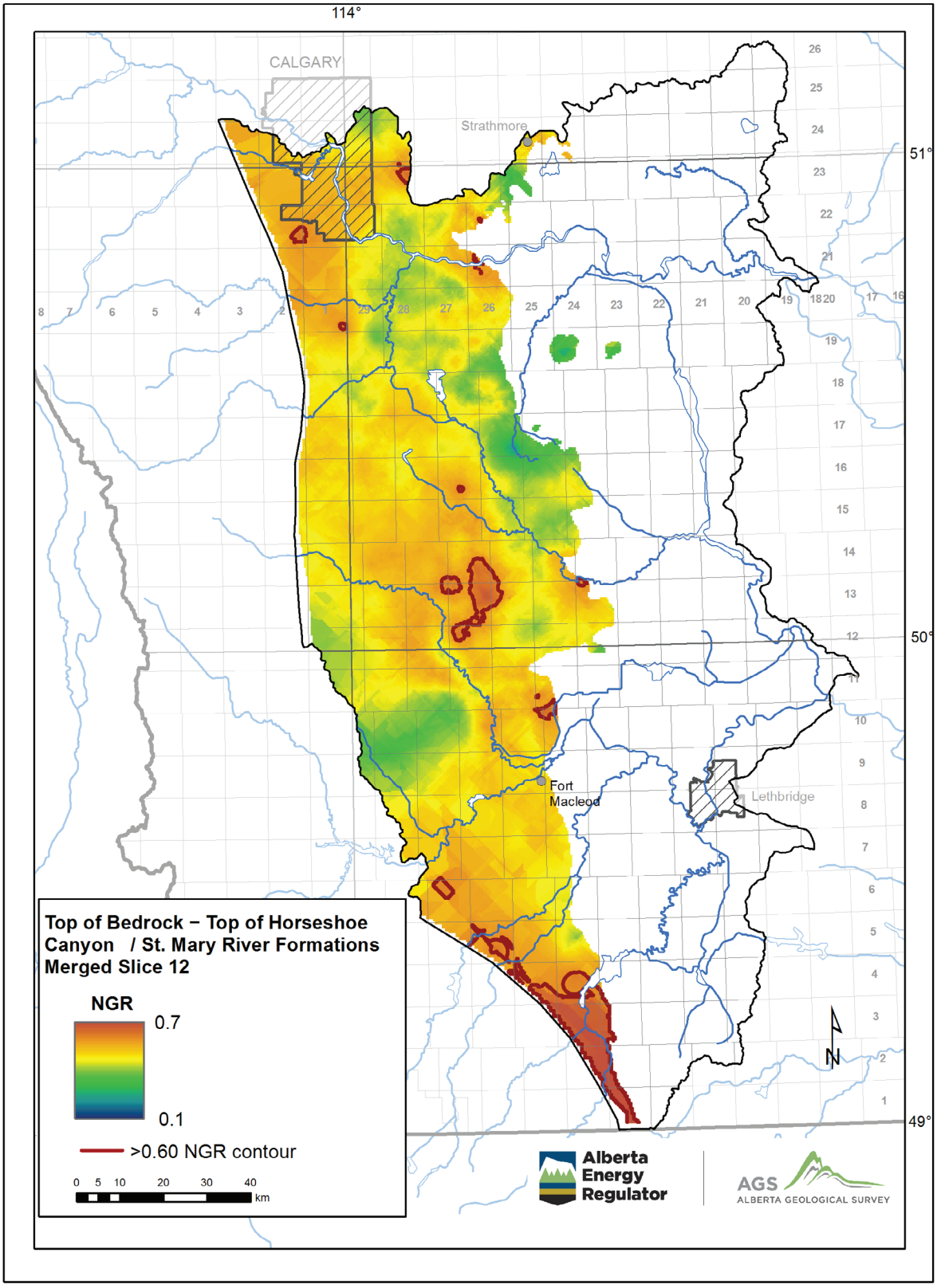

Figure A5-4. Merged slice 12 and the ≥0.60 NGR polygon.

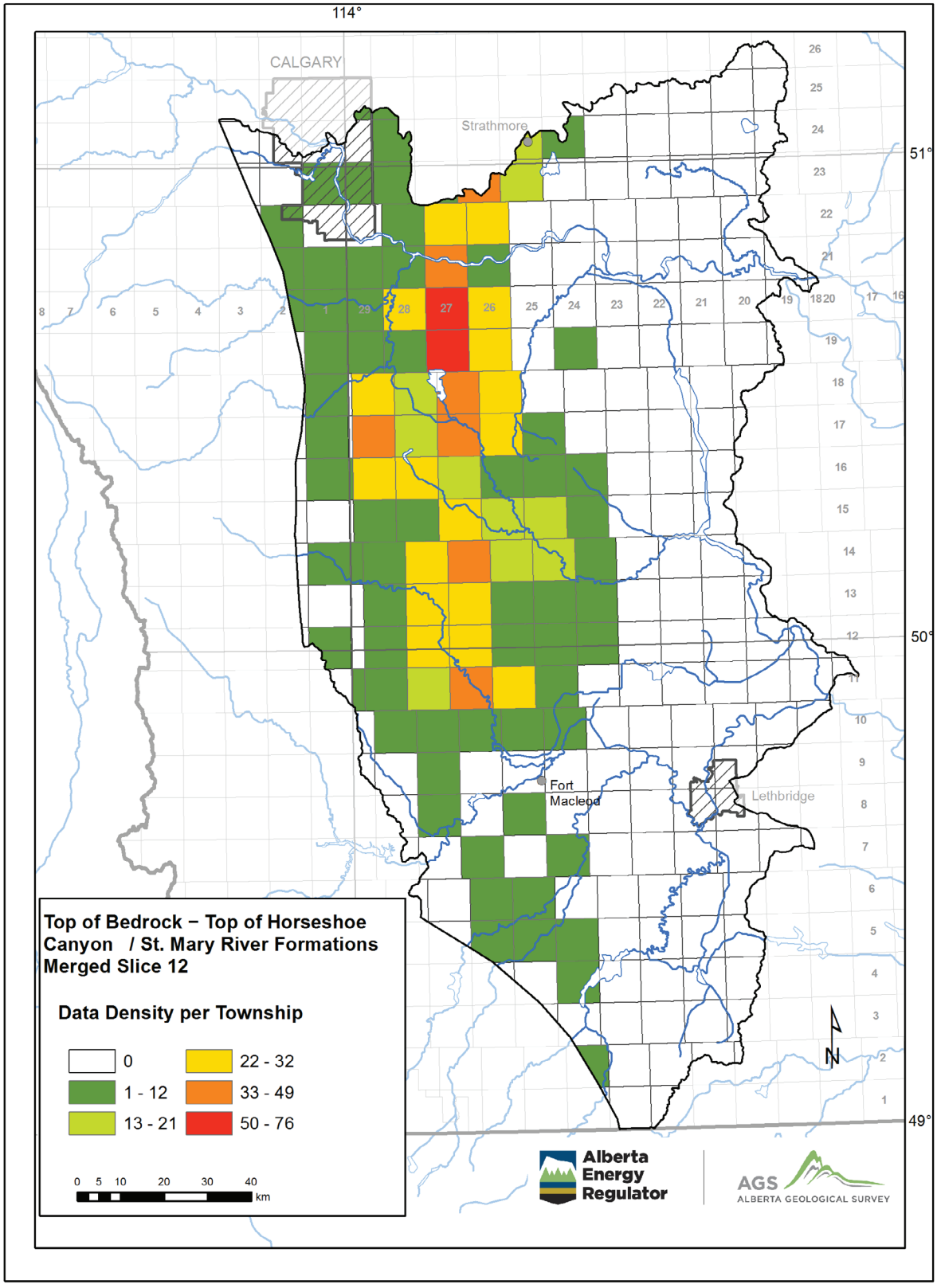

Figure A5-5. Data density map for merged slice 12.

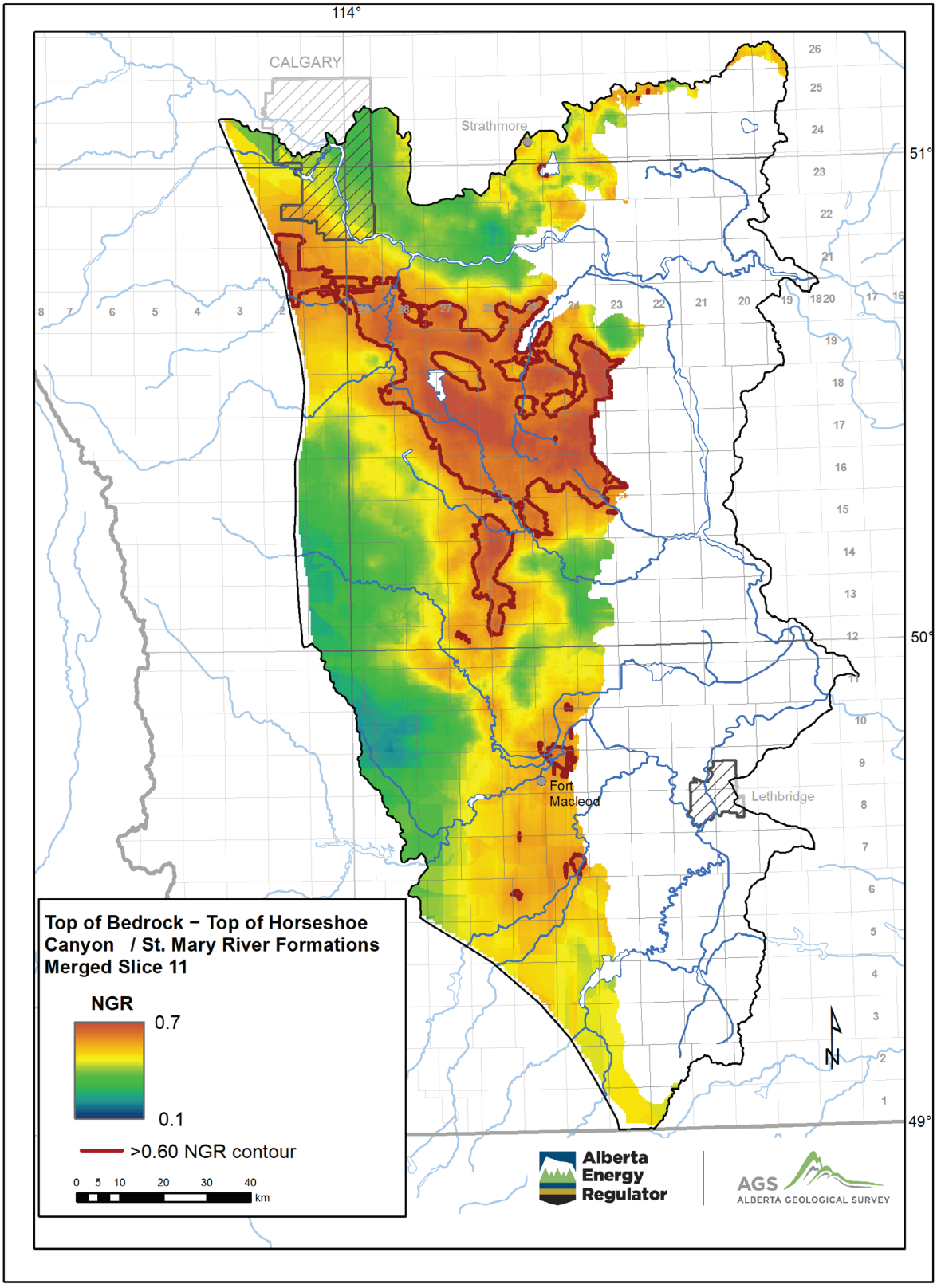

Figure A5-6. Merged slice 11 and the ≥0.60 NGR polygon.

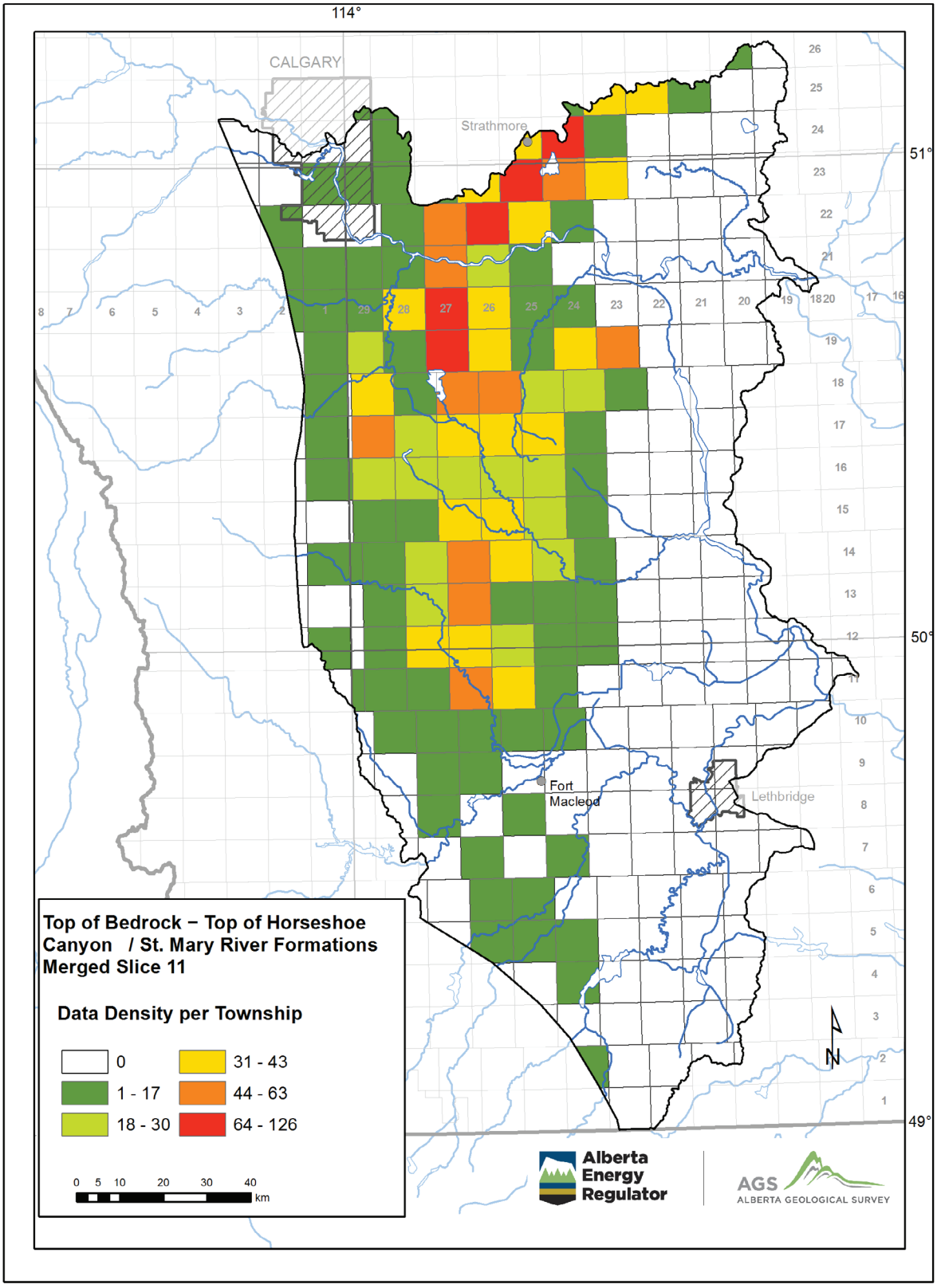

Figure A5-7. Data density map for merged slice 11.

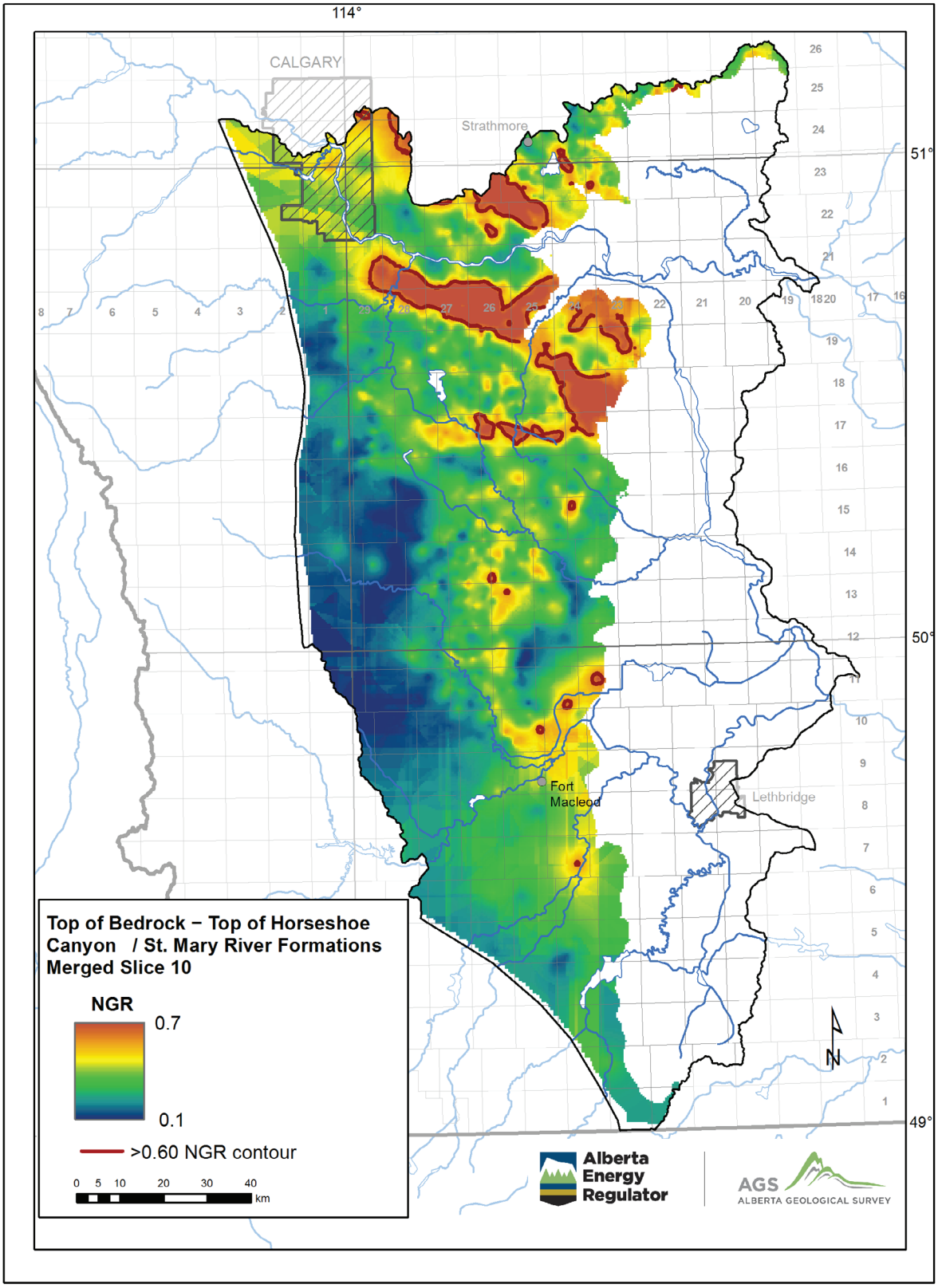

Figure A5-8. Merged slice 10 and the ≥0.60 NGR polygon.

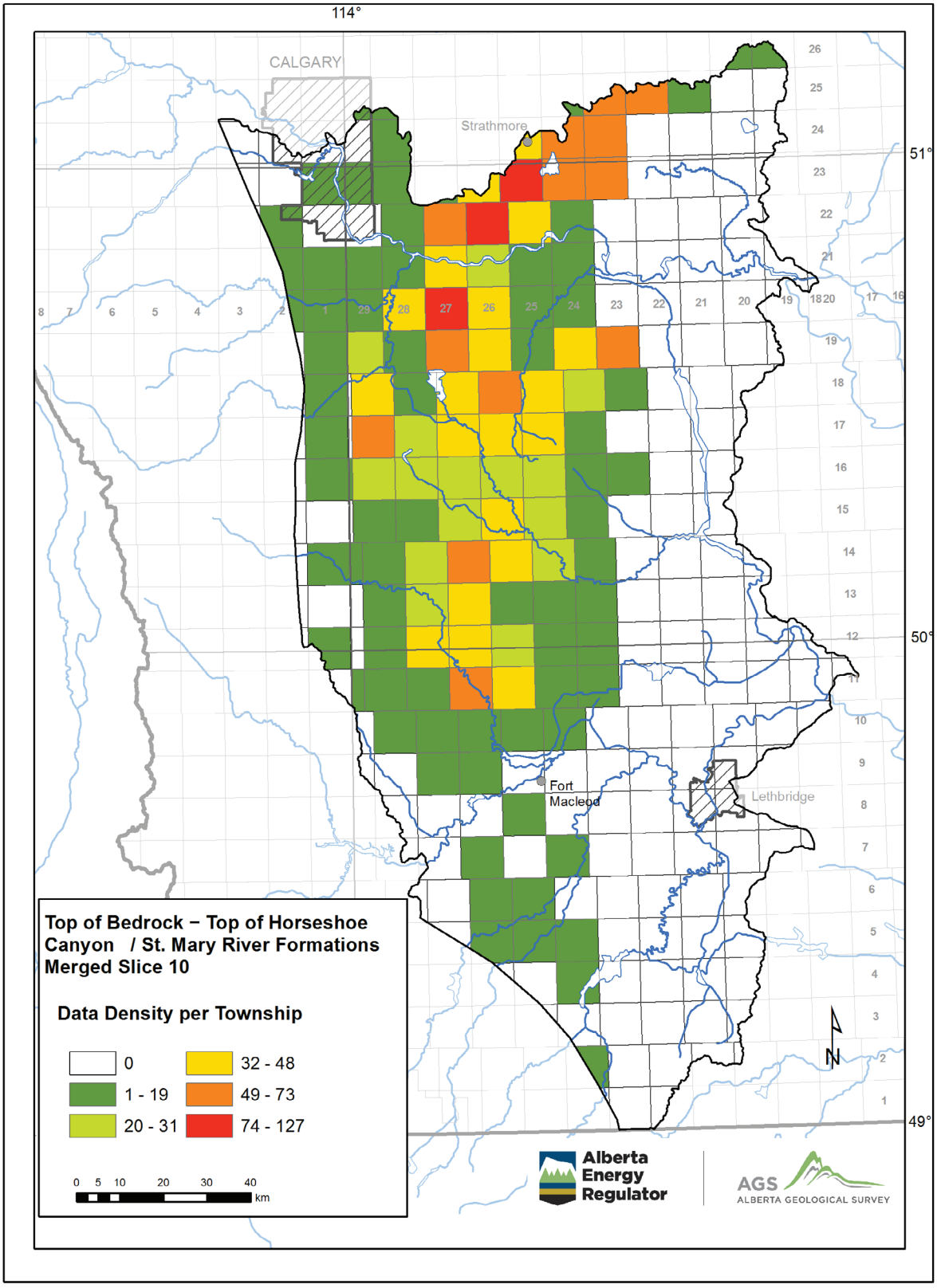

Figure A5-9. Data density map for merged slice 10.

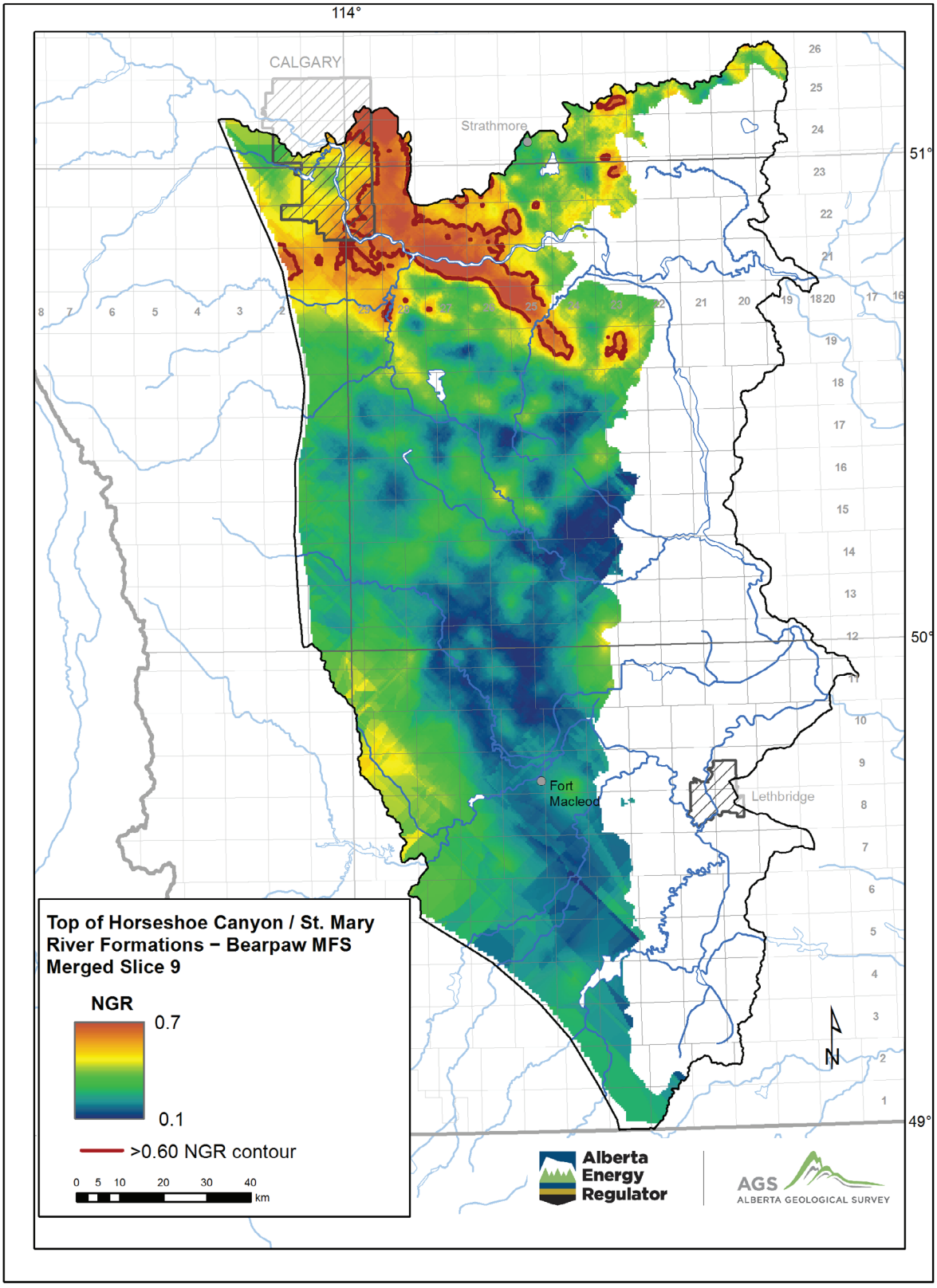

Figure A5-10. Merged slice 9 and the ≥0.60 NGR polygon.

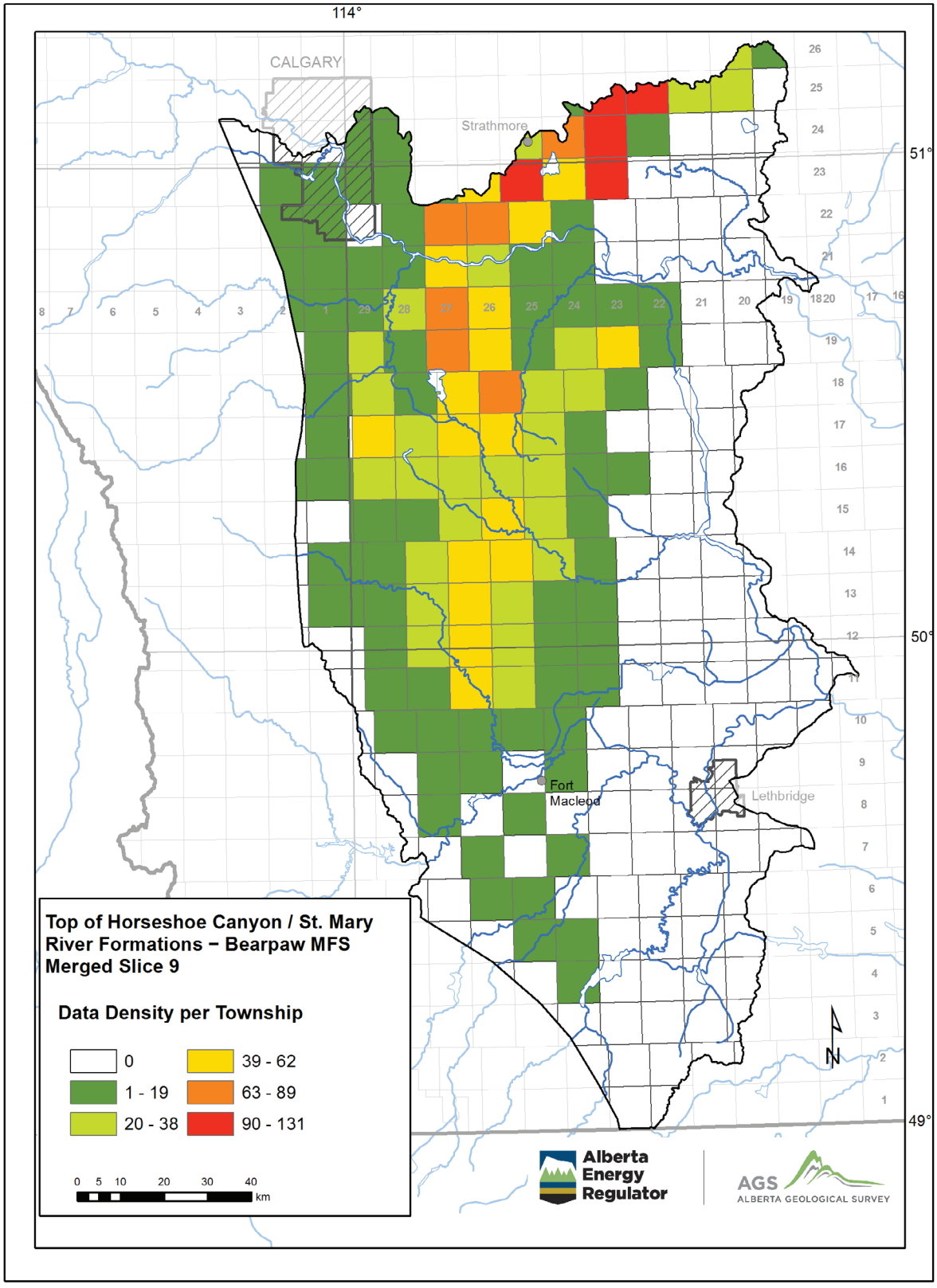

Figure A5-11. Data density map for merged slice 9.

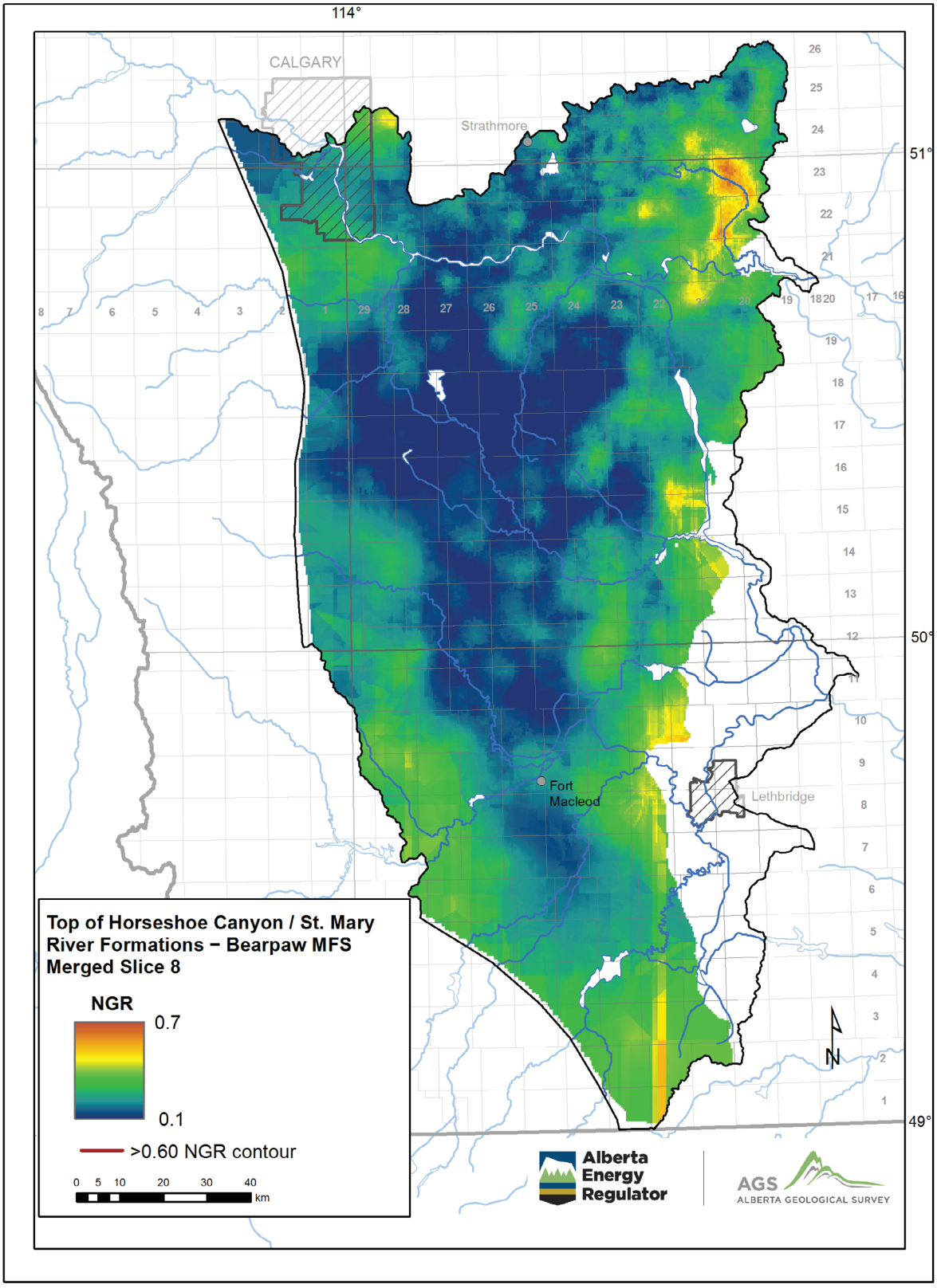

Figure A5-12. Merged slice 8 and the ≥0.60 NGR polygon.

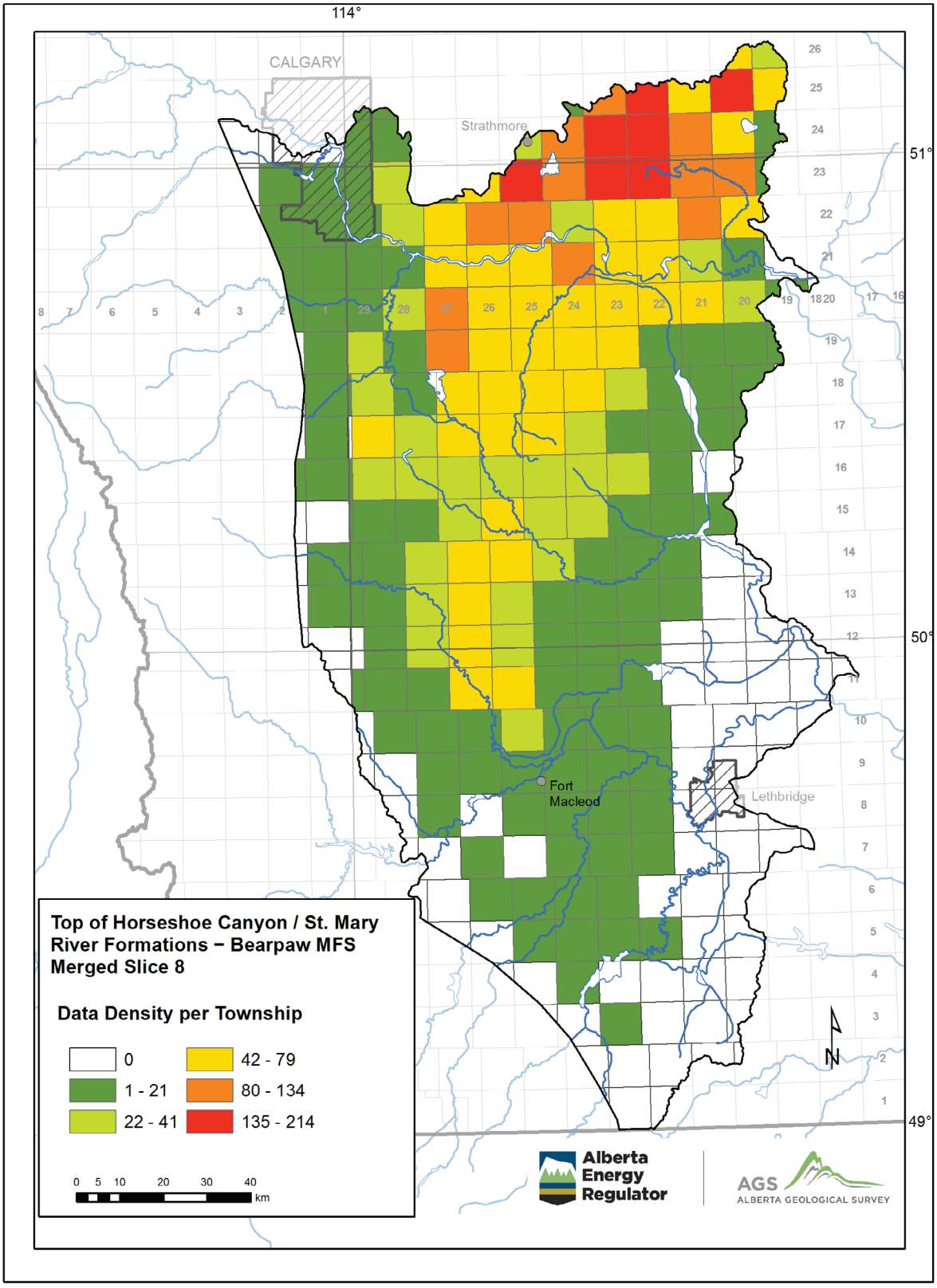

Figure A5-13. Data density map for merged slice 8.

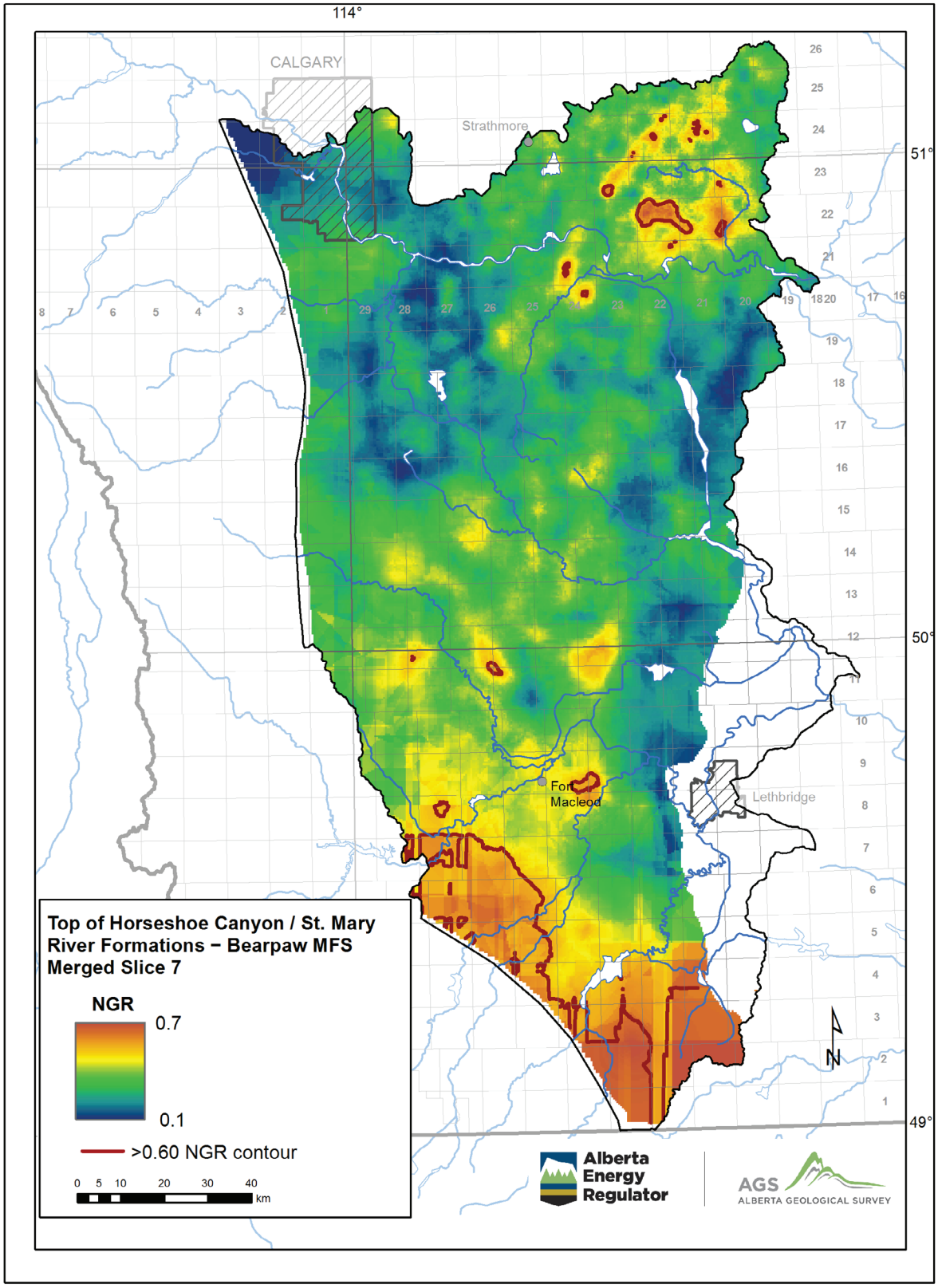

Figure A5-14. Merged slice 7 and the ≥0.60 NGR polygon.

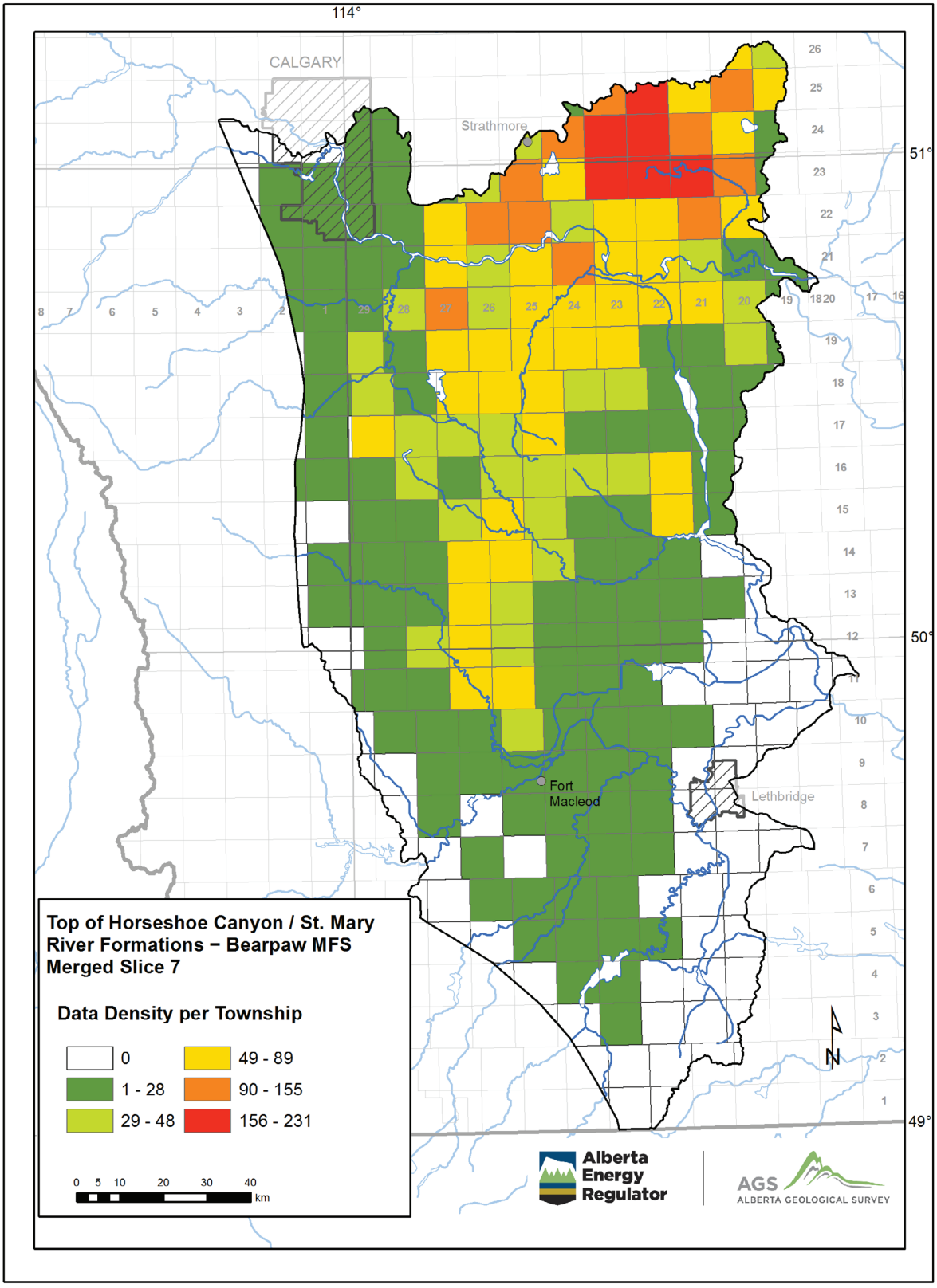

Figure A5-15. Data density map for merged slice 7.

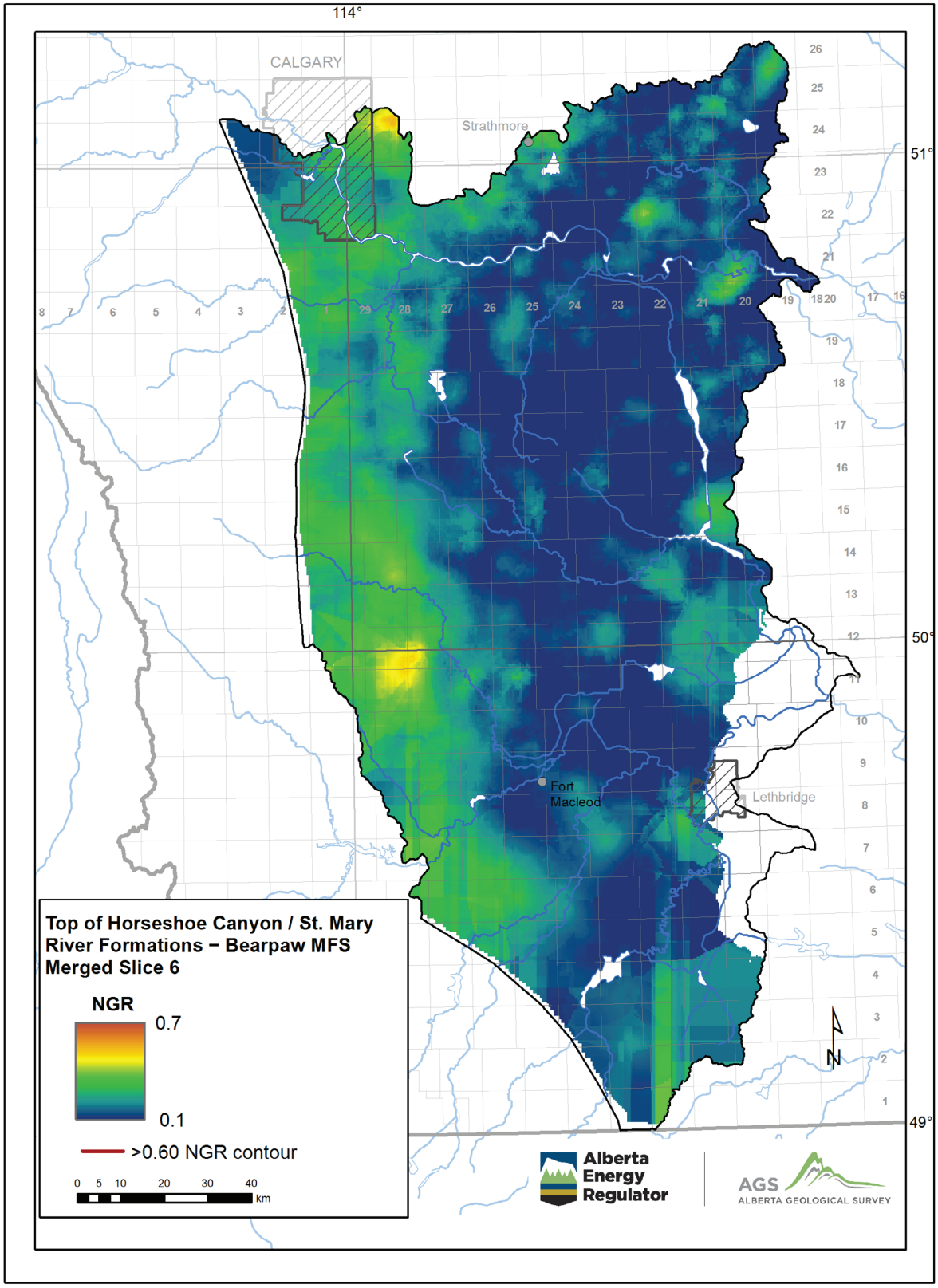

Figure A5-16. Merged slice 6 and the ≥0.60 NGR polygon.

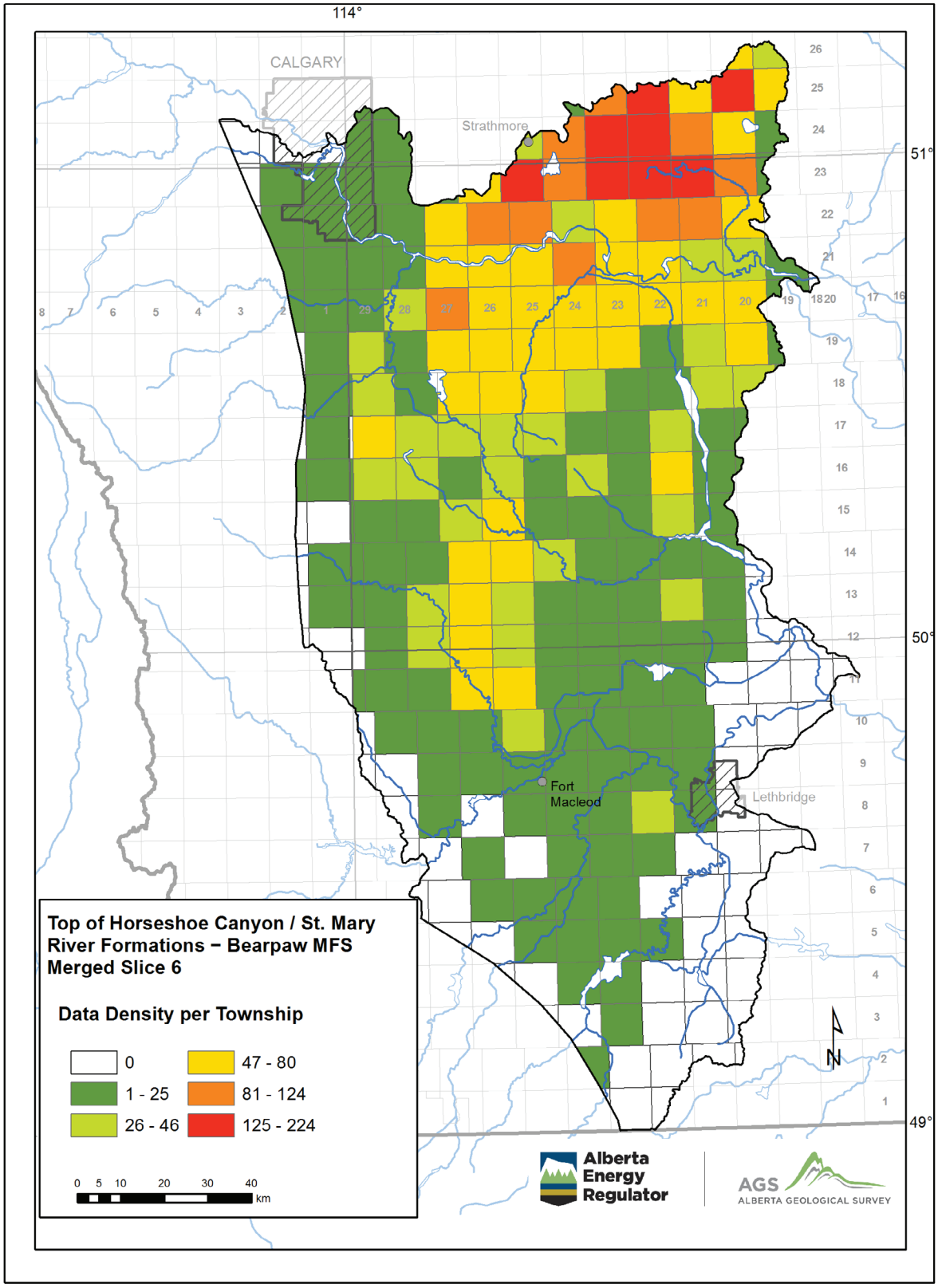

Figure A5-17. Data density map for merged slice 6.

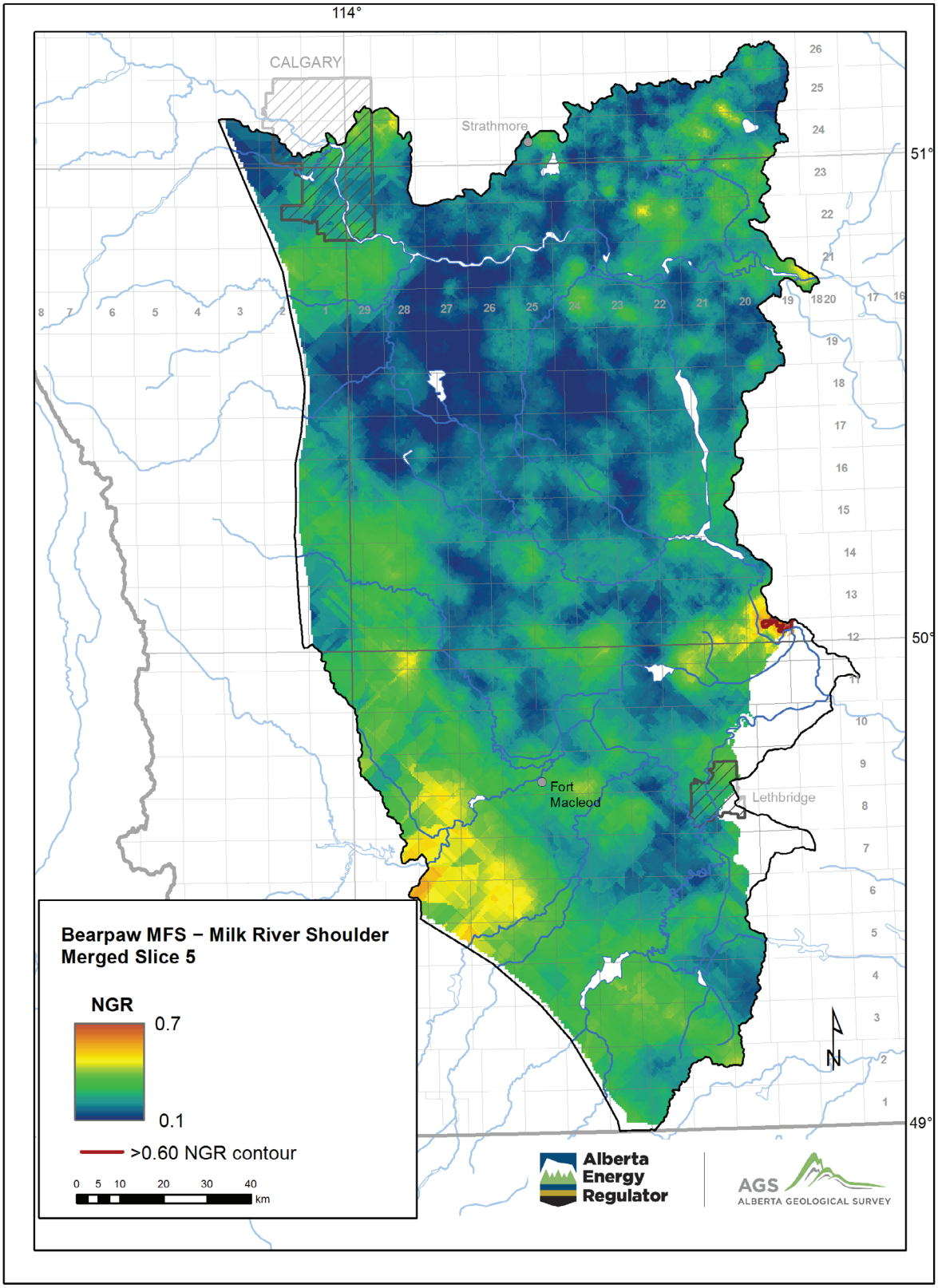

Figure A5-18. Merged slice 5 and the ≥0.60 NGR polygon.

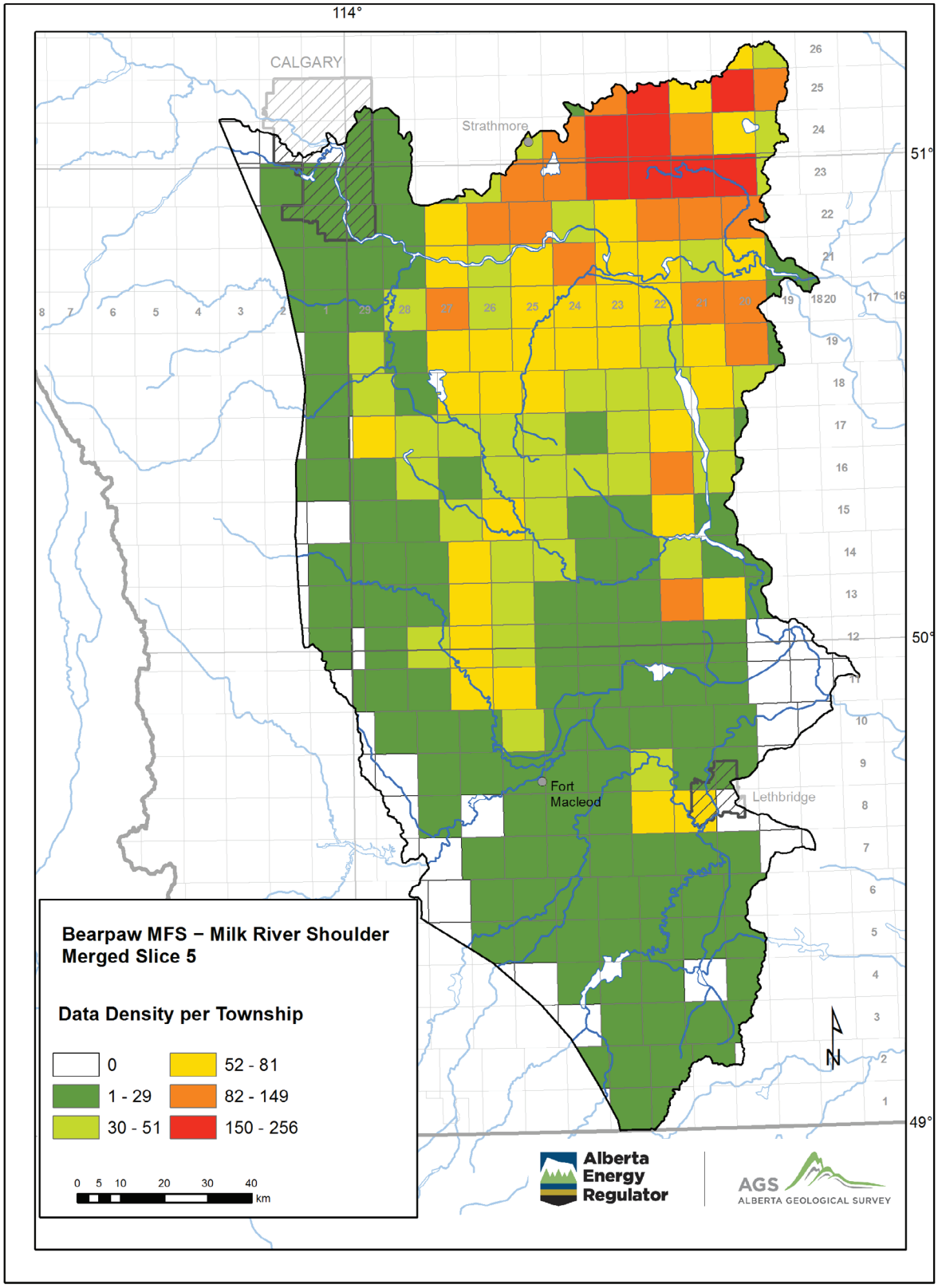

Figure A5-19. Data density map for merged slice 5.

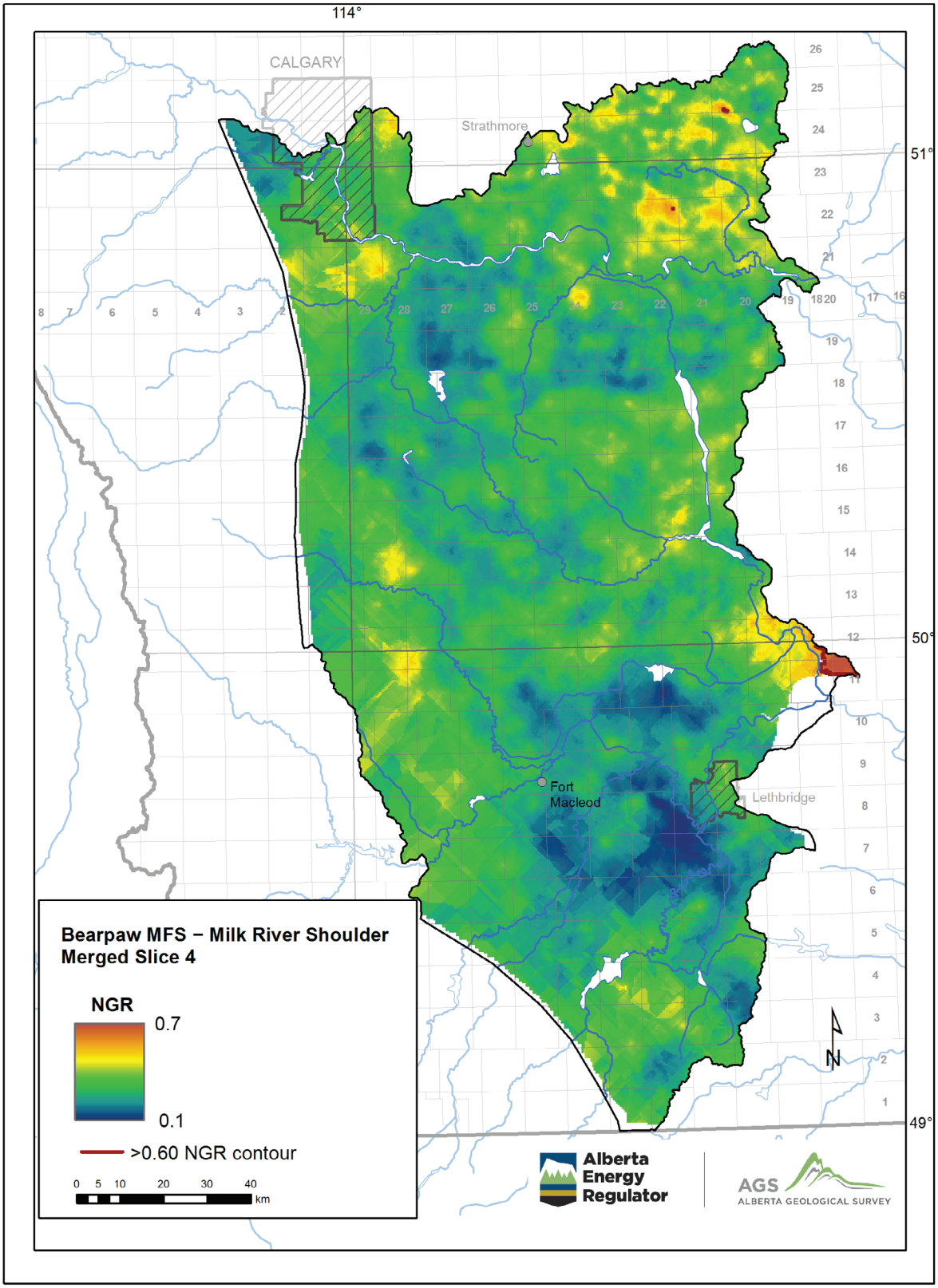

Figure A5-20. Merged slice 4 and the ≥0.60 NGR polygon.

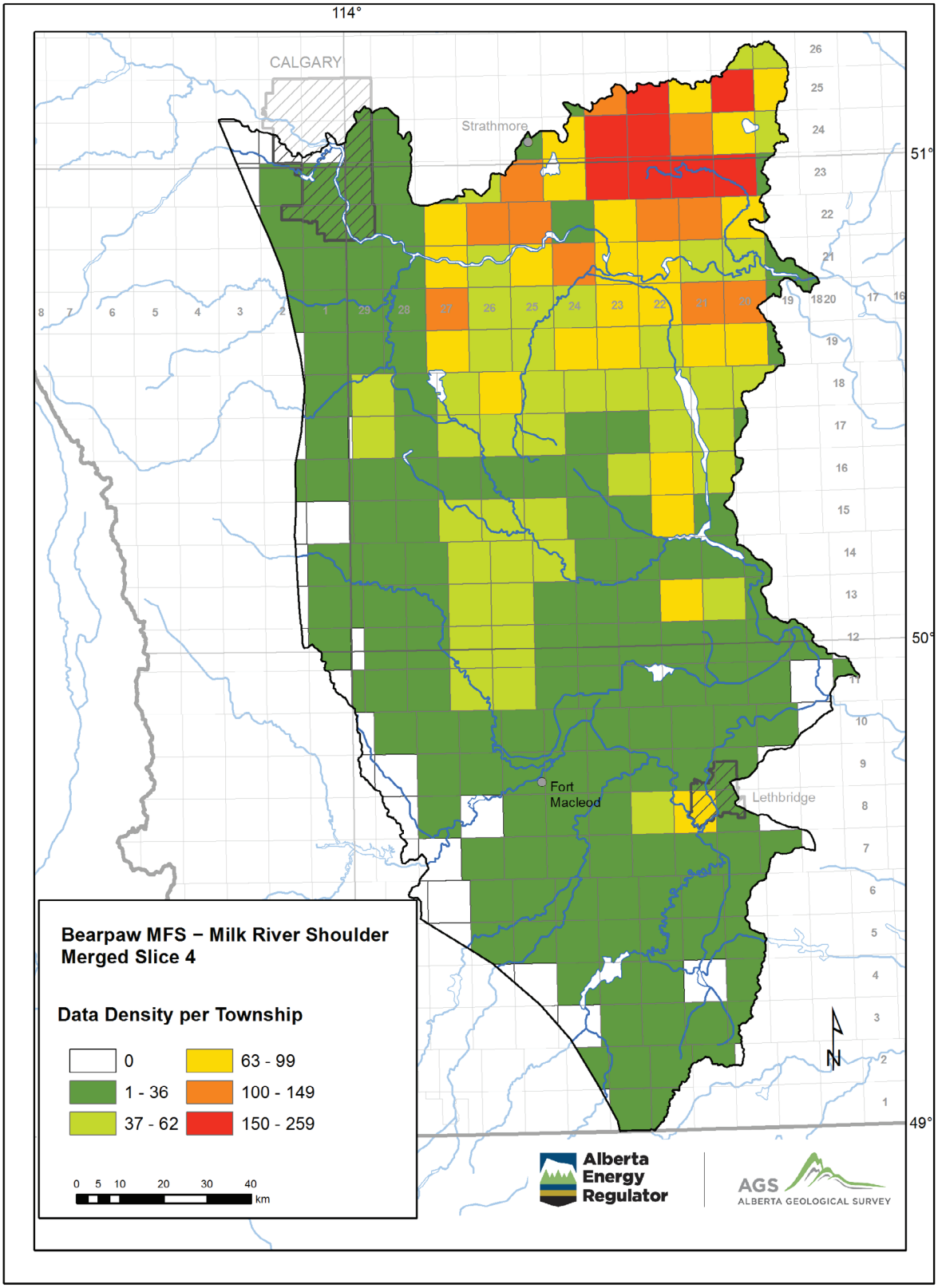

Figure A5-21. Data density map for merged slice 4.

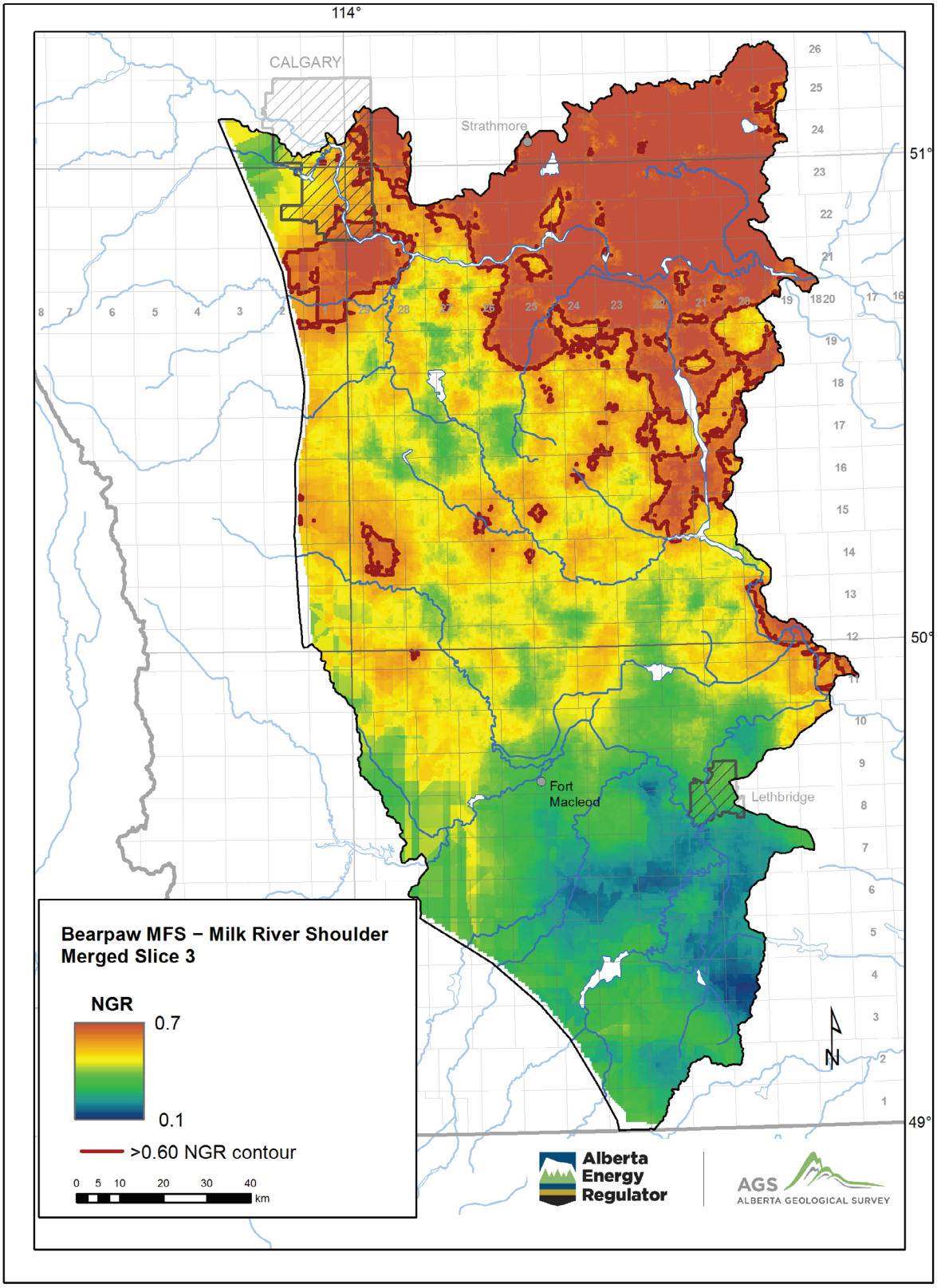

Figure A5-22. Merged slice 3 and the ≥0.60 NGR polygon.

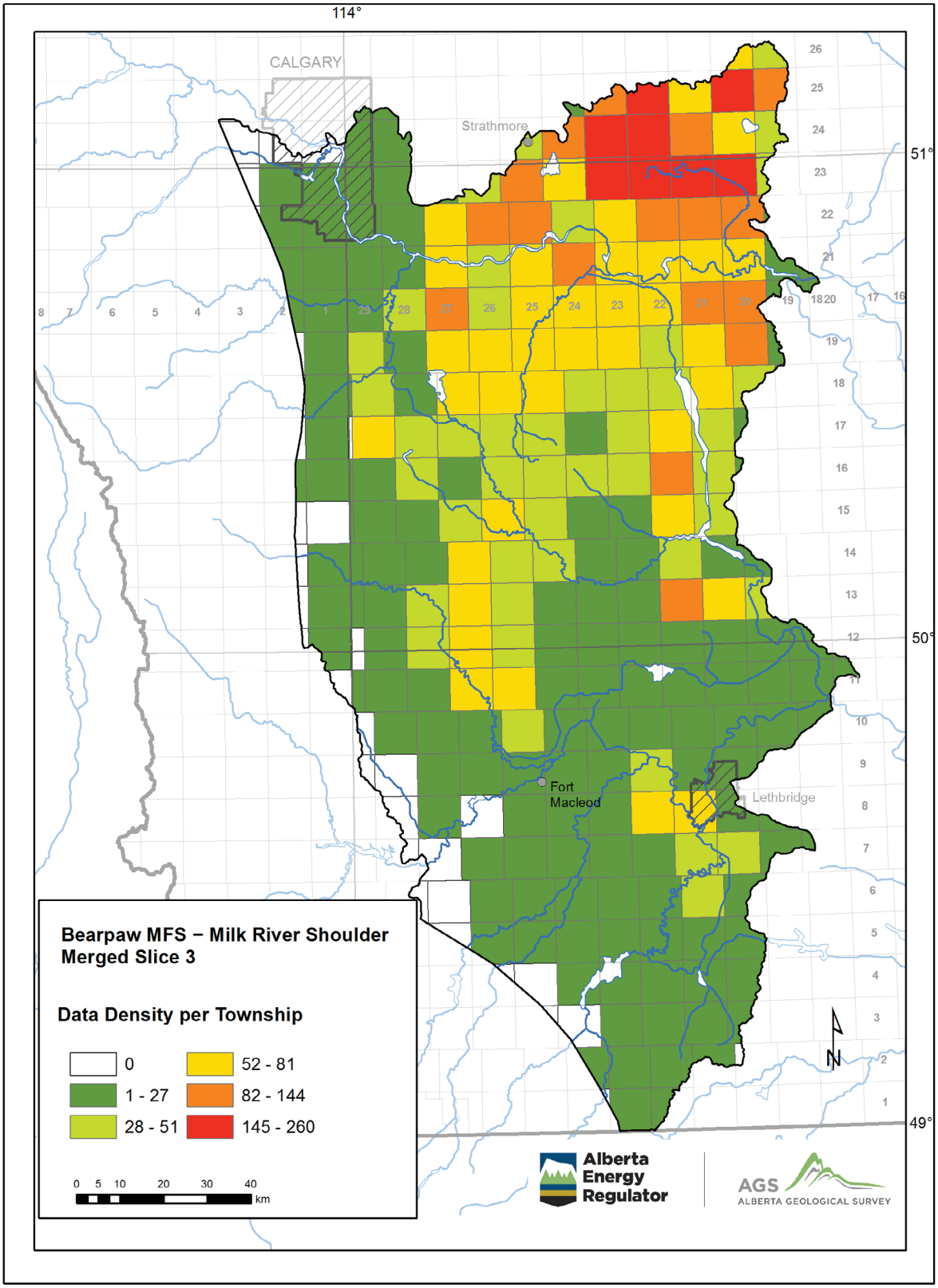

Figure A5-23. Data density map for merged slice 3.

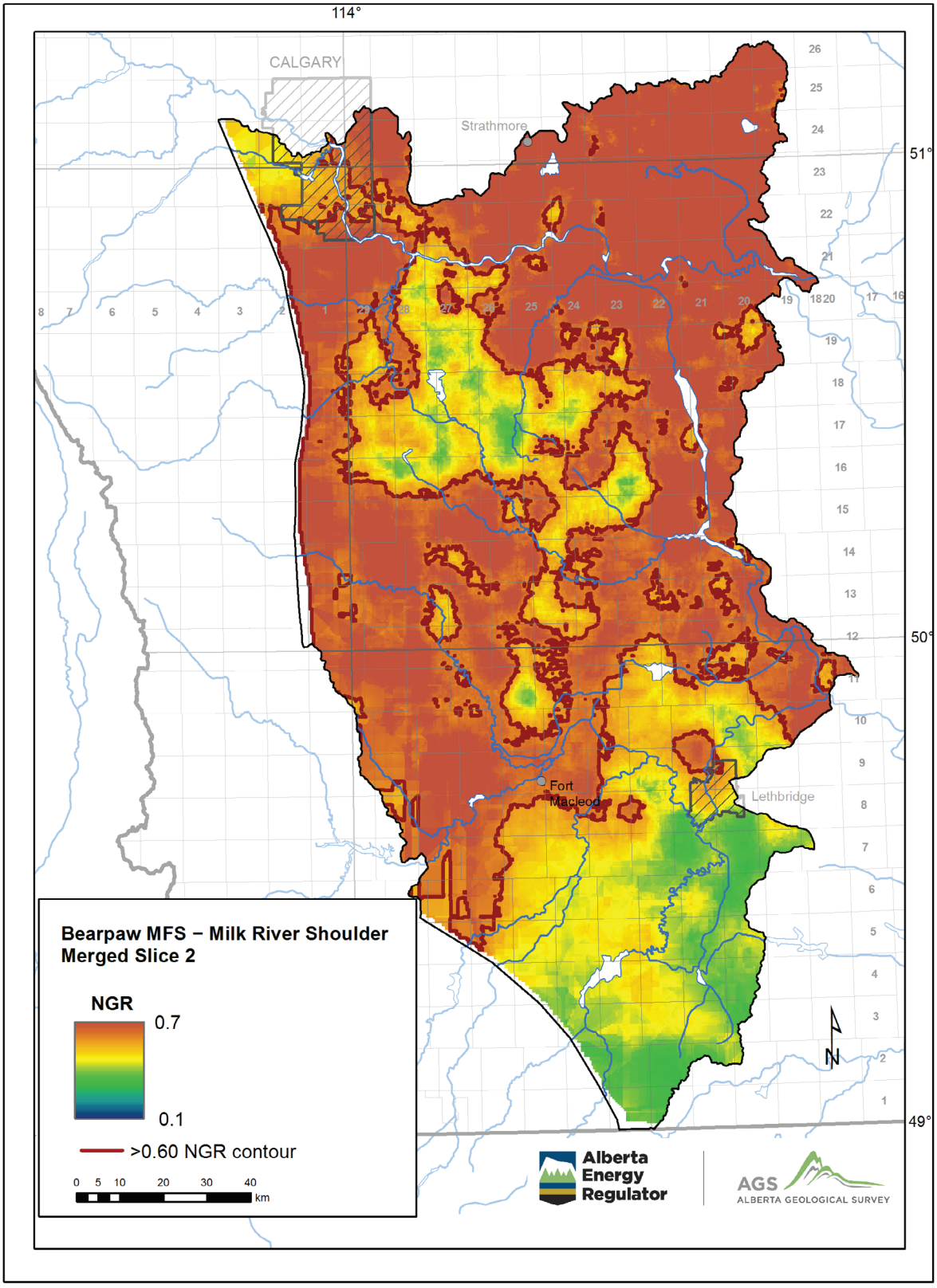

Figure A5-24. Merged slice 2 and the ≥0.60 NGR polygon.

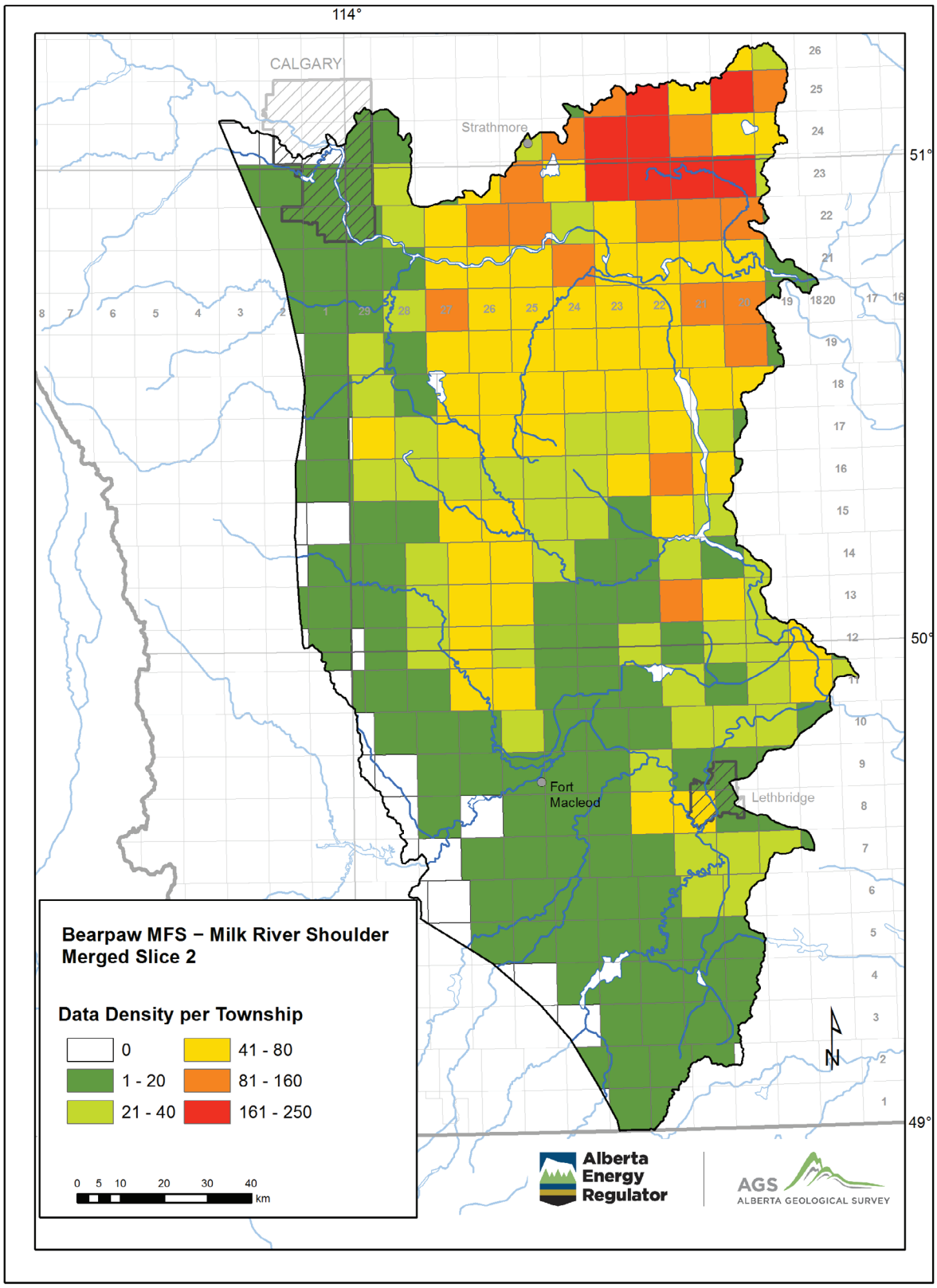

Figure A5-25. Data density map for merged slice 2.

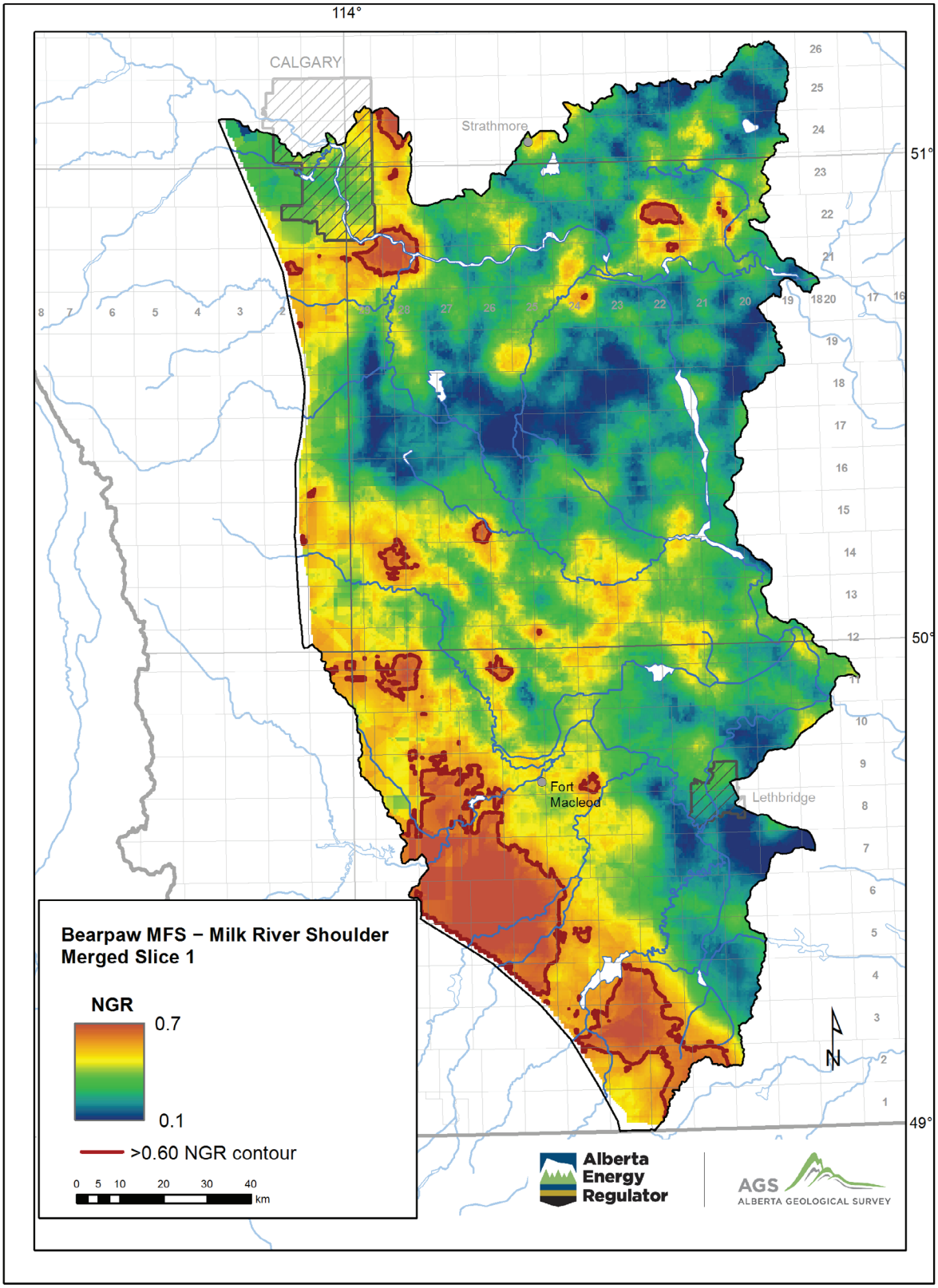

Figure A5-26. Merged slice 1 and the ≥0.60 NGR polygon.

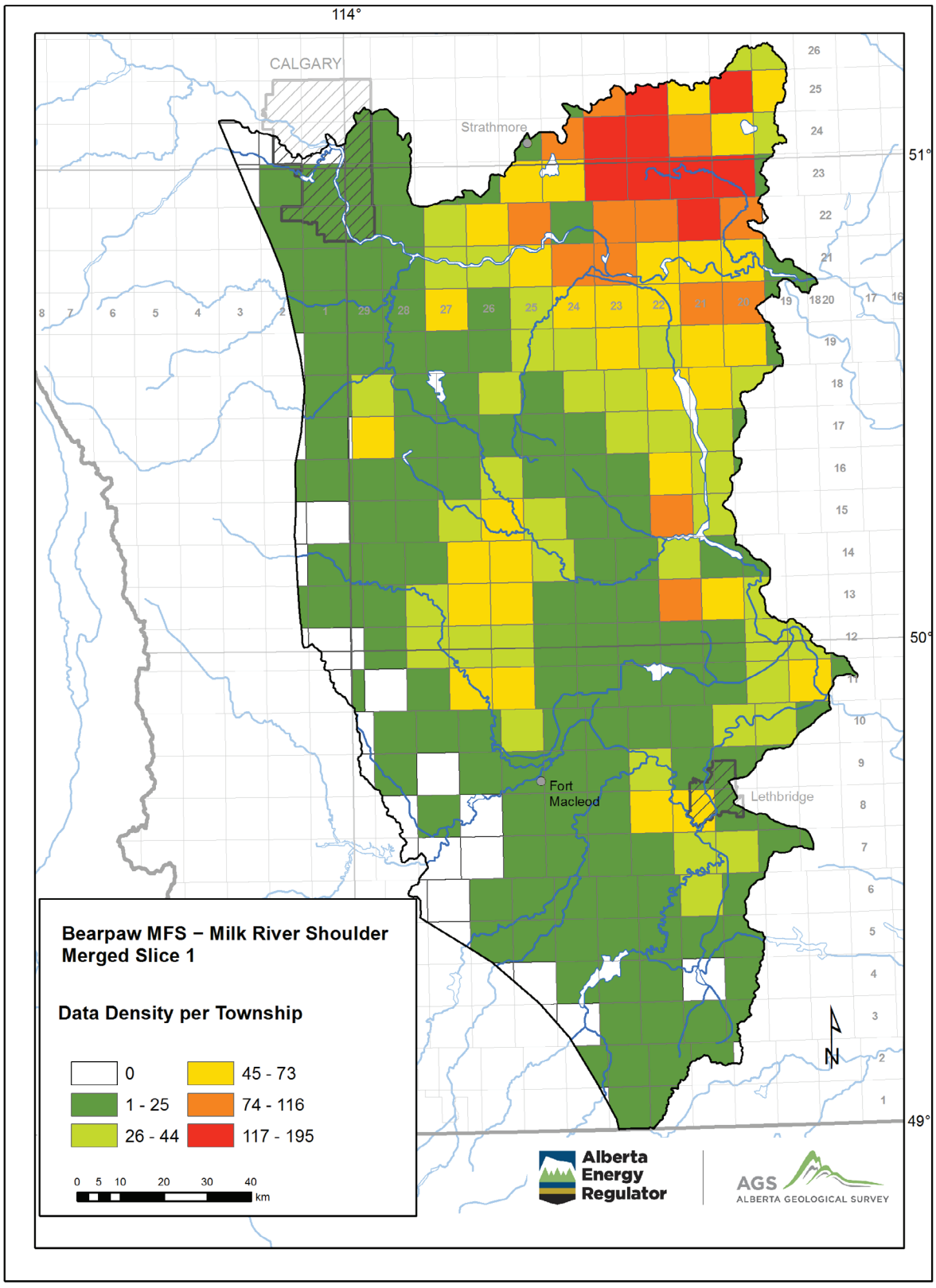

Figure A5-27. Data density map for merged slice 1.

Appendix 6 – Field Photos

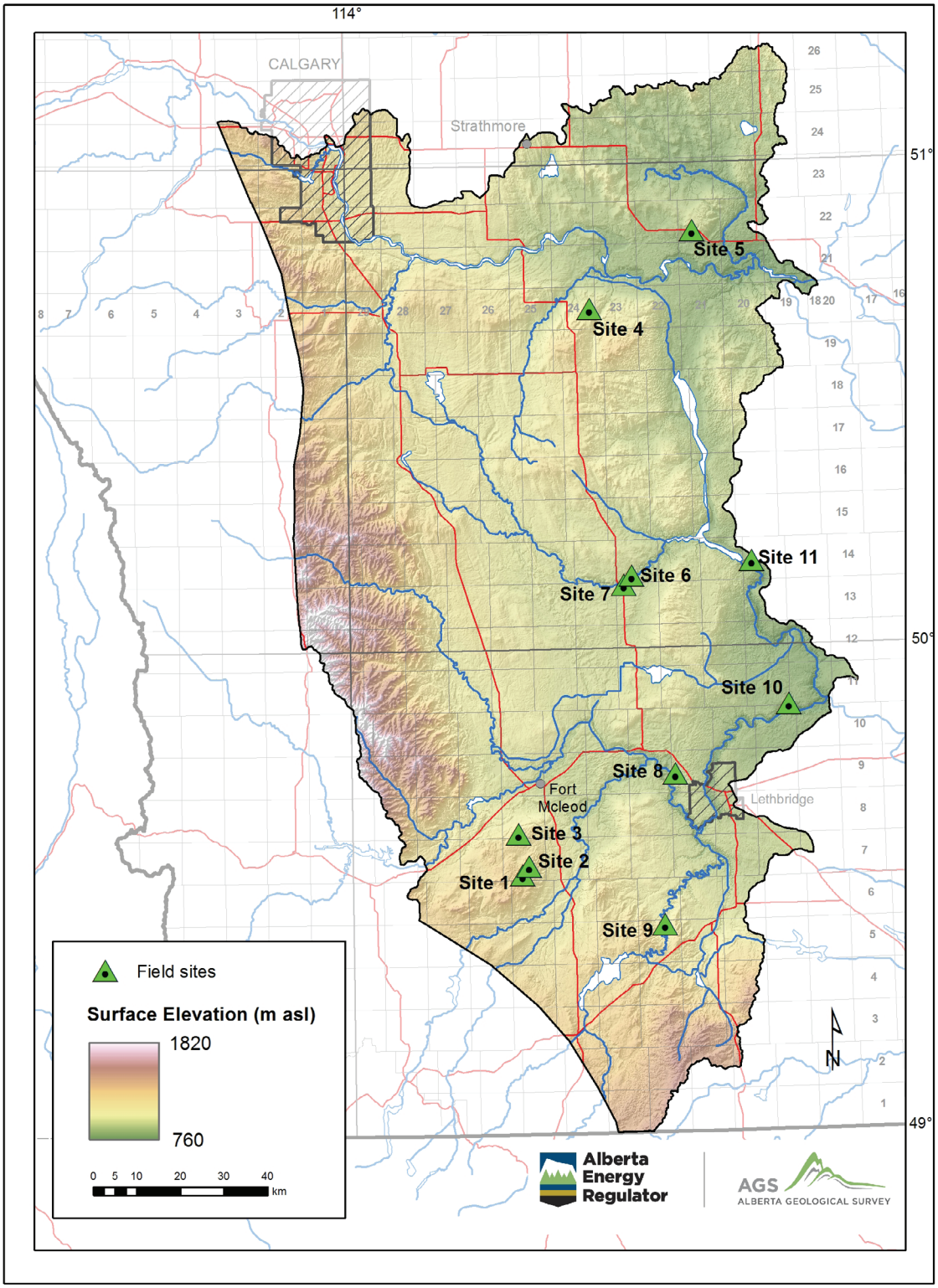

Figure A6-1. Map of field site locations within the CLC. The following figures provide selected photos from field excursions conducted to collect data for input into the hydrostratigraphic model. Most field sections are located along rivers or in excavations. Field photos of sites 6 and 11 were not taken.

Figure A6-2. Field site 1: Clast- to matrix-supported pebble–cobble gravel and sand (3 m thick) exposed in excavation.

Figure A6-3. Field site 2: Clast-supported pebble–cobble gravel and sand (3 m thick) and overlying diamicton (1 m thick) exposed in excavation.

Figure A6-4. Field site 3: Clast- to matrix-supported pebble–cobble gravel and sand (4 m thick) exposed in excavation.

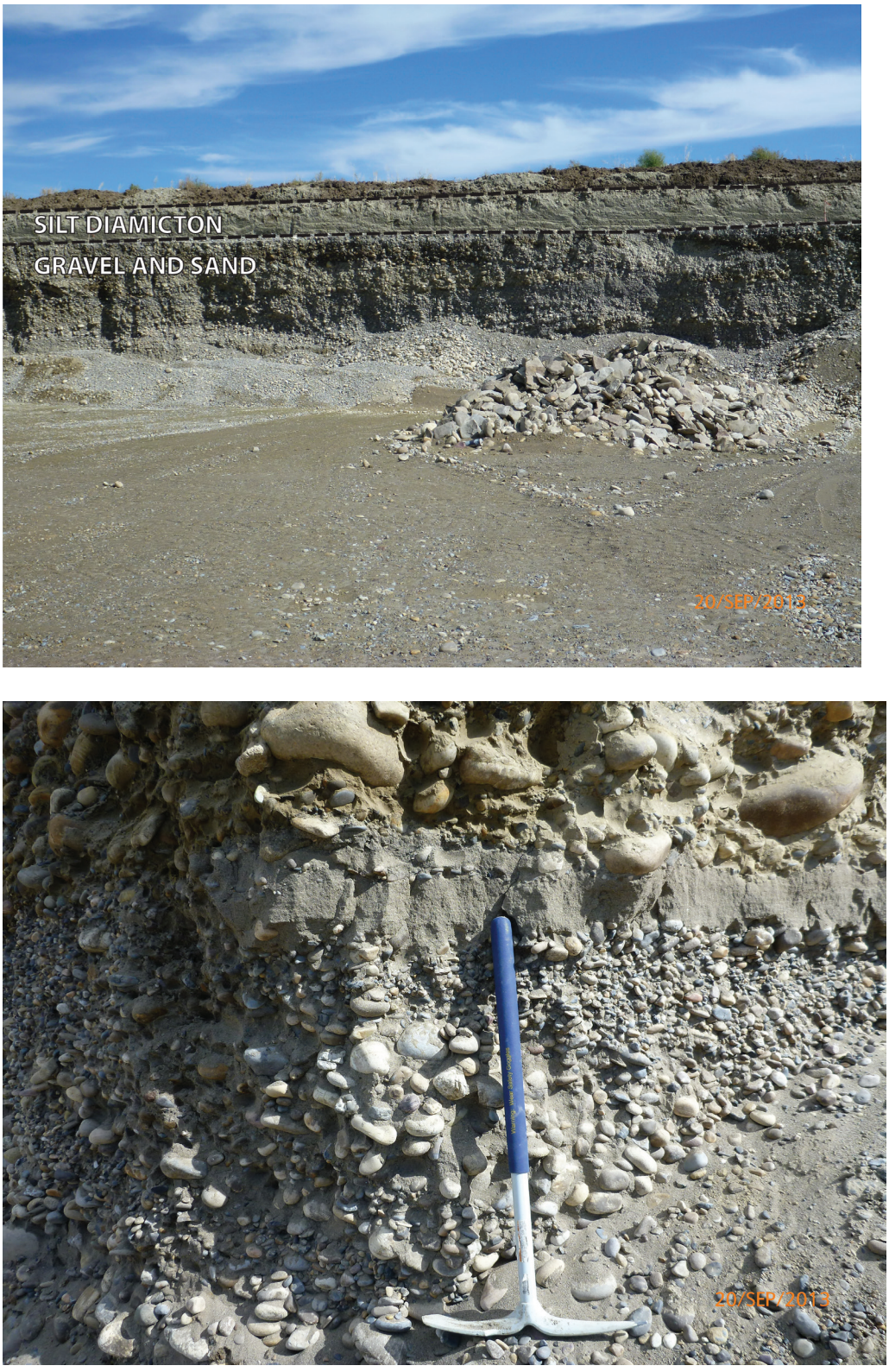

Figure A6-5. Field site 4: Crudely stratified clast-supported pebble–cobble gravel with sand lenses (6 m thick) and overlying silt diamicton (2.5 m thick) exposed in excavation.

Figure A6-6. Field site 5: Crudely bedded clast- to matrix-supported pebble–cobble gravel and sand (6 m thick) and overlying diamicton (1 m thick) exposed in excavation. Diamicton in above photos has been disturbed by gravel pit operations.

Figure A6-7. Field site 7: Interbedded sandstone/mudstone bedrock (>24 m thick) overlain by diamicton and silt/clay (approximately 8 m and 3 m thick respectively) exposed in valley wall.

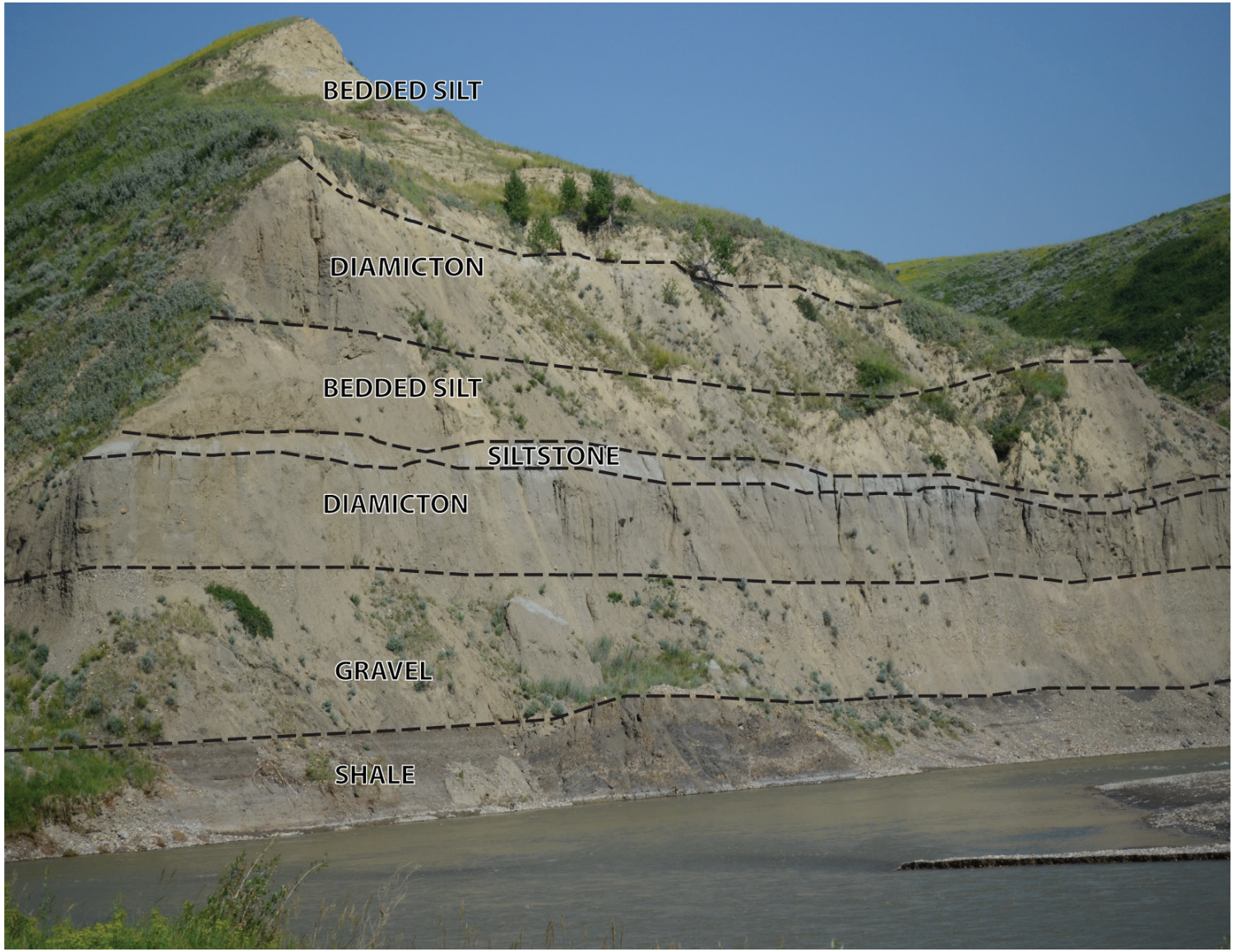

Figure A6-8. Field site 8: Units exposed in Oldman River section from bottom to top: shale (>3.5 m thick), gravel (7 m thick), diamicton (8.5 m thick), laterally extensive siltstone bedrock (1.5 m thick; displaced), bedded silt (3.5 m thick), diamicton (6.5 m thick), bedded silt (>4 m thick).

Figure A6-9. Field site 9: Interbedded sandstone/shale bedrock and overlying colluviated Quaternary material exposed in St. Mary River section. Blue line marks contact spring at base of major sandstone unit in upper photograph. Look direction of upper photograph indicated by arrow in lower photograph.

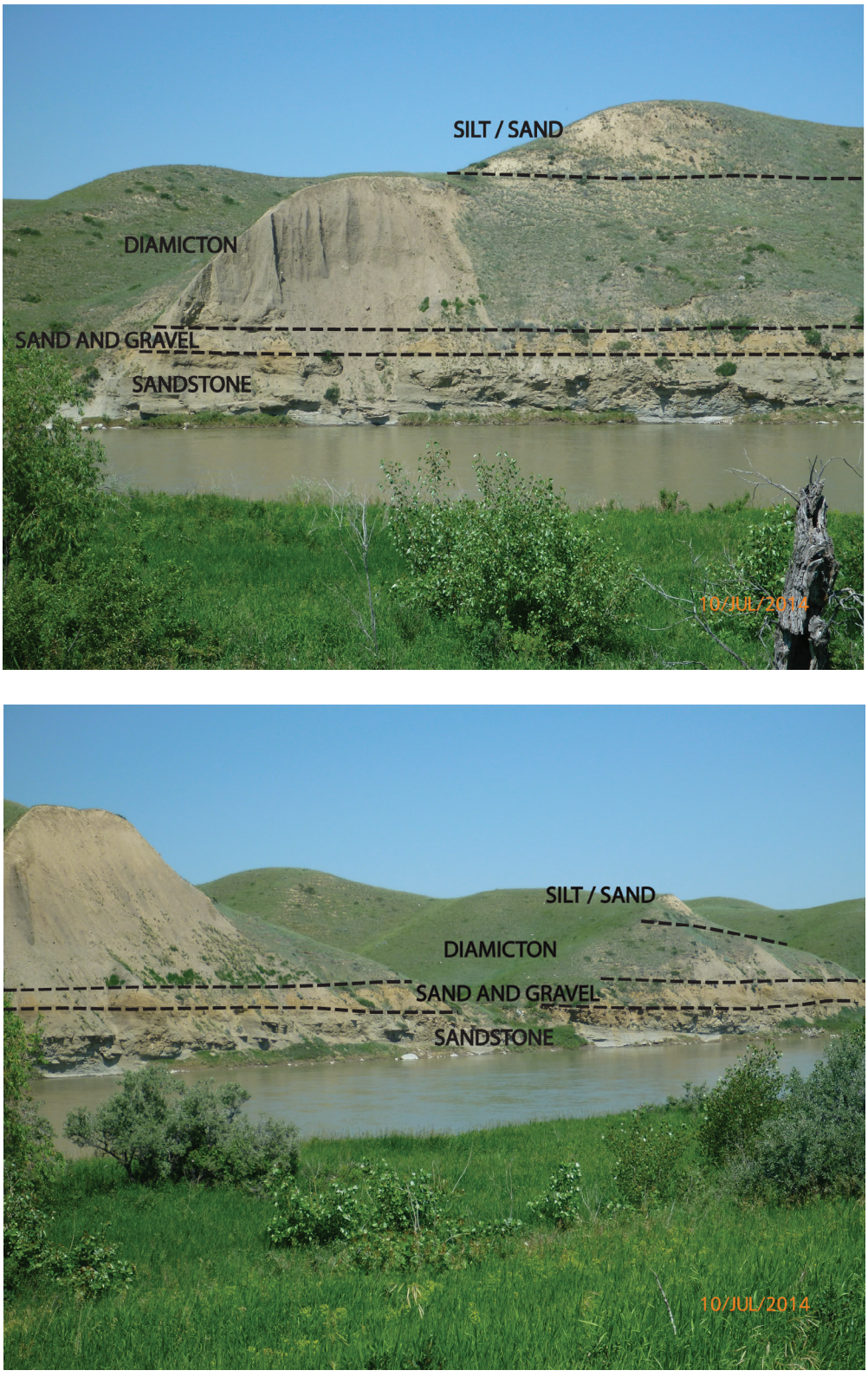

Figure A6-10. Field site 10: Units exposed in Oldman River section from bottom to top: sandstone (>8 m thick), sand and gravel (6 m thick), massive to crudely stratified diamicton (20 m thick), laminated to bedded sand and silt (12 m thick).